Linköping Studies in Science and Technology. Dissertations
No. 380

Identification of State-Space Models from Time and Frequency Data

Tomas McKelvey

Department of Electrical Engineering
Linköping University, S-581 83 Linköping, Sweden

Linköping 1995

Identification of State-Space Models from Time and Frequency Data

Dept. of Electrical Engineering
Linköping University
S-581 83 Linköping
Sweden

ISBN 91-7871-531-8 ISSN 0345-7524

Printed in Sweden by Linköpings Tryckeri AB 1995.845

To Maureen

Abstract

This dissertation considers the identification of linear multivariable systems using finite dimensional time-invariant state-space models.

Parametrization of multivariable state-space models is considered. A full parametrization, where all elements in the state-space matrices are parameters, is introduced. A model structure with full parametrization gives two important implications; low sensitivity realizations can be used and the structural issues of multivariable canonical parametrizations are circumvented. Analysis reveals that additional estimated parameters do not increase the variance of the transfer function estimate if the resulting model class is not enlarged.

Estimation and validation issues for the case of impulse response data are discussed. Identification techniques based on realization theory are linked to the prediction error method. The combination of these techniques allows for the estimation of high quality models for systems with many oscillative modes. A new model quality measure, Modal Coherence Indicator, is introduced. This indicator gives an independent quality tag for each identified mode and provides information useful for model validation and order estimation.

Two applications from the aircraft and space industry are considered. Both problems are concerned with vibrational analysis of mechanical structures. The first application is from an extensive experimental vibrational study of the airframe structure of the Saab 2000 commuter aircraft. The second stems from vibrational analysis of a launcher-satellite separation system. In both applications multi-output discrete time state-space models are estimated, which are then used to derive resonant frequencies and damping ratios.

New multivariable frequency domain identification algorithms are also introduced. Assuming primary data consist of uniformly spaced frequency response measurements, an identification algorithm based on realization theory is derived. The algorithm is shown to be robust against bounded noise as well as being consistent. The resulting estimate is shown to be asymptotically normal, and an explicit variance expression is determined. If data originate from an infinite dimensional system, it is shown that the estimated transfer function converges to the transfer function of the truncated balanced realization.

Frequency domain subspace based algorithms are also derived and analyzed when the data consist of samples of the Fourier transform of the input and output signals. These algorithms are the frequency domain counterparts of the time domain subspace based algorithms.

The frequency domain identification methods developed are applied to measured frequency data from a mechanical truss structure which exhibits many lightly damped oscillative modes. With the new methods, high quality state-space models are estimated both in continuous and discrete time.

Preface

This thesis consists of two parts: Part I deals with various aspects of estimation from time domain data. In Part II estimation methods are proposed which use frequency domain data. Some parts of the thesis have been published earlier.

Parts of Chapters 2 and 3 were presented as

> T. McKelvey. Fully parametrized state-space models in system identification. In *Proc. of the 10th IFAC Symposium on System Identification*, volume 2, pages 373–378, Copenhagen, Denmark, July 1994.

Chapter 5 is the result of joint work with Dr. Hüseyin Akçay and will appear as

> T. McKelvey and H. Akçay. Identification of infinite dimensional systems from frequency response data. In *Proc. Third European Control Conference*, Rome, Italy, 1995.

This paper has also been submitted for possible publication in *System and Control Letters*.

Section 6.4.2 will appear as

> T. McKelvey. Model validation using geometric arguments. In *Proc. Third European Control Conference*, Rome, Italy, 1995.

The material in Section 7.2 is joint work together with Thomas Abrahamsson and Lennart Ljung and has appeared in

> T. Abrahamsson, T. McKelvey, and L. Ljung. A study of some approaches to vibration data analysis. In *Proc. of the 10th IFAC Symposium on System Identification*, volume 3, pages 289–294, Copenhagen, Denmark, July 1994.

This paper has also been submitted for publication in *Automatica*.

Section 7.3 can be found in

> T. McKelvey. A combined state-space identification algorithm applied to data from a modal analysis experiment on a separation system. In *Proc. 33rd IEEE Conference on Decision and Control, Lake Buena Vista, Florida*, pages 2286–2287, December 1994.

Many of the results of Chapter 9 have been developed together with Hüseyin Akçay. Various parts of Section 9.3 has appeared as

> T. McKelvey and H. Akçay. An efficient frequency domain state-space identification algorithm. In *Proc. 33rd IEEE Conference on Decision and Control, Lake Buena Vista, Florida*, pages 3359–3364, December 1994.

and

> T. McKelvey and H. Akçay. An efficient frequency domain state-space identification algorithm: Robustness and stochastic analysis. In *Proc. 33rd IEEE Conference on Decision and Control, Lake Buena Vista, Florida*, pages 3348–3353, December 1994.

A joint paper has also been submitted to *IEEE Trans. of Automatic Control.*

Section 9.4 will appear in

> T. McKelvey and H. Akçay. Identification of infinite dimensional systems from frequency response data. In *Proc. Third European Control Conference*, Rome, Italy, 1995.

and is also being submitted to *Automatica.*

Acknowledgments

First of all I would like to express my sincere gratitude to my supervisor, Professor Lennart Ljung. He has made this work possible in many ways, primarily by providing me a place in the group and by offering me excellent guidance and encouragement during the course of this work.

Some of the material in Part II is the result of joint work with Dr. Hüseyin Akçay. I thank him for sharing his knowledge with me.

Dr. Thomas Abrahamsson, Saab Military Aircraft, and Dr. David Bayard, Jet Propulsion Laboratory, have provided me with experimental data used in this thesis. Thanks!

Two persons I am greatly indebted to are Peter Lindskog, who has carefully read the manuscript several times and provided me with numerous valuable comments, and Dr. Sören Andersson, for his excellent comments on Part I. Many thanks also go to Dr. Håkan Hjalmarsson, Anders Helmersson, Jonas Sjöberg, Håkan Fortell, Dr. Ashok Tikku and Dr. Chun Tung Chou for valuable comments and discussions regarding various parts of this work.

I am also grateful to Professor Johan Schouken at Vrije Unvirsiteit in Brussels, and Professor Bart De Moor and Dr. Peter Van Overschee at the Katholieke Universiteit in Leuven for making it possible for me to visit them. The visits were fun and served as a great source of inspiration.

I would also like to thank the rest of the people in the group of Automatic Control for their genuine generosity which makes being part of this group so nice.

Finally, I would like to thank my wife Maureen, my parents Stig and Sonja and my sister Helen for their infinite support and love.

Contents

Part I

Time Domain Methods

1

Introduction

This dissertation deals with certain topics from the area of *System Identification*. This area may be defined as a branch of system theory which deals with techniques about how to construct adequate mathematical models on the basis of available input-output data from a dynamic system. After rapid development during thirty years, System Identification is now recognized as an important engineering tool. The theory is embodied in unifying textbooks such as by Ljung [86] and Söderström and Stoica [136].

The dominating theme will be the estimation of linear state-space models in discrete time

$$x(t+1) = Ax(t) + Bu(t) + Ke(t)$$
$$y(t) = Cx(t) + Du(t) + e(t),$$

where $u(t)$, $y(t)$ and $e(t)$ are the input, output and innovation signals, respectively. The state $x(t)$ is a column vector of dimension n which equals the order of the model. In particular, we focus on such models where both $u(t)$, $y(t)$ and $e(t)$ are also vectors. These are known as *multivariable* or, equivalently, multi-input multi-output (MIMO) systems. All methods discussed are based on discrete time modeling. If certain assumptions hold, continuous-time models can be constructed by first estimating discrete time models from sampled data. The continuous-time models are then derived by a transformation of the discrete time model.

A second theme of the thesis is identification of systems of high or infinite order. In this case linear models of high orders are needed for accurate modeling. Conceptually, identification of high order models is straightforward. In practice, many factors limit the applicability of many methods to systems of low order. One such factor is the limited numerical accuracy found in all computers. This implies that for parametric model structures, it is important to find parameterizations which minimize the sensitivity of the model with respect to parameter perturbations. Many algorithms rely on a non-linear parametric optimization step, often solved by iterative search. For such methods to succeed, an initial estimate of high quality is very important.

The state-space modeling approach to identification offers some key advantages:

- High order systems can be represented as state-space models in realizations which offer low sensitivity with respect to perturbations in the parameters.
- MIMO systems are easily described as state-space models with minimal state dimensions.
- Realization and subspace based algorithms provide state-space models of high quality which can be parameterized and further improved by optimization based methods.

Thesis Outline

The material in this thesis naturally divides into two parts. Part I concerns identification from data in the time domain. Part II focuses on methods which are applicable when the primary data is in the frequency domain. These two orthogonal parts are held together by the common approach of subspace based state-space modeling of higher order systems.

Part I

In Chapter 2 multivariable state-space models suited for identification are discussed. In particular, a model structure with a full parametrization is introduced. This type of parametrization has two properties. Firstly, all systems of a given order can be described in this fully parametrized model structure. This removes the complicated structural issues inherent in "canonical" parametrizations. Secondly, the full parametrization is not identifiable, *i.e.*, one system is represented by a manifold in the parameter space. This non-uniqueness can be utilized in order to select a particular point, or a subset, on the manifold, which represent realizations with a low sensitivity to numerical inaccuracies, *e.g.*, the balanced realization.

Identification by prediction error minimization is the topic of Chapter 3. The non-uniqueness of the full parametrization require some additional measures in the parametric optimization. Two alternative routes are considered, which both aim at making the inverse of the Gauss-Newton Hessian matrix well-conditioned. The first approach is based on minimizing a regularized prediction error criterion, and the second approach uses a pseudo-inverse technique. The identification of excessive parameters is in general known to increase the variance of the model. However, we show that estimation of models with the full parametrization retains the variance properties of a minimal parametrization.

The general prediction error minimization requires a non-linear iterative search. As for all such optimizations, the success of the algorithm relies heavily on the availability of an initial model of high quality. As the model order increases, the need for a good initial model becomes even more important. The recently proposed subspace identification algorithms are methods which can be used to derive such initial models. In Chapter 4 we discuss the classical realization-based identification methods which can be used if impulse-like measurements are available. For the

special case when the excitation signal is periodic, a subspace algorithm which has low computational complexity is presented and analyzed in Chapter 5.

Some techniques applicable to system identification from impulse response measurements are considered in Chapter 6. We link the realization algorithms to prediction error minimization methods. A parametrization is introduced which minimizes the numerical complexity during the identification phase. Model order determination and model quality assessments are also discussed. A new model quality measure is developed which assesses the quality of a model with respect to an empirical impulse response by calculating a set of indicators corresponding to the modes of the system.

Two vibrational analysis applications are covered in Chapter 7. The first considers a vibrational analysis of the aircraft Saab 2000. The second example consists of a vibrational study of a satellite launcher separation system. In both applications a linear dynamical model is identified from acceleration measurements. The modeling serves the purpose of determining resonant frequencies and corresponding damping ratios, which are then to be used for evaluation and verification of other theoretical models of the mechanical structures.

Part II

Part II deals with identification from frequency data. An introduction and overview is given in Chapter 8. The dominating approaches in the area are discussed. The chapter is concluded by discussing how high order continuous-time models can be accurately identified by the use of the bilinear transformation and discrete time identification techniques.

Chapter 9 deals with the identification of state-space models from equidistant multivariable frequency response data. Several algorithms based on realization theory are proposed. The algorithms are shown to be robust against bounded noise. Consistency is proved, and the estimated transfer function is shown to be asymptotically normal. Explicit variance expressions are also given. Section 9.4 considers the case when the system is infinite dimensional. The suggested algorithm is shown to converge to a transfer function equal to the balanced truncation of the original system. This implies that the algorithm has favorable approximation properties. The algorithm is further extended in Section 9.5 to incorporate frequency weighting capabilities. This enables the user to influence the distribution of the model error of the frequencies.

Frequency domain versions of the time domain subspace based methods are discussed in Chapter 10. Here we assume that the Fourier transform of the input and output signals are known. The frequency domain version of the basic projection algorithm [31] is introduced and analyzed. Severe restrictions on the noise is required to ensure consistency of this method. A frequency domain version of the instrumental variable method in [156] is also introduced. This method is consistent under much weaker noise requirements.

Chapter 11 deals with parametric maximum-likelihood (ML) estimation of multivariable systems. The ML estimator is derived and the similarities with the time domain ML-estimator is pointed out. Some asymptotic properties of the estimates

are also briefly discussed.

Part II is concluded with an application. From measured data of a flexible mechanical structure, state-space models are estimated with the algorithms from Chapters 9 and 10. Both discrete time models and continuous-time models are estimated. The resulting models are of high order (60) and are of excellent quality.

2

State-Space Models for Identification

2.1 State-Space Models of Linear Systems

A general time-invariant discrete time *linear system* $\mathcal{S}$ can be described as

$$\mathcal{S}: \; y(t) = G_0(q)u(t) + H_0(q)e_0(t), \tag{2.1}$$

where $y(t)$ is an output vector of dimension p, $u(t)$ is an input vector of dimension m and is assumed to be known. In (2.1), q is the time shift operator. The unknown disturbances acting on the output are assumed to be generated by the second term where $e_0(t)$ is a noise vector of dimension p. $e_0(t)$ is assumed to be a sequence of independent stochastic variables satisfying

$$E\, e_0(t) = 0, \quad \text{and} \quad E\, e_0(t)e_0(t)^T = \Lambda_0 \tag{2.2}$$

where E denotes the expectation operator. The *transfer functions*[1], $G_0(q)$ and $H_0(q)$, can be characterized by their impulse responses $\{g_k\}$ and $\{h_k\}$ as

$$G_0(q) = \sum_{k=0}^{\infty} g_k q^{-k}, \quad H_0(q) = I + \sum_{k=1}^{\infty} h_k q^{-k}, \tag{2.3}$$

where $q^{-k}u(t) = u(t-k)$. $H_0(q)^{-1}$ is assumed to be a stable transfer function. We will also assume that $g_0 = 0$, *i.e.*, the direct term from $u(t)$ to $y(t)$ is missing. Inclusion of the direct term is straightforward and does not change any of the results to be presented. Furthermore we also assume that the system is finite-dimensional, *i.e.*, the transfer functions $G_0(q)$ and $H_0(q)$ can be written as a matrix where each entry is a rational function.

[1] These are actually transfer operators but we will frequently call the operator $G(q)$ as well as the z-transformed function $G(z) = \sum_{k=1}^{\infty} g_k z^{-k}$ the transfer function.

Since the system (2.1) is of finite order it can also be described in a *state-space model* formulation by introducing an auxiliary state vector $x(t)$ of dimension n, the order of the system. The input-output relation can then be described by

$$\begin{aligned} x(t+1) &= Ax(t) + Bu(t) + Ke_0(t) \\ y(t) &= Cx(t) + e_0(t). \end{aligned} \tag{2.4}$$

with $A \in \mathbb{R}^{n\times n}$, $B \in \mathbb{R}^{n\times m}$, $K \in \mathbb{R}^{n\times p}$ and $C \in \mathbb{R}^{p\times n}$. The way of representing the noise in (2.4) is called the *innovations form*. The state-space model (2.4) is equal to the system (2.1) if the matrices A, B, C and K are chosen in such a way that

$$G_0(q) = C(qI - A)^{-1}B, \quad \text{and} \quad H_0(q) = C(qI - A)^{-1}K + I. \tag{2.5}$$

The particular realization, *i.e*, the set of matrices A, B, C, K, is not unique. A change of basis for the states

$$\tilde{x}(t) = T^{-1}x(t), \tag{2.6}$$

where $T \in \mathbb{R}^{n\times n}$ is a non-singular matrix, results in a new state-space model

$$\begin{aligned} \tilde{x}(t+1) &= \tilde{A}\tilde{x}(t) + \tilde{B}u(t) + \tilde{K}e_0(t) \\ y(t) &= \tilde{C}\tilde{x}(t) + e_0(t). \end{aligned} \tag{2.7}$$

Here $\tilde{A} = T^{-1}AT$, $\tilde{B} = T^{-1}B$, $\tilde{K} = T^{-1}K$ and $\tilde{C} = CT$. It is easy to show that

$$\begin{aligned} C(qI - A)^{-1}B &= \tilde{C}(qI - \tilde{A})^{-1}\tilde{B} \\ C(qI - A)^{-1}K + I &= \tilde{C}(qI - \tilde{A})^{-1}\tilde{K} + I. \end{aligned} \tag{2.8}$$

The two state-space models are thus input-output equivalent, since their transfer functions are equal. Two system realizations with the property (2.8) will be called *similar*. The non-singular matrix T which relates the two realizations will be called a *similarity transformation*.

A natural *predictor* $\hat{y}(t)$ for the output $y(t)$ given inputs u and outputs y up to time $t-1$ is, Ljung [86],

$$\hat{y}(t) = H_0(q)^{-1}G_0(q)u(t) + [I - H_0(q)^{-1}]y(t). \tag{2.9}$$

The predictor (2.9) is the conditional expectation of $y(t)$ given information up to $t-1$ [86].

For system identification purposes it is often desirable to use *parametric models*, *i.e.*, a set of models is described by a number of real-valued parameters collected in a parameter vector $\theta \in \mathbb{R}^d$. A particular model is then represented by a value of the d-dimensional vector θ. The mapping from the space of parameters $\mathbb{R}^d$ to the space of linear models (2.1) is called a *model structure* $\mathcal{M}$.

In this thesis the focus will be on state-space model structures in innovations form

$$\mathcal{M}: \quad \begin{aligned} \hat{x}(t+1) &= A(\theta)\hat{x}(t) + B(\theta)u(t) + K(\theta)e(t) \\ y(t) &= C(\theta)\hat{x}(t) + e(t), \end{aligned} \tag{2.10}$$

where the matrices A, B, C and K are constructed from the parameter vector θ according to the model structure $\mathcal{M}$. Let

$$d_{\mathcal{M}} = \dim \theta \tag{2.11}$$

denote the dimension of the parameter vector θ and let $\mathcal{M}(\theta)$ denote the model (2.10). The model will thus have the transfer functions

$$G(q,\theta) = C(\theta)[qI - A(\theta)]^{-1}B(\theta) \tag{2.12}$$

and

$$H(q,\theta) = I + C(\theta)[qI - A(\theta)]^{-1}K(\theta). \tag{2.13}$$

By using (2.10), the predictor is given by

$$\begin{aligned} \hat{x}(t+1) &= [A(\theta) - K(\theta)C(\theta)]\hat{x}(t) + B(\theta)u(t) + K(\theta)y(t) \\ \hat{y}(t|\theta) &= C(\theta)\hat{x}(t), \end{aligned} \tag{2.14}$$

which can also be written as

$$\hat{y}(t|\theta) = W_u(q,\theta)u(t) + W_y(q,\theta)y(t) \tag{2.15}$$

where

$$W_u(q,\theta) = C(\theta)[qI - A(\theta) + K(\theta)C(\theta)]^{-1}B(\theta) \tag{2.16}$$

$$W_y(q,\theta) = C(\theta)[qI - A(\theta) + K(\theta)C(\theta)]^{-1}K(\theta). \tag{2.17}$$

In order to use the predictor (2.14) we have to ensure stability of the two corresponding transfer functions $W_u(z,\theta)$ and $W_y(z,\theta)$ and therefore we make the following definition.

Definition 2.1 Let the set of parameters $D_{\mathcal{M}} \subset \mathbb{R}^{d_{\mathcal{M}}}$ be such that

$$D_{\mathcal{M}} = \{\theta \in \mathbb{R}^{d_{\mathcal{M}}} \mid W_u(z,\theta) \text{ and } W_y(z,\theta) \text{ are stable}\}$$

□

From the structure of the state-space predictor (2.14) it follows trivially that

$$D_{\mathcal{M}} = \{\theta \in \mathbb{R}^{d_{\mathcal{M}}} \mid \text{the matrix } A(\theta) - K(\theta)C(\theta) \text{ has all eigenvalues inside the open unit disc}\}$$

for the general state-space model structure (2.10).

Definition 2.2 Two models, $\mathcal{M}_1(\theta_1)$ and $\mathcal{M}_2(\theta_2)$ are *equal* if and only if

$$G_1(e^{i\omega},\theta_1) = G_2(e^{i\omega},\theta_2) \text{ and } H_1(e^{i\omega},\theta_1) = H_2(e^{i\omega},\theta_2) \text{ for almost all } \omega \tag{2.18}$$

□

To simplify the reasoning about different models we will use the term *model set* [86] denoted by $\mathcal{M}^*$. A model structure $\mathcal{M}$ together with a parameter set $D_{\mathcal{M}}$ gives a model set

$$\mathcal{M}^* = \{\mathcal{M}(\theta) \mid \theta \in D_{\mathcal{M}}\}. \tag{2.19}$$

2.2 Parametrization and Identifiability of State-Space Models

The *parametrization* of models used in system identification is often closely tied to the concept of *identifiability*.

Definition 2.3 [86] A model structure $\mathcal{M}$ is *globally identifiable at* θ^* if

$$\mathcal{M}(\theta) = \mathcal{M}(\theta^*) \Rightarrow \theta = \theta^* \tag{2.20}$$

□

An identifiable model structure thus has a one to one correspondence between the models, *i.e.*, the transfer functions, and the value of the parameter vector θ.

Traditionally, see [86, 136], model structures which are identifiable have been favored for the purpose of system identification. The use of an identifiable model structure has a clear advantage; a unique value of θ represents a unique model. However, the parametrization of multivariable state-space models, which are identifiable, is a much discussed and notoriously difficult problem in system identification, see *e.g.*, [33, 42, 66, 92, 99] or [40, 50, 51, 149]. The root of the problem is that there is not one single, smooth identifiable parametrization of all multi-output systems (2.10). Typically, one has to work with a large number of different possible parametrizations depending on the internal structure of the system. Moreover, for some systems it is difficult to find an identifiable parametrization which is well-conditioned [87]. The identifiable model structure we will use was introduced in [149] and can be defined as:

> Let $A(\theta)$ initially be a matrix filled with zeros and with ones along the super diagonal. Let then the rows numbered $r_1, r_2, \ldots, r_p$, where $r_p = n$, be filled with parameters. Take $r_0 = 0$ and let $C(\theta)$ be filled with zeros, and then let row i have a one in column $r_{i-1} + 1$. Let $B(\theta)$ and $K(\theta)$ be filled with parameters. (2.21)

Denote this model structure $\mathcal{M}_I$. In (2.21) p is the dimension of $y(t)$ in (2.10). This parametrization is uniquely characterized by the p numbers r_i which are to be chosen by the user. Instead of r_i we will use the numbers

$$\nu_i = r_i - r_{i-1}$$

and call

$$\bar{\nu}_n = \{\nu_1, \ldots, \nu_p\} \tag{2.22}$$

the *multi-index* associated with the model structure (2.21). Notice that

$$\sum_{k=1}^{p} \nu_k = n. \tag{2.23}$$

The parametrization (2.21) is well-defined if $p \leq n$. For systems with more outputs than states an identifiable form is obtained if (2.21) is used for the n first outputs. The $p-n$ last rows of the full $p \times n$ C matrix are then filled with parameters. Hence, for this case A, B, K and the $n-p$ last rows of C are filled with parameters while the first n rows of the C matrix form a sub matrix equal to the $n \times n$ identity matrix.

Example 2.1 An identifiable state-space parametrization (2.21) of a system with four states, one input and two outputs with multi-index $\bar{\nu}_4 = \{1, 3\}$ is given by

$$\begin{aligned} \hat{x}(t+1) &= \begin{pmatrix} \theta_1 & \theta_2 & \theta_3 & \theta_4 \\ 0 & 0 & 1 & 0 \\ 0 & 0 & 0 & 1 \\ \theta_5 & \theta_6 & \theta_7 & \theta_8 \end{pmatrix} \hat{x}(t) + \begin{pmatrix} \theta_9 \\ \theta_{10} \\ \theta_{11} \\ \theta_{12} \end{pmatrix} u(t) + \begin{pmatrix} \theta_{13} & \theta_{14} \\ \theta_{15} & \theta_{16} \\ \theta_{17} & \theta_{18} \\ \theta_{19} & \theta_{20} \end{pmatrix} e(t) \\ \hat{y}(t) &= \begin{pmatrix} 1 & 0 & 0 & 0 \\ 0 & 1 & 0 & 0 \end{pmatrix} \hat{x}(t) + e(t). \end{aligned} \tag{2.24}$$

□

Theorem 2.1 *The state-space model structure $\mathcal{M}_I$ defined by (2.21) is globally identifiable at θ^* if and only if $\{A(\theta^*), [B(\theta^*)\, K(\theta^*)]\}$ is controllable.*

Proof. See [86], Theorem 4A.2. □

From the definition of the identifiable model structure (2.21) it follows that the dimension of the parameter vector is

$$d_{\mathcal{M}_I} = nm + 2np. \tag{2.25}$$

For a given system order n and number of outputs p there exists $\binom{n-1}{p-1}$ different multi-indices. From [86] we also have:

Theorem 2.2 *Any linear system that can be represented in state-space form of order n can also be represented in the particular form (2.21) for some multi-index $\bar{\nu}_n$.* □

Thus, if we consider the union of all model sets $\mathcal{M}^*_{\bar{\nu}_n}$ generated by the model structures given by all different multi-indices we have

$$\mathcal{S} \in \bigcup_{\bar{\nu}_n} \mathcal{M}^*_{\bar{\nu}_n}$$

for all possible linear systems $\mathcal{S}$ of order n. When identifying a multivariable system of a given order n using an identifiable parametrization we can, in principle, not use one single parametrization and thus we have to search for the best model among all model structures defined by the multi-indices. However, as pointed out in [86], the different model structures overlap considerably and one particular multi-index

is capable of describing *almost all* n-dimensional linear systems. The price paid is that the identification might result in a numerically ill-conditioned model.

Based on the *balanced realizations*, introduced by Moore in [109], Kabamba [65] described a canonical/identifiable parametrization for continuous-time systems with distinct Hankel singular values. This result was generalized by Ober to arbitrary systems in [114] including an extension to discrete time systems by utilizing the bilinear transformation. With this parametrization the parameters can be continuously varied within a region without resulting in a non-minimal system. Another advantage, compared to the observability forms (2.21), is that balanced realizations are known to possess better numerical properties. However, the structural indices must be known a priori also for this type of parametrization. Chou [23] uses the balanced parametrization for system identification.

The concept of identifiable model structures is important if we are interested in the values of the parameters themselves, *e.g.*, change detection techniques where a change in the parameters indicates a change in the underlying system. In black-box modeling, when we are only interested in the input-output relation $G(q,\theta)$, the value of each parameter is of no interest. The parameters can then be seen as vehicles to describe the interesting characteristics of the system.

It is also known that some systems described in their canonical/identifiable forms have transfer functions with a very high sensitivity with respect to perturbations of the parameters θ. In a computer implementation, these transfer functions are thus sensitive to finite word length effects occurring in a computer [144]. These effects can be divided into two separate problems: (i) the round-off errors introduced when truncating the sum after adding two numbers, (ii) the coefficients in the state-space matrices are represented by numbers with finite word length and the introduced truncation of the parameters will alter the transfer function. These effects are highly dependent on the parametrization used. The following example clearly illustrates that the identifiable parametrization (2.21) is very sensitive.

Example 2.2 Consider the transfer function

$$G(q) = \frac{1}{(q-0.99)^4}. \tag{2.26}$$

A state-space realization of $G(q)$ using the identifiable model structure (2.21) will have an A matrix of the following form

$$A(\theta) = \begin{pmatrix} 0 & 1 & 0 & 0 \\ 0 & 0 & 1 & 0 \\ 0 & 0 & 0 & 1 \\ \theta_1 & \theta_2 & \theta_3 & \theta_4 \end{pmatrix}, \tag{2.27}$$

where

$$\theta = \begin{pmatrix} -0.9606 & 3.8812 & -5.8806 & 3.9600 \end{pmatrix}^T \tag{2.28}$$

are the values of the parameters shown with 4 decimals. The eigenvalues of the $A(\theta)$ matrix, which all are equal to 0.99, are extremely sensitive to perturbations

of the parameters. An additive change of 2×10^{-8} in any of the four parameters will perturb one of the eigenvalues to be larger than one. A small perturbation thus leads to instability of the model. □

In the next section we will propose a new model structure which circumvents the model structure selection problem as well as reduces the sensitivity of the transfer function with respect to perturbations of the parameter vector.

2.2.1 Fully Parametrized State-Space Models

If we consider the state-space model (2.10) and choose to fill all the matrices A, B, C, K with parameters, we clearly over-parametrize the model and thus loose identifiability (2.20). To formalize we have:

> Let all the elements of the matrices $A(\theta), B(\theta), C(\theta)$ and $K(\theta)$ in the model (2.10) be parameters. Collect all these in the parameter vector $\theta \in D_{\mathcal{M}}$ and let the corresponding model structure be called *fully parametrized* . (2.29)

Let $\mathcal{M}_F$ denote the above model structure.

Example 2.3 A third order model with two inputs and two outputs is parametrized according to

$$\begin{aligned} \hat{x}(t+1) &= \begin{pmatrix} \theta_1 & \theta_4 & \theta_7 \\ \theta_2 & \theta_5 & \theta_8 \\ \theta_3 & \theta_6 & \theta_9 \end{pmatrix} \hat{x}(t) + \begin{pmatrix} \theta_{10} & \theta_{13} \\ \theta_{11} & \theta_{14} \\ \theta_{12} & \theta_{15} \end{pmatrix} u(t) + \begin{pmatrix} \theta_{16} & \theta_{19} \\ \theta_{17} & \theta_{20} \\ \theta_{18} & \theta_{21} \end{pmatrix} e(t) \\ y(t) &= \begin{pmatrix} \theta_{22} & \theta_{24} & \theta_{26} \\ \theta_{23} & \theta_{25} & \theta_{27} \end{pmatrix} x(t) + e(t) \end{aligned} \tag{2.30}$$

when the full parametrization (2.29) is employed. □

The number of parameters needed for the model structure (2.29) is

$$d_{\mathcal{M}_F} = n^2 + 2np + nm. \tag{2.31}$$

The fully parametrized model structure thus has an additional n^2 number of parameters compared to an identifiable model structure (2.21).

For completeness we have the following trivial statement.

Property 2.1 *Any linear system $\mathcal{S}$ that can be represented in state-space form of order n can also be represented by a model from the fully parametrized model structure (2.29).* □

Using this model structure for the purpose of identification has two interesting implications. First, this state-space model structure would relieve us from the search through the many different forms defined by the multi-indices when dealing with multivariable systems since the proposed model structure trivially includes all

possible systems of a given order n. Secondly, the quality of the estimated model might increase if we use a flexible model structure which not only can describe the underlying system but also allows a numerically well-conditioned description. This is a major difference compared with the identifiable model structures (2.21), which by definition only have one realization for each system $\mathcal{S}$. Since we are confined to computers with limited accuracy for all calculations it is important to be able to use models which are numerically well-conditioned.

It might be important to point out that even if the proposed model structure has more parameters than the corresponding identifiable model structure, the two models will have exactly the same flexibility with respect to the transfer functions. This can formally be stated as

$$\mathcal{M}_F^* = \bigcup_{\bar{\nu}_n} \mathcal{M}_{\bar{\nu}_n}^*,$$

where $\mathcal{M}_F^*$ denotes the model set generated by the fully parametrized model structure (2.29).

2.2.2 Relations Between Realizations

Definition 2.4 Let the true system $\mathcal{S}$ be described by (2.1) and consider a model structure $\mathcal{M}$ of minimal order n such that $\mathcal{S} \in \mathcal{M}^*$. Then the set of *true parameters* is defined as

$$D_T = \{\theta \in D_{\mathcal{M}} \,|\, G_0(z) = G(z,\theta), H_0(z) = H(z,\theta),\ \forall z \in \mathbb{C}\}. \tag{2.32}$$

□

For an identifiable model structure (2.21) the set D_T contains only one point. This follows directly from (2.20) and Theorem 2.1. If the model structure is a fully parametrized state-space model structure (2.29), the elements in D_T will be related as follows.

Lemma 2.1 *Consider the fully parametrized model structure (2.29) with n states. Then*

$$\forall \theta_i \in D_T,\ i = 1,2,\ \exists \text{ a unique invertible } T \in \mathbb{R}^{n\times n}: \tag{2.33}$$

$$\begin{aligned} A(\theta_1) &= T^{-1}A(\theta_2)T, \qquad C(\theta_1) = C(\theta_2)T \\ B(\theta_1) &= T^{-1}B(\theta_2), \qquad K(\theta_1) = T^{-1}K(\theta_2) \end{aligned} \tag{2.34}$$

Proof. See [66], Theorem 6.2.4. □

Let the parameter vector θ be composed as

$$\theta = [\ \mathrm{vec}\,(A)^T\ \ \mathrm{vec}\,(B)^T\ \ \mathrm{vec}\,(K)^T\ \ \mathrm{vec}\,(C)^T\ ]^T, \tag{2.35}$$

where $\text{vec}\,(\cdot)$ is the operator which forms a vector from a matrix by stacking its columns. The following relation for matrices X, Y, Z of compatible dimensions

$$\text{vec}\,(XYZ) = Z^T \otimes X\,\text{vec}\,(Y) \tag{2.36}$$

holds. Here $\otimes$ denotes the Kronecker product, [45],

$$X \otimes Y = \begin{pmatrix} x_{11}Y & x_{12}Y & \dots & x_{1n}Y \\ x_{21}Y & x_{22}Y & \dots & x_{2n}Y \\ \vdots & \vdots & & \vdots \\ x_{m1}Y & x_{m2}Y & \dots & x_{mn}Y \end{pmatrix},$$

where X is of dimension $m \times n$.

The relationship between the vectors θ_1 and θ_2 in Lemma 2.1 can be written as

$$\theta_1 = \bar{T}(T)\theta_2, \tag{2.37}$$

where

$$\bar{T}(T) = \begin{pmatrix} T^T \otimes T^{-1} & 0 & 0 & 0 \\ 0 & I_m \otimes T^{-1} & 0 & 0 \\ 0 & 0 & I_m \otimes T^{-1} & 0 \\ 0 & 0 & 0 & T^T \otimes I_p \end{pmatrix}. \tag{2.38}$$

We have thus proved the following lemma.

Lemma 2.2 *Consider the fully parametrized model structure $\mathcal{M}_F$ in (2.29) with n states, m inputs and p outputs. Then*

$$\forall \theta_i \in D_T,\ i = 1, 2,\ \exists \text{ a unique invertible } T \in \mathbb{R}^{n\times n} :\ \theta_1 = \bar{T}(T)\theta_2$$

where $\bar{T}(T)$ is given by (2.38). □

Lemma 2.3 *Let $\bar{T}$ be defined by (2.38). Then*

$$\bar{T}^T\bar{T} = I \Leftrightarrow T^TT = I$$

Proof. This follows immediately from the fact that

$$\bar{T}^T\bar{T} = \begin{pmatrix} TT^T \otimes (TT^T)^{-1} & 0 & 0 & 0 \\ 0 & I_m \otimes (TT^T)^{-1} & 0 & 0 \\ 0 & 0 & I_m \otimes (TT^T)^{-1} & 0 \\ 0 & 0 & 0 & T^TT \otimes I_p) \end{pmatrix}.$$

□

2.3 Numerical Sensitivity

In the area of digital filter synthesis, numerical sensitivity of different filter structures has been addressed by several authors, among others the work by Mullis and Roberts [110, 111]. They model the fixed-point calculation round-off error as noise and give conditions which minimize the output noise. From a system identification point of view it is interesting to mention that the so obtained optimal filter structures yield a significantly less round-off error compared to the standard canonical forms. Other more recent results have focused on the sensitivity of the transfer function with respect to the parameters [60, 79, 94]. The results indicate that balanced realizations, see below for the definition, have low sensitivity and will thus yield numerically well-conditioned models.

The question of sensitivity in combination with system identification is, however, not at all as developed in the literature. Some of the work has been focused on replacing the delay operator q with something else in ARX models [44, 80]. In some cases, this results in well-conditioned parameter estimates. In [39] Gevers and Li give an overview of the low sensitivity parametrization problem with the focus on digital controllers, digital filters and adaptive parameter estimators. To use balanced state-space models for identification was suggested by Maciejowski [95] and further developed by Chou [23].

2.3.1 A Review of Some Basic Results

In this section we will consider stable state-space systems of the form (2.10) without noise[2], *i.e.*, $H(q) = 0$. The matrix

$$W_o = \sum_{k=0}^{\infty} (A^T)^k C^T C A^k \tag{2.39}$$

is known as the *observability Gramian* for the state-space system (2.10). The eigenvalues of this matrix describe how the initial state variable $x(0)$ influence the output signal $y(t)$ when $u(t) \equiv 0$. This matrix also satisfies the following Lyapunov equation

$$W_o = A^T W_o A + C^T C. \tag{2.40}$$

The dual matrix

$$W_c = \sum_{k=0}^{\infty} A^k B B^T (A^T)^k \tag{2.41}$$

is called the *controllability Gramian*. This matrix describes how the inputs u influence the state vector x. W_c also satisfies

$$W_c = A W_c A^T + B B^T. \tag{2.42}$$

[2] We could also consider the noise $e(t)$ as an an unknown input and let $\bar{B} = [B \; K]$.

The Gramian matrices are symmetric by construction and if the state-space realization is minimal they are also positive definite.

Definition 2.5 A state-space realization is *balanced* or *internally balanced* if

$$W_o = W_c = \Sigma = \text{diag}\,(\sigma_1, \ldots, \sigma_n) \tag{2.43}$$

with $\sigma_1 \geq \ldots \geq \sigma_n > 0$ □

Balanced realizations of dynamic systems have emerged in the literature several times. In [111], Mullis and Roberts show that the output of a digital filter have lowest sensitivity to round-off errors if the filter is in balanced form. The continuous-time version of balancing is used by Moore [109] for model reduction purposes. In [117], Pernebo and Silverman present results on stability and minimality of reduced models using balanced realizations, considering both continuous and discrete time systems.

A change of basis of the state vector $\tilde{x} = T^{-1}x$ will transform the Gramian matrices to

$$\tilde{W}_c = T^{-1} W_c T^{-T}$$

and

$$\tilde{W}_o = T^T W_o T.$$

An important result is that all stable minimal systems can be converted to a balanced realization, see [109].

The set of eigenvalues of the matrix $W_c W_o$ is invariant under similarity transformations T and constitutes a realization invariant set [41].

Definition 2.6 The *Hankel singular values* of the stable linear system (A, B, C) are

$$\sigma_i = [\lambda_i(W_c W_o)]^{1/2}, \quad i = 1, \ldots, n. \tag{2.44}$$

where W_o and W_c are given by (2.39) and (2.41) respectively. □

In (2.44), $\lambda_i(X)$ denotes the ith eigenvalue of the matrix X. From Definition 2.5 and (2.44) it is clear that the diagonal of the Gramian matrices of a balanced realization is equal to the Hankel singular values. The Hankel singular values are also known as the second order modes of the system [111].

2.3.2 The Sensitivity Problem

In computer implementations it is important to consider so-called finite-word-length effects, *i.e.*, what effect the use of finite representation of real numbers have for an algorithm. In our case we are interested in which state-space realizations are least sensitive to these effects and thus to minimize the degradation of the system performance. In Example 2.2, the sensitivity of the eigenvalues with respect to perturbations of the matrix elements were illustrated. Another very interesting question is what effect perturbations of the matrix elements have on the

transfer function of the system. Furthermore, it is interesting to know which types of realizations (basis of the states) that minimize this sensitivity. As a measure of sensitivity of a transfer function

$$G(z) = C(zI - A)^{-1}B, \tag{2.45}$$

with respect to perturbations in the parameters we will use the expression in [142]

$$M = \left(\frac{1}{2\pi} \int_{-\pi}^{\pi} \left\| \frac{\partial G(e^{i\omega})}{\partial A} \right\|_F d\omega \right)^2 + \frac{1}{2\pi} \int_{-\pi}^{\pi} \left\| \frac{\partial G(e^{i\omega})}{\partial B} \right\|_F^2 + \left\| \frac{\partial G(e^{i\omega})}{\partial C} \right\|_F^2 d\omega, \tag{2.46}$$

where the Frobenius norm is $\|X\|_F^2 = \mathrm{tr}\,(X^H X)$ and X^H is the conjugate transpose of X. This scalar expression gives a measure of the sensitivity of the transfer function over the whole frequency range $[-\pi, \pi]$, by averaging the transfer function perturbations induced by small perturbation in every element of the matrices A, B and C. The mix between L_1 and L_2 norms is motivated by the analytical properties of the first term in (2.46). For single-input single-output systems ($m = 1, p = 1$) the measure M can be shown, [145], to have an upper bound S given by

$$M \leq S = \mathrm{tr}\,(W_c)\,\mathrm{tr}\,(W_o) + \mathrm{tr}\,(W_c) + \mathrm{tr}\,(W_o). \tag{2.47}$$

For general multivariable systems the above bound is generalized to, [94],

$$M \leq S = \mathrm{tr}\,(W_c)\,\mathrm{tr}\,(W_o) + p\ \mathrm{tr}\,(W_c) + m\ \mathrm{tr}\,(W_o) \tag{2.48}$$

where p and m are the numbers of system outputs and inputs, respectively.

Theorem 2.3 *Let W_c and W_o be the $n \times n$ Gramian matrices for a minimal state-space realization of a transfer function $G(z)$.*

Then

$$S = \mathrm{tr}\,(W_c)\,\mathrm{tr}\,(W_o) + p\ \mathrm{tr}\,(W_c) + m\ \mathrm{tr}\,(W_o) \geq \left(\sum_{i=1}^{n} \sigma_i \right)^2 + 2 \sum_{i=1}^{n} \sigma_i$$

where $\{\sigma_i\}$ are the Hankel singular values of $G(z)$. Equality holds if and only if

$$p\,W_c = m\,W_o.$$

Proof. See [94]. □

In [145] it is shown that realizations of systems with $p = m = 1$ (SISO) which satisfy $W_c = W_o$ also minimize the true measure M. From the theorem it immediately follows that balanced realizations of square multivariable systems $p = m$ achieve the minimal value of the upper bound S. If the multivariable system has $p \neq m$ a minimum sensitivity realization is obtained from a balanced realization via a state transformation matrix $T = (p/m)^{1/4} I$. We also note that if a realization satisfies $W_c = W_o$, then an orthonormal state transformation T ($TT^T = I$) will also give a new realization with the Gramian matrices still equal. This shows that there exists infinitely many realizations which satisfy $W_c = W_o$.

2.3.3 Calculation of the Balanced Realization

The following algorithm is due to Laub [73] and given a general minimal stable system (A, B, C), it will find a similarity transformation matrix T such that $(T^{-1}AT, T^{-1}B, CT)$ is in internally balanced form. Begin by forming W_o and W_c by solving the two Lyapunov equations (2.40),(2.42). Use the Cholesky factorization to obtain

$$W_o = R^T R, \tag{2.49}$$

with $R \in \mathbb{R}^{n \times n}$, and the singular value decomposition

$$RW_c R^T = U\Sigma^2 U^T \tag{2.50}$$

with $U \in \mathbb{R}^{n \times n}$, $U^T U = I$ and the diagonal matrix $\Sigma \in \mathbb{R}^{n \times n}$. The similarity transformation matrix is then given by

$$T = R^{-1} U \Sigma^{1/2}. \tag{2.51}$$

If W_o is close to singular, the Cholesky factorization (2.49) can be replaced by the numerically more stable singular value decomposition. Let

$$W_0 = U_w \Sigma_w U_w^T \tag{2.52}$$

be the singular value decomposition. R is then given by

$$R = \Sigma_w^{1/2} U_w^T. \tag{2.53}$$

An even further improved algorithm is described by Laub *et al.* in [74].

2.3.4 Using Balanced Realizations for Identification

The fully parametrized model structure (2.29) provides a degree of freedom which can be utilized in order to obtain well-conditioned models. The set D_T, from Definition 2.4, is a manifold in the parameter space and theoretically any point $\theta_0 \in D_T$ is an equally good description of the system. However, if we consider the sensitivity of the model with respect to perturbations in the parameters we can in the process of identification choose to use a low sensitivity structure, *e.g.*, the balanced realization.

Maciejowski [95] showed that a constrained balanced realization implicitly defines a canonical form and suggested to use this balanced form for system identification. Ober [114] derived an explicit parametrization of a balanced realization which have been used in system identification applications by Chou [23].

In the next chapter we shall propose a different approach by using the full parametrization and let the model in the identification adapt itself to be close to a balanced realization by means of an appropriate choice of regularization.

3

Prediction Error Minimization

3.1 Parameter Estimation by Minimizing Prediction Errors

In order to investigate the properties of the proposed model structure we will focus on system identification techniques based on the minimization of the prediction errors (PEM). The standard setting can thus be described as: Given estimation data consisting of an input sequence $\{u(t)\}$ and an output sequence $\{y(t)\}$ by

$$Z^N = \{y(t), u(t) \,|t = 1, \dots, N\}, \tag{3.1}$$

and model structure $\mathcal{M}$ defining a mapping from the parameter space $D_{\mathcal{M}}$ to the predictor $\hat{y}(t|\theta)$, the objective is to find the value $\hat{\theta}$ which minimizes a criterion $V_N(\theta)$.

Let us define the criterion to be

$$V_N(\theta) = \frac{1}{N} \sum_{t=1}^{N} |\varepsilon(t, \theta)|^2, \tag{3.2}$$

where $|\cdot|$ is the Euclidian l_2-norm. The *prediction error* is the vector

$$\varepsilon(t, \theta) = y(t) - \hat{y}(t|\theta) \tag{3.3}$$

with the predictor $\hat{y}(t|\theta)$ given by (2.14). The minimizing parameter vector is defined by

$$\hat{\theta}_N = \arg \min_{\theta \in D_{\mathcal{M}}} V_N(\theta), \tag{3.4}$$

where "arg min" denotes the operator which returns the argument which minimizes the function. This problem formulation is well-known and there exists a vast literature on how to minimize (3.2) as well as properties of the resulting estimate $\hat{\theta}_N$

(3.4) under varying assumptions on the model structure $\mathcal{M}$ and the data Z^N. See Ljung [86] or Stoica and Söderström [136] for a general discussion on the topic. For scalar systems (SISO) and the assumption that the noise $e(t)$ is Gaussian, (3.4) also coincides with the maximum likelihood estimator.

3.1.1 PEM for Fully Parametrized Models

If we use (3.2) together with the proposed model structure $\mathcal{M}_F$, the minimal value of $V_N(\theta)$ will be attained on a manifold in the parameter space. The minimizing argument $\hat{\theta}$ is thus not unique. This follows from the fact that there exist infinitely many parameter values θ in the set D_T of (2.32). The non-uniqueness usually leads to convergence problems if standard optimization algorithms are employed for the minimization of (3.2). This is because most algorithms use the inverse of the Hessian

$$\frac{d^2}{d\theta^2} V_N(\theta)$$

and in our case the Hessian will be singular. This problem can be dealt with by replacing the Hessian by some positive definite approximation. Another possibility is to further constrain the solution. We will here focus on *regularization*, which is a standard technique for ill-conditioned estimation problems, see, *e.g.*, [35]. In Section 3.4 we consider a modified search algorithm which uses a pseudo-inverse technique.

Regularization means that the criterion (3.2) is augmented with a term, which often has the form

$$W_N^\delta(\theta) = V_N(\theta) + \frac{\delta}{2}|\theta - \theta^\#|^2, \quad \delta > 0 \tag{3.5}$$

where $|\cdot|$ denotes the Euclidian norm. A more general regularization term is an arbitrary function $r(\theta, \theta^\#)$ having a positive definite Hessian. The regularization $\delta/2|\theta - \theta^\#|^2$ has the effect that the resulting estimate

$$\hat{\theta}_N^\delta = \arg\min_{\theta \in D_\mathcal{M}} W_N^\delta(\theta) \tag{3.6}$$

is a compromise between minimizing $V_N(\theta)$ and being close to $\theta^\#$. Since our objective is to find the θ which minimizes $V_N(\theta)$ it is clear that the choice of $\theta^\#$ will influence the result. In the next section we will address this question as well as present an identification algorithm for fully parametrized models.

3.1.2 Numerical Solution by Iterative Search

The state-space predictor $\hat{y}(t|\theta)$ (2.14) is in general a non-linear function of the parameters θ. This implies that an analytical solution to (3.4) is not feasible. The minimizing parameter $\hat{\theta}_N$ thus has to be searched for in the parameter space $D_\mathcal{M}$ by some iterative method. A well-known method [34] is that of Newton, which can be described as follows.

$$\hat{\theta}^{i+1} = \hat{\theta}^i - [V''(\hat{\theta}^i)]^{-1} V_N'(\hat{\theta}^i), \tag{3.7}$$

where $\hat{\theta}^i$ is the estimate at the ith step in the iterative algorithm and

$$V'_N(\theta) = \frac{d}{d\theta}V_N(\theta) = -\frac{2}{N}\sum_{t=1}^{N}\psi(t,\theta)\varepsilon(t,\theta) \tag{3.8}$$

with

$$\psi(t,\theta) = \frac{d}{d\theta}\hat{y}(t|\theta) \tag{3.9}$$

being the gradient of $V_N(\theta)$ with respect to the parameters θ. Furthermore[1],

$$V''_N(\theta) = \frac{d^2}{d\theta^2}V_N(\theta) = \frac{2}{N}\sum_{t=1}^{N}(\psi(t,\theta)\psi(t,\theta)^T - \psi'(t,\theta)\varepsilon(t,\theta)) \tag{3.10}$$

is the Hessian. In a neighborhood of the minimum $\theta = \theta_0$, the Hessian $V''_N(\theta)$ can be approximated by

$$H(\theta) = \frac{1}{N}\sum_{t=1}^{N}\psi(t,\theta)\psi(t,\theta)^T, \tag{3.11}$$

since $\varepsilon(t,\theta_0)$ and $\psi'(t,\theta_0)$ are independent, see [34]. If we use this approximation together with an adjustable step length we obtain the damped Gauss-Newton method

$$\hat{\theta}^{i+1} = \hat{\theta}^i - \mu^i[H(\hat{\theta}^i)]^{-1}V'_N(\hat{\theta}^i). \tag{3.12}$$

The scalar step length μ^i is used to perform a line search along the Gauss-Newton direction in order to find a lower value of the criterion $V_N(\theta)$. One often used method is to take $\mu^i = 1$ as the initial value which then is decreased by bisection until a lower value of the criterion is reached [88]. If we choose $H = I$, we obtain a gradient method which is fairly inefficient close to the minimum compared to the Gauss-Newton method. A thorough treatment of Newton methods can be found in [34].

Regularization

A condition which has to be met in order to be able to use a Newton method is that the Hessian $V''_N(\theta)$ must be non-singular in order to ensure that its inverse is well-defined. If the data set Z^N is informative [86] the identifiable model structures satisfies this condition in the neighborhood of the minimum. However, the proposed fully parametrized model structure does not meet this condition since $V_N(\theta)$ will not have a unique minimizing argument θ^*. The introduction of regularization and the minimization of (3.5) instead of (3.2) solves this problem if the approximate Hessian is calculated as

$$H(\theta) = \frac{2}{N}\sum_{t=1}^{N}\psi(t,\theta)\psi(t,\theta)^T + \delta I, \tag{3.13}$$

[1] The notation is not strict since $\psi'(t,\theta)$ is a tensor.

which is always positive definite. By a proper choice of δ, the regularization parameter, the inverse of $H(\theta)$ can be formed and the Gauss-Newton direction will be well-conditioned.

3.1.3 Finding an Initial Estimate

Every practical non-linear minimization procedure is exposed to the risk of getting trapped in a local minimum. The only possible "counter-measure" is to provide the minimization algorithm with an initial estimate in the neighborhood of the minimum. A good initial value will also often significantly improve the speed of convergence. The most simple method to employ is to estimate an ARX-model using a linear least-squares technique and then realize this model in a state-space realization. If the system is operating in open loop the four stage IV4 method [86] can be used to enhance the statistical properties of the estimate. The non-iterative subspace identification algorithms [152, 157] are also excellent tools for providing good initial estimates. See Viberg [158] for an overview on subspace based identification methods.

If also a noise model is to be estimated it is important to find an initial value of K such that the predictor $\hat{y}(t|\theta)$ (2.14) is stable. A straightforward choice is to let K be the solution to the Kalman filtering problem with the noise covariance equal to the identity matrix.

3.2 The Algorithm

In this section we present an identification algorithm using the proposed fully parametrized model structure defined by (2.29). The algorithm is designed to provide accurate models with low sensitivity with respect to finite word length representations.

The results on sensitivity presented in the previous chapter suggest that a good strategy would be to try to devise an algorithm which has a balanced realization as the convergence point in D_T (2.32). This is easily achieved if we after each step in (3.53) adjust the vector $\hat{\theta}^k$ to correspond to a balanced realization through a change of basis T. This means that we not only in the limit obtain a balanced realization, but that we also use it in each step of the identification. Based on this discussion the following algorithm emerges:

Algorithm 3.1

1. *Obtain an initial state-space estimate by some method described in Section 3.1.3.*

2. *Use the algorithm (2.49)-(2.51) to convert the system to a balanced realization and let the corresponding parameter vector be* $\hat{\theta}_b^0$.

3. *Let* $k = 1$.

4. *Solve the minimization problem*

$$\hat{\theta}^k = \arg\min_{\theta \in D_{\mathcal{M}}} \left[V_N(\theta) + \frac{\delta}{2} |\theta - \hat{\theta}_b^{k-1}|^2 \right]$$

by employing the Gauss-Newton optimization procedure outlined in Section 3.1.2.

5. *Convert the obtained estimate to correspond to a balanced realization.*

$$\hat{\theta}_b^k = b(\hat{\theta}^k),$$

where $b(\cdot)$ represents the balancing algorithm (2.49)–(2.51).

6. *Let $k = k + 1$ and repeat steps $4 - 6$ until*

$$V_N(\hat{\theta}_b^{k-2}) - V_N(\hat{\theta}_b^{k-1}) < \epsilon$$

where ϵ is some a priori given constant.

□

A different version of the algorithm is obtained if only one numerical iteration is performed in step 4. Practical use show that both methods have similar convergence properties. The halting criterion in step 6 could also be augmented by also terminate the algorithm if the norm of the gradient falls below a certain value.

The design of the algorithm is based on the following principles.

- One single model structure covers all systems, given the number of states, inputs and outputs.
- A good initial estimate is crucial for the success of the non-linear optimization.
- The model is close to the numerical favorable balanced realization during the estimation.
- Regularization is utilized in order to use the Gauss-Newton optimization scheme.
- The bias of the estimate, introduced by the regularization, is reduced by the iterative procedure of the steps $4 - 6$. See Section 3.3.2.

The main disadvantage with this identification algorithm is the increased numerical complexity compared with the use of an identifiable model structure. The fully parametrized model structure uses n^2 additional parameters. However, as we shall see in the following section there is no "statistical penalty" associated with the parameter excess, *i.e.*, the variance of the prediction errors of the estimated fully parametrized model equals that of an identifiably parametrized model.

3.3 Analysis

3.3.1 Statistical Analysis of the Prediction Quality

In the statistical literature, *parsimony* [19, 136] is a key concept: "Use the simplest model with as few parameters as possible". A model should have as few parameters as possible in order to obtain low variance of the estimated parameters. In the work by Akaike [5] this idea is formulated as the minimization of the average information distance or entropy. He proposes the estimate

$$\hat{\theta}_{AIC}(Z^N) = \arg\min_{\theta} \left\{ V_N(\theta) + \frac{\dim \theta}{N} \right\}, \tag{3.14}$$

which is Akaike's information theoretic criterion (AIC). By considering the statistical properties of the prediction error from an estimated model, an expression similar to AIC is obtained [136].

An identifiable state-space model of a given order has, by definition, a minimal number of parameters and is thus in accordance with this concept. Even though a fully parametrized model has more parameters than a corresponding identifiable model, we will in this section show that regularization restores the statistical properties of an identifiable model. In [134] some statistical properties are studied considering neural networks as non-linear predictor models. These results also apply to a fully parametrized model structure which is pointed out in [135]. In the sequel we will perform the analysis focusing on fully parametrized state-space models.

The main objective with the analysis is to show that the prediction error variance of an estimated model from the fully parametrized model structure is equal to the variance of a model estimated from the identifiable model structure.

First we will prove a lemma which plays a key role in the main theorem. Consider a minimal model from the fully parametrized model structure (2.29), $\mathcal{M}_F(\theta_F)$. From Theorem 2.2 we know that there exists a multi-index $\bar{\nu}_n$ and a corresponding identifiable model structure (2.21), $\mathcal{M}_I$, and a $\theta_I \in D_{\mathcal{M}_I}$ such that

$$\mathcal{M}_I(\theta_I) = \mathcal{M}_F(\theta_F). \tag{3.15}$$

Let

$$\bar{\theta}_I = [\, \operatorname{vec} A(\theta_I)^T \;\; \operatorname{vec} B(\theta_I)^T \;\; \operatorname{vec} K(\theta_I)^T \;\; \operatorname{vec} C(\theta_I)^T]^T.$$

This vector consists of the fixed ones and zeros as given by the model structure definition (2.21) and the parameters from the vector θ_I. Since the two models are equal, we have from Lemma 2.2

$$\exists \text{ a unique } T(\theta_F) : \; \bar{\theta}_I = \bar{T}(T(\theta_F))\theta_F$$

where the matrix $\bar{T}(\cdot)$ is given by (2.38). Here, we denote by $T(\theta_F)$ the similarity transformation to explicitly show the dependence on θ_F. $T(\theta_F)$ is easily constructed from the observability matrix given by the matrices in $\mathcal{M}_F(\theta_F)$ together with the

multi-index $\bar{\nu}_n$ [66]. Let

$$\mathcal{O}(\theta_F) = \begin{pmatrix} C(\theta_F) \\ C(\theta_F)A(\theta_F) \\ \vdots \\ C(\theta_F)A^{n-1}(\theta_F) \end{pmatrix} \tag{3.16}$$

be the observability matrix of the fully parametrized model. The rows of the inverse of $T(\theta_F)$ is obtained from the n rows of $\mathcal{O}(\theta_F)$ given by the set

$$\underline{r} = \{k \,|\, k = jp + i,\, i \in [1, \ldots, p],\, j \in [0, \ldots, \nu_i - 1]\}. \tag{3.17}$$

The equality of the two models (3.15) implies that the identifiable model structure contains the model and hence that the rows given by $\underline{r}$ are linearly independent. $T^{-1}(\theta_F)$ is thus a non-singular matrix and, hence, so is also $T(\theta_F)$. All the matrix elements in $T^{-1}(\theta_F)$ are polynomials in θ_F. $T(\theta_F)$ will then have elements which are rational functions of θ_F. It is now easy to construct a mapping g from $D_{\mathcal{M}_F}$ to $D_{\mathcal{M}_I}$ which is valid in the neighborhood of θ_F. The mapping can be constructed as

$$g(\theta) = S\bar{T}(T(\theta))\theta, \tag{3.18}$$

where S is a matrix which selects the non-fixed parameters from $\bar{\theta}_I$. The mapping g is thus differentiable at $\theta = \theta_F$ since all the elements of the matrix $\bar{T}(T(\theta))$ are rational functions of θ. Hence, we have shown the following lemma.

Lemma 3.1 *For all minimal state-space models $\mathcal{M}(\theta_F)$, $\theta_F \in D_{\mathcal{M}_F}$ we can find a multi-index $\bar{\nu}_n$ with the corresponding identifiable model structure $\mathcal{M}_I$ (2.21) such that the mapping g (3.18) is differentiable at $\theta = \theta_F$.*

Lemma 3.2 *Any matrices $A \in \mathbb{R}^{m\times n}$ and $B \in \mathbb{R}^{n\times p}$ satisfy*

$$\operatorname{rank} A + \operatorname{rank} B - n \leq \operatorname{rank}(AB) \leq \min(\operatorname{rank} A, \operatorname{rank} B). \tag{3.19}$$

Proof. [113] Section 5.5. □

The gradient of the predictor $\hat{y}(t|\theta)$ is defined as

$$\psi(t,\theta) = \frac{d}{d\theta}\hat{y}(t|\theta) = \begin{pmatrix} \frac{d}{d\theta_1}\hat{y}_1(t|\theta) & \cdots & \frac{d}{d\theta_1}\hat{y}_p(t|\theta) \\ \vdots & & \vdots \\ \frac{d}{d\theta_{d_\mathcal{M}}}\hat{y}_1(t|\theta) & \cdots & \frac{d}{d\theta_{d_\mathcal{M}}}\hat{y}_p(t|\theta) \end{pmatrix}, \tag{3.20}$$

i.e., it is a matrix of dimension $d_\mathcal{M} \times p$. The subscript k in $\hat{y}_k(t|\theta)$ denotes the position in the vector.

Lemma 3.3 *Let the predictor $\hat{y}^F(t|\theta_F)$ be given by a fully parametrized model structure $\mathcal{M}_F$ (2.29). Then*

$$\operatorname{rank}\left\{\frac{1}{N}\sum_{t=1}^{N}\psi^F(t,\theta_F)\psi^F(t,\theta_F)^T\right\} \leq d_{\mathcal{M}_I},$$

where $\psi^F(t,\theta_F)$ is given by (3.20) and $d_{\mathcal{M}_I}$ by (2.25).

Proof. Select an identifiable model structure (2.21) and a θ_I such that

$$\mathcal{M}_I(\theta_I) = \mathcal{M}_F(\theta_F)$$

and the mapping $g(\theta)$ (3.18) is differentiable. Then, using Lemma 3.1, we have

$$\psi^F(t,\theta_F) = \frac{d}{d\theta_F}\hat{y}^F(t|\theta_F) = \frac{d}{d\theta_F}\hat{y}^I(t|g(\theta_F)) = \frac{\partial}{\partial\theta_F}g(\theta_F)\cdot\psi^I(t,\theta_I),$$

which gives

$$\frac{1}{N}\sum_{t=1}^{N}\psi^F(t,\theta_F)\psi^F(t,\theta_F)^T = \frac{\partial}{\partial\theta_F}g(\theta_F)\cdot\left[\frac{1}{N}\sum_{t=1}^{N}\psi^I(t,\theta_I)\psi^I(t,\theta_I)^T\right]\cdot\left(\frac{\partial}{\partial\theta_F}g(\theta_F)\right)^T.$$

The proof is concluded by observing that $\psi^I(t,\theta_I)\psi^I(t,\theta_I)^T$ has dimension $d_{\mathcal{M}_I}\times d_{\mathcal{M}_I}$ and applying Lemma 3.2. □

We will continue by introducing some assumptions which are needed in order to carry out the convergence analysis.

The set Z^N from (3.1), *i.e.*, the measured input and output data, is our source of information about the true system. A model structure $\mathcal{M}$ together with the parameter space $D_{\mathcal{M}}$ constitutes the model set $\mathcal{M}^*$. A natural question to pose is whether the data set contains enough information to distinguish between different models in the model set.

Definition 3.1 [86] A data set Z^N is *informative* with respect to a model structure $\mathcal{M}$ if

$$E\lim_{N\to\infty}\frac{1}{N}\sum_{t=1}^{N}|\hat{y}(t|\theta_1)-\hat{y}(t|\theta_2)|^2 = 0 \;\Rightarrow\; \mathcal{M}(\theta_1)=\mathcal{M}(\theta_2). \tag{3.21}$$

□

Chapter 14 in [86] contains a comprehensive discussion about informative data.

Assumption A1 The data set Z^N from (3.1) is subject to the following conditions.

- It has been generated by the system (2.10).
- It is informative according to (3.21).
- It satisfies the technical condition D1 in [86].

□

From [86] we have the following convergence result.

Theorem 3.1 *Let $\hat{\theta}_N$ be defined by (3.4) and let the data Z^N satisfy A1. Then*

$$\inf_{\bar{\theta} \in D_T} |\hat{\theta}_N - \bar{\theta}| \to 0, \quad w.p.\ 1 \text{ as } N \to \infty. \tag{3.22}$$

□

Consider the regularized version of the criterion (3.5) and let $\theta^\# = \theta_0 \in D_T$. Then $\hat{\theta}_N^\delta \to \theta_0$ as $N \to \infty$ since both terms in the criterion simultaneously reach their respective minimum at $\theta = \theta_0$. This proves the following theorem.

Theorem 3.2 *Let $\hat{\theta}_N^\delta$ be defined by (3.5) and (3.6) with $\theta^\# = \theta_0 \in D_T$ and the data Z^N satisfy A1. Then*

$$\hat{\theta}_N^\delta \to \theta_0, \quad w.p.\ 1 \text{ as } N \to \infty. \tag{3.23}$$

□

This choice of $\theta^\#$ is artificial, since we in reality do not know θ_0 *a priori*. In spite of this, the theoretical implications from the analysis to follow are still interesting since we shall have $\theta^\#$ approach a $\theta_0 \in D_T$ in the algorithm. For the analysis, we need also the following result.

Lemma 3.4 *Let the predictor be defined by (2.14), the gradient by (3.20) and the data set Z^N satisfy A1. Then $\forall \theta \in D_{\mathcal{M}}$*

$$\lim_{N \to \infty} E \frac{1}{N} \sum_{k=1}^{N} \psi(t, \theta) \psi(t, \theta)^T < \infty. \tag{3.24}$$

Proof. Follows from Lemma 4.2 and Theorem 2.3 both in [86]. □

The notation $M < \infty$ in (3.24) should be interpreted as all elements in the matrix M are bounded.

We shall now derive a statistical model-quality measure for fully parametrized models obtained via minimization of the regularized prediction error criterion (3.5) and (3.6) with $\theta^\# = \theta_0 \in D_T$. For a finite data set Z^N the obtained estimate $\hat{\theta}_N^\delta$ will deviate a little from θ_0. As a measure of the quality of the estimated model using finite data we consider the scalar

$$\bar{V}(\theta) = \lim_{N \to \infty} E V_N(\theta). \tag{3.25}$$

For all estimates $\hat{\theta}_N^\delta$ we have $\bar{V}(\hat{\theta}_N^\delta) \geq \bar{V}(\theta_0) = \operatorname{tr}(\Lambda_0)$, $\theta_0 \in D_T$ and the increase of $\bar{V}(\hat{\theta}_N^\delta)$ due to the parameter deviation should be as low as possible. Recall that Λ_0, from (2.2), is the covariance matrix of the innovations. This assessment criterion thus considers the trace of the variance of the one-step prediction error, when the estimated model is applied to future data. Finally, we define

$$\bar{V}_N^\delta = E\,\bar{V}(\hat{\theta}_N^\delta) \tag{3.26}$$

with the expectation taken over the estimated parameters, as a performance measure "on the average" for the estimated model.

At the minimum of the criterion (3.5) we clearly have

$$W_N^{\delta\,\prime}(\hat{\theta}_N^\delta) \triangleq \frac{d}{d\theta} W_N^\delta(\theta)\Big|_{\theta=\hat{\theta}_N^\delta} = 0. \tag{3.27}$$

A Taylor expansion around the limiting estimate θ_0 then gives[2]

$$0 = W_N^{\delta\,\prime}(\theta_0) + W_N^{\delta\,\prime\prime}(\xi_N)(\hat{\theta}_N^\delta - \theta_0) \tag{3.28}$$

with ξ_N between $\hat{\theta}_N^\delta$ and θ_0 and

$$W_N^{\delta\,\prime\prime}(\xi_N) \triangleq \frac{d^2}{d\theta^2} W_N^\delta(\theta)\Big|_{\theta=\xi_N}.$$

From [86, p. 270] we find

$$W_N^{\delta\,\prime\prime}(\xi_N) \to \bar{W}^{\delta\,\prime\prime}(\theta_0) \ \text{ w.p. } 1 \text{ as } N \to \infty, \tag{3.29}$$

where

$$\bar{W}^{\delta\,\prime\prime}(\theta_0) = \lim_{N\to\infty} E\,\frac{1}{N}\sum_{i=1}^{N} W_N^{\delta\,\prime\prime}(\theta_0). \tag{3.30}$$

Thus, for sufficiently large N, we can write

$$\hat{\theta}_N^\delta - \theta_0 \approx -[\bar{W}^{\delta\,\prime\prime}(\theta_0)]^{-1} W_N^{\delta\,\prime}(\theta_0). \tag{3.31}$$

We also have

$$W_N^{\delta\,\prime}(\theta) = V_N'(\theta) + \delta(\theta - \theta_0) \tag{3.32}$$

with

$$V_N'(\theta) = -\frac{2}{N}\sum_{t=1}^{N} \psi(t,\theta)\varepsilon(t,\theta) \tag{3.33}$$

[2] The application of the Taylor expansion (3.28) may require different ξ_N in different rows of this vector expression.

and[3]

$$V_N''(\theta) = \frac{2}{N}\sum_{t=1}^{N}(\psi(t,\theta)\psi(t,\theta)^T - \psi'(t,\theta)\varepsilon(t,\theta)). \tag{3.34}$$

This gives

$$\bar{W^\delta}''(\theta_0) = \bar{V}''(\theta_0) + \delta I = Q + \delta I \tag{3.35}$$

where

$$Q = \bar{V}''(\theta_0) = \lim_{N\to\infty} E\,\frac{2}{N}\sum_{t=1}^{N}\psi(t,\theta_0)\psi(t,\theta_0)^T \tag{3.36}$$

since $\varepsilon(t,\theta_0) = e_0(t)$ and $\psi'(t,\theta_0)$ are independent. Lemma 3.4 shows that the sum (3.36) is convergent.

Now, by a Taylor expansion of $\bar{V}_N^\delta$ from (3.26) around θ_0, we obtain

$$\bar{V}_N^\delta = E\,\{\bar{V}(\theta_0) + (\hat{\theta}_N^\delta - \theta_0)^T\bar{V}'(\theta_0) + \frac{1}{2}(\hat{\theta}_N^\delta - \theta_0)^T\bar{V}''(\theta_0)(\hat{\theta}_N^\delta - \theta_0)\} \tag{3.37}$$

neglecting higher order terms. The second term in (3.37) is zero since $\bar{V}'(\theta_0) = 0$. If we now insert (3.31) into (3.37) and use well-known properties of the trace operator we obtain

$$\bar{V}_N^\delta = \operatorname{tr}(\Lambda_0) + \frac{1}{2}\operatorname{tr}\{E\,W_N^\delta{}'(\theta_0)(W_N^\delta{}'(\theta_0))^T[Q+\delta I]^{-1}Q[Q+\delta I]^{-1}\}. \tag{3.38}$$

By assuming $\Lambda_0 = \lambda_0 I$, from (2.2), we find

$$\lim_{N\to\infty} N\,E\,W_N^\delta{}'(\theta_0)(W_N^\delta{}'(\theta_0))^T = 2\lambda_0 Q. \tag{3.39}$$

Equation (3.38) will then be

$$\bar{V}_N^\delta \sim \lambda_0\left(p + \frac{1}{N}\operatorname{tr}\{Q[Q+\delta I]^{-1}Q[Q+\delta I]^{-1}\}\right) \tag{3.40}$$

where we use $\sim$ to mark that this expression is asymptotic in N. Since Q is a symmetric positive semi-definite matrix we can simultaneously make Q and $Q+\delta I$ diagonal. This gives

$$\bar{V}_N^\delta \sim \lambda_0\left(p + \frac{1}{N}\sum_{i=1}^{d_{\mathcal{M}_F}}\frac{\sigma_i^2}{(\sigma_i+\delta)^2}\right), \tag{3.41}$$

[3] Note that the equation is written in an informal way since $\psi'(t,\theta)$ is a tensor.

where σ_i are the eigenvalues of the matrix Q and $d_{\mathcal{M}_F}$ is given by (2.31). From Lemma 3.3 we know that the matrix Q at most have $d_{\mathcal{M}_I}$ non-zero eigenvalues. If we choose δ to satisfy

$$0 < \delta \ll \sigma_i, \ \forall \sigma_i \neq 0 \tag{3.42}$$

we arrive at

$$\bar{V}_N^\delta \sim \lambda_0 \left(p + \frac{\text{rank } Q}{N} \right) + O(\delta). \tag{3.43}$$

Thus, we have proved the following theorem.

Theorem 3.3 *Consider a fully parametrized model structure (2.29) which defines a predictor (2.14). Let the data set Z^N satisfy A1 and be generated by a true system with $\Lambda_0 = \lambda_0 I$. Furthermore, let $\hat{\theta}_N^\delta$ be given by (3.5-3.6) with $\theta^\# = \theta_0 \in D_T$. Then*

$$\lim_{\delta \to 0} \bar{V}_N^\delta \sim \lambda_0 \left(p + \frac{rank\ Q}{N} \right), \tag{3.44}$$

where $\bar{V}_N^\delta$ is given by (3.25) and (3.26), $p = \dim y(t)$, Q is defined by (3.36) and N is the number of estimation data. □

Recall that the notation $\sim$ in (3.44) is used to show that the expression is asymptotic in N.

The expression (3.44) is similar to the expression

$$\bar{V}_N \sim \lambda_0 \left(p + \frac{d_{\mathcal{M}}}{N} \right) \tag{3.45}$$

for identifiable model structures [86, 136], where $\bar{V}_N = E\,\bar{V}(\hat{\theta}_N)$ and $\hat{\theta}_N$ given by (3.4). The expression (3.45) clearly demonstrates the trade-off between model accuracy versus number of estimated parameters. However, Theorem 3.3 shows that the fully parametrized model retains the same properties since, by Lemma 3.3, the rank of Q can at most be $d_{\mathcal{M}_I}$, which is the number of parameters in a corresponding identifiable model. Hence, the fully parametrized predictor model has in fact the *same* statistical properties, *i.e.*, the same prediction error variance, as an identifiable model. All this imply that the parsimony principle should describe the model quality in terms of the size of the model set rather than the number of parameters used in the model structure.

Example 3.1 In this example we provide some empirical evidence that the result in Theorem 3.3 also applies to models estimated using Algorithm 3.1. We use Monte-Carlo simulations to generate data and estimate models using the fully parametrized model structure as well as models using an identifiable model structure.

Consider the state-space model of order 3 in innovations form:

$$\begin{aligned} x(t+1) &= \begin{pmatrix} 0.9806 & 0.1942 & 0 \\ -0.1942 & 0.9417 & 0 \\ 0 & 0 & 0.95 \end{pmatrix} x(t) + \begin{pmatrix} 0.0971 \\ 0.9709 \\ 0 \end{pmatrix} u(t) + \begin{pmatrix} 0 \\ 0 \\ 1 \end{pmatrix} e(t) \\ y(t) &= \begin{pmatrix} 0.1981 & 0.0194 & 1 \end{pmatrix} x(t) + 0.0097\, u(t) + e(t) \end{aligned} \tag{3.46}$$

where $e(t)$ is a zero mean Gaussian random variable with variance $\lambda_0 = E\, e(t)e(t) = 10^{-2}$.

By employing the model (3.46), 100 estimation data set realizations, each with 500 samples, were generated with $u(t)$ selected as a zero mean Gaussian random variable with variance $E\, u(t)u(t) = 1$. Moreover, 100 validation data set realizations were generated using independent innovation realizations but with the same input realization.

Two models, one with an identifiable parametrization (2.21) and one with the full parametrization (2.29), were estimated from each estimation data set realization. In each identification the two different models were initialized by an ARX estimate obtained from the data.

The model from the identifiable model structure was obtained by minimizing (3.2) using a Gauss-Newton iterative algorithm as described in Section 3.1.2. The halting criteria for the algorithm were either of the following:

- 60 iterations.
- No lower value of the criterion (3.2) were obtained after 10 bisections of the Gauss-Newton direction and 10 bisections of the gradient direction.
- The norm of the Gauss-Newton step falls below 10^{-8}.

The identification of the fully parametrized model was performed according to Algorithm 3.1. The minimization in step 4 of the algorithm was performed using the same Gauss-Newton method with the same stop criteria as above except a maximum of 20 iterations. Steps 4 to 6 in the algorithm are repeated twice to obtain a maximum number of 60 iterations. The regularization parameter δ was chosen to 10^{-10}.

Both estimated models are confronted with the validation data set and a sample prediction error variance is calculated as

$$\hat{\overline{V}}_N(\theta) = \frac{1}{N} \sum_{t=1}^{N} |y(t) - \hat{y}(t|\theta)|^2 \tag{3.47}$$

In Figure 3.1, (3.47) is depicted for each identified model and validation data realization. The values are sorted for increasing values of $\hat{\overline{V}}_N(\theta)$ with (+) denoting the values obtained with the identifiable models and (o) the values of the fully parametrized models. The mean value over the 100 values of $\hat{\overline{V}}_N(\theta)$ is 1.12×10^{-2} for the fully parametrized models and 1.17×10^{-2} for the models with an identifiable parametrization. This example then confirms that, in this example, the

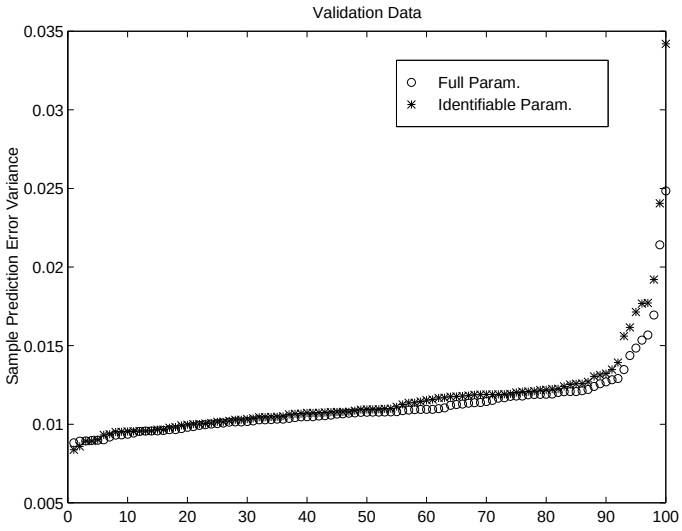

Figure 3.1: Sample prediction error variance $\hat{\bar{V}}_N(\theta)$ calculated for the identifiable models (+) and for the fully parametrized models (o).

fully parametrized model structure does not increase the prediction error variance due to too many parameters. On the contrary the mean value is lower than the identifiable models. A possible explanation is that the optimization algorithm is more probable to reach a local minimum if the identifiable parametrization is used. □

The example gives support to the claim that the derived theoretical result indeed applies also to models identified using Algorithm 3.1.

3.3.2 Convergence Analysis

In practice we cannot choose $\theta^{\#} = \theta_0$. Therefore we have to find a good guess based on *a priori* knowledge. One possibility, as described in Algorithm 3.1, is to perform a sequence of minimizations of (3.5) and use the obtained parameter estimate $\hat{\theta}_N^{\delta}$ as $\theta^{\#}$ in the next minimization. We shall now show that this scheme is locally convergent, *i.e.*, if the algorithm is started sufficiently close to the set D_T (2.32), the set of true parameters, the convergence point will be in D_T.

To simplify the discussion we will consider the minimization of $\bar{V}(\theta)$, defined in (3.25). Consider a truncated Taylor expansion of $\bar{V}(\theta)$ around a $\theta_0 \in D_T$

$$\bar{V}(\theta) \approx \bar{V}(\theta_0) + (\theta - \theta_0)^T \bar{V}'(\theta_0) + \frac{1}{2}(\theta - \theta_0)^T Q(\theta - \theta_0), \tag{3.48}$$

where

$$Q = \bar{V}''(\theta_0) = \lim_{N\to\infty} E\,\frac{2}{N}\sum_{t=1}^{N} \psi(t,\theta_0)\psi(t,\theta_0)^T$$

and assume θ is close to θ_0. The second term in (3.48) is zero since $\theta_0 \in D_T$ is a minimizing argument of $\bar{V}(\theta)$. If all higher order terms are small, the approximation is valid locally. If we assume equality in (3.48) we obtain a loss function which is purely quadratic in the parameters. We could thus interpret $\bar{V}(\theta)$ as the loss function originating from the linear regression problem with the data generating system given as

$$\mathcal{S}: \; y(t) = \psi(t,\theta_0)^T\theta_0 + e(t), \tag{3.49}$$

and the parametrized predictor

$$\mathcal{M}: \; \hat{y}(t|\theta) = \psi(t,\theta_0)^T\theta, \tag{3.50}$$

where $\psi(t,\theta_0)$ are regressors constructed from data.

Since we shall carry out the analysis locally, we may simplify the discussion by considering the linear regression set-up (3.49) and (3.50) and applying the iterative method of Algorithm 3.1.

Let the data Z^N be generated by the system (3.49). The noise, $e(t)$, is assumed to be a sequence of independent stochastic variables with zero mean $E\,e(t) = 0$, variance $E\,e(t)^T e(t) = \Lambda$ and independent of the regressors. Let the prediction model be (3.50).

Consider the criterion

$$\bar{V}(\theta) = \lim_{N\to\infty} E\,V_N(\theta). \tag{3.51}$$

This gives

$$\bar{V}(\theta) = \text{tr}\,(\Lambda) + \frac{1}{2}(\theta_0 - \theta)^T Q\,(\theta_0 - \theta).$$

Now assume that the matrix Q is singular and of rank r. This implies that $\bar{V}(\theta)$ obtains its minimum value $\text{tr}\,(\Lambda)$ for all $\theta = \theta_0 + z$, $z \in \mathcal{N}(Q)$; the null space of Q.

If we let the data set Z^N be informative, then the set D_T of the true parameters for this model structure is given by

$$D_T = \{\theta \,|\, \theta = \theta_0 + z,\, z \in \mathcal{N}(Q)\}. \tag{3.52}$$

To find the minimum of (3.51), we consider the iterative scheme

$$\hat{\theta}^k = \arg\min_{\theta\in D_{\mathcal{M}}} \left[\bar{V}(\theta) + \frac{\delta}{2}|\theta - \hat{\theta}^{k-1}|^2\right]. \tag{3.53}$$

Without loss of generality we can assume that $\theta_0 = 0$. The right hand side of (3.53) is then equal to

$$\text{tr}\,(\Lambda) + \frac{1}{2}\theta^T Q\theta + \frac{\delta}{2}(\theta - \hat{\theta}^{k-1})^T(\theta - \hat{\theta}^{k-1}),$$

which is a quadratic expression in θ. Completing the squares gives

$$\frac{1}{2}(\theta - \delta(Q+\delta I)^{-1}\hat{\theta}^{k-1})^T(Q+\delta I)(\theta - \delta(Q+\delta I)^{-1}\hat{\theta}^{k-1}) + c$$

where c contains all the θ-independent terms. The minimum is thus given by

$$\hat{\theta}^k = \delta(Q + \delta I)^{-1}\hat{\theta}^{k-1}.$$

Let T be a square non-singular matrix such that $TQT^{-1} = S$ is diagonal and define $\tilde{\theta}^k = T\hat{\theta}^k$. Furthermore, let the diagonal elements of S be given in a descending order. This gives

$$\tilde{\theta}^k = \delta(S + \delta I)^{-1}\tilde{\theta}^{k-1}.$$

By exploiting the diagonal form of S we obtain

$$\tilde{\theta}^k = R\tilde{\theta}^{k-1},$$

with

$$R = \begin{pmatrix} \frac{\delta}{\delta+s_1} & 0 & \cdots & \cdots & \cdots & 0 \\ 0 & \ddots & \ddots & & & \vdots \\ \vdots & \ddots & \frac{\delta}{\delta+s_r} & \ddots & & \vdots \\ \vdots & & \ddots & 1 & \ddots & \vdots \\ \vdots & & & \ddots & \ddots & 0 \\ 0 & \cdots & \cdots & \cdots & 0 & 1 \end{pmatrix},$$

where $s_i,\ i = 1, \ldots, r$ are the non-zero eigenvalues of Q. Recall that $\operatorname{rank} Q = r$. Expressed in terms of the initial estimate $\tilde{\theta}^0$, the estimate after k steps is given by

$$\tilde{\theta}^k = R^k\tilde{\theta}^0.$$

If we study the limiting estimate as k tends to infinity we notice that

$$R^\infty = \lim_{k\to\infty} R^k = \begin{pmatrix} 0 & 0 & \cdots & \cdots & \cdots & 0 \\ 0 & \ddots & \ddots & & & \vdots \\ \vdots & \ddots & 0 & \ddots & & \vdots \\ \vdots & & \ddots & 1 & \ddots & \vdots \\ \vdots & & & \ddots & \ddots & 0 \\ 0 & \cdots & \cdots & \cdots & 0 & 1 \end{pmatrix}$$

with r zeros on the diagonal. It is then obvious that

$$SR^\infty = 0.$$

The limiting estimate

$$\tilde{\theta}^\infty = \lim_{k\to\infty} \tilde{\theta}^k = R^\infty\tilde{\theta}^0$$

is easily seen to belong to the null space of S since

$$S\tilde{\theta}^\infty = SR^\infty\tilde{\theta}^0 = 0.$$

This is equivalent to

$$\lim_{k\to\infty} \hat{\theta}^k \in \mathcal{N}(Q).$$

This proves the following theorem.

Theorem 3.4 *Let the data set Z^N be generated by the system (3.49) and be informative. Furthermore, let the predictor be given by (3.50) with the sequence of estimates given by (3.53) with $\delta > 0$, and D_T be given by (3.52). Then*

$$\lim_{k\to\infty} \inf_{\bar{\theta}\in D_T} |\hat{\theta}^k - \bar{\theta}| = 0.$$

□

The result implies that the iterative minimization scheme (3.53) will be locally convergent also for the fully parametrized state-space model structures if the initial estimate $\hat{\theta}^0$ is close enough to the set D_T.

Degree of Regularization

From a regularization point of view, the iterative scheme (3.53) will decrease the actual regularization effect compared to minimization of (3.5), where $\theta^\#$ is a fixed value. But in the light of Theorem 3.3, this is fine since δ can become arbitrarily small and in the case (3.5) δ is a measure of the degree of regularization.

3.3.3 Discussion

In this section we have analyzed the use of the fully parametrized model structure together with the Algorithm 3.1. Theorem 3.4 proves that the iterative scheme (3.53) locally restores the convergence properties of the standard prediction error techniques, *i.e.*, the limiting estimate belongs to the set D_T, the true parameters. Our main goal is thus achieved; we have *one* model structure which include all possible multivariable systems, the introduced regularization gives the estimated predictors the same statistical quality as identifiable models as stated by Theorem 3.3. However, we can not directly apply Theorem 3.3 to the iterative scheme (3.53) since $\theta^\# = \hat{\theta}^k$ is a stochastic variable.

3.4 Direct Minimization

From the theoretical analysis, resulting in Theorem 3.3, we found that the regularization parameter δ can be chosen arbitrarily small. However, for practical purposes we need a value large enough to make the inverse of the approximate Hessian (3.13) well-conditioned (used in the Gauss-Newton optimization).

In the prediction error minimization the aim is to minimize $V_N(\theta)$ defined in (3.2). With the fully parametrized model structure the minimizing argument of $V_N(\theta)$ is a manifold in the parameter space. Possible minimization methods are then gradient methods or Ridge-Regression, also called Levenberg-Marquard [34]. In Ridge-Regression the approximate Hessian is calculated as

$$H(\theta, \delta) = V_N''(\theta) + \delta I, \tag{3.54}$$

where δ is chosen large enough to make the Hessian non-singular.

Here we will consider an alternative to Ridge-Regression. In the calculation of the Gauss-Newton direction we employ the pseudo-inverse of the approximate Hessian

$$H(\theta) = \frac{1}{N}\sum_{t=1}^{N} \psi(t,\theta)\psi(t,\theta)^T \tag{3.55}$$

of the standard prediction error criterion (3.2). When forming the pseudo-inverse we utilize the singular value decomposition of the approximate Hessian and a threshold β for the singular values to determine the correct rank, see [43].

Alternatively, if we consider informative data we can assume the rank of (3.55) to be $d_{\mathcal{M}_I} = n(m+p)$ since the theoretical rank of $H(\theta)$, according to Lemma 3.3, never exceeds $d_{\mathcal{M}_I}$. The Gauss-Newton iterations can then be described according to

$$\hat{\theta}^{i+1} = \hat{\theta}^i - \mu^i [H(\hat{\theta}^i)]^\dagger V_N'(\hat{\theta}^i). \tag{3.56}$$

In each iteration step, $\hat{\theta}^{i+1}$ can be interpreted as the minimum 2-norm solution to the under-determined equation [43]

$$(\hat{\theta}^i - \hat{\theta}^{i+1}) H(\hat{\theta}^i) = \mu^i V_N'(\hat{\theta}^i).$$

By using the minimum 2-norm solution, the parameters stay bounded in each iteration.

The main advantage of this approach is that we have returned to minimization of the true prediction error criteria (3.2), which will give us unbiased estimates. For the single output case, we now derive a result similar to Theorem 3.3 for the case when the estimate is given by (3.4). As before we consider the prediction error variance of the average model as

$$\bar{V}_N = E\,\bar{V}(\hat{\theta}_N), \tag{3.57}$$

where the expectation is over the estimated parameters and $\bar{V}(\theta)$ is given by (3.25).

Theorem 3.5 *Let the true system $\mathcal{S}$ be a single output system, $p = 1$. Consider a fully parametrized model structure $\mathcal{M}_F$ (2.29) which defines a predictor (2.14). Denote by $\mathcal{M}_I$ the identifiable model structure (2.21), whose model set contains the true system, $\mathcal{S} \in \mathcal{M}_I^*$. Let the data set Z^N satisfy A1 and be generated by the true system $\mathcal{S}$. Furthermore, let $\hat{\theta}_N$ be given by (3.4) using the model structure $\mathcal{M}_F$. Then*

$$\bar{V}_N \sim \lambda_0 \left(1 + \frac{d_{\mathcal{M}_I}}{N}\right), \tag{3.58}$$

where $\bar{V}_N$ is given by (3.57), $d_{\mathcal{M}_I}$ is the number of parameters in the identifiable model structure $\mathcal{M}_I$ and N is the number of estimation data.

Proof. Since the the system only have one output the identifiable model structure and the fully parametrized model structure both generate the same model set, *i.e.*,

$$\mathcal{M}_F^* = \mathcal{M}_I^*. \tag{3.59}$$

Let $\hat{\theta}_N$ and $\hat{\theta}_N^I$ denote the estimates from (3.4) for the fully parametrized and the identifiable model structure, respectively. Assumption A1 and (3.59) now imply equality of the estimated models

$$\mathcal{M}_F(\hat{\theta}_N) = \mathcal{M}_I(\hat{\theta}_N^I).$$

Since the estimated models are equal for any N and any noise realization, the two estimates are equal in any sense. Particularly, since (3.58) holds for the identifiable model structure, [136, p. 440], it also holds for the fully parametrized model structure. □

The following example serves as an illustration of the result above.

Example 3.2 Consider the same system as in Example 3.1. Exactly the same identification procedure is applied with the only difference that the fully parametrized system is estimated using the standard prediction error criteria (3.2) with the Gauss-Newton error iterations (3.56). We select $\beta = 10^{-5}$ to be the singular value threshold for the rank determination. In Figure 3.2, the sorted sample prediction error variance $\hat{\overline{V}}(\theta)$ calculated using independent validation data is shown for the 100 estimated systems. The mean value of $\hat{\overline{V}}_N(\theta)$ calculated over the 100 estimated models were 0.0119 for the models with the identifiable parametrization and 0.0116 for the models with full parametrization. As a comparison, the theoretical value is $\lambda_0(1 + d_{\mathcal{M}_I}/N) = 0.0102$, from (3.45). The estimation algorithm used as an average 33.3 Gauss-Newton iterations for the fully parametrized models. For the identifiable models the corresponding value is 37.5. For both type of models 15 of the 100 estimations used the maximum of 60 Gauss-Newton iterations. Hence, the additional n^2 parameters to estimate in the fully parametrized model structure does not seem to require more Gauss-Newton iterations. □

3.5 Norm-Minimal Realizations

We shall now consider an alternative to Algorithm 3.1 by using $\theta^\# = 0$ in (3.5). The criterion we minimize is then

$$W_N^\delta(\theta) = V(\theta) + \frac{\delta}{2}|\theta|^2 \tag{3.60}$$

and the resulting estimate is

$$\hat{\theta}_N^\delta = \arg\min_{\theta \in D_{\mathcal{M}}} W_N^\delta(\theta). \tag{3.61}$$

The key result is that the obtained realization is norm-minimal. Moreover, if the system is of a particularly simple form this also implies that the realization is a balanced one (except for an orthonormal state transformation).

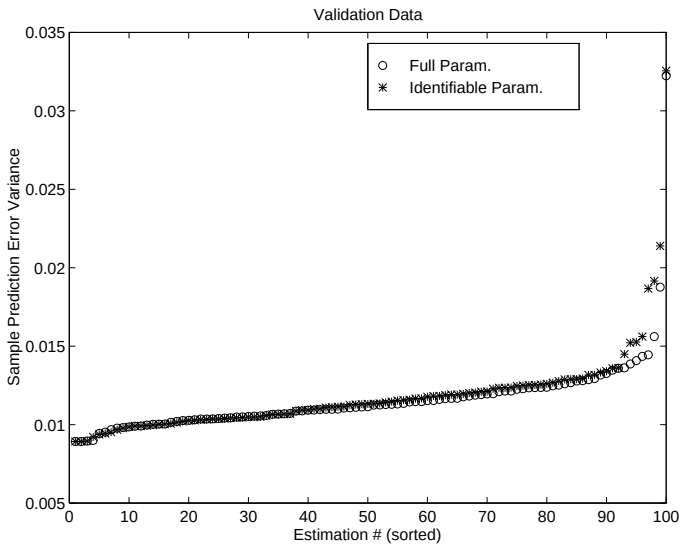

Figure 3.2: Sample prediction error covariance $\hat{\overline{V}}_N(\theta)$ calculated for the identifiable models (+) and for the fully parametrized models (o).

A further specialization of the set in Definition 2.4 will define norm-minimal realizations.

Definition 3.2 Consider a fully parametrized model structure (2.29) and the set of parameters D_T from Definition 2.4. The subset of D_T defined by

$$D_N = \{\theta \,|\, \theta = \arg\min_{\theta \in D_T} |\theta|\} \tag{3.62}$$

results in a set of models

$$\{\mathcal{M}(\theta) \,|\, \theta \in D_N\}$$

which are called *norm-minimal realizations.* □

Consider a state-space system which is given as a norm-minimal realization. Let $\theta \in D_N$ be the corresponding parameter vector. All other realizations of this system can be reached with non-singular similarity transformations T and new parameter vectors $\bar{\theta} = \bar{T}(T)\theta$, where the matrix $\bar{T}(T)$ is given by (2.38). The set of all norm minimal realizations of a system is then spanned by all transformations T which do not change the norm $|\theta|$ of the parameter vector. The following lemma details the structure of such a family of T.

Lemma 3.5 *Consider the fully parametrized model structure (2.29). Then*

$$\forall \theta_i \in D_N,\ i = 1, 2,\ \exists \bar{T} :\ \theta_1 = \bar{T}\theta_2 \ \ \textit{and}\ \ \bar{T}^T\bar{T} = I$$

Proof. The existence of a $\bar{T}$ which relates two realizations θ_1 and θ_2 of the same system is established by Lemma 2.2. In [54] it is proven that the state transformation matrix T satisfies $T^TT = I$ if both realizations are norm-minimal. By applying Lemma 2.3, the proof is concluded. □

The above lemma demonstrates that the set $D_N \subset D_T$ does *not* contain a singleton, but is a manifold in the parameter space $D_{\mathcal{M}}$. This has an interesting consequence for the regularized prediction error criterion $W_N^\delta(\theta)$, defined by (3.60). Any minimizing argument $\hat{\theta}_N^\delta$ of $W_N^\delta(\theta)$ will be non-unique since every $\bar{\theta} = \bar{T}(T)\hat{\theta}_N^\delta$ with $TT^T = I$ is also a minimizing argument of $W_N^\delta(\theta)$.

The following theorem shows that we will obtain a norm-minimal realization (in the limit) if we use the regularized prediction error criterion with the special choice $\theta^\# = 0$.

Theorem 3.6 *Let the data set Z^N satisfy A1 and consider a fully parametrized model structure (2.29) which contains the true system. Moreover , let $\hat{\theta}_N^\delta$ be defined by (3.5) and (3.6) with $\theta^\# = 0$.*

Then

$$\lim_{\delta \to 0} \lim_{N \to \infty} \inf_{\bar{\theta} \in D_N} |\hat{\theta}_N^\delta - \bar{\theta}| = 0, \qquad \text{w.p. 1.}$$

where D_N is defined by (3.62).

Proof. We can consider (3.6) as a penalty method to solve the following constrained minimization problem;

$$\min |\theta|^2 \text{ subject to}$$

$$E \lim_{N \to \infty} V_N(\theta) = \bar{V}(\theta) = \text{tr } \Lambda_0$$

since we know from Theorem 3.1 that $\bar{V}(\theta) \geq \text{tr } \Lambda_0$ and obtains its minimum for $\theta \in D_T$ (w.p. 1). An application of the theorem in [93, pp. 366-368] guarantees convergence of the sequence

$$\hat{\theta}_\infty^\delta = \lim_{N \to \infty} \hat{\theta}_N^\delta$$

to D_N as $\delta \to 0$ which concludes the proof. □

The set of models $\mathcal{M}(\theta), \theta \in D_N$ can also be characterized by a simple matrix equation. The following theorem by Helmke [54] gives the details.

Theorem 3.7 *Consider a model $\mathcal{M}_F(\bar{\theta})$ using the fully parametrized model structure (2.29) with state-space matrices $\bar{A}, \bar{B}, \bar{C}, \bar{K}$. Then*

$$\bar{A}\bar{A}^T + \bar{B}\bar{B}^T + \bar{K}\bar{K}^T = \bar{A}^T\bar{A} + \bar{C}^T\bar{C}$$

if and only if

$$\bar{\theta} \in D_N.$$

Proof. See [54].

Model	FM	IM $\bar{\nu}_6 = \{1,5\}$	IM $\bar{\nu}_6 = \{2,4\}$
$\hat{\overline{V}}$	0.0056	0.0070	0.0123
Model	IM $\bar{\nu}_6 = \{3,3\}$	IM $\bar{\nu}_6 = \{4,2\}$	IM $\bar{\nu}_6 = \{5,1\}$
$\hat{\overline{V}}$	0.0177	0.0056	0.0059

Table 3.1: Sample prediction error variance, $\hat{\overline{V}}$, evaluated using independent data from Example 3.3. (FM) is the value for the fully parametrized model. The results of the models for the five different identifiable parametrizations (IM) are shown together with the corresponding multi-index $\bar{\nu}_6$.

3.6 Examples

In this section we present some examples illustrating the previously discussed properties of the proposed identification algorithm and model structure.

Example 3.3 In Appendix A.2 of [96] a turbo generator model with two inputs, two outputs and six states is described. We use the continuous-time model to generate an estimation data set and a validation set using piecewise constant random binary $(-1,+1)$ signals as inputs and sample the inputs and outputs using a sample time of 0.05 seconds. The estimation data set and the validation set is, respectively, 500 and 300 samples long. The the output sequences is also corrupted with white zero mean Gaussian noise with variance $\Lambda_0 = 0.0025 \cdot I_2$ (which makes the system of output-error type).

The estimation is performed on estimation data according to Algorithm 3.1 using a fully parametrized model with six states. This gives a total of 64 parameters to estimate which can be compared with the 40 parameters for any identifiable model structure, *i.e.*, (2.21). The regularization parameter δ is set to 10^{-5} which makes the numerics well-conditioned. To assess the quality of the estimated model we evaluate

$$\hat{\overline{V}} = \frac{1}{N}\sum_{t=1}^{N} |y(t) - \hat{y}(t|\hat{\theta}_N)|^2$$

for the independent validation set.

To compare the proposed parametrization of the model with conventional identifiable parametrizations (2.21), we identified the five different models possible (corresponding to five sets of multi-indices $\bar{\nu}_6$ (2.22)). The results are given in Table 3.1. This clearly shows that the fully parametrized model (FM) is equally good as the best identifiable model (IM). It is also of interest to note that all the other identifiable models have a less good performance. □

Example 3.4 In this example we will illustrate how different types of parametrizations influence the quality of the identified model if the parameters in the model are constrained to have finite precision.

		# Digits			
	$\hat{\overline{V}}(\theta)$	6	7	8	9
Model	Ident.	1.95×10^{4}	99.3	6.53	0.101
	Full	3.78×10^{-4}	1.63×10^{-4}	1.24×10^{-6}	1.26×10^{-6}

Table 3.2: The mean value of the sample prediction errors, $\hat{\overline{V}}(\theta)$, calculated over 100 estimated models. The parameters of the models were constrained to 6-9 digits of significance.

Consider the simple third order discrete time system

$$y(t) = \frac{1}{(q-0.98)^3}u(t) + e(t), \tag{3.63}$$

where q is the forward time shift operator and $e(t)$ is a sequence of zero mean Gaussian random variables with variance 10^{-4}. With $u(t)$ selected as a random signal with unit variance, we use system (3.63) to generate 100 data sets each with 500 samples of $u(t)$ and $y(t)$. Using these 100 data sets we estimate two different kinds of output-error models; the fully parametrized state-space model and a state-space model with a minimal identifiable parametrization in observability canonical form. For each data record an initial ARX model is estimated. This estimate is then converted to the two different model structures. The fully parametrized model is minimized according to Algorithm 3.1, whereas the identifiable model is estimated by minimizing (3.2). For each model structure we estimate four different models and the parameters of each model is during the identification restricted to have 6,7,8 or 9 significant digits, respectively. For each data set a total number of eight models is estimated. The Gauss-Newton iterations are performed in the same fashion as in Example 3.1 using a maximum of 60 iterations. The quality of each model is evaluated by calculating the sample prediction error variance $\hat{\overline{V}}(\theta)$ from a simulation of the estimated model $\hat{y}(t|\hat{\theta}_N)$ and a noise free simulation of the true system (3.63) using the same input realization

$$\hat{\overline{V}}(\theta) = \frac{1}{N}\sum_{t=1}^{N}(y(t) - \hat{y}(t|\theta))^2. \tag{3.64}$$

The mean values of $\hat{\overline{V}}(\theta)$, calculated over the 100 estimated models are shown in Table 3.2. The extreme difference between the fully parametrized and the identifiable models is quite striking. However, from an information theory point of view, the result is quite natural since we used only 6 parameters in the identifiable model compared to 15 in the fully parametrized one. The discrete set of possible models is thus much larger for the fully parametrized model set than for the identifiable model set; hence, the set of attainable models are much denser. In Figure 3.3, the distribution of the errors are shown for the estimated models with 9 digits of significance. We can also see a tendency for the identifiable models to be more probable to reach a local a local minimum, instead of finding the global one. □

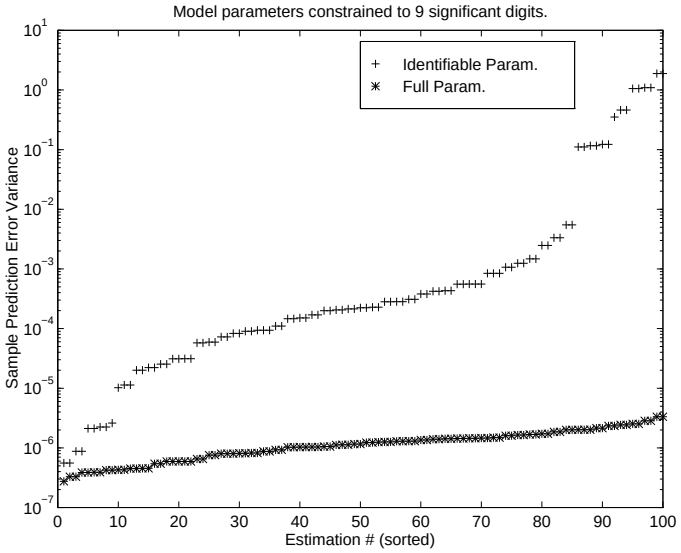

Figure 3.3: Sample prediction error variance calculated for 100 estimated models. The graph shows models identified where all parameters were constrained to 9 digits of significance. (*) Denotes fully parametrized models and (+) the identifiable parametrized models.

Example 3.5 In this example measured data from a glass oven process are used to identify state-space models. Van Overschee and De Moor [151] have estimated state-space models from these data using the subspace algorithm N4SID. The system consists of 3 inputs and 6 outputs and is modeled as a system of order $n = 5$. Using the same data and our fully parametrized state-space model structure we identify two different models using Algorithm 3.1. One output error model, *i.e.*, $K(\theta) = 0$ in (2.10) and one model (2.10) also including $K(\theta)$. In Table 3.3, the prediction error measure P (used in [151]) of the two estimated models is compared with the model obtained by [151], where

$$P = \frac{1}{6}\sum_{k=1}^{6}\sqrt{\frac{1}{N}\sum_{t=1}^{N}\frac{(y_k(t)-\hat{y}_k(t))^2}{y_k(t)^2}}$$

is evaluated on a validation data set. The fully parametrized OE-model has the best performance of the models in simulations. The other fully parametrized model performs slightly worse than the subspace identified model. This example shows that identification using real data works quite well for the proposed model structure compared with the subspace identification method.

□

Model	Simulation	1 step prediction
Subspace [151]	0.536	0.108
Full param. with K	0.547	0.135
Full param. $K = 0$	0.511	*n. a.*

Table 3.3: Performance P of the estimated models in Example 3.5

3.7 Discussion

The fully parametrized model structure introduced in Chapter 2 has in this chapter been further analyzed. The main idea is that a single model structure covers all systems of a given order. In order to employ an efficient numerical method for minimizing the prediction errors for the fully parametrized model, a prediction error criterion augmented with a regularization term have been considered. It is shown that the use of regularization automatically gives us the same statistical properties as those obtained from an identifiable model structure, even though the fully parametrized model structure contains more parameters to estimate.

An identification algorithm is presented which utilizes the numerically well-conditioned balanced realization during the identification process. This is done by means of a special choice of regularization. The convergence property of the proposed algorithm has also been discussed.

It is also shown that the use of a particular type of regularization will give a model which is norm-minimal. A connection between low sensitivity and norm-minimal realizations is also established.

4

Realization Algorithms

In this chapter we will address the question of how to obtain a state-space realization of a discrete time linear system if a finite amount of the impulse response coefficients are at hand. We will focus completely on an algebraic approach based on factorization of the *Hankel matrix* constructed from the impulse response. (See (4.7) below.) Most of the material is of review character.

This problem has been studied by many authors, both from a system theoretical or algebraic point of view as well as from more practical system identification aspects. Some early work is by Kronecker, [70], wherein he noted that a sequence of impulse response coefficients admits a finite dimensional realization of order n if and only if the rank of the Hankel matrix is less than or equal to n. Ho and Kalman [57], Youla and Tissi [166] and Silverman [132] all proposed algorithms to solve the realization problem via a factorization of the Hankel matrix. These algorithms relied upon exact knowledge of the impulse response. The lower order approximation problem is closely related to the realization problem. In [10] Aplevich describes an algorithm which approximates a given impulse response with a lower order state-space system. The resulting algorithm has close relations to the algorithm by Ho and Kalman.

From a system identification point of view it is interesting to consider the problem of identification of a state-space system using noisy measurements of the impulse response

$$\tilde{g}_k = g_k + w_k, \tag{4.1}$$

where $\tilde{g}_k$ is the measured impulse response and w_k is noise. A direct use of the realization algorithms on these noisy impulse responses is difficult since the Hankel matrix will generally be of full rank. The singular value decomposition was first proposed by Zeiger and McEwen [169] to obtain a low rank approximation of the Hankel matrix and later by Kung [71], where also some theoretical results on the approximation error caused by the noise can be found. In [62] the algorithm by Zeiger and McEwen is generalized to some extent.

In the field of signal processing we find the same type of algorithms, *e.g.*, fitting of exponentials to data [28] or the ESPRIT algorithm [125].

Most of the realization theory is based on quite old results which is seen from the references quoted above. All algorithms require numerical algebra tools such as the singular value decomposition and matrix inversion. With the development of "easy to use" numerical algebra packages, *e.g.*, MATLAB [143] and fast computers, implementation of the algorithms has become easy and large scale problems can be solved. Hence, it is only during the last 10 years we find successful applications of the realization algorithms to real data problems, [12, 13, 62, 76, 161].

We shall concentrate on linear state-space systems. Throughout this chapter we will use the following deterministic state-space model

$$\begin{aligned} x(t+1) &= Ax(t) + Bu(t) \\ y(t) &= Cx(t) + Du(t), \end{aligned} \tag{4.2}$$

with m inputs and p outputs. Furthermore, we assume (4.2) to be both observable and controllable and hence of minimal order n. We denote the system (4.2) with the quadruple (A, B, C, D) and obtain thereby an explicit realization. The impulse response coefficients of the system are given by

$$g_k = \begin{cases} D, & k = 0 \\ CA^{k-1}B, & k > 0, \end{cases} \tag{4.3}$$

which uniquely defines the input/output properties of the system via

$$y(t) = \sum_{k=0}^{\infty} g_k u(t-k). \tag{4.4}$$

To simplify the presentation, we will omit the D matrix from the discussion since it simply is equal to g_0. The triple (A, B, C) will then denote a system (4.2) with $D = 0$.

Let the extended observability and controllability matrices $\mathcal{O}_i$ and $\mathcal{C}_j$ be defined as

$$\mathcal{O}_i = \begin{pmatrix} C \\ CA \\ \vdots \\ CA^{i-1} \end{pmatrix} \tag{4.5}$$

$$\mathcal{C}_j = \begin{pmatrix} B & AB & \cdots & A^{j-1}B \end{pmatrix} \tag{4.6}$$

with the dimensions $\mathcal{O}_i \in \mathbb{R}^{pi \times n}$ and $\mathcal{C}_j \in \mathbb{R}^{n \times mj}$. The minimality of (A, B, C) now implies that, if $\min(i, j) \geq n$, $\mathcal{O}_i$ and $\mathcal{C}_j$ have both rank n.

4.1 Properties of the Impulse Response Hankel Matrix

In this section we begin by introducing the Hankel matrix constructed from the impulse response. We then proceed by discussing the rank deficiency property of the Hankel matrix and also introduce the Hankel operator.

Consider the block Hankel matrix $\mathcal{H}_{ij}$ constructed from the impulse response coefficients

$$\mathcal{H}_{ij} = \begin{pmatrix} g_1 & g_2 & \cdots & g_j \\ g_2 & g_3 & \cdots & g_{j+1} \\ \vdots & \vdots & \vdots & \vdots \\ g_i & g_{i+1} & \cdots & g_{i+j-1} \end{pmatrix}, \tag{4.7}$$

where $\mathcal{H}_{ij} \in \mathbb{R}^{pi \times mj}$. From the structure of the Hankel matrix and the definition of the impulse response (4.3), it is easy to see that we can write the Hankel matrix as the product

$$\mathcal{H}_{ij} = \mathcal{O}_i \mathcal{C}_j. \tag{4.8}$$

For all dimensions $\min(i, j) \geq n$, $\mathcal{H}_{ij}$ is always of rank n, see [57]. This fact can be used to infer an unknown system order if the impulse response coefficients are given. However, the rank of a matrix is very sensitive to perturbations in the matrix elements. A Hankel matrix $\tilde{\mathcal{H}}_{ij}$ constructed using noisy impulse response measurements $\tilde{g}_k$ will almost always be of full rank. The closeness of $\tilde{\mathcal{H}}_{ij}$ to a low-rank matrix can then be tested using the singular value decomposition [43]. We shall later return to this issue.

The necessary conditions for a block Hankel matrix to correspond to a minimal realization (4.2) is given by the *partial realizability criterion* [27]

$$\text{rank}(\mathcal{H}_{ij}) = \text{rank}(H^1) = \text{rank}(H^2) = n, \ \forall i, j \ \min(i, j) > n, \tag{4.9}$$

where H^1 is the $(i-1)p \times jm$ sub-matrix obtained from $\mathcal{H}_{ij}$ by removing the last block row and H^2 is the $ip \times (j-1)m$ sub-matrix obtained by removing the last block column.

Consider the double infinite Hankel matrix $\mathcal{H}_{\infty\infty}$ where both the number of block rows i and columns j are infinite. This matrix is known as the *Hankel operator* of the system (4.2), see [41]. Assume the input $u(t)$ is zero for all $t \geq 0$. The output from the system can then be written as

$$\begin{pmatrix} y(1) \\ y(2) \\ y(3) \\ \vdots \end{pmatrix} = \mathcal{H}_{\infty\infty} \begin{pmatrix} u(-1) \\ u(-2) \\ u(-3) \\ \vdots \end{pmatrix}. \tag{4.10}$$

The Hankel operator thus describes how past inputs influence future outputs. The n non-zero singular values of $\mathcal{H}_{\infty\infty}$ are equal to the Hankel singular values (2.44)

of the system (4.2). From the definition it is clear that the set of Hankel singular values does not depend on any particular realization and is therefore a realization invariant set.

The Hankel norm of a system is defined as

$$\|G\|_H = \bar{\sigma}(\mathcal{H}_{\infty\infty}), \tag{4.11}$$

where $\bar{\sigma}(X)$ denotes the largest singular value of the matrix X. The Hankel norm can thus be seen as the maximal gain of the Hankel operator of the system. Let

$$G(z) = C(zI - A)^{-1}B \tag{4.12}$$

denote the transfer function of the system. For stable systems the Hankel norm can also be shown to satisfy, see [41]

$$\|G\|_2 \leq \|G\|_H \leq \|G\|_\infty, \tag{4.13}$$

where

$$\|G\|_2^2 = \bar{\sigma}\left(\frac{1}{2\pi}\int_0^{2\pi} G(e^{i\omega})G(e^{-i\omega})^T\, d\omega\right) \tag{4.14}$$

and

$$\|G\|_\infty = \sup_\omega \bar{\sigma}\left(G(e^{i\omega})\right). \tag{4.15}$$

In an early paper by Ho and Kalman [57] it was shown that the Hankel matrix with the impulse response coefficients can be used to obtain a state-space model of the system. If the impulse response is corrupted by noise, the rank determination becomes difficult. In [169] Zeiger and McEwen proposed to use the singular value decomposition to find a low-rank approximation. It is possible to estimate the A and C matrices using only the range space of the observability matrix $\mathcal{O}_i$; this was shown by Kung in [71]. Kung's approach is of additional interest, since the observability range space can be recovered also from input-output measurements of a system. This fact is utilized in the more recent so-called subspace identification algorithms.

4.2 The Algorithm by Zeiger-McEwen

Using the algebraic ideas in [57], Zeiger and McEwen [169] introduced the singular value decomposition to solve the rank determination problem when considering noisy data. The algorithm can be described as follows.

Let $\underline{\mathcal{H}}_{ij} \in \mathbb{R}^{pi\times mj}$ be the block Hankel matrix with g_2 as the top left element but with the same matrix size as $\mathcal{H}_{ij}$ (4.7). Assume that $\min(i,j) \geq n$, where n is the system order. Define the SVD

$$\mathcal{H}_{ij} = \begin{pmatrix} U_s & U_o \end{pmatrix} \begin{pmatrix} \Sigma_s & 0 \\ 0 & \Sigma_o \end{pmatrix} \begin{pmatrix} V_s^T \\ V_o^T \end{pmatrix}, \tag{4.16}$$

where Σ_s is a diagonal matrix which contains the n largest singular values. The SVD decomposes the Hankel matrix into two terms, the signal term $U_s\Sigma_s V_s^T$ and the term which is orthogonal $U_o\Sigma_o V_o^T$. If the impulse response g_k is noise free, Σ_o is equal to zero. Use the SVD to factor the Hankel matrix as

$$\mathcal{H}_{ij} = (U_s\Sigma_s^{1/2})(\Sigma_s^{1/2}V_s^T). \tag{4.17}$$

Hence, it is straightforward to take

$$\hat{\mathcal{O}}_i = U_s\Sigma_s^{1/2}, \quad \hat{\mathcal{C}}_r = \Sigma_s^{1/2}V_s^T \tag{4.18}$$

as estimates of the observability and controllability matrices, respectively. It can be shown [29] that there exists a non-singular matrix $T \in \mathbb{R}^{n\times n}$ such that

$$\mathcal{O}_i = \hat{\mathcal{O}}_i T, \;\; \mathcal{C}_j = T^{-1}\hat{\mathcal{C}}_j, \tag{4.19}$$

where $\mathcal{O}_i$ and $\mathcal{C}_j$ are the extended observability and controllability matrices constructed from the realization (4.2). The factorization obtained with the SVD thus gives the observability and controllability matrices for some realization $(\hat{A}, \hat{B}, \hat{C})$ of the system (4.2). From the block-shift properties of the extended observability and controllability matrices, we notice that the matrix $\underline{\mathcal{H}}_{ij}$ can be written as

$$\underline{\mathcal{H}}_{ij} = \mathcal{O}_i A \mathcal{C}_j = \hat{\mathcal{O}}_i \hat{A} \hat{\mathcal{C}}_j. \tag{4.20}$$

Since the system is minimal both $\hat{\mathcal{O}}_i$ and $\hat{\mathcal{C}}_j$ have full rank. An estimate of $\hat{A}$ is then obtained as

$$\hat{A} = \hat{\mathcal{O}}_i^{\dagger}\underline{\mathcal{H}}_{ij}\hat{\mathcal{C}}_j^{\dagger}, \tag{4.21}$$

where $(\cdot)^{\dagger}$ denotes the Moore-Penrose pseudo-inverse [43]. By utilizing the original SVD of $\mathcal{H}_{ij}$ from (4.16) and (4.18), it is easy to see that (4.21) simplifies to

$$\hat{A} = \Sigma_s^{-1/2}U_s^T\underline{\mathcal{H}}_{ij}V_s\Sigma_s^{-1/2}. \tag{4.22}$$

B and C are obtained from the estimated observability and controllability matrices as

$$\hat{C} = \begin{pmatrix} I_p & 0_{p\times(i-1)p} \end{pmatrix}\hat{\mathcal{O}}_i \tag{4.23}$$

$$\hat{B} = \hat{\mathcal{C}}_j \begin{pmatrix} I_m & 0_{m\times(j-1)m} \end{pmatrix}^T. \tag{4.24}$$

The Eigensystem Realization Algorithm (ERA) by Juang and Pappa [62] is a slight generalization of the algorithm by Zeiger and McEwen. In ERA, a generalized Hankel matrix

$$\mathcal{H}_{ij}(k) = \begin{pmatrix} g_k & g_{k+t_1} & \cdots & g_{k+t_{j-1}} \\ g_{k+s_1} & g_{k+s_1+t_1} & \cdots & g_{k+s_1+t_{j-1}} \\ \vdots & \vdots & & \vdots \\ g_{k+s_{i-1}} & g_{k+s_{i-1}+t_1} & \cdots & g_{k+s_{i-1}+t_{j-1}} \end{pmatrix}, \tag{4.25}$$

where t_k, $k = 1, \ldots, j-1$ and s_k, $k = 1, \ldots, i-1$ are arbitrary positive integers. The algorithm follows the same steps as the algorithm by Zeiger-McEwen with the only difference that $\mathcal{H}_{ij}(1)$ and $\mathcal{H}_{ij}(2)$ are used instead of $\mathcal{H}_{ij}$ and $\underline{\mathcal{H}}_{ij}$.

4.3 The Algorithm by Kung

A different method for estimating the A matrix was proposed by Kung in [71] where the shift invariant property of the observability or the controllability matrix is utilized. Consider the estimate $\hat{\mathcal{O}}_j = U_s \Sigma_s^{1/2}$ in (4.18) of the observability matrix and define $\overline{U}_s$ and $\underline{U}_s$ as the sub-matrices formed by deleting the p last and p first rows from U_s, respectively. Notice that the shift invariant property of the observability matrix gives

$$\overline{U}_s \Sigma_s^{1/2} \hat{A} = \underline{U}_s \Sigma_s^{1/2}. \tag{4.26}$$

$\overline{U}_s$ is the extended observability matrix of dimension $(i-1)p \times n$. If $i-1 \geq n$, $\overline{U}_s$ is of full rank since the system is assumed to be minimal; hence, a pseudo-inverse exists. This gives the estimate

$$\hat{A} = \Sigma_s^{-1/2} (\overline{U}_s^T \overline{U}_s)^{-1} \overline{U}_s^T \underline{U}_s \Sigma_s^{1/2}. \tag{4.27}$$

B and C are estimated according to (4.24) and (4.23). The advantage with this estimation method is that it only requires the construction of one Hankel matrix and that only the observability range space is needed to obtain $\hat{A}$ and $\hat{C}$ of some realization of the system. This property is extensively used in more recent subspace based identification algorithms, see [158] for an excellent overview. By duality between the controllability and the observability matrices, the A matrix can be estimated in a similar fashion using the shift invariant structure of the controllability matrix.

4.4 The Low-Rank Approximation

If the Hankel matrix is constructed from a noise free impulse response from a system of order n, $\mathcal{H}_{ij}$ will be of exactly rank n and the factorization obtained from using the SVD (4.16) will be exact. In the case of noisy measurements of the impulse response, $\tilde{g}_k$ in (4.1), the low-rank approximation obtained by the SVD

$$\hat{\mathcal{H}}_{ij} = \hat{\mathcal{O}}_i \hat{\mathcal{C}}_j \tag{4.28}$$

is a rank n matrix which is the best approximation of $\tilde{\mathcal{H}}_{ij}$, the Hankel matrix with the noisy impulse response. The approximation is optimal in the sense that it minimizes the 2-norm of the approximation error [43]. However, $\hat{H}$ will in general not be a Hankel matrix, and neither $\hat{\mathcal{O}}_i$ nor $\hat{\mathcal{C}}_j$ will have the shift invariant property. Consequently, the rest of the realization algorithm will then only be approximately correct. For infinite Hankel matrices $\mathcal{H}_{\infty\infty}$ it has been shown by Adamjan, Arov and Krein [2] that there exists a rank n Hankel matrix which obtains the same 2-norm as any other general rank n matrix. For general finite dimensional Hankel matrices the optimal closeness to a low-rank Hankel matrix is still unknown [71].

It is sometimes proposed in the literature to use realization algorithms for model reduction purposes [14]. The idea is to calculate the impulse response coefficients g_k from the high order system and then apply Kung's algorithm to obtain a lower order approximate model. However, no theoretical results exist on the approximation

error resulting from this type of approach. The approach of truncated balanced realizations [117] or Hankel approximation techniques [41] provide theoretically more sound model reduction methods.

If the algorithms used for Hankel approximation encounter numerical problems and fail, the realization algorithm approach can then be an alternative.

4.5 Properties of the Models

In this section we briefly discuss some properties of the estimated models obtained from the realization algorithms by Zeiger-McEwen and Kung. Let

$$W_o^i = \sum_{k=0}^{i-1} (A^T)^k C^T C A^k \tag{4.29}$$

and

$$W_c^j = \sum_{k=0}^{j-1} A^k B B^T (A^T)^k \tag{4.30}$$

denote the finite observability and controllability Gramians of orders i and j, respectively. Assuming that the system is asymptotically stable, these matrices converge to the Gramian matrices W_o (2.39) and W_c (2.41), introduced in Chapter 2, as both i and j tend to infinity. Consider a model $(\hat{A}, \hat{B}, \hat{C})$ estimated with one of the realization algorithms. From (4.18) it follows that

$$W_o^i = \hat{\mathcal{O}}_i^T \hat{\mathcal{O}}_i = \Sigma_s \tag{4.31}$$

$$W_c^j = \hat{\mathcal{C}}_j \hat{\mathcal{C}}_j^T = \Sigma_s. \tag{4.32}$$

Hence, $W_o^i = W_c^j = \Sigma_s$. If $i = j$, this realization is referred to as $i - balanced$ in [95] or *approximately balanced* in [71].

Definition 4.1 A state-space model (A, B, C) is ij-*balanced* if the i-extended observability matrix (4.5) and j-extended controllability matrix (4.6) satisfy the relations

$$\mathcal{O}_i^T \mathcal{O}_i = \mathcal{C}_j \mathcal{C}_j^T = \Sigma \tag{4.33}$$

where $\Sigma = \text{diag}(\sigma_1, \sigma_2, \ldots, \sigma_n)$ with $\sigma_1 \geq \sigma_2 \geq \ldots \geq \sigma_n \geq 0$. □

We note the following property of Σ.

Lemma 4.1 *If the system* (A, B, C) *is minimal and* $\min(i, j) \geq n$, *then* $\sigma_n > 0$ *in (4.33).*

Proof. The minimality and the choice of i and j directly implies that $\mathcal{O}_i$ and $\mathcal{C}_j$ both are of rank n. The construction of Σ then directly shows that rank(Σ) = n which in turn implies that $\sigma_n > 0$. □

For a minimal system the rank of $\mathcal{O}_i^T\mathcal{O}_j$ and $\mathcal{C}_j\mathcal{C}_j^T$ is always n, independently of the basis chosen for the state variables.

Assume that the Hankel matrix is doubly infinite ($i = j = \infty$) and constructed from a system of order n. A (theoretical) estimation of a state-space model of order n using the algorithm by Zeiger-McEwen or Kung then results in an internally balanced realization (2.43) with $W_o = W_c = \Sigma_s$, where the diagonal elements of Σ_s are the Hankel singular values of the system.

4.6 Noise Effects

In general, all methods are of limited practical use unless they are robust against noisy data or inexact measurements. In this section we shall mention some results concerning bounds on the error caused by noise and also discuss the choice of number of rows vs. number of columns in the Hankel matrix.

Analysis of noise effects is not very developed in the literature. We can mention some results from [71], where a bound on the impulse response errors is derived under the assumption that the impulse response dies out completely in finite time. A pure simulation study is performed in [63] wherein the performance of the ERA algorithm is evaluated using different levels of noise. De Groen and De Moor present some theoretical results in [28] which we will review below.

Assume that the measurements are corrupted by noise w_k. Then we have

$$\tilde{g}_k = g_k + w_k, \quad \tilde{\mathcal{H}}_{ij} = \mathcal{H}_{ij} + W, \quad \|W\| < \epsilon, \tag{4.34}$$

where $\tilde{\mathcal{H}}_{ij}$ and $\tilde{g}_k$ denote the noise perturbed counterparts of $\mathcal{H}_{ij}$ and g_k, respectively. $\|\cdot\|$ denotes some consistent matrix norm and W denotes the Hankel matrix constructed from the noise w_k. Consider the SVD

$$\tilde{\mathcal{H}}_{ij} = \begin{pmatrix} \tilde{U}_s & \tilde{U}_o \end{pmatrix} \begin{pmatrix} \tilde{\Sigma}_s & 0 \\ 0 & \tilde{\Sigma}_o \end{pmatrix} \begin{pmatrix} \tilde{V}_s^T \\ \tilde{V}_o^T \end{pmatrix}, \tag{4.35}$$

where $\tilde{\Sigma}_s$ contains the n largest singular values. Use $\tilde{U}_s\tilde{\Sigma}_s\tilde{V}_s^T$ as the rank n approximation of $\tilde{\mathcal{H}}_{ij}$. The approximations of the system matrix A given by the methods by Zeiger-McEwen and Kung, respectively, yield an error which can be estimated by the norm of the noise matrix and the difference between the singular values of $\tilde{\Sigma}_s$ and $\tilde{\Sigma}_o$.

Theorem 4.1 [28] *For each of the approximate system matrices $\hat{A}$ from (4.21) or from (4.27), there exists a similarity transformation T and a constant c, such that*

$$\|\hat{A} - T^{-1}AT\| < c\frac{\|W\| + \sigma_{n+1}}{\sigma_n - \sigma_{n+1}}, \tag{4.36}$$

provided that $\|W\| + \sigma_{n+1} < 2(\sigma_n - \sigma_{n+1})$. *Here* $\{\sigma_i\}$ *denotes the singular values of* $\tilde{\mathcal{H}}_{ij}$, *in a decreasing order.*

From the theorem we see that if $\|W\| \to 0 \Rightarrow \sigma_{n+1} \to 0$. Hence, the system matrix satisfies $\|\hat{A} - T^{-1}AT\| \to 0$ for some T.

Consider the case of additive zero mean stochastic noise with the following properties

$$\begin{aligned} E\, w_i w_j^T &= \delta(i-j)\sigma I \\ E\, g_i w_j^T &= 0, \quad \forall i, j, \end{aligned} \tag{4.37}$$

where E denotes the expectation operator and $\delta(i-j)$ is the Kronecker delta. It is easy to show [28] that the "covariance matrix" $E\,\tilde{\mathcal{H}}_{ij}\tilde{\mathcal{H}}_{ij}^T$ satisfies

$$E\,\tilde{\mathcal{H}}_{ij}\tilde{\mathcal{H}}_{ij}^T = \mathcal{H}_{ij}\mathcal{H}_{ij}^T + pi\sigma I, \tag{4.38}$$

where pi is the number of rows in the Hankel matrix (4.7). The singular value decomposition of (4.38) is obtained as

$$E\,\tilde{\mathcal{H}}_{ij}\tilde{\mathcal{H}}_{ij}^T = \begin{pmatrix} U_s & U_o \end{pmatrix} \begin{pmatrix} \Sigma_s + pi\sigma I & 0 \\ 0 & pi\sigma I \end{pmatrix} \begin{pmatrix} U_s^T \\ U_o^T \end{pmatrix}, \tag{4.39}$$

where U_s and Σ_s originate from (4.16). The observability range space is thus recovered from U_s. Hence, if the number of samples are large enough (j chosen large), the law of large numbers applies to $\tilde{\mathcal{H}}_{ij}\tilde{\mathcal{H}}_{ij}^T$ and a good estimate of the observability range space can be expected from $\tilde{U}_s$ in (4.35).

For a fixed number of data, $N = i + j - 1$, the best choice would be to choose $i = n + 1$ and $j = N - n$. However, it turns out that the singular values in Σ_s decrease as j increases with $N = i + j - 1$ held constant. This means that the smallest singular value in Σ_s approaches the largest one of the noise and, hence, the corresponding left singular vector becomes less accurate. In [28] the recommendation is to choose $pi = mj$, *i.e.* a square Hankel matrix.

4.7 Discussion

The realization algorithms provide a straightforward method to calculate a state-space model from the impulse response. Accompanied by the singular value decomposition, the algorithms can be used for identification purposes when the impulse response is noise corrupted. The methods are non-iterative and can handle systems of high orders ($n \sim 500$). The singular value decomposition of the Hankel matrix $\mathcal{H}_{ij}$ is the step which requires the major part of the computational time. Once the SVD is calculated, the determination of all systems of order $n < i$, where i is the number of block rows of $\mathcal{H}_{ij}$ is quickly accomplished. The only computation involved is to solve one linear equation (4.20) or (4.26). It is thus possible, with a relatively small effort, to estimate a set of models with different model orders. This set of models provides insight into the complexity of the data and the choice of an appropriate model order.

5

Periodic Excitation Signals

An identification algorithm for use with data generated by periodic inputs is presented in this chapter. The algorithm is based on the geometrical properties of the resulting periodic output signal and a state-space model is derived from the signal subspace of a Hankel matrix. It is shown that only $2n + 1$ noise-free output measurements are required to identify an nth order system. The algorithm is demonstrated to be consistent when the output measurements are corrupted by zero mean noise characterized by decaying covariances. The computational complexity of the algorithm is lower by several orders of magnitude than standard methods.

5.1 Introduction

Methods which identify state-space models by means of geometrical properties of the input and output sequences are commonly known as *subspace methods* and have received much attention in the literature. The early subspace identification methods by De Moor and Vandewalle [31], Moonen and De Moor [107] and Verhaegen [155] focused on deterministic systems with errors present at the outputs. Such models are known as output-error models. By extending these methods, consistent algorithms have been obtained when the errors are described by colored noise, see Van Overschee and De Moor [152] and Verhaegen [156, 157]. A comprehensive overview of these methods is given by Viberg in [158]. One of the advantages with the methods is the absence of a parametric iterative optimization step. In classical prediction error minimization [86], such a step is necessary for most model structures.

The aim of this chapter is to consider the case when a system is excited by periodic inputs. Excitation signals which are periodic have long been used in the area of frequency domain identification [129]. Some advantages with periodic excitation also for time domain algorithms are presented in [130]. By applying a

periodic excitation signal on a stable system, the output signals becomes periodic after an initial transient. From one period of noise-free outputs, it is possible to construct a state-space model in a similar way as with the other subspace methods. The algorithm to be presented is closely related to a frequency domain method which we return to in Chapter 9. One objective for developing a subspace algorithm for the special case of periodic inputs is that the resulting algorithm is quite simple and the computational complexity is orders of magnitudes less than the general subspace based algorithms.

5.2 Identification Algorithm

Consider the following stable, discrete-time invariant, linear system in the state-space form

$$\begin{aligned} x(t+1) &= Ax(t) + Bu(t) \\ y(t) &= Cx(t) + Du(t) + v(t), \end{aligned} \tag{5.1}$$

where $y(t) \in \mathbb{R}^p$ is the output, $u(t) \in \mathbb{R}^m$ the input and $v(t)$ is an additive noise term. Furthermore, $x(t) \in \mathbb{R}^n$ is the state-vector assumed to be of minimal dimension which implies that the system is both observable and controllable. The model (5.1) is of output-error type since the noise term only affects the output. The system can also be characterized by the transfer function

$$G(z) = C(zI - A)^{-1}B + D,$$

which describes the input-output properties and is thus independent of the particular state-space basis used for the realization (5.1).

The aim of the identification is to retrieve the system (5.1) from input-output data. Assuming (5.1) is excited by a single M-periodic input signal

$$u(t) = u(t \pm kM); \quad t, k = 0, 1, \cdots, \tag{5.2}$$

we will now derive a simple identification algorithm. Note that (5.2) implies stationary conditions at $t = 0$.

The fundamentals of the algorithm will first be presented by considering the noise-free case $v(t) = 0$ and $m = 1$ in (5.1). Using the impulse response $\{g_k\}$ of the system (5.1), the measured outputs can be described by

$$y(t) = \sum_{k=0}^{\infty} g_k u(t-k), \tag{5.3}$$

where

$$g_k = \begin{cases} D, & k = 0 \\ CA^{k-1}B, & k > 0 \end{cases}. \tag{5.4}$$

By introducing the circulant Toeplitz matrix

$$U = \begin{pmatrix} u(0) & u(1) & \cdots & u(M-1) \\ u(M-1) & u(0) & \cdots & u(M-2) \\ \vdots & \vdots & \ddots & \vdots \\ u(1) & u(2) & \cdots & u(0) \end{pmatrix} \tag{5.5}$$

and $p \times M$ matrices

$$\underline{g}_i = \begin{pmatrix} g_{iM} & \cdots & g_{iM+M-1} \end{pmatrix}; \quad \underline{y}_i = \begin{pmatrix} y(iM) & \cdots & y(iM+M-1) \end{pmatrix} \tag{5.6}$$

we can write (5.3) as

$$\underline{y}_i = \underline{h}\, U, \quad i \geq 0, \tag{5.7}$$

where

$$\underline{h} = \begin{pmatrix} h_0 & h_1 & \cdots & h_{M-1} \end{pmatrix} = \sum_{k=0}^{\infty} \underline{g}_k. \tag{5.8}$$

Assuming U is non-singular, which is closely related to the notion of persistent excitation [86], we obtain

$$\underline{h} = \underline{y}_i\, U^{-1}, \quad i \geq 0. \tag{5.9}$$

Using (5.4) and (5.8), each column of $\underline{h}$ can be written as

$$h_i = \sum_{k=0}^{\infty} g_{i+kM} = \begin{cases} D + CA^{M-1}(I - A^M)^{-1}B, & i = 0 \\ CA^{i-1}(I - A^M)^{-1}B, & i > 0 \end{cases}. \tag{5.10}$$

Now consider the Hankel matrix

$$H_{ij} = \begin{pmatrix} h_1 & h_2 & \cdots & h_j \\ h_2 & h_3 & \cdots & h_{j+1} \\ \vdots & \vdots & \vdots & \vdots \\ h_i & h_{i+1} & \cdots & h_{i+j-1} \end{pmatrix}, \tag{5.11}$$

where size $i > n$ and $i + j = M$. By using the extended observability and controllability matrices

$$\mathcal{O}_i = \begin{pmatrix} C \\ CA \\ \vdots \\ CA^{i-1} \end{pmatrix}; \tag{5.12}$$

$$\mathcal{C}_j = \begin{pmatrix} B & AB & \cdots & A^{j-1}B \end{pmatrix} \tag{5.13}$$

the Hankel matrix (5.11) can be expressed as

$$H_{ij} = \mathcal{O}_i (I - A^M)^{-1} \mathcal{C}_j. \tag{5.14}$$

Since the system (5.1) is minimal both $\mathcal{O}_i$ and $\mathcal{C}_j$ have full rank n for all $i, j \geq n$. Because the system is stable, all eigenvalues of A are inside the unit disc which in turn implies the non-singularity of $I - A^M$. Hence we conclude that H_{ij} is also of rank n. Thus the range space of H_{ij} equals the range space of the observability matrix $\mathcal{O}_i$. It is well known that C and A matrices of some realization similar to the original can be determined from this space [71, 107]. It will now be demonstrated how a full state-space model can be determined from H_{ij}.

A singular value decomposition of H_{ij} can be written as

$$H_{ij} = \begin{pmatrix} U_s & U_o \end{pmatrix} \begin{pmatrix} \Sigma_s & 0 \\ 0 & \Sigma_o \end{pmatrix} \begin{pmatrix} V_s^T \\ V_o^T \end{pmatrix}, \tag{5.15}$$

where Σ_s contains the n non-zero singular values on the diagonal and $\Sigma_o = 0$ since H_{ij} is of rank n. Since (5.14) is valid for any realization, we take the realization which makes $\mathcal{O}_i = U_s$. Let $(\hat{A}, \hat{B}, \hat{C}, \hat{D})$ denote this particular realization. Notice that $\hat{D} = D$. Define

$$\overline{U} = \begin{pmatrix} I_{p(i-1)} & 0 \end{pmatrix} U_s; \qquad \underline{U} = \begin{pmatrix} 0 & I_{p(i-1)} \end{pmatrix} U_s. \tag{5.16}$$

From the shift invariant structure of $\mathcal{O}_i$, it follows that $\overline{U}\hat{A} = \underline{U}$. Since the system is minimal and $i > n$, $\overline{U}$ is an (extended) observability matrix of full rank n. This implies that $\hat{A}$ can be determined uniquely by

$$\hat{A} = \overline{U}^{\dagger} \underline{U}, \tag{5.17}$$

where $(\cdot)^{\dagger}$ is the Moore-Penrose pseudo inverse. The matrix $\hat{C}$ is simply equal to the first p rows of U and therefore

$$\hat{C} = \begin{pmatrix} I_p & 0 \end{pmatrix} U_s. \tag{5.18}$$

Since $H_{ij} = U_s \Sigma_s V_s^T$ and $\mathcal{O}_i = U_s$, it is clear that

$$\mathcal{C}_j = (I - \hat{A}^M) \Sigma_s V_s^T. \tag{5.19}$$

Since $\hat{B}$ is equal to the first column of $\mathcal{C}_j$ we have

$$\hat{B} = (I - \hat{A}^M) \Sigma_s V_s^T \begin{pmatrix} 1 \\ 0_{(j-1)\times 1} \end{pmatrix}. \tag{5.20}$$

From (5.10) we see that $\hat{D}$ can be calculated as

$$\hat{D} = h_0 - \hat{C} \hat{A}^{M-1} (I - \hat{A}^M)^{-1} \hat{B}. \tag{5.21}$$

In the algorithm, it suffices to let $i = n + 1$ and $j = n$. Thus M can be taken as $M \geq 2n + 1$. Since an nth order single-input single-output system has $2n + 1$ unknown parameters, the length of the experiment is then the shortest possible.

We summarize the result in the following theorem.

Theorem 5.1 *Assume that the system (5.1) of order n is excited with an $M \geq 2n+1$ periodic single input from $t = -\infty$ and U in (5.5) is of full rank. Furthermore, let M noise-free output measurements be available. Then the state-space model calculated above is similar to the state-space model (5.1).*

Multi-input systems can be handled by the algorithm if a different experiment is performed for each input. The resulting h_i for each experiment forms matrices of size $p \times m$ which are used in the block Hankel matrix (5.11).

5.2.1 Analysis

Consider the general case when $v(t)$ is assumed to be some noise sequence. Since the deterministic system is stationary, the noise influence can be reduced by averaging the outputs $y(t)$ over several periods. Assuming the outputs to be measured for N periods, which yields a total of NM measurements, the estimate of $\underline{h}$ is then

$$\tilde{\underline{h}}^N = \frac{1}{N} \sum_{k=0}^{N-1} \underline{y}_k U^{-1}, \tag{5.22}$$

where superscript N shows the dependence on the number of periods. These perturbed estimates are used in the Hankel matrix (5.11) which we denote by $\tilde{H}_{ij}$. This matrix is now generically of full rank and in the SVD (5.15) we let Σ_s contain the n largest singular values and let $U_s \Sigma_s V_s^T$ be an estimate of the noise free Hankel matrix H_{ij} and $(\hat{A}, \hat{B}, \hat{C}, \hat{D})$ are derived by (5.17–5.21).

Let us assume that the noise term $v(t)$ is a zero mean random variable with covariance function

$$R_v(t,s) = E\, v(t) v(s)^T$$

satisfying

$$\|R_v(t,s)\|_F < c \frac{t^\alpha + s^\alpha}{1 + |t-s|^\beta} \tag{5.23}$$

for some constants $c > 0$, $0 \leq 2\alpha < \beta < 1$. The assumption (5.23) is rather weak and includes many colored noise sequences. The main consistency result is then:

Theorem 5.2 *The identification algorithm is strongly consistent if the noise term $v(t)$ satisfies (5.23), i.e., the estimated transfer function $\hat{G}(z)$ satisfies*

$$\lim_{N \to \infty} \sup_{|z|=1} \|\hat{G}(z) - G(z)\|_F = 0, \quad \textit{w.p. 1}$$

Proof. Let $\Delta \underline{h}^N := \tilde{\underline{h}}^N - \underline{h}$ and let Δh_i^N denote its ith column. Let $[U^{-1}]_{i,j}$ denote the (i,j)th element of U^{-1}. From (5.22), we have

$$\Delta h_i^N = \frac{1}{N} \sum_{k=0}^{N-1} \sum_{m=1}^{M} v(m+kM) [U^{-1}]_{m,i} = \sum_{m=1}^{M} [U^{-1}]_{m,i} \frac{1}{N} \sum_{k=0}^{N-1} v(m+kM), \tag{5.24}$$

where $v(t)$ is the noise vector. The last sum in (5.24) has the limiting value

$$\lim_{N\to\infty} \frac{1}{N} \sum_{k=0}^{N-1} v(m+kM) = 0, \text{ w.p. } 1, \quad \forall m, M < \infty,$$

see [25, p. 94]. Since U^{-1} is assumed to be invertible, all elements in U^{-1} are bounded and we obtain

$$\lim_{N\to\infty} \|\tilde{H}_{ij} - H_{ij}\|_F = 0, \quad \text{w.p. } 1.$$

The proof is concluded by applying the robustness result Theorem 9.2 in Chapter 9. □

5.2.2 Efficient Implementation

Equation (5.7) can be interpreted as the circular convolution between the periodic sequences $u(t)$ and h_k and consequently equation (5.9) is the circular deconvolution. Since the circular convolution of two time sequences are equal to the multiplication of their corresponding discrete Fourier transforms [20], an alternative to forming the matrix inverse U^{-1} in (5.9) is to deconvolve the sequences in the frequency domain. Let

$$U_i = \sum_{k=0}^{M-1} u(k) e^{-j2\pi ki/M}, \quad i = 0, \ldots, M-1$$

be the discrete Fourier transform of $u(t)$ and conformally let Y_i be the DFT of $y(t)$. h_k is then given as the inverse DFT of the fraction $\frac{Y_i}{U_i}$ as

$$h_k = \frac{1}{M} \sum_{i=0}^{M-1} \frac{Y_i}{U_i} e^{j2\pi ki/M}, \quad k = 0, \ldots, M-1. \tag{5.25}$$

This alternative expression for h_k reveals the necessary condition for the inverse of U given in (5.5) to exist; the input signal must have an M-point DFT which is non-zero for all M frequencies. If M is equal to 2^k for some integer k the DFT and inverse DFT in (5.25) can be formed by the computationally efficient fast Fourier transform (FFT) [20]. In Chapter 9 we will develop a very similar frequency domain identification algorithm.

5.2.3 Discussion

If U is an identity matrix, *i.e*, the system is excited by an M-periodic unit pulse sequence, then $U^{-1} = I$ and $h_k = y(k)$, $k = 0, \ldots, M-1$. If we also let $M \to \infty$, we obtain the well-known realization algorithm by Kung [71]. In Kung's algorithm, a realization is obtained from a finite number of unbiased Markov parameters (impulse response coefficients). In our algorithm, on the other hand, an unbiased state-space realization is constructed from a finite sequence of biased Markov parameters using a persistently exciting input.

Robustness analysis of the presented algorithm follows the same lines as for the frequency domain algorithm presented in Chapter 9. See the proof of Theorem 9.2 for details.

5.3 Example

To illustrate some properties of the proposed algorithm, we will perform a comparison by identifying the dynamics of a fourth order deterministic system using three different approaches: the proposed algorithm, the recent subspace method N4SID[1] [152] and the method of prediction error minimization PEM [86, 88]. The aim of the identification is to determine the deterministic system such that $\|G - \hat{G}\|_\infty$ is "small" where G is the deterministic system and $\hat{G}$ the estimated model.

Let G, the deterministic system, be of fourth order with two oscillatory modes having damping factors equal to 0.01. Furthermore, let the measured output consist of the deterministic output additively perturbed by a noise sequence generated by white noise filtered through a first order system with a pole at 0.95. The system is given by

$$y(t) = \frac{100\,(0.3187\,q^4 + 1.2749\,q^3 + 1.9123\,q^2 + 1.2749\,q + 0.3187)}{q^4 - 3.2534\,q^3 + 4.6070\,q^2 - 3.2165\,q + 0.9777}\,u(t) + \frac{10^{-3}}{q - 0.95}\,e(t), \quad (5.26)$$

where q is the forward shift operator and $e(t)$ zero mean Gaussian distributed random variables with unit variance. The magnitude of the transfer function from u to y is shown in figure 5.1 and the system has the infinity norm $\|G\|_\infty = 40$.

The input is constructed by repeating a random sequence of length 20, 200 times which gives an input sequence of length 4000. The deterministic output is calculated from the input sequence with an initial condition x_0 chosen such that stationary conditions prevail. The measured output is constructed by adding the noise sequence to the deterministic output sequence. Also, a second data set is constructed with initial condition zero.

The input and measured output sequences are used for identification using the three algorithms. The algorithms can be divided into two classes; output-error methods and methods which explicitly estimate a noise model. The new algorithm is an output error method while N4SID and PEM explicitly identify a noise model. Since we know that the noise model has one state, we let N4SID and PEM estimate state-space systems with a total of five states in innovation form [86], while the new algorithm estimates output-error state-space models with four states. To illustrate the influence of the length of the data sequence on the quality of the estimate, we use subsequences of length $N = 500, 1000, 2000$ and 4000 in different identification experiments. This represents using 25, 50, 100 and 200 periods of the periodic excitation signal. To obtain a measure of average performance a Monte Carlo simulation is performed. 100 sets of data, each one with an independent noise realization, is used to estimate 100 models for each method and data length N. Also 100 models are estimated using the data set with zero initial condition. Since a zero initial condition violates the assumption of stationarity of the deterministic system we only use the last 2000 samples for the estimation to reduce this effect when using the new algorithm.

[1] The software implementation of N4SID was provided by Peter Van Overschee, Katholieke Universiteit Leuven, Belgium.

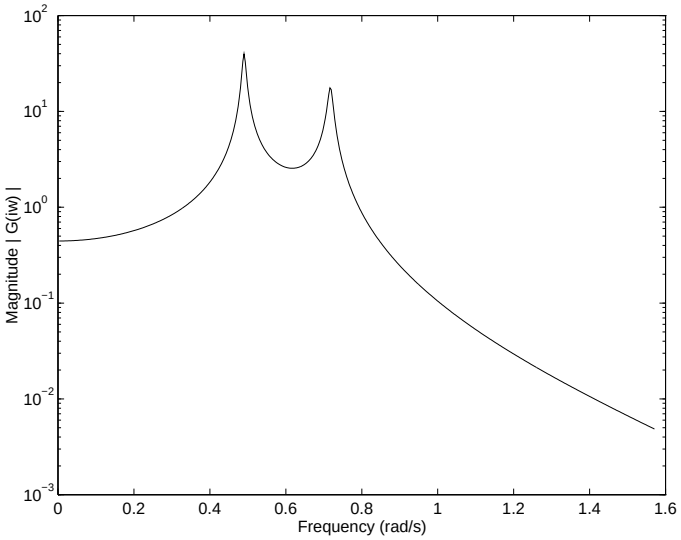

Figure 5.1: The magnitude of the transfer function of the system used in the example.

The prediction error estimation (PEM) starts by using N4SID to obtain an initial estimate which is transformed to observability canonical form [86] followed by Gauss-Newton iterations [34] minimizing the norm of the prediction error sequence. When the norm of the Gauss-Newton step falls below 10^{-8} or when no decrease in the loss function can be observed the iterations are terminated.

5.3.1 Results

The results of the identifications are given in Table 5.1 and 5.2. The new algorithm has a performance which is close to the statistically efficient prediction error method. N4SID does not perform well on these data when the system has a non-zero initial condition. For a zero-initial condition (last line in Table 5.1) N4SID performs well. For a zero initial condition we violate the basic assumption of the new algorithm but it still performs quite well. In Figure 5.2 the average of the error magnitude is shown for the three methods with a non-zero initial condition. From the figure we again see that the models estimated by PEM has the lowest error. The average number of floating point operations used to estimate one model is shown in Table 5.2. The new algorithm has by far the lowest complexity. This stems from the simple averaging (5.22) which performs a significant data reduction. N4SID and PEM has a much higher complexity since these methods are not tuned to the special case of periodic input signals.

Initial Cond.	N	Average $\|G-\hat{G}\|_\infty$ New	N4SID	PEM	Max $\|G-\hat{G}\|_\infty$ New	N4SID	PEM
$x(0) \neq 0$	500	5.10	26.1	4.38	14.2	38.2	13.1
	1000	3.89	24.5	2.80	11.4	38.1	8.68
	2000	2.53	21.4	1.98	7.73	36.8	5.08
	4000	1.75	19.4	1.51	5.63	34.5	3.59
$x(0) = 0$	4000	1.98	1.72	0.08	5.81	3.57	0.21

Table 5.1: Results from Monte Carlo simulations using 100 different noise realizations. For each noise realization and estimation method four models are estimated using different data lengths (N). The left part of the table shows the estimation error $\|G-\hat{G}\|_\infty$ averaged over the 100 estimations. The right part of the table shows the worst case error of the 100 estimations. The last line gives the results when the system is excited from a zero initial condition.

N	FLOPS ($\times 10^3$) New	N4SID	PEM
500	35	3.7×10^3	32×10^3
1000	36	5.3×10^3	60×10^3
2000	37	8.7×10^3	119×10^3
4000	39	15×10^3	192×10^3

Table 5.2: Computational complexity of the the new algorithm, N4SID and PEM demonstrated as the number of floating point operations (FLOPS) required to estimate one model as a function of the data set length (N). The number of operations for PEM also includes the operations used in N4SID for the initial model estimation.

5.3.2 Discussion

The prediction error method with an explicit noise model theoretically gives statistically efficient estimates of the system asymptotically in data, *i.e.*, the variance of the estimated model reaches the Cramér-Rao lower bound [86]. From the Monte Carlo simulations we notice that the best models were estimated by the statistically efficient prediction error method. The price paid for this statistical efficiency is a significant computational load. If accurate and fast methods are needed the presented algorithm as a viable alternative.

5.4 Conclusions

By using periodic inputs to excite a linear system of order n, we have demonstrated that a state-space model can be correctly estimated using only $2n+1$ noise-free samples of the output signal. If noise is present simple averaging can be applied to reduce its effect on the estimates. The algorithm is shown to be consistent under

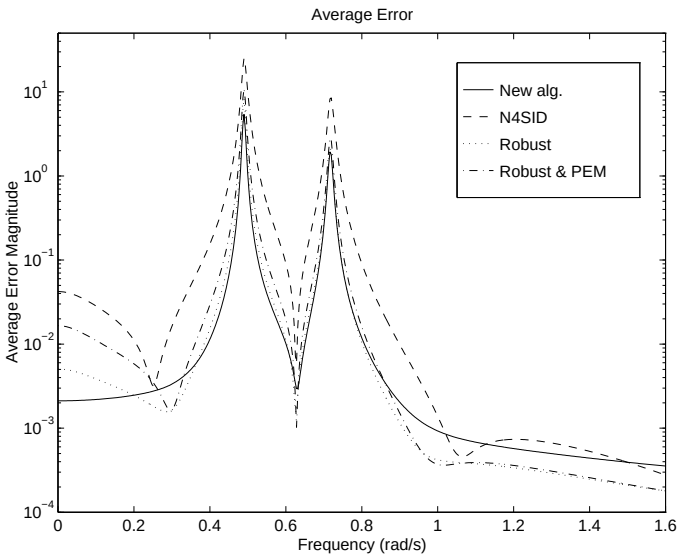

Figure 5.2: Average error magnitude $|G - \hat{G}|$ from the Monte Carlo simulation. The average is calculated over 100 estimations using $N = 4000$.

the mild assumptions that the noise is zero mean and has a covariance function which is decreasing. An example is presented comparing the estimation properties of the proposed algorithm with two known algorithms, N4SID and PEM. The results show that the new algorithm and PEM gives comparable results. Regarding computational speed, the new algorithm uses several magnitudes less floating point operations compared with the other methods.

6

System Identification From Impulse Response Measurements

In many applications the system under consideration is excited using an input of impulse like character. This is particularly so in some mechanical vibration analysis test situations, where the test specimen is excited with a pulse-like input, *e.g.*, the system is struck by a hammer or a structure is released from an initial position in which the structure contains potential energy. Typically, the characteristics of these types of systems are that the model order is quite large and many modes are poorly damped. The purpose of this chapter is to describe some identification tools and methods which are applicable for this type of data. The methods described below provide a foundation for the applications studied in the following chapter.

The problem of estimating a linear model from impulse response data is equivalent to that of estimating the parameters of damped or undamped sinusoids hidden in noise, *i.e.*, to fit a weighted sum of exponentials

$$y(t) = \sum_{i=1}^{n} \beta_i e^{\alpha_i t}, \tag{6.1}$$

with unknown exponents α_i and coefficients β_i, to a given set of noisy data $\tilde{y}(t)$. The first solution to the problem is due to Prony [32] and variations of his method are described in several books on numerical analysis, [56, 68, 72]. More recent methods are the realization based algorithms by Zeiger and McEwen [169], Kung [71], Roy *et al.* [126], De Groen and De Moor [28], and optimal maximum likelihood methods, for undamped signals, Stoica *et al.* [140]. Vibrational analysis applications using realization type algorithms are described by Vold and Russel [161], Juang and Pappa [62], Benveniste and Fuchs [17], Prevosto *et al.* [123] and Lew *et al.* [76].

If noise is present a consistency problem occurs. If the system is stable, the impulse response decays exponentially and, hence, so does the signal-to-noise ratio. This means that statistical consistency cannot be obtained by increasing the number of measurements. However, if we are allowed to perform several experiments we can consistently estimate the system by letting the number of experiments tend to infinity. We will return to this question in Section 6.5.

In this chapter we shall discuss some issues which are important in the identification process in order to obtain good estimates of the system under consideration. Our main contribution is to link the prediction error approach of standard system identification to subspace based realization algorithms. By merging these two very different approaches we obtain a method which utilizes the advantages of both. The key idea is to use the non-iterative realization algorithms to obtain an initial estimate of a state-space model. The state-space model so obtained is then converted to a state-space realization well suited for parametrization. Finally, the parametrized model is used as an initial estimate for the iterative prediction error method. Experience suggests that this last step can significantly improve the fit of the model to measured data. If the model order is high, the initial estimate provided by the realization algorithm step is crucial since the prediction error methods typically are trapped in local minima if the initial estimate is far from being able to describe the true system. The parametrization problem will be discussed in Section 6.3 where a parametrization well suited for vibrational models will be derived.

In Section 6.4 we shall also discuss the process of model order selection and introduce a new model quality measure which can be useful in the model order selection step, as well as in the model validation step. The new method compares an impulse response, usually measured, to a state-space model in a distributed way. For each pole of the estimated model, a quality measure is derived describing the accuracy of the estimated pole. The measure can be used to determine the accuracy of the estimated poles with respect to a measured impulse response and also for determination of the model order.

6.1 Preliminaries

Consider a linear time-invariant state-space system (A, B, C, D) of order n. Suppose we apply an impulse at input channel k

$$u(t) = \begin{cases} e_k, & t = 0 \\ 0, & t > 0, \end{cases} \tag{6.2}$$

where e_k is a zero vector except for a one in position k. The output of the system, assuming $x(0) \equiv 0$, is then equal to the kth column of the impulse response of the system

$$y^k(t) = g_t^k, \;\; t \geq 0, \tag{6.3}$$

where the superscript denotes the column number. For an m-input system, m impulse response experiments must be carried out in order to obtain the whole impulse response matrix at time t

$$\begin{pmatrix} y^1(0) & y^2(0) & \cdots & y^m(0) \end{pmatrix} = D, \tag{6.4}$$

$$\begin{pmatrix} y^1(t) & y^2(t) & \cdots & y^m(t) \end{pmatrix} = CA^{t-1}B, \;\; t > 0. \tag{6.5}$$

A freely decaying motion of a system can also be interpreted from the point of view that the initial state x_0 of the system is non-zero and $u(t) \equiv 0$. The measurements $y(t)$ are then described by

$$y(t) = CA^{t-1}x_0, \quad t > 0. \tag{6.6}$$

If M experiments are performed we obtain the relation

$$\begin{pmatrix} y^1(t) & y^2(t) & \cdots & y^M(t) \end{pmatrix} = CA^{t-1} \begin{pmatrix} x_0^1 & x_0^2 & \cdots & x_0^M \end{pmatrix}, \quad t > 0. \tag{6.7}$$

By interpreting the initial states x_0^i as the columns of a B matrix the measurements $y^i(t)$ are the impulse responses from a system with $D = 0$.

The only difference between the two descriptions is that the direct coupling between the input and output in the first description is given by $D = g_0 = y(0)$, whereas in the latter one no information of a direct coupling is given. If only output measurements are given and some uncertainty exists about the exact time when the impulse was applied, it might be more advantageous to use the latter description with some proper choice of initial time such as $t = 0$ and discard the D matrix in the model. If only the poles of the system are of interest, this approach is more appropriate.

6.1.1 Modal Parameters in Vibrational Analysis

The acceleration at each point of a vibrating structure is a superposition of damped sinusoids, each with a natural frequency and a damping ratio. Each sinusoid is referred to as a vibrational mode. The amplitudes and phases for one mode at different locations of the structure is called the *modal shape* of the structure. The frequencies along with the corresponding damping ratios and the modal shapes are altogether referred to as *modal parameters* of the structure.

The acceleration at a discrete set of locations on a vibrating mechanical structure can accurately be modeled by a linear multi-output state-space model (4.2). The p output channels of the model $y(t) \in \mathbb{R}^p$ describes the acceleration at p points of the structure. In the linear state-space model (4.2) each vibrating mode is associated with a complex conjugate pair of poles or, equivalently, eigenvalues of the A matrix of the model. From this eigenvalue pair the frequency and damping ratio can easily be calculated. The modal shape is equivalent to the columns of the C matrix of a complex diagonal realization of the system (see (6.21)). A state-space model with n states can describe $n/2$ different vibrational modes.

The modal parameters of a mechanical system can be determined from a state-space model of the acceleration. If the structure is excited with an impulse or is released from an initial state, a state-space model can be constructed from accelerometer measurements at the points of interest of the mechanical structure. The modal parameters can also be determined by pure sinusoidal excitation at discrete frequencies which then gives an alternative, but more complicated way of model estimation.

Frequencies and Damping Ratios

The eigenvalues of the matrix A, from the model (4.2), contain the information about frequencies and damping ratios for all structural modes described by the model. Denote by f the sampling frequency and by $\lambda_k(A),\ k = 1, \ldots, n$, the eigenvalues of A from the state-space model. For the kth mode the time multiplier function

$$e^{-\zeta_k \Omega_k t} \sin(\omega_k t) \tag{6.8}$$

is observed during a free decaying motion. It is characterized by the frequency ω_k (in rad/s) and relative damping ratio ζ_k. These modal parameters are associated with a complex conjugate eigenvalue pair from the real matrix A such that

$$\omega_k = \mathrm{Im}(\log \lambda_k^+) f \tag{6.9}$$

$$\zeta_k = -\mathrm{Re}(\log \lambda_k^+) f / \Omega_k \tag{6.10}$$

with

$$\Omega_k = \omega_k / \sqrt{1 - \zeta_k^2} \tag{6.11}$$

where λ_k^+ is given from A as the eigenvalue of the complex conjugate pair having the positive imaginary part.

6.2 Identification Methods

The realization algorithms are excellent tools for obtaining state-space models from impulse response data. However, the lack of an explicit criterion to minimize reduces the possibility of obtaining statistically efficient estimates. Moreover, it is possible to find examples where significantly better models can be estimated using the classical prediction error minimization (PEM) method. The success of PEM methods, which normally include a non-linear parametric optimization, is heavily dependent on the availability of a good initial estimate.

In this section, we will combine realization algorithms with prediction error minimization methods. The proposed identification scheme begins by making use of a realization algorithm to obtain an initial estimate. A computational inexpensive re-estimation, involving a linear least-squares solution of the matrices B and D (or C and D), then follows. As a final step we invoke the standard prediction error minimization using some appropriate parametrization. The first and second steps, which both are non-iterative, provide a model which usually is close to the prediction error minimum. The final step, which involves an iterative non-linear minimization, will provide some final adjustments of the model to the data.

6.2.1 Data Pre-Processing

Before inserting a measured impulse response, or free decay measurements, into the numerical identification algorithms it is important to consider some measures to make the data easier to handle.

Filtering

Filtering should always be considered if the frequency range of interest is known and noise reduction can be expected. A simple band-pass filtering can then be applied. The correct way of filtering is to filter both the output signal (the impulse response) as well as the input signal (the impulse). The input signal to use is then simply the impulse response of the filter. This way of filtering will shape the spectrum of the noise [86]. The estimation problem is then, however, no longer an impulse response estimation problem since the filtered input is not equal to an impulse. Standard identification techniques should then be applied which utilize both the input signal as well as the output signal. A useful approach for this case is to use one of the recent subspace based algorithms [152, 157] to provide an initial input-output model and then proceed with PEM.

If the impulse response arises from a complex system containing a large number of frequencies it may be interesting to zoom in on a fraction of the frequencies. In this case, the aim is not only to shape the spectrum of the noise but also to suppress some modes arising from the complex system. This can be achieved if the filtered impulse response is still considered to be an impulse response. Assume that the measured impulse response is described as

$$\tilde{g}_t = g_t + w_t,$$

where g_t is the true impulse response and w_t is the noise term. A filtered impulse response $\tilde{g}_t^f$ is described by

$$\begin{pmatrix} x(t+1) \\ x_f(t+1) \end{pmatrix} = \begin{pmatrix} A & 0 \\ B_f C & A_f \end{pmatrix} \begin{pmatrix} x(t) \\ x_f(t) \end{pmatrix} + \begin{pmatrix} B \\ 0 \end{pmatrix} \delta(t) + \begin{pmatrix} 0 \\ B_f \end{pmatrix} w_t$$
$$\tilde{g}_t^f = \begin{pmatrix} 0 & C_f \end{pmatrix} \begin{pmatrix} x(t) \\ x_f(t) \end{pmatrix} + D_f D \delta(t) + D_f w_t, \tag{6.12}$$

where (A_f, B_f, C_f, D_f) is a state-space realization of the filter used and $x_f(t)$ is the corresponding state vector. In (6.12) $\delta(t)$ is the Kronecker delta. The filtered impulse response is thus a superposition of the filtered true impulse response and the filtered noise

$$\tilde{g}_t^f = g_t^f + w_t^f, \tag{6.13}$$

where w_t^f denotes the filtered noise term. A straightforward application of the realization algorithm to the filtered impulse response would thus yield a model containing both the system dynamics and the filter dynamics. However, if the modes of interest have low damping ratios, accurate low order models can be estimated by using the band-pass filtered impulse response as an impulse response and estimate an approximate low order model. The majority of the energy in the filtered impulse response will originate from the system modes having frequencies in the pass-band of the filter and having low damping ratios. A low order approximation will then accurately capture these modes.

If non-causal zero-phase filtering is used, the time instant when the impulse was applied will be smoothed out in the filtered data. A good rule is to choose

the $t = 0$ sample by inspection and assume a free decay output from that point and on. In this case we will get no estimate of the D matrix. If the D matrix is important, other identification methods with inputs that are persistently exciting should be used.

Decimation

If the measured data set is very long, the last part may contain mostly noise since the signal part decays at an exponential rate. A plot of the signals and visual inspection easily reveals if the last part of the data set should be discarded.

If the measured data is sampled at a very high sample frequency compared to the frequency range of interest, it is advisable to decimate the data set by some appropriate factor to improve numerical accuracy. A very high sampling frequency results in a discrete time system with all poles close to 1. If filtering is also considered, it should be performed prior to the decimation step. From a statistical point of view, we loose information by decimation but it is our experience that the realization algorithms sometimes perform better on decimated data.

6.2.2 Initial Estimates From Realization Algorithms

The realization algorithms presented in Chapter 4 require very little user interaction except for the choice of Hankel matrix dimension; the number of block rows i and block columns j. If the data set is large, then the computational requirements are reduced if we use a wide ($mj > pi$) Hankel matrix. The singular value decomposition is more demanding for a square matrix than a wide matrix if the number of data $N = i + j - 1$ is fixed. However, the noise influence is minimized for a square $\mathcal{H}_{ij}$, $pi = mj$, as discussed in Chapter 4. It is our recommendation to use a Hankel matrix which is as close to a square matrix as the computer resources allow.

6.2.3 Linear Least-Squares Estimation

From the initial estimate obtained from one of the realization algorithms, it is fairly simple to improve the model quality by re-estimating the B and D matrices from the estimation data by assuming A and C fixed. This can be done by means of minimizing the squared prediction error, which in this case is

$$\varepsilon_k = \tilde{g}_k - \hat{g}_k. \tag{6.14}$$

For fixed $\hat{A}$ and $\hat{C}$, the impulse response $\hat{g}_k$ is linear in B and D. Thus, the estimation is easily accomplished by an ordinary least-squares solution.

Assume that $\tilde{g}_k$, $k = 0, \ldots, N$, is the noisy impulse response. We can then write (see (6.5))

$$\tilde{g}_0 = D + w_0 \tag{6.15}$$

$$\begin{pmatrix} \tilde{g}_1 \\ \tilde{g}_2 \\ \vdots \\ \tilde{g}_N \end{pmatrix} = \hat{\mathcal{O}}_N B + \begin{pmatrix} w_1 \\ w_2 \\ \vdots \\ w_N \end{pmatrix}, \tag{6.16}$$

where $\hat{\mathcal{O}}_N$ is the N block row extended observability matrix (4.5) constructed from $\hat{A}$ and $\hat{C}$. Assume that the initial estimates $\hat{A}$ and $\hat{C}$ are close to the true ones (except for a similarity transformation). We can now use the least-squares solutions to estimate D and B as

$$\hat{D} = \tilde{g}_0 \tag{6.17}$$

$$\hat{B} = \hat{\mathcal{O}}_N^{\dagger} \begin{pmatrix} \tilde{g}_1 \\ \tilde{g}_2 \\ \vdots \\ \tilde{g}_N \end{pmatrix}, \tag{6.18}$$

where $(\cdot)^{\dagger}$ is the Moore-Penrose pseudo-inverse. If $(\hat{A}, \hat{C})$ is an observable pair $\hat{\mathcal{O}}_N$ will be of full rank and the solution $\hat{B}$ is unique.

A completely dual approach is obtained if we consider the estimation of C and D, assuming $\hat{A}$ and $\hat{B}$ are fixed. The least-squares estimate is then obtained as

$$\hat{C} = \begin{pmatrix} \tilde{g}_1 & \tilde{g}_2 & \cdots & \tilde{g}_N \end{pmatrix} \hat{\mathcal{C}}_N^{\dagger}, \tag{6.19}$$

where $\hat{\mathcal{C}}_N$ is the extended controllability matrix (4.6), which have full rank if $(\hat{A}, \hat{B})$ is a controllable pair.

Either of these least-square steps will move the model closer to the prediction error minimum and thus improve the speed of convergence for the final step, *i.e.*, the non-linear iterative prediction error minimization.

6.2.4 Prediction Error Minimization

The state-space model, obtained from the realization algorithm and further refined with the least-squares estimation, is now an excellent initial model for prediction error minimization. In order to perform the non-linear optimization by the Gauss-Newton method we need a parametrization of the state-space model. The parametrization should be designed with the focus on vibrational analysis applications. The characteristics are thus single-input systems with a large number of complex poles as well as a large number of outputs.

6.3 Numerically Efficient Parametrizations

During the prediction error minimization using a Gauss-Newton method (see Chapter 3.1.2) the main computational effort lies in calculating the gradient and in the search for a lower value of the criterion along the Gauss-Newton direction. In

both calculations, most of the computational time is spent on solving the system equations (2.1) forward in time. For a state-space model without any particular structure, the number of floating point operations (flops) are $N\mathbf{O}(n^2)$ where n is the system order and N is the number of samples calculated. If we instead consider a model with the identifiable parametrization (2.21) the number of flops required is only $N\mathbf{O}(pn)$, where p is the number of outputs. This difference becomes quite significant if the model order is high and $p \ll n$. As we already have discussed in Chapter 2.3, the identifiable parametrization (2.21) becomes very ill-conditioned when model order increases and, hence, is not a good parametrization candidate for systems of high order. The fully parametrized model structure (2.29) could also be considered, but here we will focus on a different parametrization from which the poles are easily accessible. By restricting to systems having an A matrix which can be made diagonal, we can derive a parametrization which is both minimal, numerically efficient and well-conditioned.

6.3.1 The Complex Diagonal Form

Consider a system (A, B, C) such that the eigenvalues of A are distinct. Then there exists a non-singular matrix $T \in \mathbb{C}^{n\times n}$ such that

$$T^{-1}AT = \Lambda = \operatorname{diag}(\lambda_1, \lambda_2, \ldots, \lambda_n), \tag{6.20}$$

where $\lambda_i \in \mathbb{C}$ are the poles of the system. We also impose a total ordering of the eigenvalues such that the primary ordering is by the real part in a non-decreasing order and the secondary ordering is based on the imaginary part in a non-decreasing order. Since A is a real matrix, there exists for each complex eigenvalue λ_i a $j \neq i$ such that $\lambda_i = \lambda_j^*$, where $(\cdot)^*$ denotes complex conjugate. If we use T as the complex similarity transformation, we obtain the system

$$(\Lambda, \tilde{B}, \tilde{C}) = (T^{-1}AT, T^{-1}B, CT). \tag{6.21}$$

Let

$$\underline{i} = \{i \,|\, \operatorname{Im}(\lambda_i) > 0\} \tag{6.22}$$

and

$$\overline{i} = \{i \,|\, \operatorname{Im}(\lambda_i) = 0\} \tag{6.23}$$

be the set of indices of the complex eigenvalues with positive imaginary part and the set of indices having real eigenvalues, respectively. Let the cardinality of the sets $\underline{i}$ and $\overline{i}$ be denoted by $\underline{n}$ and $\overline{n}$, respectively.

Now, since the original system is real valued $(y(t), u(t) \in \mathbb{R})$ we notice that the following relations hold for each complex eigenvalue pair $\lambda_i = \lambda_j^*$:

$$\tilde{B}_i = \tilde{B}_j^*, \text{ and } \tilde{C}_i = \tilde{C}_j^*, \tag{6.24}$$

where $\tilde{B}_i$ denotes the ith row of $\tilde{B}$ and $\tilde{C}_j$ denotes the jth column of $\tilde{C}$. Note also that for all real eigenvalues $\lambda_i \in \mathbb{R}$ the corresponding $\tilde{B}_i$ and $\tilde{C}_i$ are real. We

can describe the same system dynamics with a reduced order model consisting of $\underline{n}$ complex states $\underline{x}(t)$ and $\overline{n}$ real states $\overline{x}(t)$ using the matrices

$$\underline{\Lambda} = \operatorname{diag}(\lambda_{\underline{i}_1}, \ldots, \lambda_{\underline{i}_{\underline{n}}}), \quad \overline{\Lambda} = \operatorname{diag}(\lambda_{\overline{i}_1}, \ldots, \lambda_{\overline{i}_{\overline{n}}}) \tag{6.25}$$

$$\underline{B} = \begin{pmatrix} \tilde{B}_{\underline{i}_1} \\ \vdots \\ \tilde{B}_{\underline{i}_{\underline{n}}} \end{pmatrix}, \quad \overline{B} = \begin{pmatrix} \tilde{B}_{\overline{i}_1} \\ \vdots \\ \tilde{B}_{\overline{i}_{\overline{n}}} \end{pmatrix} \tag{6.26}$$

$$\underline{C} = \begin{pmatrix} \tilde{C}_{\underline{i}_1} & \cdots & \tilde{C}_{\underline{i}_{\underline{n}}} \end{pmatrix}, \quad \overline{C} = \begin{pmatrix} \tilde{C}_{\overline{i}_1} & \cdots & \tilde{C}_{\overline{i}_{\overline{n}}} \end{pmatrix}, \tag{6.27}$$

where $\underline{i}_j$ and $\overline{i}_j$ denote the elements in the sets $\underline{i}$ and $\overline{i}$, respectively. The input-output relation can be written as

$$\begin{aligned} \overline{x}(t+1) &= \overline{\Lambda}\overline{x}(t) + \overline{B}u(t) \\ \underline{x}(t+1) &= \underline{\Lambda}\underline{x}(t) + \underline{B}u(t) \\ y(t) &= \overline{C}\overline{x}(t) + 2\operatorname{Re}(\underline{C}\underline{x}(t)) + Du(t) \end{aligned} \tag{6.28}$$

using the reduced order complex state-space description. The calculation of the complex states in (6.28) is particularly simple, because all states are completely decoupled since both $\overline{\Lambda}$ and $\underline{\Lambda}$ are diagonal matrices. This model structure thus shows $\mathbf{O}(n)$ complexity when calculating the output $y(t)$ and results in a more advantageous parametrization with respect to parametric sensitivity, *i.e.*, the diagonals of $\overline{\Lambda}$ and $\underline{\Lambda}$ contain the poles of the system (the real poles and the complex ones with positive imaginary part).

6.3.2 An Identifiable Parametrization

The diagonal form described above offers a possibility to parametrize the system using a minimal number of parameters, provided that certain conditions are imposed on the system.

For simplicity, consider a single input system ($m = 1$) with n states and p outputs with a minimal realization (A, B, C) and assume that the A matrix has distinct eigenvalues. The complex diagonal form (6.21) does not provide an identifiable parametrization since the diagonal form is preserved by diagonal non-singular similarity transformations

$$T = \operatorname{diag}(t_1, \ldots, t_n). \tag{6.29}$$

An identifiable parametrization is obtained if we add the constraint

$$\tilde{B} = \begin{pmatrix} 1 & \cdots & 1 \end{pmatrix}^T \tag{6.30}$$

on the system. The minimality of the system implies that this choice of $\tilde{B}$ always is possible. The two conditions, the ordered diagonal form of Λ and (6.30), make

this form identifiable since it is not possible to find any similarity transformation which preserves this structure.

The number of real-valued parameters required for this model structure is then n parameters in the diagonal of Λ and pn in the $\tilde{C}$ matrix which gives a total number of $n(p+1)$ real valued parameters. This coincides with the number of parameters in the identifiable model structure (2.21).

If we consider a general multivariable system with distinct poles, the described diagonal form can easily be extended to multi-input systems if we add the assumption that the system is controllable from the first input. An identifiable parametrization will then be obtained by adding parameters to the second up to the mth column of $\tilde{B}$, while keeping fixed ones in the first column. In this case, the total number of parameters becomes $n(p+m)$ which again is identical to the number of parameters of model structure (2.21). The controllability requirement from the first input can be relaxed if a more complex method of fixing ones in the $\tilde{B}$ matrix is devised. This leads to a set of non-overlapping parametrizations.

The main advantages of this type of parametrization is the clear coupling between parameters and poles of the system as well as, for a free decaying system, relative amplitude and phase between different outputs. The decoupling of the states also, as stated before, leads to a low computational load. The main disadvantage is the restriction to systems which have distinct poles and, for the multi-input case, that the system is required to be controllable from the first input.

6.3.3 Block Diagonal Identifiable Parametrization

It is sometimes required that the parametrization results in a state-space system with real valued matrices. It is easy to derive such a form from the complex diagonal realization (6.21) with the added constraint on $\tilde{B}$ (6.30). The columns of $\tilde{C}$ and rows $\tilde{B}$ corresponding to real-valued eigenvalues are also real-valued and thus need no change.

For the sub-system corresponding to complex eigenvalues we can obtain a block diagonal form by employing a block diagonal similarity transformation matrix

$$T_b = \frac{1}{\sqrt{2}} \operatorname{diag}\left(\begin{pmatrix} 1 & i \\ 1 & -i \end{pmatrix}, \ldots, \begin{pmatrix} 1 & i \\ 1 & -i \end{pmatrix} \right). \tag{6.31}$$

With this transformation the block diagonal sub-system results in a realization

$$(A_b, B_b, C_b) = (T_b^{-1}\Lambda T_b, T_b^{-1}\tilde{B}, \tilde{C}T_b). \tag{6.32}$$

Here, A_b is a block diagonal matrix where each block element on the diagonal has the form

$$\{A_b\}_{kk} = \begin{pmatrix} \mathrm{Re}(\lambda_k^+) & -\mathrm{Im}(\lambda_k^+) \\ \mathrm{Im}(\lambda_k^+) & \mathrm{Re}(\lambda_k^+) \end{pmatrix}, \tag{6.33}$$

where $\{\lambda_k^+\}$ are the $n/2$ eigenvalues with positive imaginary parts. The B_b matrix is of the form

$$B_b = \begin{pmatrix} 1 & 0 & 1 & 0 & \ldots & 1 & 0 \end{pmatrix}^T. \tag{6.34}$$

The C_b matrix becomes real but without any particular structure. The number of parameters in this structure is $n(p+1)$ as before.

Example 6.1 A fourth order system with two outputs has a block diagonal parametrization given by

$$\begin{aligned} x(t+1) &= \begin{pmatrix} \theta_1 & -\theta_2 & 0 & 0 \\ \theta_2 & \theta_1 & 0 & 0 \\ 0 & 0 & \theta_3 & -\theta_4 \\ 0 & 0 & \theta_4 & \theta_3 \end{pmatrix} x(t) + \begin{pmatrix} 1 \\ 0 \\ 1 \\ 0 \end{pmatrix} u(t) \\ y(t) &= \begin{pmatrix} \theta_5 & \theta_7 & \theta_9 & \theta_{11} \\ \theta_6 & \theta_8 & \theta_{10} & \theta_{12} \end{pmatrix} x(t). \end{aligned} \tag{6.35}$$

□

6.4 Model Order Determination and Model Quality Assessment

During the identification process the user has to decide on which model order to use. A low-order model may be too simple for accurately capturing the dynamics of the underlying system, whereas a too high model order may lead to unnecessarily complicated computations and a large model uncertainty.

In order to obtain further knowledge about an estimated model, the question of model quality arises. In this chapter we discuss some different approaches which can be used during the identification process of a system. The focus will be on methods applicable to impulse response identification problems originating from vibrational analysis experiments. We shall mainly concentrate our discussion on two different concepts; cross-validation-techniques and modal coherence techniques. The important question these methods are supposed to answer is: Do we possess any information in the collected data which falsify the obtained model? It is important to remember that we can never state that a particular estimated model is the correct one. Generally, after a successful model validation step, we can only state that in the light of the data available the estimated model cannot be falsified.

The information available to be used in the model quality assessment step can be divided into four categories; the estimated model $(\hat{A}, \hat{B}, \hat{C}, \hat{D})$, the measured data used to obtain the model (estimation data set), measured data obtained from the true system not used to obtain the model (validation data set) and other prior information such as physical insight or other types of modeling of the system.

We will in the following discussion consider the model order selection as a part of the model quality assessment of the final model, since a clear coupling between model order and model quality exists. The identification process (for off-line problems) is also always of an iterative nature where different models are estimated and compared.

The model order selection problem can be recast as a hypothesis testing problem by employing a statistical framework. An overview of such methods is given in [136]. A different path is obtained by introducing criteria with a model complexity

penalty. Among these methods we mention Akaike's information criterion (AIC) [5] and the final prediction error (FPE) [4].

6.4.1 Gap Between Singular Values

In the first identification step, using the realization algorithms by Kung or Zeiger-McEwen, the singular values of the Hankel matrix (4.7) can be used as an indication of an appropriate model order. The presence of noise and structural non-linearities usually make the Hankel matrix (4.7) to be of full rank. However, if a clear size difference exists between the n largest and the rest of the singular values of (4.16), it is natural to regard the largest singular values as originating from a linear system of order n and the smallest ones from noise and non-linearities. If a clear gap does not exist, the model order decision becomes much more difficult and other techniques, such as cross-validation or modal coherence measures should be attempted.

The singular values of the Hankel matrix offer a simple and inexpensive method to determine the model order. However, from the point of view of some applications, *e.g.*, vibrational analysis, the identified modes, including frequency, damping ratio and modal shape, are the interesting properties. The connection between singular values and modes is not straightforward. A different approach which describes the quality of the estimated model for each frequency, and thus for the modes, will be discussed in the sequel.

6.4.2 Modal Coherence

The most straightforward way to determine the validity of a state-space model (A, B, C) with respect to a measured empirical impulse response is simply to calculate the impulse response of the state-space model and compare it with the empirical one, *e.g.*, calculate the norm of the errors. This type of measure only describes the total performance of the model and gives no specific information about the accuracy of each mode.

The modes are easily accessible from the eigenvalues of the A matrix but they are fairly hidden in the empirical impulse response unless a model is estimated from the impulse response. Hence, it is somewhat difficult to obtain a distributed measure which describes the quality of each of the modes of the system (A, B, C) by comparing the empirical impulse response and the system (A, B, C).

The *modal amplitude coherence*, introduced by Juang *et al.* [62], is one approach to obtain quality measures connected to each of the estimated modes of the system. This measure uses the controllability matrix of the estimated state-space model and is only defined for state-space models derived from the realization algorithm by Kung or Zeiger-McEwen. In this section, we will generalize this measure for arbitrary estimation methods and present a practical method of how to calculate it.

Assume an impulse response $\{g_k\}_{k=1}^{N}$ and a state-space realization (A, B, C) is given. The *modal coherence* is a set of indicators γ_k, $k = 1, \ldots, n$. Each indicator γ_k is associated with one eigenvalue λ_k of the matrix A. The set of indicators γ_k is derived by comparing the extended observability and controllability matrices from

the model (A, B, C) with the extended observability and controllability matrices directly derived from the empirical impulse response.

With this quality measure we obtain a distributed measure which can tell how well a certain mode (complex conjugate eigenvalue pair of A) of the state-space model (A, B, C) reproduces the corresponding mode in a given impulse response.

A fundamental problem in the comparison is that the controllability and observability matrices must be converted to a unique common basis in order to make any meaningful comparison. In what follows we will introduce a state-space realization in a normal form as well as a normal form of a singular value decomposition of a matrix. These normal forms constitute a common unique basis.

A Normal Form for the SVD of the Hankel Matrix

Definition 6.1 In the *normal form singular value decomposition* of a matrix

$$\mathcal{H}_{ij} = U\Sigma V^T, \tag{6.36}$$

the three factors U, Σ and V are unique. □

Consider the SVD (4.16) of the Hankel matrix $\mathcal{H}_{ij}$ constructed from the given impulse response. We can then consider

$$\mathcal{O}_i^d = U_s \Sigma_s^{1/2} \tag{6.37}$$

and

$$\mathcal{C}_j^d = \Sigma_s^{1/2} V_s^T, \tag{6.38}$$

respectively, as the controllability and observability matrix of a system of order n directly inferred from the given impulse response. As previously mentioned in Chapter 4, we have

$$\mathcal{O}_i^{d\,T} \mathcal{O}_i^d = \mathcal{C}_j^d \mathcal{C}_j^{d\,T} = \Sigma_s, \tag{6.39}$$

which we, from Definition 4.1, recall as ij-balancing. Hence we can say that the data-inferred observability and controllability matrices are given in ij-balanced form.

The factorization of the Hankel matrix $\mathcal{H}_{ij}$ obtained by the SVD (4.16) is not uniquely defined. By assuming that $\mathcal{H}_{ij}$ is constructed from the impulse response of an nth order system, we can write

$$\mathcal{H}_{ij} = U_s \Sigma_s V_s^T, \tag{6.40}$$

with $U_s \in \mathbb{R}^{pi \times n}$, $U_s^T U_s = I$, $V_s^T \in \mathbb{R}^{n \times mj}$, $V_s V_s^T = I$, $\Sigma_s = \text{diag}\,(\sigma_1, \ldots, \sigma_n)$ and $\sigma_1 \geq \ldots \geq \sigma_n > 0$. This factorization is unique up to a matrix $T \in \mathbb{R}^{n \times n}$, satisfying

$$T\Sigma_s = \Sigma_s T,\ TT^T = I. \tag{6.41}$$

If (6.41) holds, a valid SVD factorization is then also

$$\mathcal{H}_{ij} = \bar{U}_s \Sigma_s \bar{V}_s^T \tag{6.42}$$

with $\bar{U}_s = U_s T$ and $\bar{V}_s = V_s T$. If we limit ourself to consider the generic case of distinct singular values in Σ_s, it is easy to show that the matrices satisfying (6.41) are of the form

$$T_s = \text{diag}(s_1, s_2, \ldots, s_n), \tag{6.43}$$

where $\{s_i\}$ are either $+1$ or -1. We now introduce a normal form for the SVD for the case of distinct singular values by requiring a positive sign of the first non-zero element in each column of U_s. Let U_s^k denote the kth column of U_s. A normal form is constructed by determining the signs in the diagonal of $T_s = \text{diag}\,(s_1, \ldots, s_n)$ in the following way.

$$\begin{aligned} \forall k \in [1, \ldots, n]: \quad & \text{If the first non-zero element in } U_s^k \text{ is negative, take } s_k = -1, \\ & \text{otherwise } s_k = 1. \end{aligned} \tag{6.44}$$

Since U_s is always of full rank, at least one element in each column U_s^k is non-zero and each sign s_k will be unique. A unique SVD factorization of $\mathcal{H}_{ij}$ will then be

$$\mathcal{H}_{ij} = \bar{U}_s \Sigma_s \bar{V}_s^T \tag{6.45}$$

where $\bar{U}_s = U_s T_s$ and $\bar{V}_s = V_s T_s$. We summarize the result in a lemma.

Lemma 6.1 *Assume that the singular value decomposition of $\mathcal{H}_{ij}$ is given by (6.40) with distinct singular values Σ_s. A normal form SVD (6.36) is then defined by the steps (6.44) and (6.45).* □

With this normal form it is possible to compare two Hankel matrices by comparing the different factors.

The ij-Balanced Normal Form

We will now continue by deriving a realization in normal form for the state-space system (A, B, C) which will match the SVD factorization above. The realization will be based on the ij-balanced realization from Definition 4.1.

Given a general minimal system (A, B, C) the following algorithm [73] will define a similarity transformation matrix T such that $(T^{-1}AT, T^{-1}B, CT)$ is in ij-balanced form. Begin by forming

$$Q = \mathcal{O}_i^T \mathcal{O}_i \tag{6.46}$$

and

$$P = \mathcal{C}_j \mathcal{C}_j^T. \tag{6.47}$$

Use the Cholesky factorization [43] to obtain

$$Q = R^T R, \tag{6.48}$$

with $R \in \mathbb{R}^{n\times n}$ and the SVD

$$RPR^T = U\Sigma^2 U^T, \tag{6.49}$$

with $U \in \mathbb{R}^{n\times n}$ and $U^TU = I$ and the diagonal matrix $\Sigma \in \mathbb{R}^{n\times n}$, $\Sigma = \text{diag}\,(\sigma_1, \ldots, \sigma_n)$, $\sigma_1 \geq \sigma_2 \geq \ldots \geq \sigma_n > 0$. The similarity transformation matrix is then defined by

$$T = R^{-1}U\Sigma^{1/2} \tag{6.50}$$

Lemma 6.2 *A minimal state-space system (A, B, C) is transformed to ij-balanced form by the similarity transformation given by (6.46)–(6.50) if* $\min(i, j) \geq n$.

Proof. From the minimality and $\min(i, j) \geq n$, it follows from Lemma 4.1 that both Q and P are positive definite symmetric matrices and hence the calculations (6.46)–(6.50) are well-defined. The transformation directly gives

$$T^T\mathcal{O}_i^T\mathcal{O}_iT = \Sigma^{1/2}U^TR^{-T}R^TRR^{-1}U\Sigma^{1/2} = \Sigma \tag{6.51}$$

and

$$T^{-1}\mathcal{C}_j\mathcal{C}_j^TT^{-T} = \Sigma^{-1/2}U^TRPR^TU\Sigma^{-1/2} = \Sigma \tag{6.52}$$

which concludes the proof. □

The ij-balanced form is not a unique realization [41, 117], since state transformations T satisfying

$$\Sigma T = T\Sigma, \;\; TT^T = I \tag{6.53}$$

also results in a new ij-balanced form. A normal form is constructed if this ambiguity is removed.

Definition 6.2 If (A_1, B_1, C_1) is input-output equivalent to the realization (A_2, B_2, C_2), a normal form is a mapping

$$M : \mathbb{R}^{n\times n} \times \mathbb{R}^{n\times m} \times \mathbb{R}^{p\times m} \to \mathbb{R}^{n\times n} \times \mathbb{R}^{n\times m} \times \mathbb{R}^{p\times m}, \tag{6.54}$$

such that

$$M(A_1, B_1, C_1) = M(A_2, B_2, C_2). \tag{6.55}$$

□

A normal form is thus such that if two models are given, we can convert both to the normal form and then compare the system matrices element by element to determine system equivalence. A normal form can also be considered as a unique basis for the states of the system.

Consider a minimal state-space realization (A, B, C) which is ij-balanced. Assume all the singular values in Σ to be distinct and ordered in a descending order

according to Definition 4.1. The basis of the states of the ij-balanced form is then unique up to similarity transformations T_s (6.43). By uniquely determining the n signs of the diagonal element of T_s a normal form will emerge as (T_sAT_s, T_sB, CT_s). This can be accomplished as follows. Construct the extended observability matrix $\mathcal{O}_i$. Each column of $\mathcal{O}_i$ have at least one non-zero element since the system is observable. The diagonal elements of T_s are uniquely given by

$$\forall k \in [1, \ldots, n]: \quad \text{If the first non-zero element in } \mathcal{O}_i^k \text{ is negative, take } s_k = -1, \text{ otherwise } s_k = 1. \tag{6.56}$$

In (6.56) $\mathcal{O}_i^k$ is the kth column of $\mathcal{O}_i$.

Lemma 6.3 *The ij-balancing algorithm (6.46)–(6.50) resulting in the minimal state-space description (A, B, C) and the sign determination of the transformation matrix T_s (6.56), result in a normal form (T_sAT_s, T_sB, CT_s), provided that the diagonal elements of Σ in (4.33) are distinct.*

Proof. Given the ij-balanced realization, with Σ having distinct singular values, it is easy to show that the only state transformation matrices which preserves the ij-balanced form is of the form T_s (6.43). The minimality implies that $\mathcal{O}_i$ have full rank and thus, each column of $\mathcal{O}_i$ have a non-zero element. The introduction of the positivity condition of the first non-zero element of each column of the extended observability matrix $\mathcal{O}_i$, makes the realization unique. □

The case of non-distinct diagonal elements in Σ can also be handled if additional steps are included, see the proof of Theorem 2.1 in [95]. The generic case, however, is distinct singular values and this will suffice for our purposes.

Theorem 6.1 *Consider an ij-balanced normal form (A, B, C) with the extended observability and controllability matrices $\mathcal{O}_i$ and $\mathcal{C}_j$, respectively, and a normal form SVD factorization (6.45) of a Hankel matrix $\mathcal{H}_{ij}$ with distinct singular values Σ_s. Then*

$$\mathcal{O}_i = \bar{U}_s \Sigma_s^{1/2} \quad \text{and} \quad \mathcal{C}_j = \Sigma_s^{1/2} \bar{V}_s^T \tag{6.57}$$

if and only if $\mathcal{H}_{ij}$ is constructed from the impulse response of the system (A, B, C).

Proof. Assume $\mathcal{H}_{ij}$ is constructed from the system (A, B, C). It then follows that

$$\mathcal{H}_{ij} = \mathcal{O}_i \mathcal{C}_j. \tag{6.58}$$

From Definition 4.1 we have the relations

$$\mathcal{O}_i^T \mathcal{O}_i = \mathcal{C}_j \mathcal{C}_j^T = \Sigma. \tag{6.59}$$

From the singular value decomposition

$$\mathcal{O}_i = \tilde{U}_o \tilde{\Sigma}^{1/2} \tilde{V}_o^T \tag{6.60}$$

note that

$$\Sigma = \mathcal{O}_i^T \mathcal{O}_i = \tilde{V}_o \tilde{\Sigma} \tilde{V}_o^T \tag{6.61}$$

and hence $\tilde{\Sigma} = \Sigma$. Σ was assumed to have distinct ordered elements on the diagonal which then implies that $\tilde{V}_o = \tilde{T}_s$ for some sign matrix $\tilde{T}_s$. From Lemma 6.3 it follows that the first non-zero element in each column in $\mathcal{O}_i$ is positive. If we impose the same condition on $\tilde{U}_o$ we conclude that $\tilde{T}_s = I$. By similar arguments we can write

$$\mathcal{C}_j = \Sigma^{1/2} \tilde{V}_c^T. \tag{6.62}$$

This results in a factorization

$$\mathcal{H}_{ij} = \mathcal{O}_i \mathcal{C}_j = \tilde{U}_o \Sigma \tilde{V}_c^T. \tag{6.63}$$

Since the first non-zero element in each column of $\tilde{U}_o$ is positive we conclude, according to Lemma 6.1, that this is a normal form SVD of the Hankel matrix. Hence

$$\Sigma = \Sigma_s, \quad \tilde{U}_o = \bar{U}_s, \text{ and } \tilde{V}_c = \bar{V}_s \tag{6.64}$$

which proves the if part. The only if part is trivial since (6.57) implies

$$\mathcal{H}_{ij} = \mathcal{O}_i \mathcal{C}_j \tag{6.65}$$

which concludes the proof. □

The above result indicates a way of comparing implicit models given in impulse response form with models in state-space form. We will now consider such a quality measure which can be calculated for each eigenvalue of A and hence can be associated with the modes of the system.

Modal Coherence

We will now generalize the modal amplitude coherence introduced by Juang *et al.* [62]. The method compares the modes from an estimated state-space model with the information contained in an impulse response. We will do this by using the normal forms derived above and diagonalize the system to obtain a decoupling of the different modes.

Consider a state-space dynamic system (A, B, C) such that A can be diagonalized,

$$\exists \text{ non-singular } T \in \mathbb{C}^{n \times n}, \; T^{-1} A T = \Lambda, \tag{6.66}$$

where $\Lambda = \text{ diag}\,(\lambda_1, \lambda_2, \ldots, \lambda_n)$ and $\lambda_i \in \mathbb{C}$ are the eigenvalues of A. Let us use this transformation to obtain a state-space realization with complex matrices

$$(\Lambda, B_c, C_c) = (T^{-1} A T, T^{-1} B, C T). \tag{6.67}$$

This realization is particularly interesting since the modes (or frequencies) of the system can be associated with the diagonal elements of Λ, which are the poles of the system. Furthermore, row k of the B_c matrix and column k of the C_c matrix are associated with the kth pole of the system. We can thus write the transfer function as the sum

$$G(z) = \sum_{k=1}^{n} \frac{1}{z - \lambda_k} C_c^k B_c^k, \tag{6.68}$$

where the superscript denotes column and row numbers, respectively.

Recall that the estimated system (A, B, C) given in ij-balanced normal form has the observability and controllability matrices $\mathcal{O}_i$ and $\mathcal{C}_j$, respectively. If T is the complex similarity transformation which diagonalizes A, the corresponding complex observability and controllability matrices are

$$\mathcal{O}_i^c = \mathcal{O}_i T, \quad \mathcal{C}_j^c = T^{-1} \mathcal{C}_j. \tag{6.69}$$

Note that the kth column of $\mathcal{O}_i^c$, as well as the kth row of $\mathcal{C}_j^c$, is associated with the kth eigenvalue λ_k.

Consider the normal form SVD factorization (6.45) of the Hankel matrix $\mathcal{H}_{ij}$. If the Hankel matrix is constructed from the impulse response of the system (A, B, C), it is clear from Theorem 6.1 that

$$\mathcal{O}_i^c = \bar{U}_s \Sigma_s^{1/2} T \text{ and } \mathcal{C}_j^c = T^{-1} \Sigma_s^{1/2} \bar{V}_s^T, \tag{6.70}$$

where T is given by (6.66).

From the two relations (6.70) we can for each eigenvalue λ_k either compare the columns of the observability relation with each other or the rows of the controllability relation or both.

Definition 6.3 The *modal observability coherence* γ_k^o is defined as

$$\gamma_k^o = \frac{|(\mathcal{O}_i^c e_k)^H \bar{U}_s \Sigma_s^{1/2} T e_k|}{(|(\mathcal{O}_i^c e_k)^H \mathcal{O}_i^c e_k||(\bar{U}_s \Sigma_s^{1/2} T e_k)^H \bar{U}_s \Sigma_s^{1/2} T e_k|)^{1/2}}, \; k = [1, \ldots, n]. \tag{6.71}$$

The *modal controllability coherence* γ_k^c is defined as

$$\gamma_k^c = \frac{|e_k^T \mathcal{C}_j^c (e_k^T T^{-1} \Sigma_s^{1/2} \bar{V}_s^T)^H|}{|e_k^T \mathcal{C}_j^c (e_k^T \mathcal{C}_j^c)^H||e_k^T T^{-1} \Sigma_s^{1/2} \bar{V}_s^T (e_k^T T^{-1} \Sigma_s^{1/2} \bar{V}_s^T)^H|)^{1/2}}, \; k = [1, \ldots, n] \tag{6.72}$$

where $\mathcal{O}_i^c$ and $\mathcal{C}_j^c$ are given by (6.69) and $\bar{U}_s, \Sigma_s$ and $\bar{V}_s$ are given by (6.45), T by (6.66) and e_k is a unit vector with a one in position k.

Furthermore, the *modal coherence indicator* (MCI) is defined as

$$\gamma_k = \gamma_k^c \gamma_k^o, \quad k = 1, \ldots, n \tag{6.73}$$

□

Given a state-space model and an impulse response, the set $\{\gamma_k\}_{k=1}^n$ of modal coherence indicators describes the "coherence" between the modes of the state-space model and the impulse response and thus serves as a distributed model quality measure.

Based on Definition 6.3 we can form a corollary to Theorem 6.1.

Corollary 6.1 *The properties of the modal coherence indicators from Definition 6.3 are*

$$\gamma_k \in [0,1], \forall k \in [1,2,\ldots,n]. \tag{6.74}$$

In particular, if the Hankel matrix $\mathcal{H}_{ij}$ and the system (A,B,C) share the same impulse response coefficients we have

$$\gamma_k = 1, \forall k \in [1,2,\ldots,n]. \tag{6.75}$$

The modal controllability coherence measure from Definition 6.3 is equal to the modal amplitude coherence introduced in [62] if the state-space model (A,B,C) originates from the algorithm by Zeiger-McEwen or the ERA-algorithm. The novelty of the introduced method is that given any state-space model and an impulse response the modal coherence can be calculated.

From the definition it follows that n modal coherence indicators (MCIs) can be calculated from a system of order n. For a complex conjugate eigenvalue pair the two corresponding MCIs will be equal. For one vibrational mode we thus only need to consider one MCI. For the real eigenvalues each eigenvalue has a unique MCI.

Stabilization Diagram

The modal coherence indicators (6.73) can be used as a quality tag attached to each of the vibrational modes of an estimated model. Each vibrational mode is characterized, among other things, by the frequency ω_k (6.9). The indicators γ_k can be used in a diagram to visualize frequency location and modal accuracy. Such a diagram is called a stabilization diagram. In a stabilization diagram the horizontal axis represents frequency and the vertical axis modal coherence. A vertical bar of length γ_k is plotted for each mode at the frequency location given by ω_k. If several models of different orders are available the corresponding bar graphs can be stacked on top of each other, starting with the model with the lowest order.

The characteristics of the diagram is that for identified models with too low order some frequencies (modes) give rise to low modal coherence indicators (the bars are short). As the model order increases these split into two or more modes with higher indicators (or disappear again). As the model order increases the identified frequencies "stabilize", hence the name stabilization diagram.

Example 6.2 An impulse response of a linear system of order $n = 8$ is given at 500 sample points. The impulse response is corrupted by additive zero mean Gaussian noise with variance 10^{-2}.

Seven models with model orders $2, 4, \ldots, 14$ respectively were estimated using the algorithm by Kung followed by a least-squares estimation of the C matrix.

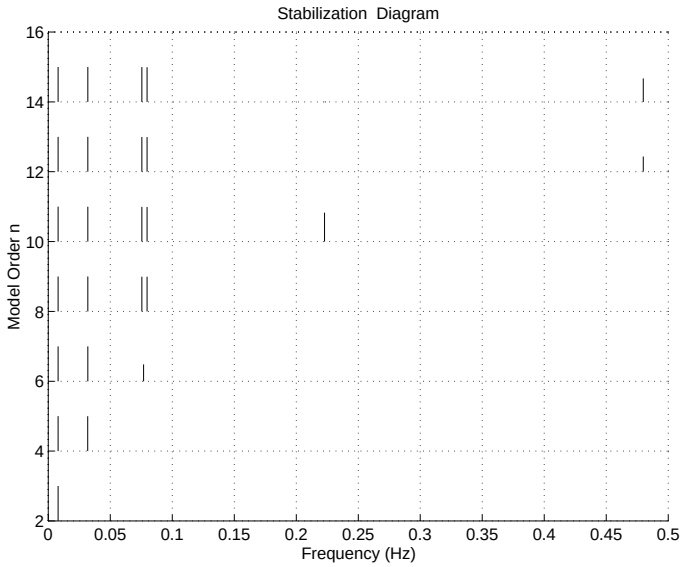

Figure 6.1: Stabilization diagram indicating identified resonance frequencies and corresponding modal coherence indicator (MCI). For each model order a bar graph is shown. The location of the bars along the horizontal axis is determined by the frequencies of the modes from the model. The length of each bar is equal to the corresponding MCI γ_k. In the figure the bar graphs for different model orders are placed on top of each other and the vertical axis show the model order. In the diagram models of orders 2 to 14 are shown.

In figure 6.1 a stabilization diagram is shown indicating the identified resonance frequencies and the corresponding modal coherence indicator (MCI). From the diagram we see that the low frequency modes (below 0.1 Hz) are accurately estimated by the lower order models. The model of order 6 (3 resonant modes) have an MCI significantly lower than 1 for the highest frequency. At model order 8 (4 resonant modes) this indicator splits up in two with high MCI. At model order 8 we see that all four indicators are high. A further increase of the model order results in low indicators for the new resonance frequencies as well as for some of the old. Based on the diagram we would thus prefer a model order of 8 (4 resonant modes) where each mode is of high quality.

□

6.4.3 Cross Validation Techniques

The most pragmatic way of validating a model is to determine its prediction performance using "fresh" data, *i.e.*, data which have not been used for the estimation of the model. A good model is such that it can accurately predict the behavior of the system even if it is confronted with data not used in the identification. The quality is easily measured if several experiments are performed on the same system

and under similar conditions. One set of measurements is then used for estimation and the other independent set to validate the model. This technique is known as cross-validation. See [86] or [139] for a more general discussion.

Cross Validation with Independent Experiments

In order to use cross validation for impulse-response-type experiments we need two data sets obtained from two impulse experiments. One data set, the estimation data, is used to obtain a state-space model. The other data set, the validation data, is used to calculate the mean square error

$$\hat{\overline{V}}(\theta) = \sum_{t=1}^{N} |\tilde{g}_t - \hat{g}_t(\theta)|^2, \tag{6.76}$$

where $\tilde{g}_t$ is the impulse response of the validation data set and $\hat{g}_t(\theta)$ is the simulated impulse response of the estimated model. Model order determination can be performed by estimating several models of different model orders and then compare the resulting values of $\hat{\overline{V}}(\theta)$. If the excitation of the different modes of the system cannot be exactly reproduced, a re-estimation of the B matrix using the validation data should be considered since the B matrix describes how the different modes are excited. This is equivalent to assuming that both the estimation data set and the validation data set originate from two free decay experiments with different initial states x_0.

Example 6.3 Consider the estimated models from Example 6.2. For each estimated model, $\hat{\overline{V}}(\theta)$ is calculated using an independent data set. The results are shown in Figure 6.2. It is clear from the graph that a suitable model order should be 8. This coincides with the order of the linear model which generated the data. □

Cross-validation Using Independent Outputs

Suppose only one data set is available, but that it consists of a large number of output channels. Then we can divide the output channels into two disjoint sets. If the division is made in such a way that all dynamic modes are present in both sets, we can estimate a model using only one set of output channels and validate using the other set. This type of validation is advantageous in some cases, *e.g.*, if non-linearities cause the damping ratio of the modes to depend on the degree of excitation. The same experiment can then also be used for validation and we are not faced with the problem of excitation levels for different experiments.

Assume that we estimate a model (A, B, C_e) using the selected estimation output channels. If we consider the validation output channels, it is easy to estimate a new output matrix C_v by minimizing the squared norm of the prediction error. This is because the impulse response is a linear function of C_v for fixed B and A. The norm of the residuals will be a measurement of the quality of the estimated model. If the residuals are small, the estimated A and B matrices thus contain all

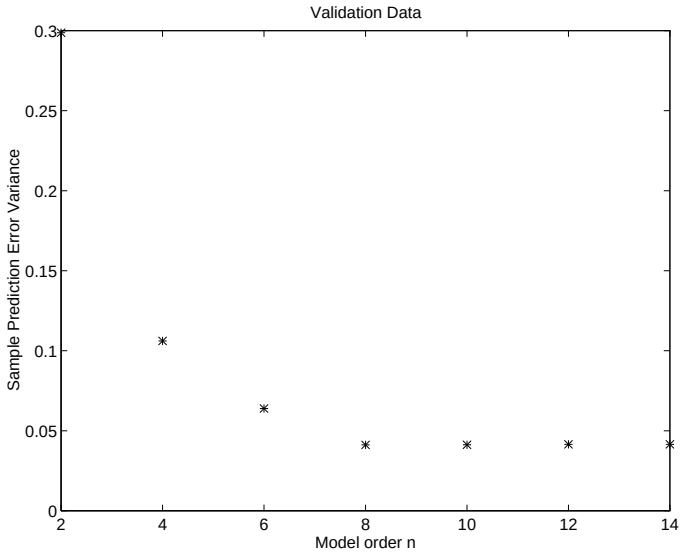

Figure 6.2: Sample prediction error variance $\hat{\overline{V}}(\theta)$ vs. model order n, calculated using independent data and the estimated models from Example 6.2.

the information relevant for predicting the validation output channels with respect to frequencies and damping ratios. The amplitudes and phases of the validation output channels are determined from the estimation of C_v.

6.5 Asymptotic Properties

As already stated in the beginning of this chapter, consistency can not be attained by letting only the number of measurements tend to infinity, since the signal-to-noise ratio tends to zero at an exponential rate for strictly stable systems.

However, if the impulse response experiment is repeated M times, each time collecting N output measurements, we can obtain a more accurate estimate of the impulse response by means of averaging over different experiments. To simplify notation we consider a single-input ($m = 1$) system. Let

$$\hat{g}_k^{(M)} = \frac{1}{M} \sum_{i=1}^{M} \tilde{g}_k^i \tag{6.77}$$

where $\tilde{g}_k^i \in \mathbb{R}^p$ is the noise corrupted measurement at time k resulting from an impulse input at time $t = 0$ in experiment i.

Assume that the measured output can be described by

$$\tilde{g}_k^i = g_k + w_k^i \tag{6.78}$$

where w_k^i are zero mean random variables with the properties

$$E\, w_k^i {w_k^j}^T = R_k \delta(i-j), \tag{6.79}$$

$$\|R_k\|_F < \infty, \quad \forall k \tag{6.80}$$

and

$$E\, w_k^i {g_j}^T = 0, \quad \forall i,k,j. \tag{6.81}$$

As a result from the law of large numbers [24], it follows that $\hat{g}_k^{(M)}$ is a consistent estimate of g_k, *i.e.*,

$$\lim_{M\to\infty} \hat{g}_k^{(M)} = g_k, \quad \text{w.p. 1.} \tag{6.82}$$

Moreover, the asymptotic variance of $\hat{g}_k^{(M)}$ will be R_k/M.

The noise influence can thus be suppressed by averaging over many experiments, which therefore always should be considered unless the noise level is negligible. Observe that assumptions (6.78)–(6.81) are rather weak, *e.g.*, noise having a rational spectrum (in time) satisfies these conditions.

6.6 Conclusions

Some techniques applicable to system identification from impulse response measurements have been considered. We have linked the realization algorithms to prediction error minimization methods. A parametrization have been introduced which minimizes the numerical complexity during the identification phase. Model order determination and model quality assessments have also been discussed. A new model quality measure have been developed which assesses the quality of a model with respect to an empirical impulse response by calculating a set of indicators corresponding to the modes of the system.

7

Applications

7.1 Introduction

In this chapter two identification applications from aircraft and space industry will be considered. Both problems are concerned with vibrational analysis of mechanical structures. Experiments, using impulse inputs, have been performed on the structures and accelerometers have been used to obtain measurements of the impulse response. The goal of the analysis, for both applications, is to verify theoretical vibrational models constructed by Finite Element Methods (FEM). The verification is done by comparing theoretical vibrational parameters with estimated quantities derived from the experimental data, *i.e.*, frequencies and damping ratios for the vibrational modes.

The purpose of our presentation is not to provide a detailed analysis of the two problems, but to show that the estimation and model quality assessment methods previously described can successfully be applied to real world problems.

The first application is from an extensive experimental vibrational analysis of the airframe structure of the Saab 2000 commuter aircraft.

The second application stems from a vibrational analysis of a rocket separation system. A separation system is a device which serves as the connection between the launcher and the payload, often a satellite. When the correct orbit is reached, after the launch, the separation system releases the payload from the launcher.

7.2 Vibration Analysis of the Saab 2000 Aircraft

7.2.1 Introduction

Analysis of vibrating structures is a very important task in the aircraft industry. This concerns both tests and analysis for validating safety and comfort properties and most often involves analyzing structural modes and damping properties.

In this section we will apply the methods described in the earlier chapters for vibration analysis and evaluate the results obtained. The data we worked with is from rather extensive tests with the new commercial aircraft Saab 2000, developed by the Saab Aircraft company.

7.2.2 The Experiments

The experimental results presented here are part of a large-scale experimental damping survey performed on the Saab 2000 aircraft. The study was aimed at revealing the damping properties and their dependence on deformation of a body-in-green fuselage/wing/nacelle assembly (see Figure 7.1). The nacelle is the outer casing of the engine. Before the test it was suspected, and verified and quantified by the test, that the damping would increase with increasing vibrational magnitude. The test was divided into two phases, the first consisting of a conventional ground vibration (normal mode) test at a low vibrational level and under stationary harmonic conditions. The second phase was a complementary high vibrational level study. The results of the tests were to be applied in the aircraft load evaluation and simulation of extremely hard landings (up to 3 m/s sink rate). The results presented in this chapter are only from the second phase of the test.

Various excitation locations and magnitudes were used during the second phase. Snap-back excitations from pre-determined deflection states were used as structural inputs. Accelerometers and load cells were used to sense the structural response. An enormous amount of data were collected during the test, out of which a selected amount has been used in this section. The results presented here were obtained during a wing-tip snap-back excitation from a moderate initial deflection state (10% of the highest excitation level used). In this test 21 accelerometers were distributed over the wings (12 accelerometers), the nacelles (6) and fuselage (3). Load cells were used to register the reactive loads on the supports and tension in the pre-stressed cables used for excitation. A sampling rate of 512 Hz was used and a total 4096 samples were collected.

7.2.3 Identification of Vibrational State-Space models

In this section we will discuss the estimation of state-space models from accelerometer data originating from the snap-back excitation.

The acceleration response to the snap-back excitation is triggered by the almost instantaneous release of cable tension. Thereafter, the accelerations are governed by the free-decay properties of the structure. In the identification procedure we considered the data as originating from an impulse excitation.

To reduce the amount of data, the measured acceleration signals were decimated with a factor of two to a sample rate of 256 Hz. To illustrate the properties of the accelerometer signals a selection of measured channels is shown in Figure 7.2. In the right hand graphs only the first 1200 samples are shown. The left graphs show the first 250 samples. We notice a large amount of resonant modes with frequencies distributed in a rather wide range.

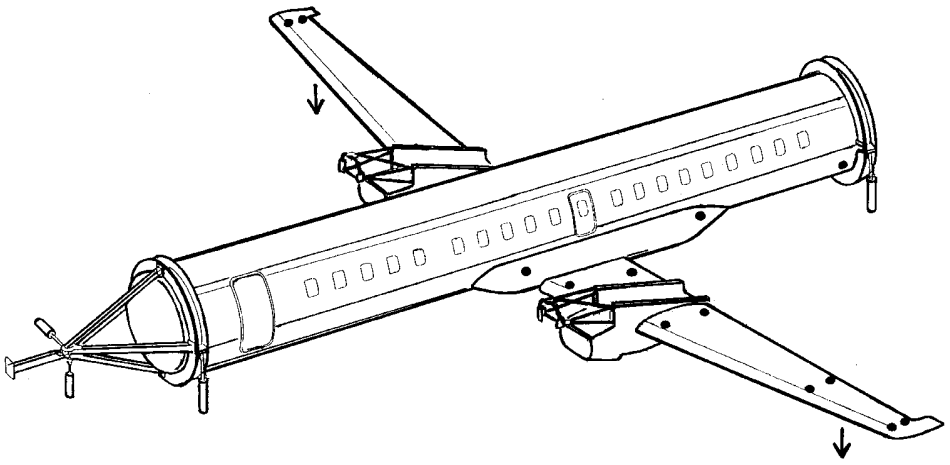

Figure 7.1: Test specimen. Location of wing and fuselage accelerometers are shown as dots (nacelle accelerometers are not shown). All shown accelerometers sense vertical accelerations. Arrows indicate location of the snap-back cables.

Based on visual inspection, the measured signals to be used in the identification were chosen to be sample numbers 26-1250. By choosing sample 26 as the first sample we assure that the snap-back excitation has fully taken place. The output channels were divided into the two disjoint sets of estimation data and validation data. The choice was based on the modal contents of each channel. The channels were grouped into 4 groups were each group represented low, low to medium, medium and high frequency content. This choice was also based on visual inspection of the 21 output channels. The validation and estimation channels were then selected by drawing from all four groups. In this way we ensured approximately the same modal contents in both data sets.

The estimation data set contains 14 accelerometer channels each consisting of 1225 samples. The validation data set contains 7 channels also with 1225 samples each. The two data sets were normalized in such a way that all signals were of equal 2-norm.

In a first step we apply Kung's algorithm, from Chapter 4. The major computational part consists of calculating the SVD of the Hankel matrix (4.7). To reduce the noise influence we choose to select $i = 80$ as the number of block rows of $\mathcal{H}_{ij}$. This choice makes the Hankel matrix almost square. For validation purposes we also calculate the SVD of the Hankel matrix of the validation data with $i = 80$. The magnitudes of the 100 largest singular values of the Hankel matrix based on the estimation data are depicted in Figure 7.3. From the figure we can draw the conclusion that a model order in the range from 10 to 30 should be considered.

In the next step, which is aimed at determining the appropriate model order we focus on both the modal coherence quality measure from Definition 6.3 and cross-validation techniques. For increasing model orders we estimate models (A, B, C) from the estimation data using Kung's algorithm and employ least-squares estima-

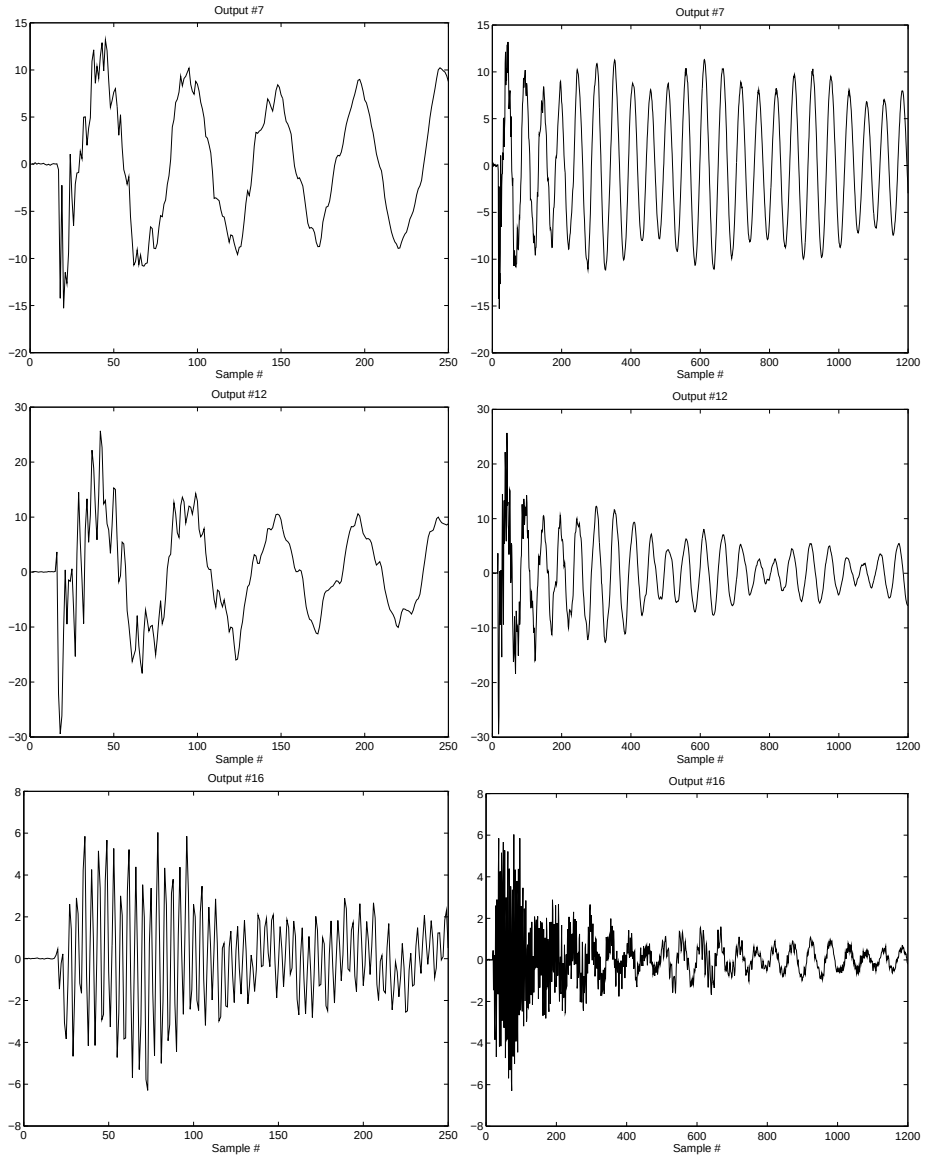

Figure 7.2: A selection of measured accelerations at different points of the test specimen from the snap-back excitation experiment. Notice the large amount of modes with frequencies distributed in a rather wide range. Left graphs show the first 250 samples of the corresponding graphs to the right. The data shown is after the decimation step and thus corresponds to a sampling frequency of 256 Hz.

tion of the C matrix to refine the models. Recall that the SVD is already calculated so each new estimation is almost instantaneous. Each estimated model is validated

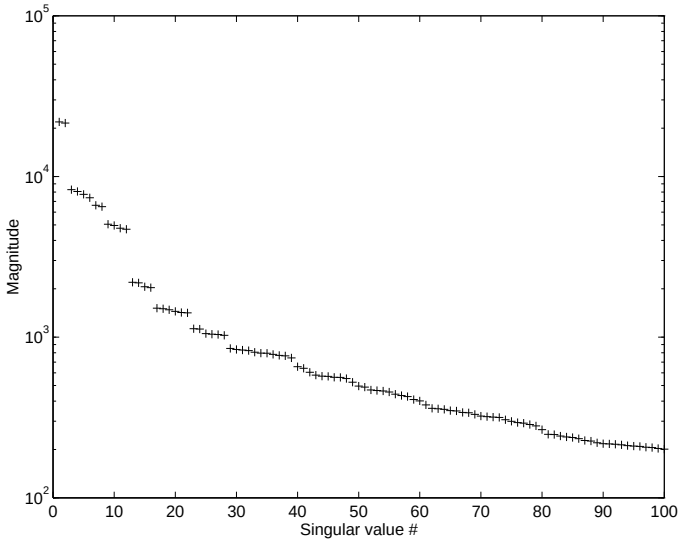

Figure 7.3: The graph shows the 100 largest singular values of the Hankel matrix based on the estimation data.

by re-estimating a C matrix, denoted by C_v, now using the validation data set. As a quality measure we use

$$\hat{\overline{V}} = \frac{1}{N}\sum_{k=1}^{N} |g_k - \hat{g}_k|^2, \tag{7.1}$$

where $\{g_k\}$ is the validation data set and $\{\hat{g}_k\}$ is the impulse response from the state-space model (A, B, C_v). Also for each estimated model we calculate the modal coherence indicators (MCI) γ_k using the estimated model (A, B, C_v) and the validation data set. In Figure 7.4 the resulting $\hat{\overline{V}}$ for models of even order from 10 to 22 is shown. The left graph depicts $\hat{\overline{V}}$ calculated on the estimation data while the right graph shows $\hat{\overline{V}}$ calculated on the validation data. From the two graphs it is not completely clear which model order to apply. However, from both graphs we can however conclude that a model order of at least 14 is required. A possible candidate is also 22 since $\hat{\overline{V}}$ calculated from the validation data is significantly reduced for this model order.

In Figure 7.5 two stabilization diagrams are shown. The left diagram is calculated using the estimation data and the right one using the validation data. Each diagram is composed of a sequence of bar graphs. For each estimated model a bar graph is drawn. The position of the bars along the horizontal axis is determined by the frequency of the estimated modes. The length of each bar is equal to γ_k, the corresponding MCI. A tall bar (maximum is 1) indicates modes of high qual-

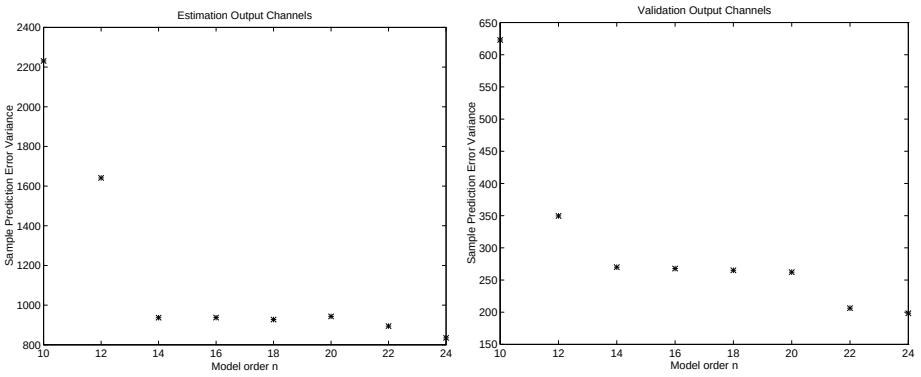

Figure 7.4: $\overline{\hat{V}}$ calculated from the estimation data set (left graph) and from the validation data set (right graph). In the graphs the result from estimated models of orders 10 to 24 are depicted. The models are estimated using Kung's algorithm followed by a re-estimation of the C matrix.

ity. In the left diagram which corresponds to the estimation data we can identify 7 modes with high MCI for models of order 14 and higher. Two, in frequency, closely spaced modes around 5 Hz can only be seen as one bar in the diagram. In the right graph, corresponding to the validation data, the same modes except one also have high indicators. A possible explanation to why the MCI for the mode at 60 Hz is low is that the validation channels do not contain this mode. Hence, the division between estimation and validation channels is not appropriate. For models with orders larger and equal to 22 a high quality mode appears in the right diagram. This might indicate that the validation channels contain a mode which is not very significant in the estimation data.

Based on this we decide to use model order 14 in the subsequent identification work since it adequately models the 7 dominant modes.

Once the model order is decided upon we now focus on prediction error minimization by parametrizing the model and perform a Gauss-Newton optimization. We use all 21 accelerometer channels to obtain the best possible model given the data at hand. A new Hankel matrix is constructed with the number of block rows $i = 55$. Kung's algorithm is employed to estimate a model of order 14 and it is followed by the least-squares estimation of C (6.19). This initial model is transformed to the block-diagonal form (6.32) to allow a minimal parametrization. This model structure has 14 parameters in the block diagonal A matrix and 14×21 parameters in the C matrix which yields a total of 308 parameters to be estimated. This might seem as a very large amount of parameters for a non-linear optimization. However, since the major part of the parameters originate from the C matrix, the corresponding gradient calculations for these parameters are particularly simple. The results from the estimation are presented in the next section.

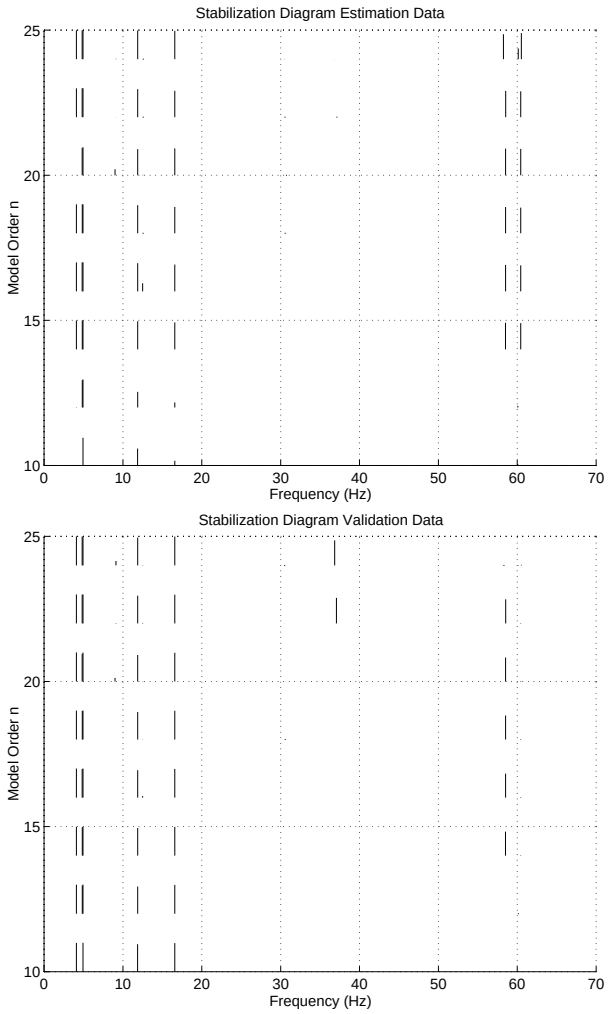

Figure 7.5: Stabilization diagram calculated from the estimation data and the estimated models (top graph) and from validation data (bottom graph). In the diagrams estimated models of order 10 to 24 are shown. The models are obtained by employing Kung's algorithm followed by least-squares estimation of the C matrix. For each model order a bar graph is shown. The location of the bars along the horizontal axis is determined by the frequencies of the modes in the model. The length of each bar is equal to the corresponding MCI γ_k. In the figure the bar graphs for different model orders are placed on top of each other and the vertical axis shows the corresponding model order.

7.2.4 Results

The results from the three subsequent identification steps are detailed in Table 7.1. Calculated on all data the loss function $\overline{\hat{V}}$ from (7.1) is reduced from the initial

	Kung's alg.	C re-est.	PEM
$\hat{\overline{V}}$	1235	1221	1177

Table 7.1: Model quality for estimated models of order 14. The quality measure $\hat{\overline{V}}$ (7.1) is the average squared 2-norm of the difference between the measured signals and the model.

Kung's alg			PEM		
f (Hz)	ζ (%)	MCI γ	f (Hz)	ζ (%)	MCI γ
4.1031	0.4594	0.9980	4.1056	0.4685	0.9985
4.8445	-0.0402	0.9974	4.8376	0.0264	0.9966
4.9398	0.4512	0.9994	4.9420	0.4139	0.9997
11.8644	1.1942	0.9910	11.8756	1.1677	0.9861
16.5732	1.1685	0.9891	16.5857	1.1580	0.9960
58.4829	1.1304	0.9536	58.3674	1.3413	0.9560
60.4157	0.3013	0.9730	60.4292	0.4157	0.9850
	Average:	0.9859		Average:	0.9883

Table 7.2: Modal parameters of estimated model of order 14. All 21 output channels have been used in the estimation. Notice that one mode, $f = 4.84$, of the the initial model delivered by Kung's algorithm is unstable.

value of 1235 to 1177. The least-squares estimation of C followed by the prediction error minimization reduced $\hat{\overline{V}}$ by 4.7%.

In Table 7.2 the estimated modal frequencies, damping ratios and corresponding MCIs are presented. Notice that one mode, $f = 4.84$, of the the initial model delivered by Kung's algorithm is unstable. The subsequent PEM iterations, however, yielded a stable model.

From the high modal coherence indicators we can conclude that all identified frequencies are of high quality.

In Table 7.2 the average of the MCIs γ_k are shown. We see from the average values that the prediction error minimization step improved the overall modal coherence. The PEM step has moved the frequencies only marginally but the damping ratios are more affected.

A comparison between the simulated impulse response from the estimated model and the measured signals are shown in Figure 7.6 for a selection of three accelerometer channels. The left graphs depict the initial 150 samples of the graphs shown to the right. All the graphs indicate that the estimated model is of high quality both for high frequency modes as well as for the low frequency ones.

7.2.5 Discussion

We have found that the identification methods described in the previous chapters have produced a state-space vibrational model which describes the measured accel-

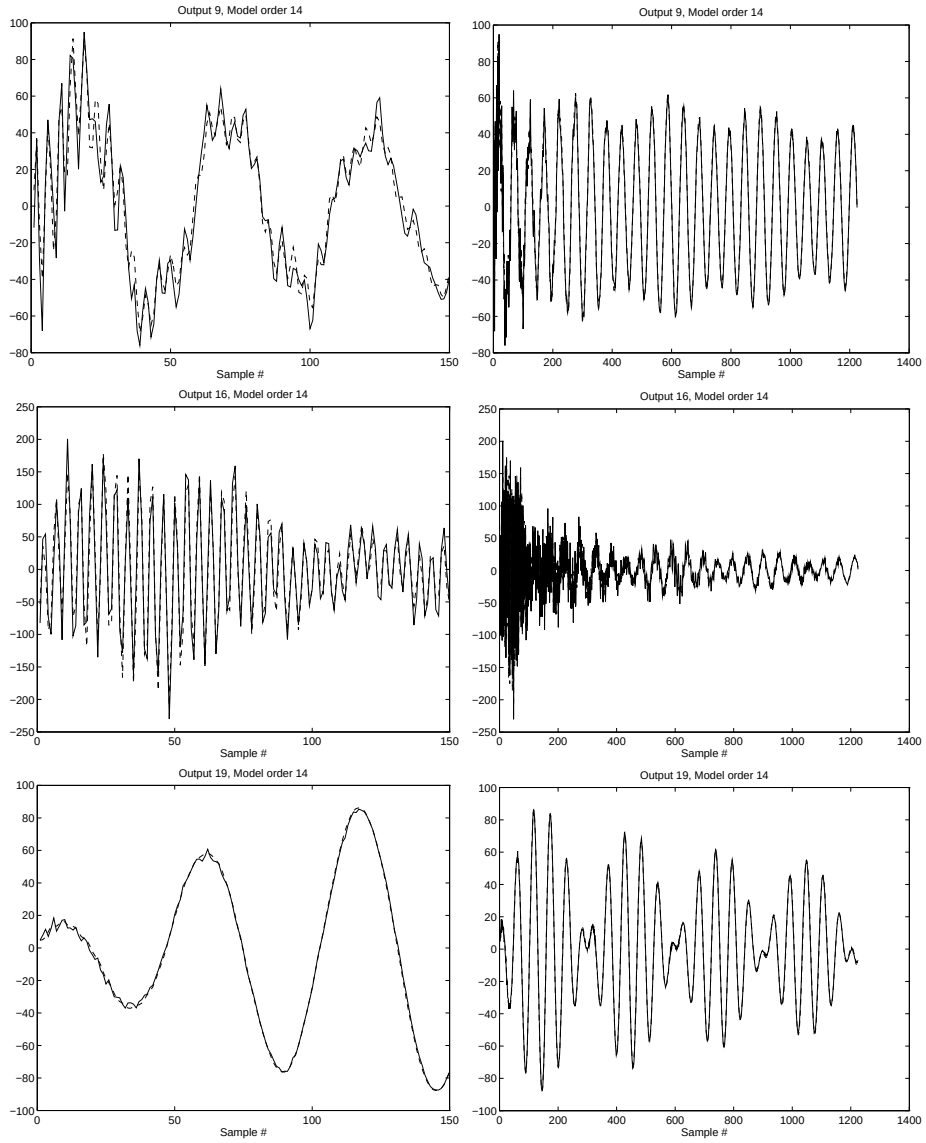

Figure 7.6: Selected measured (solid) and simulated (dashed) normalized accelerations. The simulated outputs originate from an estimated model of order 14. Top graphs show wing tip vertical acceleration. Middle graphs show nacelle lateral acceleration and bottom graphs show vertical acceleration of rear fuselage. The left graphs show the 150 first samples of the corresponding right graphs.

erations with high accuracy. In particular we found that Kung's algorithm provides models of high quality. However, subsequent minimization of the prediction errors improves the model quality even further. Moreover, the modal coherence quality

measure provides significant aid, both when deciding model order and in the evaluation of the final model. As a result, the estimated modal frequencies and damping ratios can be used to validate the analytical FEM model. Even though the amount of data is quite large the computational load is manageable.

We can also mention that the computationally inexpensive re-estimation of the C matrix always provided significant improvements compared to the initial model obtained from Kung's algorithm.

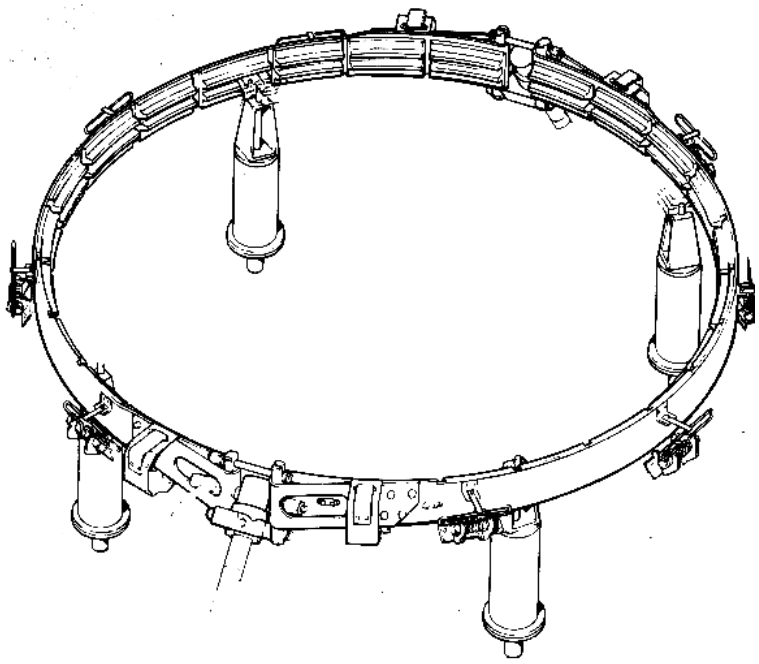

Figure 7.7: A clamp band of a separation system which attaches the satellite to the rocket launcher.

7.3 Vibration Analysis of a Satellite Separation System

7.3.1 Introduction

A separation system is a mechanical device which attaches a satellite to a rocket-launcher. It serves the purpose of keeping the satellite in place on top of the launcher during the launch phase and when the launcher has reached the correct orbit, releases it from the launcher. The system consists of a clamp band, a clamp band retention set, a separation spring set and pyro bolt cutters. The clamp band consists of two steel band halves, joined together by two connecting bolts. The band tension provides a pressure on the clamp which attaches the satellite to the launcher. The pyro bolt cutters cut the connecting steel bolts, thereby releasing the band halves and freeing the satellite from the launcher. The clamp band retention set consists of extractors and catchers which are fastened to the adaptor structure and attached to the clamp band. The retention set is extracting and parking the clamp band after the release of the satellites. The separation springs are mounted on the adaptor and exert the requested energy for a safe satellite separation. In Figure 7.7 an illustration of a clamp band of a separation system is shown.

The manufacturer, Saab Ericsson Space AB, uses vibrational measurements from release experiments in order to evaluate performance and determine the op-

timal tension in the clamp band. Requested features of the system are, among others, high load capability, low shock generation and, of course, reliability.

The experimental vibrational data has been made available to the author by courtesy of Saab Ericsson Space AB, Linköping, Sweden.

7.3.2 The Vibration Experiment

The vibrational data consist of measurements from a separation experiment. When the bolts are cut by the explosive charge the tension in the clamp band induces oscillations. Three accelerometers are sensing radial accelerations on the clamp band. During the experiments a sampling frequency of $f = 32768$ Hz was used. For each of the three channels 4096 samples were collected. In Figure 7.8 the full measurement records are shown.

From finite element modeling (FEM) it is expected that two vibrational modes in the range from 1000-1500 Hz should exist. Our goal is to try to verify the existence of such modes from the experimental data and provide accurate information about frequencies and damping ratios.

7.3.3 Identification

By studying the graphs in Figure 7.8, as well as the corresponding spectra obtained from the fast Fourier transform, it is clear that a large part of the signal energy is located above the frequency band of interest. We therefore employ pre-filtering of the accelerometer signals to zoom in on the interesting frequency interval. A Butterworth band-pass filter of order 10 with pass-band between 1000 to 1460 Hz is used on the data. From the filtered data, samples 331 to 2000 were retained for the identification. All accelerometer channels were normalized to achieve equal 2-norms. Since only three channels are available we use all in the identification. Hence, cross-validation cannot be performed.

A Hankel matrix with $i = 75$ block rows were constructed. This choice of block rows, which not provides a square Hankel matrix, originates from numerical problems with the SVD algorithm. All choices of a larger i resulted in convergence problems for the SVD algorithm.

Initially, a set of models with model order ranging from 2 to 20 were estimated with Kung's algorithm and refined by least-squares estimation of the C matrix. For each of the estimated models we calculate the Modal Coherence Indicators (MCI) as well as the sample prediction error variance $\hat{\overline{V}}$. In Figure 7.9 the results are shown in the form of a stabilization diagram and a plot of $\hat{\overline{V}}$. In the stabilization diagram we notice two frequencies with rather high MCIs, one around 1350 Hz and the other around 1230 Hz. The sample prediction errors have a rather inconsistent behavior. This might be an indication of non-linearities occurring in the data. The result is that Kung's algorithm seems to provide less accurate estimate for model orders 10, 12 and 14. A model order of 16 is decided upon since it provided high MCIs for the previous mentioned frequencies as well as a low value of $\hat{\overline{V}}$.

The initial state-space model provided by Kung's algorithm is converted to the block diagonal form (6.32) and parametrized accordingly. With the para-

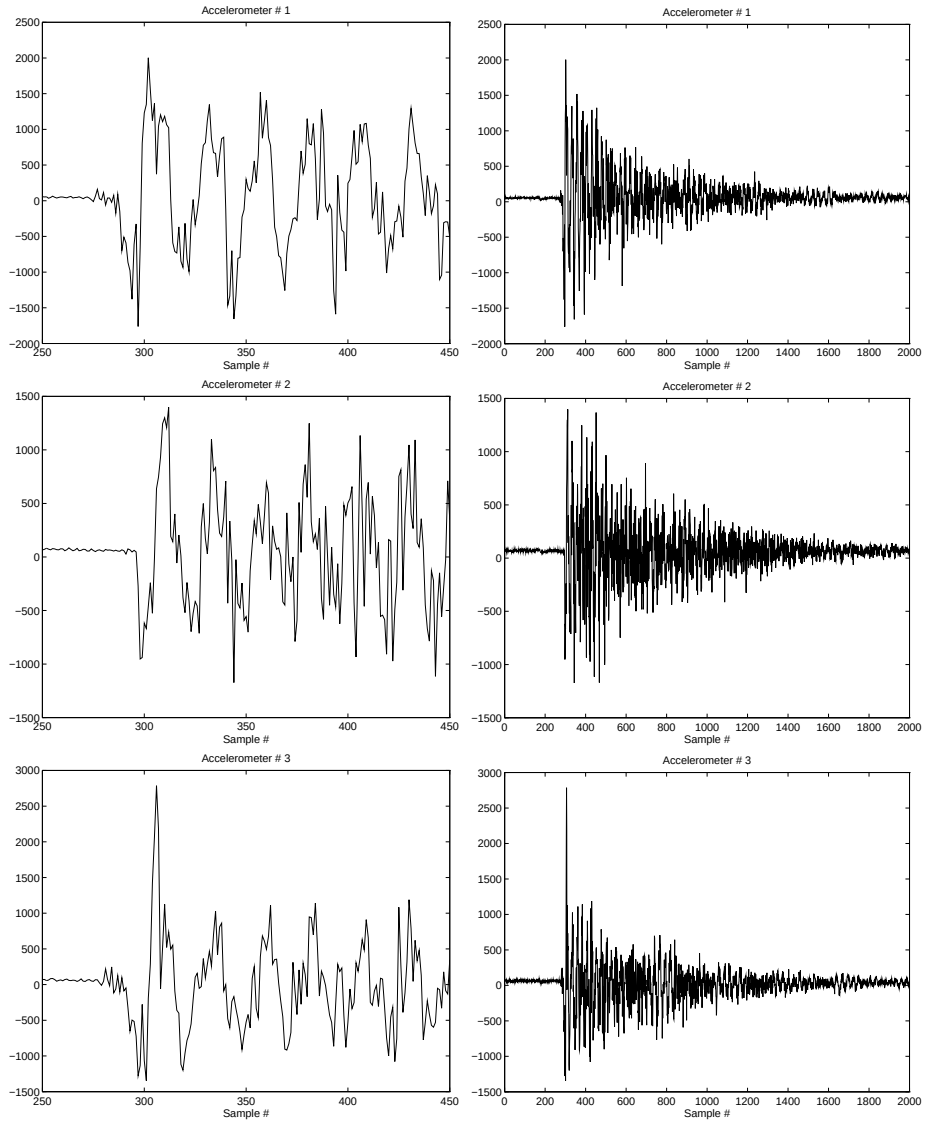

Figure 7.8: Radial acceleration measurements of the clamp band of a separation system. The measurements originate from a separation experiment simulating the release of a satellite from the launching rocket. Left graphs shows the first 200 samples of the right graphs in more detail. The measured data is obtained at a sampling frequency of 32768 Hz.

metrized model, prediction error minimization was performed by employing the Gauss-Newton algorithm outlined in Chapter 3.1.2.

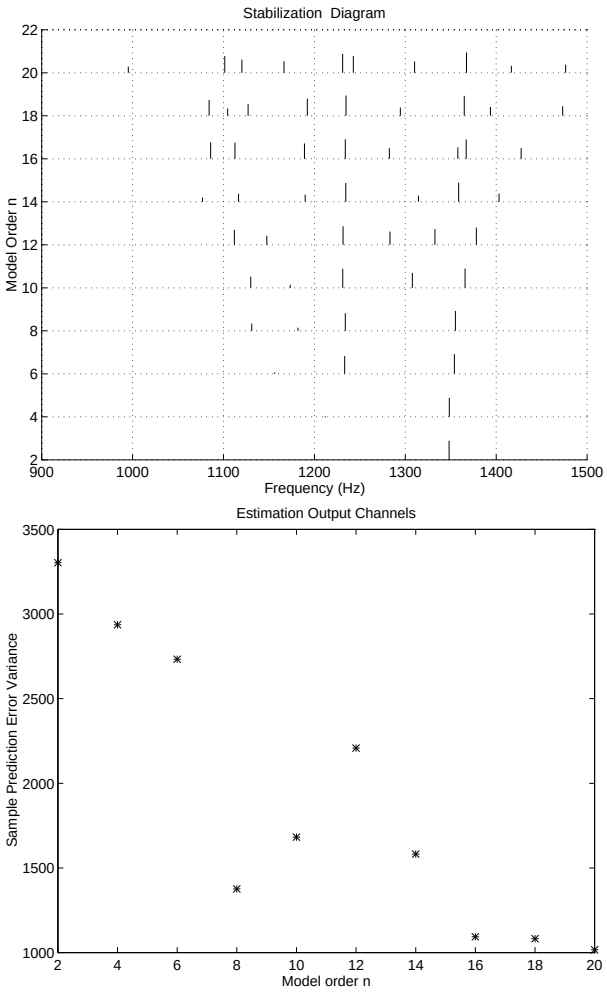

Figure 7.9: Stabilization diagram (top) and sample prediction error variance $\hat{\overline{V}}$ (bottom). The models are estimated from the bandpass filtered data employing Kung's algorithm and least-squares estimation of the C matrix. The graphs show estimated models of order 2 to 20.

7.3.4 Results

The non-linear prediction error minimization reduced the prediction errors considerably. In Table 7.3 the sample prediction error variance are shown for the 16th order model after each identification step. The improvement provided by the second and third steps reduces $\hat{\overline{V}}$ by 92%.

The identified frequencies and damping ratios are shown in Table 7.4 together with the corresponding MCIs γ_k. The two modes with frequencies 1235.7 and

	Kung's alg.	C-est.	PEM
$\hat{\overline{V}}$	1094	530.1	92.22

Table 7.3: Model quality for estimated model of order 16. $\hat{\overline{V}}$ is the average squared 2-norm of the difference between measured impulse response and the impulse response from the estimated model.

		Kung's alg.			PEM
f (Hz)	ζ (%)	MCI γ	f (Hz)	ζ (%)	MCI γ
1085.9	6.0169	0.6861	1123.9	4.2357	0.3563
1112.6	0.6875	0.5921	1125.6	1.0321	0.5449
1189.1	1.0392	0.7619	1187.2	1.8926	0.5558
1234.0	0.7066	0.8730	1235.7	0.6332	0.9351
1282.5	0.4668	0.5082	1310.1	1.4891	0.6250
1357.9	0.2507	0.5816	1351.3	0.7351	0.8093
1367.0	1.2983	0.9173	1357.9	1.1559	0.8735
1427.4	1.1080	0.6619	1426.1	3.9496	0.6511
	Average	0.6978		Average	0.6689

Table 7.4: Frequencies, damping ratios and corresponding modal coherence indicators (MCI) for estimated models of order 16.

1357.9 have the highest MCIs. We notice that the average MCI decreases after the PEM iterations. This gives us another indication that the data might contain non-linear components.

Since we used a band-pass pre-filter to zoom in, we might have ended up estimating the poles of the filter as well as the poles of the system. In Table 7.5 the frequencies and damping ratios of the poles of the Butterworth filter are shown. By comparing frequency locations and damping ratios from Tables 7.4 and 7.5 we conclude that the identified modes do not directly originate from the filter.

A comparison between the filtered measured accelerations and the resulting impulse response of the estimated model is illustrated by Figure 7.10. The fit between the two signals is very good. The linear model describes the measured data very well. However, most of the estimated modes are uncertain in the light of the MCI in Table 7.4. A possible explanation is that the vibrations originate from only a few modes but do not completely linearly propagate through the mechanical structure. An improved fit can thus be achieved by increasing the model order and identifying more "linear modes" which are not true vibrational modes. This would explain why only a few modes obtain high MCI in spite of a quite good fit between measured and simulated data.

f (Hz)	ζ (%)
1007.2	5.8038
1066.8	15.3353
1187.0	19.0473
1337.6	15.2741
1444.8	5.7656

Table 7.5: Frequencies, damping ratios for the 10th order Butterworth filter used in the pre-filtering.

7.3.5 Discussion

In this real-world application we are faced with data which not entirely lends itself to be modeled with a linear dynamic model. Kung's algorithm does not provide models which are close to the minimum of the prediction error criteria. If the goal is to minimize the prediction errors the non-linear prediction error minimization is crucial for these data. The use of a band-pass pre-filter provides the desired frequency zooming effect and does not seem to perturb the obtained results.

7.4 Conclusions

The applications treated in this chapter are concerned with vibrational experiments of mechanical structures. The realization algorithm by Kung, which is outlined in Chapter 4, have been used together with prediction error minimization, as described in Chapter 6, to estimate discrete time linear state-space models. It is pointed out that the model quality can be significantly improved by employing the PEM method with the model from Kung's algorithm as an initial model. In the second application the fit between measured and simulated signals improved by 92%. The models obtained are analyzed and validated by means of both Cross-Validation and by studying the modal coherence indicators introduced in Section 6.4.2. The MCIs gave significant guidance in the model order selection step as well as for assessing the quality of the estimated models.

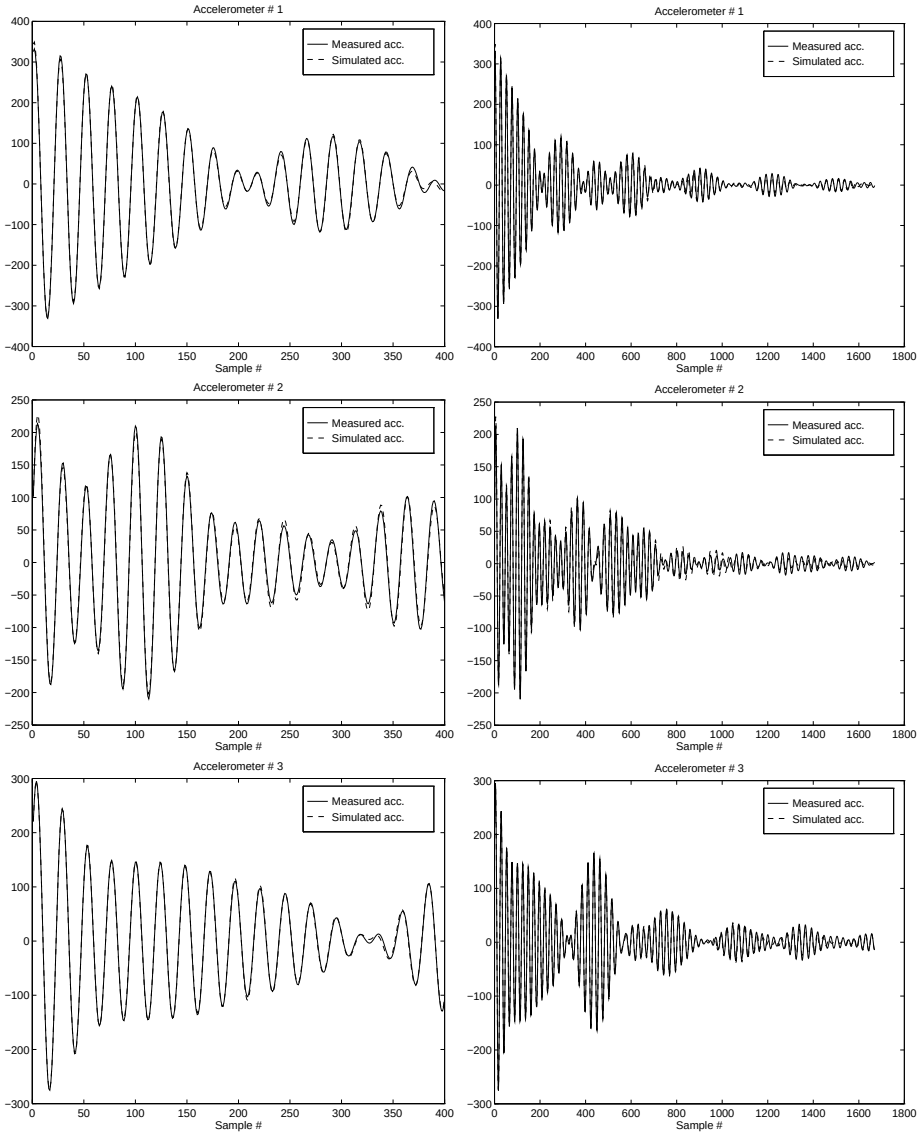

Figure 7.10: Filtered normalized radial acceleration measurements used in the estimation (solid) and simulated from a model of order 16 (dashed). Left graphs shows the first 200 samples of the right graphs in more detail.

Part II

Frequency Domain Methods

8

Frequency Domain Identification

This chapter introduces the subject of identification in the frequency domain. Although most primary measurements of physical systems are done in the time domain, it can in many cases be fruitful to view frequency domain quantities as the primary measurements. In many applications, such as control engineering, it is common practice to characterize systems and signals by their frequency domain properties, *e.g.*, the properties of a closed loop control system can be predicted from either the Nyquist plot or the Bode diagram of the open loop transfer function.

A number of so called non-parametric methods exist which transform time domain measurements into the frequency domain. The Fourier transform techniques play a key part in such methods and in particular the fast Fourier transform (FFT). In modern measuring equipment, such as HP spectrum analyzers, it is possible to directly obtain samples of the Fourier transforms as primary data. In the step from time domain measurements to frequency domain data most techniques also incorporate some sort of data and noise reduction.

The goal of this chapter is to display and discuss some advantages which are particular for frequency domain identification methods in order to motivate the study and development of new frequency domain identification algorithms. We will also briefly review some of the dominating approaches in the area.

8.1 Introduction

The Fourier Transform

Let $x(t)$ be a continuous-time signal belonging to the class

$$\mathcal{L}_1 = \left\{ x(t) \;\middle|\; \int_{-\infty}^{\infty} |x(t)|\, dt < \infty \right\}.$$

For $\mathcal{L}_1$ signals the continuous-time Fourier transform is defined as

$$X(\omega) = \int_{-\infty}^{\infty} x(t)e^{-j\omega t}\,dt,$$

and the inverse transform is given by

$$x(t) = \frac{1}{2\pi}\int_{-\infty}^{\infty} X(\omega)e^{j\omega t}\,d\omega.$$

Let $x(k)$ denote the discrete time signal obtained by uniformly sampling of $x(t)$ at the time instants $t = kT$, $k = 0, \pm 1, \pm 2, \ldots$. Here T denotes the sampling period. $x(k)$ will then belong to the class

$$\ell_1 = \left\{ x(k) \;\middle|\; \sum_{k=-\infty}^{\infty} |x(k)| < \infty, \right\}$$

and the time-discrete Fourier transform of $x(k)$ is given by

$$X_T(\omega) = T\sum_{k=-\infty}^{\infty} x(k)e^{-j\omega kT}.$$

The inverse time-discrete Fourier transform is given by

$$x(k) = \frac{1}{2\pi}\int_{-\frac{\pi}{T}}^{\frac{\pi}{T}} X_T(\omega)e^{j\omega kT}\,d\omega.$$

The relation between the continuous-time Fourier transform of a signal $x(t)$ and the time-discrete Fourier transform of the sampled signal is given by Poisson's summation formulae

$$X_T(\omega) = \sum_{k=-\infty}^{\infty} X(\omega + k\omega_s), \quad -\frac{\omega_s}{2} \le \omega \le \frac{\omega_s}{2},$$

where $\omega_s = \frac{2\pi}{T}$ is the sample frequency in (rad/s). For the important case of a band limited signal, *i.e.,*

$$X(\omega) \equiv 0, \quad |\omega| \ge \frac{\omega_s}{2},$$

the two transforms coincide

$$X_T(\omega) = X(\omega),$$

and we can exactly reconstruct the continuous-time signal from the sampled counterpart. For signals with infinite energy, scaled transforms can be introduced to ensure finiteness of the Fourier transform. Most often we shall assume $T = 1$, and drop the explicit notation of T. The notation $X(\omega)$ will be used for both transforms and we let the context resolve any ambiguities.

In practice, only a finite number of data are available. For this case we define the discrete Fourier transform (DFT)

$$X(\omega) = \sum_{k=0}^{M-1} x(k)e^{-j\omega k},$$

which is equal to the time-discrete Fourier transform if we assume $x(k) = 0$ for $k < 0$ and $k \geq M$. If we calculate the transform at M frequencies

$$\omega_k = \frac{2\pi k}{M}, \quad k = 0, \ldots, M-1,$$

the original signal can be recovered by the inverse DFT

$$x(k) = \frac{1}{M} \sum_{t=0}^{M-1} X(\frac{2\pi t}{M}) e^{j2\pi kt/M}.$$

If the number of data is an integer power of 2, *e.i.* $M = 2^k$, the DFT can be calculated with a fast radix-2 algorithm called the fast Fourier Transform (FFT) [115].

Linear Dynamic Models

Often linear dynamic models are sought which can reproduce the data to an acceptable accuracy. Such a system identification step can also be considered as data reduction, since the complexity of the identified model in most cases is much less than the amount of primary data used to produce the model.

The relationship between the transformed input and output signals for linear systems is conveniently given by the transfer functions of the systems. For continuous-time causal systems, the input-output relation is given by

$$y(t) = \int_0^\infty h(\tau)u(t-\tau)\,d\tau + g_0 u(t),$$

where $y(t) \in \mathbb{R}^p$ is the output, $u(t) \in \mathbb{R}^m$ is the input and $h(t) \in \mathbb{R}^{p\times m}$ is the weighting function. By defining the Markov parameters [66]

$$g_{k+1} = \left.\frac{d^k h(t)}{dt^k}\right|_{t=0}, \quad k = 0, 1, \ldots$$

the frequency domain formulation becomes

$$Y(\omega) = G(j\omega)U(\omega),$$

where $G(s)$ is the transfer function of the continuous-time system given by

$$G(s) = \sum_{k=0}^{\infty} g_k s^{-k}.$$

For the discrete time case, the input-output relation is given by the convolution

$$y(t) = \sum_{k=0}^{\infty} g_k u(t-k),$$

where $g_k \in \mathbb{R}^{p\times m}$ is the impulse response. The frequency domain formulation is

$$Y(\omega) = G(e^{j\omega})U(\omega),$$

where $G(z)$ is the discrete time transfer function given by

$$G(z) = \sum_{k=0}^{\infty} g_k z^{-1}.$$

In the frequency domain the only difference between continuous-time and discrete time models is which argument, s and $j\omega$ or z and $e^{j\omega}$, we use in the transfer function. To simplify notation we introduce the generic symbol ξ to denote the transform variable in either domain.

Excitation Signals

The periodic excitation signals

$$u(t) = u(t \pm Mk), \quad k = 0, 1, \ldots$$

of period time M form a class of signals important for frequency domain identification. This stems from the fact that after the initial transient of a linear system, the output signal $y(t)$ also becomes periodic. In the single input case, the discrete Fourier transform over one period of the input and output signals exactly satisfy [20]

$$G(e^{j\omega_k}) = \frac{Y(\omega_k)}{U(\omega_k)}, \quad \omega_k = \frac{2\pi k}{M}, \quad k = 0, \ldots, M-1$$

if $U(\omega_k) \neq 0$, $\forall k$.

The harmonic excitation method is a classical way of directly measuring the frequency response. A pure sinusoid of frequency ω is applied to the input. When the system becomes stationary the amplitude and phase-shift equal the frequency response function at $j\omega$. By averaging over many periods, a significant noise reduction can be obtained directly at the measurement site.

A much deeper discussion about various kinds of excitation signals and their properties is given by Schoukens and Pintelon in [129].

The Identification Problem

If samples of the transform functions $Y(\omega)$ and $U(\omega)$ are known at a set of frequencies ω_k, the issue of transfer function identification arises. What is sought is a linear model in the form of a transfer function $\hat{G}(\xi)$ such that

$$Y(\omega_k) = \hat{G}(\xi_k)\, U(\omega_k), \quad k = 1, \ldots, M \tag{8.1}$$

holds. Here $\xi_k = j\omega_k$ for continuous-time models and $\xi_k = e^{j\omega_k}$ for discrete time models. In general, (8.1) is not feasible since all real world systems are nonlinear and/or the measured input and output signals are subject to errors due to measurement noise and other forms of inaccuracies. Depending on what prior information is available and the intended use of the model, a large number of methods are available. Most existing frequency domain identification methods for SISO systems use a parametric model structure of the form

$$G(\xi,\theta) = \frac{b(\xi,\theta)}{a(\xi,\theta)}, \tag{8.2}$$

where $b(\xi,\theta)$ and $a(\xi,\theta)$ are polynomials in ξ of some predetermined degree. We will return to the issue of model structures in Section 8.3. Most estimation algorithms determine the model G by a parametric optimization of some weighted least-squares criterion

$$\hat{\theta} = \arg\min_{\theta} \frac{1}{M} \sum_{k=1}^{M} W(\xi_k,\theta) \left| a(\xi_k,\theta)Y(\omega_k) - b(\xi_k,\theta)U(\omega_k) \right|^2 .$$

Different choices of weighting functions $W(\xi_k,\theta)$ reveal different estimators described in the literature, see *e.g.*, [120].

Before we start to discuss various aspects of frequency domain identification in detail, we first consider a small identification example.

Time versus Frequency Domain

In this introductory example we apply both a time domain technique as well as a frequency domain technique to identify a simple second order system. The system is given by the difference equation

$$y(t) = \frac{q + 0.5}{q^2 - 1.5\,q + 0.7} u(t) + e(t), \tag{8.3}$$

where $e(t)$ is a white noise sequence of zero mean and variance equal to 5. A data set of length 400 is generated by applying a pseudo-random binary sequence $(+1, -1)$ as the input to the system with zero initial conditions. The input signal has most energy in the lower frequencies.

A time domain model is estimated using the standard prediction error minimization procedure with an output error model structure of order 2. The estimation is performed using the command `oe` in MATLAB's System Identification Toolbox [88], *i.e.*,

$$\hat{\theta} = \arg\min_{\theta} \sum_{k=1}^{M} |y(t) - \frac{b(q,\theta)}{a(q,\theta)} u(t)|^2,$$

and the estimate is determined by Gauss-Newton iterative numerical search. The frequency domain estimation starts by forming the finite discrete Fourier transforms (DFT) of the inputs and outputs, $U(\omega_k)$ and $Y(\omega_k)$, and subsequently solves

$$\hat{\theta} = \arg\min_{\theta} \sum_{k=1}^{M} |Y(\omega_k) - \frac{b(e^{j\omega_k},\theta)}{a(e^{j\omega_k},\theta)} U(\omega_k)|^2$$

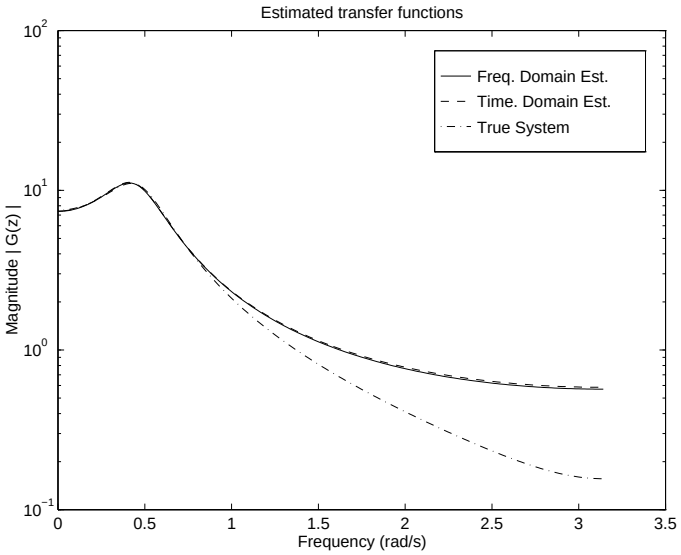

Figure 8.1: Identification results.

also using Gauss-Newton iterations.

The estimated transfer functions are depicted together with the true transfer function in Figure 8.1. The estimated transfer functions are almost identical. The deviations between the true system and the estimated models in the higher frequencies are due to a rather low signal to noise ratio. The zero initial condition implies that the Fourier transform of the output signal is subject to leakage since the system output is not a periodic signal. Leakage is when the energy of a spectral line is smeared throughout the frequencies in the form of side lobes in the DFT [68, 129]. This is due to finite measurement time. Only if the DFT is formed from a full period of a periodic signal, the DFT will be free from leakage. However, for this example, this fact does not disturb the result compared to the time domain estimated model. The time domain estimation could be expected to perform better since the zero-initial condition is implicitly assumed in this method.

To summarize, this trivial example shows that frequency domain identification can be applied in a straightforward way in the frequency domain with almost identical results as obtained from the time domain method.

8.2 Frequency Domain Advantages

Many distinct features can be associated with the frequency domain approach and we shall here list a few of them. A more extensive treatment of this subject can be found in [129].

Pre-filtering

Pre-filtering of the data is an important tool which allows the user to influence the model error. In the frequency domain, filtering is equivalent to multiplication. In the identification this corresponds to assigning frequency dependent weights of the identification criterion. Perfect band pass filtering is particularly simple to implement.

Periodic Inputs

The frequency domain identification approach depends on an appropriate choice of excitation signal. The finite discrete Fourier transform is subject to leakage unless the signal is periodic and observed over exactly one or multiple, full periods [129]. For a given finite input signal there always exist an initial condition of the system, such that the observed output has a leakage free Fourier transform. The standard approach to ensure this is to use a periodic input signal and start measuring the output after the initial transient has decreased sufficiently. The advantage of periodic inputs is the extremely simple noise reduction possibility: Just average the measured signals over several periods before applying the discrete Fourier transform.

A sufficient condition for a leakage free Fourier transform is a periodic excitation signal applied at $t = -\infty$. On the other hand, most time domain methods implicitly assume the system to have zero initial conditions, *i.e.*, inputs prior to time 0 are assumed to be zero. Whichever assumption about the past behavior is the correct one should thus influence the final choice of identification method.

Data Reduction

Very large data sets have to be collected when the system has wide spread time constants. In such data sets neighboring values of the time domain data of dynamic systems carry the high frequency information content. If simple decimation is used for the purpose of data reduction, the high frequency information will be lost. After conversion to the frequency domain, each sample of the frequency response carry the information at that frequency. Data reduction can simply be done by discarding samples at frequencies which is of no interest for the use of the final model. Particularly, samples at frequencies where no excitation is present should be removed. Significant noise reduction can also be gained by averaging over neighboring frequencies. The particular choice of degree of averaging gives a clear trade-off between noise reduction and frequency resolution.

Combining Experiments

Often information about a system is given by many independent experiments. In the frequency domain approach, frequency data from many experiments can simultaneously be used in the estimation step. This gives the user a high degree of flexibility. If the model estimated with existing data is not adequate over a certain frequency band, a new experiment can be designed which only emphasis

information around these frequencies. Using the union of the new and old data a new improved model can be identified.

Band-Limited Signals and Continuous-Time Models

If the actual input signal is band-limited (BL), *i.e.*, the signal has no power above the Nyquist frequency, the continuous-time Fourier transform can be reconstructed from sampled data. This presents the possibility to construct continuous-time models in a straightforward fashion.

8.3 Model Structures

The choice of model structure and identification algorithm is often intimately connected and in the literature these two concepts are often presented intertwined. This section only focuses on different types of model structures used for frequency domain identification.

The simplest and historically most used model structure is to model the transfer function G as a fraction of two parametrized polynomials

$$G(\xi,\theta) = \frac{b(\xi,\theta)}{a(\xi,\theta)} = \frac{\sum_{k=0}^{nb-1} b_k \xi^k}{\sum_{k=0}^{na} a_k \xi^k}, \tag{8.4}$$

where

$$\theta^T = (a_0, a_1, \ldots, a_{na-1}, b_0, b_1, \ldots, b_{nb-1})\,.$$

The popularity of this particular form and its derivates originates from the possibility to form an identification criterion which can be minimized analytically with respect to the parameters θ. In order to obtain an identifiable parametrization, an extra constraint on the the parameter vector θ is needed. The most common constraints used are [120]

$$\theta_j = 1, \quad \text{for some } j$$

or

$$|\theta| = 1.$$

Under-modeling occur when the true system has a larger dimension than the chosen model order. In this case the constraint chosen influences the bias of the estimation error [30]. As previously discussed in Chapter 2, the un-factored polynomial representation (8.4) yields transfer functions which are sensitive with respect to small parameter changes, especially if the model order is high. High order continuous-time transfer functions are also known to be more sensitive than the discrete time versions.

Different, and more numerically reliable parametrizations are obtained by using partial fraction expansion, or pole-zero factorization representations. These parametrizations require the knowledge of the pole multiplicity *a priori* [61]. Another parametrization is obtained by a second order expansion of the transfer function [118, 137]. In this form the parameters will represent natural frequencies and damping factors and is similar to the block diagonal state-space parametrization

described in Section 6.3. In the partial fraction parametrizations the transfer function numerator and denominator will not be linear in the parameters and one have to rely on iterative numerical minimization.

The use of normalized frequencies and Chebyshev polynomials improves the estimation accuracy for higher order models [3]. By introducing orthogonal polynomials [38] well-conditioned high order models can be identified and the pole and zero locations can be determined in a numerically robust fashion [124].

Multi-Output Case

The parametrization of multi-input single-output systems is straightforward by letting the numerator polynomial become a row vector of polynomials. The general case with multiple outputs is much more involved if an identifiable parametrization is required. For this case the state-space form is one of the more convenient model structures. For different, and well-conditioned parametrizations of the state-space models, see Chapters 2 and 6.

If we relax the requirement on identifiability, the simple extension of the polynomial fraction model is obtained by using a polynomial matrix $B(\xi,\theta)$ [16]

$$G(\xi,\theta) = \frac{B(\xi,\theta)}{a(\xi,\theta)}.$$

Polynomial matrix fraction descriptions have also been used [22],

$$G(\xi,\theta) = A(\xi,\theta)^{-1}B(\xi,\theta)$$

where $A(\xi,\theta)$ and $B(\xi,\theta)$ are parametrized polynomial matrices. A multi-output version of the partial fraction expansion, the pole residue parametrization, is presented in [61]. This parametrization also suffers from being over-parametrized, *i.e.*, non-unique and requires an *a priori* knowledge of how many real and complex poles the system has, respectively. A MIMO extension of the Chebyshev polynomial SISO model structure is described in [26]. In [81] each element in the transfer function matrix is modeled as the fraction of two polynomials. After identification, using SISO techniques, a model reduction step is conducted to obtain a minimal state-space realization.

Linear Parametrizations

All the above model structures have a common disadvantage: The transfer function $G(\xi,\theta)$ is in general a non-linear function of its parameters. An alternative choice of model structure is to consider transfer functions described by

$$G(\xi,\theta) = \sum_{k=0}^{d-1} \theta_k B_k(\xi), \tag{8.5}$$

where the $B_k(\xi)$ are a set of fixed transfer functions. The transfer function (8.5) is linear in the parameters which simplifies the estimation problem considerably. The simple choice (which is orthogonal)

$$B_k(\xi) = z^{-k}$$

yields the well known finite impulse representation (FIR). Other types of orthogonal basis functions are the family of Laguerre filters [162] or Kautz filters [163]. These ideas are further generalized by the generation of an orthogonal basis function from stable linear dynamic systems [55]. Wavelet bases has also been considered as a possible model structure for identification [112]. If prior knowledge is available about the system, the basis function can be tuned such that only few terms in the expansion are required to accurately describe the transfer function. The obvious disadvantage is that if no such knowledge is at hand, a very large number of terms could be required in order to accurately model a small finite-dimensional system. If a low order model is required, modeling with orthogonal basis functions often needs a secondary model reduction step.

A frequency domain oriented model structure along these lines can be formed by letting the basis function consist of a set of narrow band-pass filters [90]. The width of the filters and thus also their density over the frequency axis can be tuned to match each particular modeling problem. A high density of basis functions yields a high frequency resolution but also a higher noise sensitivity.

8.4 Identification Methods

Some of the existing identification approaches will be summarized in this section. Based on the resulting algorithms, the methods to be described are divided as:

- Optimization based algorithms. These methods determine the system by means of a parametric optimization of some criterion. They can be divided further into two main groups:
  - Deterministic algorithms, which also can be described as complex curve fitting techniques.
  - Algorithms derived from an assumption of stochastic errors.
- Subspace based methods. The subspace methods identify state-space models by utilizing the geometrical properties of the input and output signals of the system. We divide these into two groups:
  - Realization based methods.
  - Input-output based methods.

8.4.1 Optimization Based Methods

All algorithms in this section determine the parameters θ, and hence also the model, by a parametric optimization

$$\hat{\theta} = \arg\min_{\theta} V(\theta),$$

where $V(\theta)$ is a criterion function. Pintelon *et al.* provide a thorough survey of single-input single-output methods based on parametric optimization in [120].

Measured frequency data come in two forms, either as samples of the transfer function

$$G_k = G(\omega_k), \quad k = 1, \ldots, M,$$

or as samples of the input and output Fourier transforms

$$Y_k = Y(\omega_k), \quad U_k = Y(\omega_k), \quad k = 1, \ldots, M.$$

If the method requires samples of the frequency response they can easily be formed as

$$G_k = \frac{Y_k}{U_k}.$$

If U_k is small or zero, the input signal $u(t)$ contains little or no power at the frequency and the sample should be discarded to reduce the noise influence. If the inputs are corrupted by noise of known character it is favorable to use the input and output samples directly in the identification. If the noise level on the input signal is low this distinction becomes much less important [120].

Deterministic Algorithms

The estimation methods given in this section all try to minimize the criterion

$$V_{NLS}(\theta) = \sum_{k=1}^{M} \|G_k - G(\xi_k, \theta)\|_F^2 , \tag{8.6}$$

which for most model structures is a non-quadratic function of the parameters. This estimator is consistent as $M \to \infty$ if G_k are unbiased measurements of the transfer function. In order to find the minimizing argument $\hat{\theta}$ an iterative parametric optimization has to be applied. Since the criterion is a sum of squares, the Gauss-Newton method, [34], is applicable. The single-input single-output problem is treated by Van den Enden *et al.* [147] and is extended to multi-input multi-output systems by Bayard [16], by utilizing a numerical stable sparse QR-factorization method. The success of the optimization is highly dependent on the availability of a high quality initial model. Initial models can be obtained by forming an approximate criterion which is quadratic in the parameters, or by the use subspace based techniques.

If the transfer function is modeled according to (8.4), a first approximation of (8.6) was given by Levy [75]

$$V_{LS}(\theta) = \sum_{k=1}^{M} |G_k a(\xi_k, \theta) - b(\xi_k, \theta)|^2 . \tag{8.7}$$

Since the parameters θ are quadratic in (8.7), $V_{LS}(\theta)$ can be minimized analytically by the ordinary linear least-squares algorithm. However, the approach has a serious deficiency. The model error $G_k - G(\xi_k, \theta)$ is weighted by the magnitude of the denominator polynomial $a(\xi_k, \theta)$. In most cases this gives an overemphasis of the fit at high frequencies, and consequently produce models with a poor low frequency

behavior. The Levy estimator is not statistically consistent, unless the noise has a spectrum proportional to $1/|a(\xi,\hat{\theta})|^2$.

The bad fit at low frequencies of the Levy estimate (8.7) can be removed if a frequency dependent weighting is introduced and an iterative approach is taken. This leads to the class of iterative weighted least-squares methods, with the criterion

$$V^i_{IWLS}(\theta) = \sum_{k=1}^{M} W(\xi_k, \hat{\theta}^{i-1}) \left\| G_k\, a(\xi_k,\theta) - b(\xi_k,\theta) \right\|_F^2 , \tag{8.8}$$

and the ith iteration gives the estimate

$$\hat{\theta}^i = \arg\min_{\theta} V^i_{IWLS}(\theta).$$

Sanathanan and Koerner [128] suggests the following weight

$$W(\xi_k,\theta) = \frac{1}{|a(\xi_k,\theta)|^2}$$

which gives an improved low frequency fit. However, if convergent, Whitfield [164] shows that the method is not guaranteed to converge to the solution of the nonlinear least squares solution (8.6). A range of algorithms using different weights have been published and we refer to [120] for a unifying treatment.

All estimators above use the parameter constraint $a_{na-1} = 1$. In some cases this constraint can give numerical problems if the constrained parameter should be zero or close to zero. In this case we can constrain θ by imposing the norm $\theta^T\theta = 1$ which leads to a total least squares (TLS) solution [43]. If applied to the Levy estimate we obtain the criterion [120]

$$V_{TLS}(\theta) = \frac{1}{\theta^T\theta} \sum_{k=1}^{M} \left| G_k\, a(\xi_k,\theta) - b(\xi_k,\theta) \right|^2 .$$

Since the weighting is frequency independent the TLS estimator suffers from the same deficiencies as the Levy estimate (8.7).

An alternative identification strategy is to minimize the maximum deviation between model and measured frequency response

$$V_{MAX}(\theta) = \max_k \left\| G_k - G(\xi_k,\theta) \right\|_F^2 . \tag{8.9}$$

In [53] Hakvoort presents an algorithm which solves the min-max problem by the use of a constrained non-linear optimization. The algorithm uses a parametrization of the denominator in the form of products of second order polynomials. With this parametrization, stability of the estimated model can be ensured by using linear constraints.

The Stochastic Approach

In this section we consider two approaches which differ by the noise assumptions. In the first approach we assume the Fourier transform of the input signal to be exactly

known and the transform of the output signal is corrupted by zero mean noise with *unknown* frequency dependent covariances. In the other approach we assume that both the input transform as well as the output transform are corrupted with zero mean noise with *known* second order properties. This assumption leads to the frequency domain errors-in-variables identification problem. Which assumption is the best is highly dependent on how the data are obtained, what prior knowledge is available, and the intended use of the model. If a discrete time model from computer to process output is sought, the assumption that the input signal is noise free is quite natural. These type of models are often required for control design intended for computer based control. If, on the other hand, the input signal indeed is measured by some sensor then the errors-in-variables assumption is more valid. It is important to remember that the noise statistics have to be known in order to apply the errors-in-variables algorithm. If measurements of only the noise are available these quantities can be estimated prior to the identification [129].

Output Errors The assumption that the input is exactly known and uncorrelated with the noise on the output is the mainstream assumption in time-domain identification of systems operating in open-loop [86]. In a frequency domain formulation we assume the data to be generated by

$$Y(\omega) = G(\xi,\theta)U(\omega) + H(\xi,\theta)E(\omega) \tag{8.10}$$

for some unknown value of θ. The noise is given by the term $H(\xi,\theta)E(\omega)$, where $H(\xi,\theta)$ is assumed to be a stable and inversely stable transfer function with no poles or zeros on the unit circle and $E(\omega)$ are the frequency domain innovation signal which we assume to be zero mean and independent between different frequencies [90]. Furthermore, assume that $E(\omega)$ is complex Normal [21]

$$E(\omega) \in N^c(0,\lambda),$$

then the maximum likelihood (ML) estimator for a single-output system is given by

$$\begin{aligned}
\hat{\theta}_M &= \arg\min_{\theta} \left[\log W_M(\theta) + \frac{1}{M}\sum_{k=1}^{M} \log |H(\xi_k,\theta)|^2 \right] \\
W_M(\theta) &= \frac{1}{M}\sum_{k=1}^{M} |H(\xi_k,\theta)^{-1}|^2 \, |Y(\omega_k) - G(\xi_k,\theta)U(\omega_k)|^2 \\
\hat{\lambda}_M &= W_M(\hat{\theta}_M),
\end{aligned} \tag{8.11}$$

see Ljung [90]. If the spectrum of the noise is known the ML-estimator equals a weighted NLS estimator. In Chapter 11 we will return to ML-estimators and derive the frequency domain multi-output ML-estimator.

Errors-In-Variables Let us now consider the case when both input and output signals are corrupted with noise. If we denote by $X(\omega)$ the noise free input signal

we have the following relations

$$Y(\omega) = G(\omega)X(\omega) + E_y(\omega)$$
$$U(\omega) = X(\omega) + E_u(\omega).$$

When faced with measurements where both the input and the output signal are corrupted with noise the errors-in-variables approach have to be applied Kalman [67], Anderson and Deistler [8]. A serious restriction applies for this framework. The power spectrums of the input and output noise, or at least the ratio between them, have to be known *a priori*, in order to uniquely determine the system Anderson [7]. In the comprehensive book on frequency domain identification methods by Schoukens and Pintelon [129], a frequency domain errors-in-variables estimation algorithm, ELiS, is derived and analyzed. In ELiS the system $G(\xi)$ is modeled as the fraction of two parametrized polynomials (8.4). If the two noise sources are complex normal random variables, ELiS is the maximum-likelihood estimator. Knowing the input and output power spectrums of the noise, denoted by $\sigma_U^2(\omega)$ and $\sigma_Y^2(\omega)$, respectively, the maximum-likelihood estimate is given by [129]

$$\hat{\theta}_{ELiS} = \arg\min_{\theta} \sum_{k=1}^{M} \frac{|b(\xi_k,\theta)U(\omega_k) - a(\xi_k,\theta)Y(\omega_k)|^2}{\sigma_U^2(\omega_k)|b(\xi_k,\theta)|^2 + \sigma_Y^2(\omega_k)|a(\xi_k,\theta)|^2} \tag{8.12}$$

if the input and output noise sources are uncorrelated. For correlated noise

$$\rho(\omega) = E\, N_Y(\omega)N_X(\omega)^* \neq 0$$

the correction

$$2\,\mathrm{Re}\,(\rho(\omega_k)b(\xi_k,\theta)a(\xi_k,\theta)^*)$$

is subtracted from the denominator in (8.12). As well as the time domain maximum-liklihood estimator is consistent for a large class of noise distributions [86], sufficient conditions for consistency of ELiS is zero mean noise sources $N_U(\omega)$ and $N_Y(\omega)$ with bounded fourth-order moments and uncorrelated over frequency up to the fourth-order moments [121]. Since the denominator in (8.12) is parametrized, an analytical solution is not feasible and non-linear parametric optimization is required. In order to avoid local minima it is important to start the optimization from a high quality initial model.

Logarithmic Least Squares The non-linear least square estimate (8.6) often gives poor estimates of the zero locations. The magnitude of the frequency response at these points is very small and consequently a large error gives very little contribution to the criterion function.

A possible solution is fitting the logarithm of the frequency data to the logarithm of the model [52, 61, 131]

$$V_{LOG}(\theta) = \sum_{k=1}^{M} \|\log G_k - \log G(\xi_k,\theta)\|_F^2 . \tag{8.13}$$

This cost function simultaneously weights the differences in the logarithm of the magnitudes and the difference in phase [131]. The log estimator has been analyzed in a stochastic setting [52] with the conclusion that it is more robust against lack of prior noise information and to outliers compared with the errors-in-variables ML-method. It has also been noted, [61], that the LOG estimator often has better convergence properties than the regular NLS estimator.

If noise is present, inaccuracies at frequencies where the transfer function has a small magnitude might be a result induced by a small signal to noise ratio at these frequencies. The NLS estimator (8.6) is the maximum-likelihood estimator if the noise spectrum is constant. Using a log estimator for the case of a flat noise spectrum would only lead to less accurate models.

8.4.2 Subspace Methods

These methods identify linear state-space models

$$\begin{aligned} x(t+1) &= Ax(t) + Bu(t) \\ y(t) &= Cx(t) + Du(t), \end{aligned}$$

by utilizing the geometrical properties of signals from a linear dynamic system. The name *subspace* stems from a key algorithmic step in all these methods; the extraction of the signal subspace of a matrix built from observed data. Any matrix which spans this subspace can be used as an estimate of the extended observability matrix of some realization. The particular features of subspace based modeling are:

- Multi-input multi-output systems of high orders can "easily" be identified.
- A particular parametrization of the state-space matrices is *not* necessary. The algorithms delivers the matrices A, B, C, D in a well-conditioned realization.
- The methods are non-iterative and hence do not suffer from deficiencies like local minima *etc.*, which are inherent problems for the optimization based techniques.

On the negative side we notice that the algorithms do not explicitly minimize any criterion which makes them more difficult to analyze.

Realization Based Methods

If the impulse response of a system is known, the realization algorithms described in Chapter 4 are practical and efficient methods for identifying state-space models of high order.

Given samples of the frequency response function at equidistant frequencies, an estimate of the impulse response is obtained by using the inverse discrete Fourier transform. A complication occurs here since, using a finite number of frequency samples, the estimated impulse response will be perturbed by aliasing effects. The degree of perturbation is related to what rate the impulse response decays to zero.

However, if the system has well damped poles or a large amount of frequency data is available, the errors are small.

By combining the inverse DFT with a realization algorithm one obtains the frequency domain algorithm described by Juang and Suzuki [64]. Gu and Misra [49] describe a similar approach which uses the obtained impulse response as an initial FIR model which, in a second step, is reduced by truncated balanced realization.

In Chapter 9 we will return to these ideas and present a new algorithm which do not suffer from the aliasing effects of the finite inverse DFT. This leads to an algorithm which exactly identifies a finite dimensional system from a finite number of frequency response measurements.

Input Output Based Methods

During the last ten years a number of subspace based time domain algorithms have appeared [31, 107, 152, 155, 157, 160], which use the geometrical properties of the Hankel matrices of the measured input and output signals. These properties also carry over to the frequency domain, where we assume samples of the Fourier transform of the input and output signals to be given at a set of frequencies. The first account of a frequency domain formulation is due to Liu *et al.* [84], where a frequency domain version of the Q-Markov-Cover algorithm [85] is presented.

A more comprehensive discussion, algorithm development, and analysis will be carried out in Chapter 10.

8.5 Identification of Continuous-Time Models

Most real world processes subject to modeling are of continuous-time character. However, measured input and output signals of the process are almost without exception in sampled form. If a discrete time model is sought, the modeling is straightforward since the measured data are in sampled form. If, on the other hand, a continuous-time model is desired, two options are available. Either we assume that the input signal is piecewise constant between the sample points, which is known as the zero order hold (ZOH) assumption, or we assume that the input signal is band limited (BL), such that the continuous-time signals exactly can be reconstructed from the given samples.

To estimate continuous-time domain models under the ZOH assumption is straightforward if the following assumptions hold [122]:

- The input signal $u(t)$ is constant between the sample instants.
- The continuous-time system is proper, *i.e.*, $\lim_{\omega\to\infty} G(j\omega) < \infty$.
- The magnitudes of the imaginary parts of the poles and zeros of the system are less than the Nyquist frequency (π/T).

A discrete time model can be estimated using the sampled data and the continuous-time model is obtained by inverse ZOH-sampling of the discrete time system. These observations hold both for time domain as well as frequency domain methods.

The BL assumption, as already mentioned, means that the input and output signals have no power above the Nyquist frequency. The estimation problem for general excitation signals should be performed in the time domain and is rather involved [133]. For the case of periodic excitation, the modeling is considerably simplified by considering identification in the frequency domain [122]. Under the BL assumption the discrete Fourier transform of the input and output signals equal their continuous-time transforms and

$$G(j\omega_k) = \frac{Y(\omega_k)}{U(\omega_k}).$$

A continuous-time transfer function $G(s)$ can thus directly be fitted to the frequency data.

It is well known that the parameter estimation problem is better conditioned for discrete time transfer functions, since powers of $e^{j\omega}$ form a natural orthogonal basis [15]. By use of the bilinear transformation the continuous-time identification problem can be solved in the discrete domain without introducing any approximation errors.

8.5.1 The Bilinear Transformation

The bilinear transformation maps the complex values in the s domain to the z domain as

$$s = \frac{2(z-1)}{T(z+1)},$$

with the inverse

$$z = \frac{2+sT}{2-sT}.$$

The parameter T is a parameter which the user is free to specify under constraint that $2/T$ is not a pole of the continuous-time system [6], and can be seen as a sort of sampling time.

If the continuous-time transfer function is given by $G(s)$ the bilinear transformation gives the discrete time transfer function

$$G\left(\frac{2(z-1)}{T(z+1)}\right) = G^d(z).$$

The bilinear transformation maps poles and zeros in the left half plane into the unit circle while the right half plane is mapped to the complement of the unit disc. The poles and zeros on imaginary axis are mapped onto the the unit circle. Stability properties are thus preserved.

The important feature of the bilinear transformation is that the frequency response is invariant if we pre-warp the frequency scale. Let the continuous-time transfer function be evaluated at $j\omega_k$ and let the bilinear transformed discrete time transfer function be evaluated at $e^{j\omega_k^d}$ then it holds that [11]

$$G\left(j\omega_k\right) = G\left(\frac{2(e^{j\omega_k^d}-1)}{T(e^{j\omega_k^d}+1)}\right) = G^d(e^{j\omega_k^d})$$

if

$$\omega_k^d = 2\,\mathrm{atan}(\frac{\omega_k T}{2}).$$

Hence, given samples of a continuous-time transfer function G_k at frequencies ω_k, the samples of the corresponding bilinear transformed discrete time transfer function can be obtained simply as

$$G_k^d = G_k, \quad k = 1, \ldots, M \tag{8.14}$$

$$\omega_k^d = 2\,\mathrm{atan}(\frac{\omega_k T}{2}), \quad k = 1, \ldots, M. \tag{8.15}$$

After the discrete time transfer function is estimated, the continuous-time transfer function is obtained through the inverse map

$$G(s) = G^d\left(\frac{2+sT}{2-sT}\right).$$

If samples of the input and output Fourier transforms are the primary data, the same approach can by applied.

State-Space Models

For state-space models, the bilinear transformation between

$$G(s) = D + C(sI - A)^{-1}B$$

and

$$G^d(z) = D^d + C^d(zI - A^d)^{-1}B^d$$

can, *e.g.*, be described by the matrix relations [6]

$$\begin{aligned} A^d &= (\frac{2}{T}I + A)(\frac{2}{T}I - A)^{-1} \\ B^d &= \frac{2}{\sqrt{T}}(\frac{2}{T}I - A)^{-1}B \\ C^d &= \frac{2}{\sqrt{T}}C(\frac{2}{T}I - A)^{-1} \\ D^d &= D + C(\frac{2}{T}I - A)^{-1}B \end{aligned} \tag{8.16}$$

which imply

$$\begin{aligned} A &= \frac{2}{T}(I + A^d)^{-1}(A^d - I) \\ B &= \frac{2}{\sqrt{T}}(I + A^d)^{-1}B^d \\ C &= \frac{2}{\sqrt{T}}C^d(I + A^d)^{-1} \\ D &= D^d - C^d(I + A^d)^{-1}B^d. \end{aligned} \tag{8.17}$$

This particular choice of transformations has an advantage. The observability and controllability Gramian matrices as well as the Hankel singular values are invariant under the bilinear transformations (8.16) and (8.17) [41]. Particularly, a balanced realization remains balanced after the bilinear transformation. This implies that the transformations retain the system in a well-conditioned basis if the original system is given in a balanced realization.

8.6 Cross Validation

When faced with real data, the process of identification is of an iterative nature. A set of models are estimated from the data and compared with each other in order to find the best model. In the assessment of estimated models, cross-validation [139] is a technique which is quite natural. In cross validation two separate data sets are used; one for estimation and one for validation. The best model is the model which performs best when the quality is assessed using the validation data. Behind this technique we can see a very reasonable structure. Data is composed of a system dependent part which can be explained by a model and a noise part which cannot be described by any model. If a model performs well on the validation data, this gives an indication that the model has captured the features of the underlying system. On the other hand if a model performs well on the estimation data this can indicate that the model might describes the underlying system but also describes the particular noise realization which the estimation data is subject to. The modeling of this particular noise realization is usually of no interest and and when faced with the validation data such a model usually will perform less god.

Consider the case when the true system indeed is a linear dynamic system of finite order. If we now estimate a sequence of models with increasing model orders, the estimation error would normally decrease when evaluated on the estimation data. If the model order is increased above the true order, the model will start to fit the noise. However when evaluated on the validation data one expects to find a model order which attains a minimum error evaluated on the validation data. One then hopes that this model order is close to the true one. If the true system however is infinite-dimensional, cross validation techniques will not give the same guidance since high order models will always approximate the underlying infinite-dimensional system better than low complexity models if the noise level is low or the amount of data is high.

In the frequency domain, cross validation is easily performed by dividing the frequency response measurements into two disjoint sets; estimation data and validation data. The most natural division is to take every other frequency point as the estimation data and the rest as validation data. This division also preserves an existing uniform spacing between frequencies. A model is then estimated using the estimation data only and the quality of the model is assessed by comparing the estimated transfer function with the validation data set.

9

Realization Based Identification

The present chapter deals with a frequency domain based identification problem. In this formulation, the experimental data are taken to be the noisy values of the frequency response of the system at a set of frequencies. In the traditional way of frequency domain identification, the linear dynamic system is modeled by a transfer function which is the fraction of two polynomials with real coefficients and a nonlinear least-squares fit to the data is sought [89, 119]. The solution to this nonlinear parametric optimization problem is obtained by iterative, numerical search. For certain noise models such identification methods can be interpreted as statistical maximum-liklihood estimators and as such they are the frequency domain counterpart to the well known time domain Prediction Error Methods [86].

For time domain identification some non-iterative, subspace based algorithms which deliver state-space models without the need for an explicit parametrization have appeared in the literature during the last years [152, 155]. Subspace based algorithms are also more robust to numerical inaccuracies than parametrized *canonical* models due to the fact that there is no need for an explicit parametrization. Existing frequency domain subspace algorithms are described in [49, 64] and [83, 84]. The algorithm given in [64] uses the inverse discrete Fourier transform (IDFT) to estimate the Markov parameters or impulse response coefficients of the system. The so estimated Markov parameters are then used as in a standard realization algorithm [62, 71, 169]. The objective for doing this is that the coefficients so obtained are close to the impulse response of the system if the number of frequency points are large and the system has well damped poles. If these two requirements are not fulfilled, the estimates deteriorates even if no noise is present. Hence, the approach taken in [64] is exact if and only if the system has a finite impulse response and therefore it may yield very poor estimates for lightly damped systems which exhibits a slowly decaying impulse response. A similar approach is described in [49] where the approximate Markov parameters obtained from the IDFT are taken as the finite impulse response of a system and then, as a second step, the model reduction technique of balanced truncation [109] is applied. The second frequency

domain subspace approach [83, 84] is based on the time domain subspace based algorithm [85] which in turn is closely related to the basic projection algorithm [31]. We will return to this type of algorithms in the next chapter, but we may already now point out that this approach is consistent only under very restricted noise assumptions.

In this chapter we will introduce a new frequency domain identification algorithm which is heavily based on the classical state-space realization algorithms described in Chapter 4. The method combines the inverse discrete Fourier transform (IDFT) and a modified realization algorithm. By studying the properties of the Hankel matrix with the coefficients obtained by the inverse discrete Fourier transform (IDFT), it follows that

$$H_{qr} = \mathcal{O}(I - A^{2M})^{-1}\mathcal{C}$$

where $\mathcal{O}$ and $\mathcal{C}$ are the extended observability and controllability matrices, respectively. It is now clear that the range space of H_{qr} equals the range space of $\mathcal{O}$ and a new algorithm can be derived. The key features of this new algorithm are:

- Any stable finite dimensional system of order n is exactly identified using $n + 2$ equidistant noise-free samples of the frequency response.
- The algorithm is robust to norm bounded perturbations in the data.
- If the data are corrupted by stochastic noise the algorithm is strongly consistent and the estimation error is asymptotically normal distributed.
- If the system under consideration is infinite dimensional the algorithm estimates finite dimensional models with an asymptotic error equal to the truncated balanced realization.
- The algorithm can easily be augmented with frequency weighting capabilites which allows the user to tune the model error over the frequencies.

The chapter is outlined as follows: First a clear problem formulation is given which forms the basis for the rest of the chapter. In Section 9.2 the algorithm is stated and some practical considerations are discussed. In the following section the algorithm is analyzed extensively under the assumption that the underlying system is finite dimensional. The case when the system is of infinite dimension is dealt with in Section 9.4. In the last section the frequency weighted algorithm is presented and analyzed.

9.1 Problem formulation

Assume that the true system G is a stable multivariable linear time-invariant discrete time system with input/output properties characterized by the impulse response coefficients g_k through the equation

$$y(t) = \sum_{k=0}^{\infty} g_k u(t-k) \tag{9.1}$$

where $y(t) \in \mathbb{R}^p$, $u(t) \in \mathbb{R}^m$ and $g_k \in \mathbb{R}^{p\times m}$. If the system is of finite order n it can be described by a state-space model

$$\begin{aligned} x(t+1) &= A_0 x(t) + B_0 u(t) \\ y(t) &= C_0 x(t) + D_0 u(t) \end{aligned}, \tag{9.2}$$

where $y(t) \in \mathbb{R}^p, u(t) \in \mathbb{R}^m$, and $x(t) \in \mathbb{R}^n$. The state-space model (9.2) is a special case of (9.1) with

$$g_k = \begin{cases} D_0, & k = 0 \\ C_0 A_0^{k-1} B_0, & k > 0 \end{cases}. \tag{9.3}$$

The frequency response of (9.1) is

$$G(e^{j\omega}) = \sum_{k=0}^{\infty} g_k e^{-j\omega k}, \tag{9.4}$$

which for the state-space model (9.2) can be written as

$$G(e^{j\omega}) = C_0 (e^{j\omega} I - A_0)^{-1} B_0 + D_0. \tag{9.5}$$

The problem formulation is then: Given the frequency response at a finite number of frequencies, possibly corrupted by noise

$$G_k = G(e^{j\omega_k}) + n_k, \;\; \omega_k \in [0, \pi], \tag{9.6}$$

find a finite dimensional state-space system (9.2) of order n. In (9.6) $G(e^{j\omega_k})$ represents the system frequency function (9.4) and n_k denotes the noise. The identification should yield an estimated model, denoted by $\hat{G}$, such that the true system and the identified model are "close" to each other. Closeness between systems is quantified by the distance between the true and estimated transfer functions and is given by

$$||\hat{G} - G||_\infty = \sup_\omega \bar{\sigma}(\hat{G}(e^{j\omega}) - G(e^{j\omega})). \tag{9.7}$$

Here $\bar{\sigma}(A)$ denote the largest singular value of the matrix A. Since $\bar{\sigma}(A) \leq \|A\|_F$ [43], we notice that

$$||\hat{G} - G||_\infty \leq \sup_\omega \|\hat{G}(e^{j\omega}) - G(e^{j\omega})\|_F.$$

9.2 The Algorithm

If the impulse response coefficients (9.3) are given, well-known realization algorithms can be used to obtain a state-space realization [57, 62, 71, 169]. The algorithm to be presented is closely related to these results, but does not require the true impulse response coefficients to be known.

Assume that frequency response data G_k on a set of uniformly spaced frequencies, $\omega_k = \frac{\pi k}{M}$, $k = 0, \ldots, M$ are given. Since G is a transfer function with a real valued impulse response (9.1), frequency response data on $[0, \pi]$ can be extended to $[0, 2\pi]$ which forms the first step of the algorithm.

Algorithm 9.1

1. *Extend the transfer function samples to cover the full unit circle*

$$G_{M+k} := G^*_{M-k}, \quad k = 1, \ldots, M-1, \tag{9.8}$$

where $(\cdot)^*$ denotes complex conjugate.

2. *Let $\hat{h}_i$ be defined by the $2M$-point Inverse Discrete Fourier Transform (IDFT)*

$$\hat{h}_i = \frac{1}{2M} \sum_{k=0}^{2M-1} G_k \; e^{j2\pi ik/2M}, \; i = 0, \ldots, q+r-1. \tag{9.9}$$

3. *Let the block Hankel matrix $\hat{H}_{qr}$ be defined as*

$$\hat{H}_{qr} = \begin{pmatrix} \hat{h}_1 & \hat{h}_2 & \ldots & \hat{h}_r \\ \hat{h}_2 & \hat{h}_3 & \ldots & \hat{h}_{r+1} \\ \vdots & \vdots & \ddots & \vdots \\ \hat{h}_q & \hat{h}_{q+1} & \ldots & \hat{h}_{q+r-1} \end{pmatrix} \in \mathbb{R}^{qp \times rm} \tag{9.10}$$

with number of block rows $q > n$ and block columns $r \geq n$. The dimension of $\hat{H}_{qr}$ is bounded by $q + r \leq M$.

4. *Let the singular value decomposition of $\hat{H}_{qr}$ be*

$$\hat{H}_{qr} = \begin{pmatrix} \hat{U}_s & \hat{U}_o \end{pmatrix} \begin{pmatrix} \hat{\Sigma}_s & 0 \\ 0 & \hat{\Sigma}_o \end{pmatrix} \begin{pmatrix} \hat{V}_s^T \\ \hat{V}_o^T \end{pmatrix} \tag{9.11}$$

where $\hat{\Sigma}_s$ contains the n largest singular values.

5. *The state-space matrices are calculated as*

$$\hat{A} = (J_1 \hat{U}_s)^\dagger J_2 \hat{U}_s \tag{9.12}$$

$$\hat{C} = J_3 \hat{U}_s \tag{9.13}$$

6.

$$\hat{B} = (I - \hat{A}^{2M}) \hat{\Sigma}_s \hat{V}_s^T J_4 \tag{9.14}$$

$$\hat{D} = \hat{h}_0 - \hat{C} \hat{A}^{2M-1} (I - \hat{A}^{2M})^{-1} \hat{B}. \tag{9.15}$$

where

$$J_1 = \begin{pmatrix} I_{(q-1)p} & 0_{(q-1)p \times p} \end{pmatrix}, \quad J_2 = \begin{pmatrix} 0_{(q-1)p \times p} & I_{(q-1)p} \end{pmatrix} \tag{9.16}$$

$$J_3 = \begin{pmatrix} I_p & 0_{p \times (q-1)p} \end{pmatrix}, \quad J_4 = \begin{pmatrix} I_m \\ 0_{(r-1)m \times m} \end{pmatrix} \tag{9.17}$$

and I_i denotes the $i \times i$ identity matrix, $0_{i \times j}$ denotes the $i \times j$ zero matrix and $X^\dagger = (X^T X)^{-1} X^T$ denotes the Moore-Penrose pseudo-inverse of the full column rank matrix X.

The important property of this algorithm, which we formally will show below, is that it exactly identifies the true system if noise free data are supplied and the system is of finite dimension.

After the IDFT step 2, the algorithm differs from Kung's [71] in two ways, the estimation of B and D, and in the selection of state-space basis. The difference in B and D stems from the fact that Algorithm 9.1 uses the coefficients $\hat{h}_k$ from the IDFT instead of the impulse response g_k.

By using $\hat{U}_s$ in (9.12) and (9.13) instead of $\hat{U}_s\hat{\Sigma}_s^{1/2}$ as in Kung's algorithm results in a different state-space basis. However, the identified transfer functions are still the same even if noisy data are used. The selection of a particular transfer function is already made when ordering the singular values and does not depend on which basis the extended observability matrix is in [146]. The transfer function indeed remains the same if the estimated extended observability matrix is taken as

$$\hat{\mathcal{O}}_q = U_s T$$

for any nonsingular $T \in \mathbb{R}^{n\times n}$.

From (9.9), notice that

$$\lim_{M\to\infty} \hat{h}_k = \int_0^{2\pi} G(e^{j2\pi\theta})\ e^{j2\pi k\theta} d\theta = g_k,\ k = 0, \ldots, q+r-1,$$

where g_k from (9.3) is the kth impulse response coefficient of G. Thus for noise free data, $\hat{H}_{qr}$ tends to a limit as M tends to infinity and equals the Hankel matrix of the impulse response studied in Chapter 4.

The realization given by the algorithm using noise free data is balanced in the sense that the q-block row observability matrix

$$\hat{\mathcal{O}}_i = \begin{pmatrix} \hat{C} \\ \hat{C}\hat{A} \\ \vdots \\ \hat{C}\hat{A}^{q-1} \end{pmatrix} \tag{9.18}$$

and the r-block column controllability matrix

$$\hat{\mathcal{C}}_r = \begin{pmatrix} \hat{B} & \hat{A}\hat{B} & \ldots & \hat{A}^{r-1}\hat{B} \end{pmatrix} \tag{9.19}$$

satisfy

$$\hat{\mathcal{O}}_q^T\hat{\mathcal{O}}_q = I,\ \ \hat{\mathcal{C}}_r\hat{\mathcal{C}}_r^T = (I-\hat{A}^{2M})\hat{\Sigma}_s^2(I-\hat{A}^{2M})^T, \tag{9.20}$$

where $\hat{\Sigma}_s$ is given by (9.11). As M, q and r jointly tend to infinity, the products (9.20) will converge to the observability and controllability Gramians, respectively, and the diagonal elements of $\hat{\Sigma}_s$ will converge to the Hankel singular values of the system. These properties will become important when we study identification of infinite dimensional systems in Section 9.4

Another way of forming B and D yields an alternative algorithm which is close to Algorithm 9.1.

Algorithm 9.2

1-5. Analogous to steps 1-5 in Algorithm 9.1.

6.

$$\hat{B},\ \hat{D} = \arg \min_{\substack{B \in \mathbb{R}^{n \times m} \\ D \in \mathbb{R}^{p \times m}}} \sum_{k=0}^{2M-1} \left\| G_k - D - \hat{C}(e^{j\omega_k} I - \hat{A})^{-1} B \right\|_F^2 . \tag{9.21}$$

This alternative way of obtaining B and D given by (9.21) deserves some further comments. Since both matrices (B and D) are linear in the transfer function assuming $\hat{A}$ and $\hat{C}$ fixed, (9.21) is directly obtained by solving the corresponding linear equations in the least squares sense. In practical examples (9.21) and Step 6 in Algorithm 9.1 yield approximately the same result.

Alternative ways of calculating A

Step 5 of Algorithm 9.1 (9.12) is based on the relation

$$J_1 \hat{U}_s \hat{A} = J_2 \hat{U}_s,$$

which exactly holds in the noise-free case. Recall the block shift structure of the extended observability matrix (9.18). In the noisy case, the expression (9.12) is the solution to

$$\hat{A} = \arg \min_{A \in \mathbb{R}^{n \times n}} \left\| J_1 \hat{U}_s A - J_2 \hat{U}_s \right\|_F .$$

Implicit in this solution is the noise model

$$J_1 \hat{U}_s \hat{A} = J_2 \hat{U}_s + N$$

and $\hat{A}$ minimizes the Frobenius norm of N. This noise model is however not consistent with the original equation since both $J_1 \hat{U}_s$ and $J_2 \hat{U}_s$ contain errors. With this more correct view we obtain the error model

$$(J_1 \hat{U}_s + N_1)\hat{A} = J_2 \hat{U}_s + N_2,$$

and the Total Least Squares (TLS) method can be applied [43]:

$$\hat{A} = \arg \min_{\substack{A \in \mathbb{R}^{n \times n} \\ (J_1 \hat{U}_s + N_1)A = J_2 \hat{U}_s + N_2}} \left\| \begin{pmatrix} N_1 & N_2 \end{pmatrix} \right\|_F . \tag{9.22}$$

The total least squares solution can be obtained by a SVD [43]. The TLS technique for calculating A is also found in the signal processing algorithm ESPRIT [125]. In [148] an overview of these methods is given. Practical experience show similar performance for the least squares solutions (9.12) and the total least squares (9.22) when applied to noisy data.

By applying the array signal processing technique of weighted subspace fitting, the poles of the system, or equivalently the eigenvalues of the matrix A, can be optimally calculated given the statistical properties of the constructed extended observability matrix. In [116, 141] these ideas are exploited in a system identification context. A disadvantage with weighted subspace fitting is the introduction of a non-linear optimization step, which have to be solved by iterative search.

Guaranteeing Stability

Many times stability is a most desirable feature of the estimated model. A stable A, (all eigenvalues inside the unit circle) can be guaranteed by the following procedure [97]:

$$\hat{A} = \hat{U}_s^\dagger \begin{pmatrix} J_2 \hat{U}_s \\ 0_{p\times n} \end{pmatrix}.$$

The price paid is that the method will not yield the true A matrix even for the noise free case unless the true system has a finite impulse response or if $q \to \infty$.

We would like to suggest a different approach to guarantee stability by adding an extra projection step 5b after (9.12). In this step all unstable eigenvalues are projected into the unit circle. The idea can be implemented in the following way:

- Transform $\hat{A}$ to the complex Schur form.
- Project any diagonal elements (eigenvalues) satisfying $1 < |\lambda_i| \leq 2$, into the unit disc by $\lambda_i := \lambda_i(\frac{2}{|\lambda_i|} - 1)$. Eigenvalues with magnitude $|\lambda_i| > 2$ are set to zero. Eigenvalues on the unit circle can be moved into the unit disc by changing the magnitude of the eigenvalue to $1 - \epsilon$ for some small positive ϵ, *i.e.*, $\lambda_i := \lambda_i(1 - \epsilon)$.
- Finally transform $\hat{A}$ back to its original form before proceeding further to determine $\hat{B}$ and $\hat{D}$.

This way of imposing stability does not suffer from consistency problems when identifying stable systems since only unstable eigenvalues are affected. A second advantage is that the magnitude of the frequency response is approximately unchanged by the projection.

9.2.1 Practical Aspects

When facing a practical identification problem many models of different orders are estimated and compared in order to find a suitable "best" model. In the presented algorithms most of the computational effort lies in the SVD factorization (9.11). Given the factorization (9.11), all models of order less than q are easily obtained from the rest of the algorithms by letting n range from 1 to $q-1$. Hence, the choice of appropriate model order can easily be accomplished by direct comparison of a wide range of models with different orders at a rather low computational cost.

9.3 Finite Dimensional Systems

In this section we will analyze the presented algorithm under the assumption that the frequency response data originate from a finite dimensional stable discrete time system of order n. First we will discuss the properties for the case when no noise is present and continue to analyze the influence of the noise.

9.3.1 Noise Free Case

Let us now assume that $n_k = 0$ in (9.6), *i.e.*, noise free measurements. Furthermore, assume that the frequency responses G_k originate from an nth order system with a state-space representation (A_0, B_0, C_0, D_0) according to (9.2) and (9.5).

Algorithm 9.1 is based on the fact that the resulting coefficients $\hat{h}_i$ from the finite IDFT of the frequency response has a Hankel matrix with the same range space as the observability matrix of the true system. It is well known that the Hankel matrix of the impulse response has this property, [57, 71], but much less known is that the Hankel matrix (9.10) also has this property. $\hat{A}$ and $\hat{C}$ are thus estimated as in Kung's algorithm. However, the estimates of $\hat{B}$ and $\hat{D}$ have to take into account that the Hankel matrix is not based on the impulse response. The factor $(I - \hat{A}^{2M})$ in (9.14) accomplishes this.

Notice that as the number of frequency response data tends to infinity, $\hat{A}^{2M}$ tends to zero since $\hat{A}$ is assumed to be stable and the algorithm equals Kung's realization algorithm [71] except for a difference in the chosen basis for the states.

The usefulness of Algorithm 9.1 in the case of finite M follows from the following key theorem.

Theorem 9.1 *Let G be an nth order stable discrete time system represented by (9.2). Then $n + 2$ noise-free equidistant frequency response measurements of G on $[0, \pi]$ are sufficient to identify a state-space realization with a transfer function equal to G by Algorithm 9.1 or Algorithm 9.2.*

Proof: Denote by $\mathcal{O}_0$ and $\mathcal{C}_0$ the extended observability (9.18) and controllability (9.19) matrices from the system realization (A_0, B_0, C_0, D_0). Let $\rho(A)$ denote the spectral radius [58] of A. Since G is a stable transfer function, it can be represented by the following Taylor series

$$\begin{aligned} G(z) &= D_0 + C_0(zI - A_0)^{-1}B_0 = D_0 + \sum_{k=1}^{\infty} C_0 A_0^{k-1} B_0 z^{-k} \\ &= \sum_{k=0}^{\infty} g_k z^{-k}, \quad \rho(A_0) < |z|. \end{aligned}$$

Notice that $\hat{h}_k$ defined by (9.9) can be written as

$$\begin{aligned} \hat{h}_k &= \frac{1}{2M} \sum_{s=0}^{2M-1} \sum_{i=0}^{\infty} g_i e^{j2\pi s(k-i)/2M} = \sum_{i=0}^{\infty} g_{k+2iM} \\ &= C_0 A_0^{k-1} \left(\sum_{i=0}^{\infty} A_0^{2iM} \right) B_0 = C_0 A_0^{k-1} (I - A_0^{2M})^{-1} B_0, \quad k > 0, \end{aligned}$$

and therefore H_{qr} can be factored as

$$\hat{H}_{qr} = \mathcal{O}_0 (I - A_0^{2M})^{-1} \mathcal{C}_0 \tag{9.23}$$

From the dimensions of the factors in (9.23) it is clear that $\hat{H}_{qr}$ has a maximal rank n. Furthermore, since the system is stable $\rho(A_0) < 1$, $(I - A_0^{2M})$ is always of rank n. Minimality of the system also implies that both $\mathcal{C}_0$ and $\mathcal{O}_0$ are of rank n and hence also $\hat{H}_{qr}$ if $r \geq n$ and $q > n$. In (9.11), then $\hat{\Sigma}_o = 0$ which means that the column range spaces of $\hat{H}_{qr}$, $\mathcal{O}_0$ and $\hat{U}_s$ will be equal. A valid extended observability matrix $\hat{\mathcal{O}}$ is then given by $\hat{U}_s$ since there exists a non-singular $n \times n$ matrix S such that

$$\hat{\mathcal{O}} = \hat{U}_s = \mathcal{O}_0 S.$$

$\hat{U}_s$ is thus an extended observability matrix from a state-space realization $(\hat{A}, \hat{B}, \hat{C}, \hat{D})$ which is similar to the original realization (A_0, B_0, C_0, D_0) from (9.2). (9.12) and (9.13) yield $\hat{A}$ and $\hat{C}$ which are related to the original realization as

$$\hat{A} = S^{-1} A_0 S \quad \hat{C} = C_0 S$$

as shown in [71].

According to the estimated $\hat{A}$ and $\hat{C}$ we notice that

$$\begin{aligned}\hat{H}_{qr} =& \mathcal{O}_0 (I - A_0^{2M})^{-1} \mathcal{C}_0 = \hat{\mathcal{O}} S^{-1} (I - A_0^{2M})^{-1} \mathcal{C}_0 \\ =& \hat{\mathcal{O}} (I - S^{-1} A_0^{2M} S)^{-1} S^{-1} \mathcal{C}_0 = \hat{\mathcal{O}} (I - \hat{A}^{2M})^{-1} \hat{\mathcal{C}}.\end{aligned}$$

From this it follows that

$$\hat{\Sigma}_s \hat{V}_s^T = (I - \hat{A}^{2M})^{-1} \hat{\mathcal{C}}.$$

Hence, we obtain

$$(I - \hat{A}^{2M}) \hat{\Sigma}_s \hat{V}_s^T J_4 = \hat{B}$$

which proves (9.14).

From the IDFT (9.9) we have

$$\hat{h}_0 = g_0 + \sum_{i=1}^{\infty} g_{2iM} = D_0 + \sum_{i=1}^{\infty} C_0 A_0^{2iM-1} B_0 = D_0 + \hat{C} \hat{A}^{2M-1} (I - \hat{A}^{2M})^{-1} \hat{B}$$

which proves (9.15). Then the state-space realizations (A, B, C, D) and (A_0, B_0, C_0, D_0) are similar and have equal transfer functions.

The least square estimate of Algorithm 9.2 will also yield the true values since with the true values of $\hat{B}$ and $\hat{D}$ the model will exactly reproduce the $M + 1$ noise free frequency response data G_k. Since the system is assumed to be minimal the solution $\hat{B}$ and $\hat{D}$ is also unique if $M + 1 > n + 1$.

Letting $q = n+1$, $r = n$, $M = n+2$, we satisfy the condition $q + r < 2M$ which completes the proof. □

Uniqueness of the Realization

The realization obtained by the algorithm is not completely unique. The non-uniqueness originates from the SVD (9.11). If the singular values Σ_s are assumed to be distinct and in a descending order the only non-uniqueness origins from possible sign changes in the left and right singular vectors. A unique SVD can in

this case be imposed with the additional constraint that the first non-zero element in each of the left singular vectors (column vectors of $\hat{U}_s$) must be positive. If some of the singular values are equal a more involved procedure can be undertaken. A possible way is to use a modified version of the procedure outlined in the proof of Theorem 2.1 in [95]. For all practical identification applications there is however no need for a unique realization since the goal is only to obtain the transfer function.

9.3.2 The Noisy Case

In the previous section, we demonstrated that an nth order system can be recovered by a simple algorithm involving only the IDFT, SVD, and simple algebraic manipulations using $n+2$ frequency response measurements. The assumption that the system which generated the data is finite dimensional with a known order is not realistic and we will admit the possibility of some "small unmodeled dynamics" which is not captured by any finite dimensional model set. First, we will derive expressions of the perturbation of the transfer function and demonstrate that the proposed algorithm is robust to unmodeled dynamics and noise. Secondly, we analyze the algorithm by stochastic analysis and show consistency as well as derive an approximate variance expression of the estimated transfer function. To simplify the presentation we will drop most size-indicating subscripts of most symbols in what follows.

In the noisy case we can write

$$\hat{H} = H + \Delta H,$$

where $\hat{H}$ is given by (9.10). Here H denotes the noise-free Hankel matrix originating from the true system and ΔH represents the Hankel matrix of the noise part. In general $\hat{H} \in \mathbb{R}^{qp \times rm}$ will be of full rank ($= \min(qp, mr)$) because of the perturbation matrix ΔH. If the largest singular value of ΔH is significantly smaller than the smallest singular value of H, the n largest singular values $\hat{\Sigma}_s$ of $\hat{H}$ and corresponding left singular vectors $\hat{U}_s$ will be close to the unperturbed counterparts and the estimated system will be close to the true system. The SVD of the identification algorithm will thus have a noise threshold and when the noise level increases over this level, the resulting estimates will not be reliable since the singular vectors in $\hat{U}_s$ might change places. In the next section we will discuss how the estimated system is perturbed when ΔH is "small".

Bounded Noise

Suppose that frequency response data G_k as in (9.6) where G is the finite dimensional nominal model are given and n_k captures unmodeled dynamics and noise. First we consider the case when n_k is uniformly bounded

$$\|n\|_\infty = \sup_k \|n_k\|_F \leq \epsilon. \tag{9.24}$$

Later on we will also investigate the properties when we assume n_k to be a stochastic variable.

The noise term n_k gives an additive perturbation on the noise free coefficient h_k and consequently we find

$$\hat{h}_k = h_k + \Delta h_k,$$

where Δh_k are the IDFT of n_k

$$\Delta h_k = \frac{1}{2M} \sum_{i=0}^{2M-1} n_i e^{j2\pi ki/(2M)}. \tag{9.25}$$

The perturbed Hankel matrix is given by

$$\hat{H} = H + \Delta H$$

where H is the unperturbed Hankel matrix and ΔH is the perturbation matrix with elements

$$[\Delta H]_{i,j} = \Delta h_{i+j-1}. \tag{9.26}$$

Here we have dropped the subscript of the Hankel matrix to simplify the notation. The norm of ΔH is bounded by

$$\|\Delta H\|_F \leq \sqrt{qr}\,\epsilon$$

where ϵ is the bound in (9.24).

Let the singular value decompositions of the unperturbed Hankel matrix be given as

$$H = \begin{pmatrix} U_s & U_o \end{pmatrix} \begin{pmatrix} \Sigma_s & 0 \\ 0 & 0 \end{pmatrix} \begin{pmatrix} V_s^T \\ V_o^T \end{pmatrix} \tag{9.27}$$

where Σ_s has n positive singular values on the diagonal in a non-increasing order. Since the system is assumed to have order n, H has rank n and the nth singular value of H, denoted by $\sigma_n(H)$, will be some positive number. In the identification algorithm the SVD plays an important role or more precisely the left singular vectors U_s of the Hankel matrix. The following result describes how the noise will influence this quantity.

Lemma 9.1 *Let $\hat{H} = H + \Delta H$ and $\|\Delta H\|_F \leq \epsilon$. Let $\hat{U}_s$ be given by (9.11) and U_s and U_o by (9.27). Furthermore assume that $\sigma_n(H) > 0$ and*

$$\epsilon < \sigma_n(H)/4. \tag{9.28}$$

Then there exists a nonsingular matrix $T \in \mathbb{R}^{n\times n}$ such that

$$\hat{U}_s = (U_s + U_o P)T \tag{9.29}$$

and

$$\|P\|_F \leq \frac{4}{\sigma_n(H)}\,\epsilon. \tag{9.30}$$

Proof. Let

$$\begin{pmatrix} U_s^T \\ U_o^T \end{pmatrix} \Delta H \begin{pmatrix} V_s & V_o \end{pmatrix} = \begin{pmatrix} E_{11} & E_{12} \\ E_{21} & E_{22} \end{pmatrix} = E. \tag{9.31}$$

From (9.31) we notice that $\|E\|_F = \|\Delta H\|_F \leq \epsilon$ and also, $\|E_{ij}\|_2 \leq \|E_{ij}\|_F$ since the spectral norm is upper bounded by the Frobenius norm. Therefore it is clear that

$$\begin{aligned} \delta = \sigma_n(H) - \|E_{11}\|_2 - \|E_{22}\|_2 &\geq \sigma_n(H) - \|E_{11}\|_F - \|E_{22}\|_F \\ &\geq \sigma_n(H) - 2\epsilon \geq \frac{1}{2}\sigma_n(H) > 0 \end{aligned} \tag{9.32}$$

by assumption (9.28). We also have

$$\frac{\|E_{21} \;\; E_{12}^T\|_F}{\delta} \leq \frac{\epsilon}{\frac{1}{2}\sigma_n(H)} \leq \frac{1}{2}.$$

Then by Theorem 8.3.5 in [43] there exists a matrix P satisfying

$$\|P\|_F \leq \frac{2\epsilon}{\delta} \leq \frac{4\epsilon}{\sigma_n(H)}$$

such that range($\hat{U}_s$) and range($U_s + U_o P$) are equal. Since the range spaces are equal and U_s is of full rank there exists a unique non-singular matrix T such that (9.29) is satisfied. □

It is clear from the result above that the resulting subspace spanned by $\hat{U}_s$ is close to the subspace spanned by U_s if the noise level is low. Since only the range space of the two matrices are close we had to introduce the matrix T in order to relate $\hat{U}_s$ and U_s directly. This *a priori* unknown T represents the "unknown" basis resulting from the identification. This would lead one to expect a difficulty in bounding the transfer function perturbation. However, we will show that this fact does not represent any problem since different state-space basis do not alter the resulting transfer function.

Theorem 9.2 *Let the frequency data be given by (9.6) with the noise uniformly bounded $\|n_k\|_\infty \leq \epsilon$ and let G be a stable nth order linear system with transfer function $G(z)$. Let $(\hat{A}, \hat{B}, \hat{C}, \hat{D})$ be the identified state-space model given by Algorithm 9.1 and let $\hat{G}(z)$ be the corresponding transfer function. Then $\exists\, \epsilon_0, c > 0$ such that $\forall\, \epsilon \leq \epsilon_0$*

$$\sup_{\|n_k\|_\infty \leq \epsilon} \sup_{|z|=1} \|\hat{G}(z) - G(z)\|_F \leq c\,\epsilon \tag{9.33}$$

Proof. First we bound the perturbation of the estimated state-space matrices with the aid of a change of basis represented by the unknown but non-singular T from Lemma 9.1. These bounds are then used to finally bound the transfer function

itself. Throughout the proof we let c denote a bounded real constant which might have different values.

Let (A, B, C, D) denote the state-space realization of the true system which is a result from applying noise free data to Algorithm 9.1. First consider the estimation of the A matrix (9.12). Let ϵ be small enough in order to use the result from Lemma 9.1. Then $\hat{U}_s = (U_s + U_o P)T$. Therefore

$$\hat{A} = (J_1(U_s + U_o P)T)^\dagger J_2(U_s + U_o P)T$$

which can be written

$$T\hat{A}T^{-1} = (J_1(U_s + U_o P))^\dagger J_2(U_s + U_o P)$$

where we used the fact that $(XT)^\dagger = T^{-1}(X)^\dagger$. Hence we can write

$$\begin{aligned}\|T\hat{A}T^{-1} - A\|_F &= \|(J_1(U_s + U_o P))^\dagger J_2(U_s + U_o P) - (J_1 U_s)^\dagger J_2 U_s\|_F \\ &\leq \|(J_1(U_s + U_o P))^\dagger J_2 U_o P\|_F + \|(J_1(U_s + U_o P))^\dagger - (J_1 U_s)^\dagger\|_F \|J_2 U_s\|\end{aligned}$$

Since U_s is an extended observability matrix of an nth order minimal system $J_1 U_s$ is of full rank. The matrix $J_1(U_s + U_o P)$ will thus also be of full rank for all sufficiently small vales of ϵ. We can thus use Lemma A.1 in Appendix A to obtain

$$\begin{aligned}\|T\hat{A}T^{-1} - A\|_F \leq\ & \|(J_1(U_s + U_o P))^\dagger J_2 U_o P\|_F \\ & + \|(J_1(U_s + U_o P))^\dagger\|_2 \|(J_1 U_s)^\dagger\|_2 \|J_1 U_o P\|_F \|J_2 U_s\|_F\end{aligned}$$

By using Lemma A.2 we know that the pseudo-inverse is bounded for all sufficiently small ϵ and $\|P\|_F \leq c\epsilon$. All this yields

$$\|T\hat{A}T^{-1} - A\|_F \leq c\,\epsilon, \quad \forall\, \epsilon < \epsilon_A, \tag{9.34}$$

for some $\epsilon_A > 0$. For convenience let $\Delta A = T\hat{A}T^{-1} - A$.

For $\hat{B}$ from (9.14) we obtain

$$\hat{B} = (I - \hat{A}^{2M})\hat{U}_s^T \hat{H} J_4 = T^{-1}(I - (A + \Delta A)^{2M})TT^T(U_s^T + P^T U_o^T)(H + \Delta H)J_4$$

Since $\hat{U}_s^T \hat{U}_s = I = T^T(U_s^T + P^T U_o^T)(U_s + U_o P)T = T^T + T^T P^T P T$ we can write $T^T = T^{-1} - T^T P^T P$. Also we can write[1]

$$(A + \Delta A)^{2M} = A^{2M} + \sum_{k=1}^{2M} \binom{2M}{k} A^{2M-k} \Delta A^k.$$

With this we get

$$\begin{aligned}\hat{B} = T^{-1} &\left[I - A^{2M} + \sum_{k=1}^{M} \binom{2M}{k} A^{2M-k} \Delta A^k \right] \\ &\times (I - TT^T P^T P)(U_s^T + P^T U_o^T)(H + \Delta H)J_4 \\ &= T^{-1}B + O(\epsilon)\end{aligned}$$

[1] This is actually abuse of notation unless ΔA and A commutes.

Hence we obtain

$$\|T\hat{B} - B\|_F = O(\epsilon) \leq c\,\epsilon, \quad \forall \epsilon < \epsilon_B, \tag{9.35}$$

for some $\epsilon_B > 0$. The $\hat{C}$ matrix is straightforward computed as

$$\hat{C} = J_3(U_s + U_o P)T$$

which directly gives

$$\|\hat{C}T^{-1} - C\| \leq c\,\epsilon, \quad \forall \epsilon < \epsilon_A. \tag{9.36}$$

Let $\Delta B = T\hat{B} - B$ and $\Delta C = \hat{C}T^{-1} - C$. For $\hat{D}$ we have

$$\hat{D} = D + CA^{2M-1}(I - A^{2M})^{-1}B + \Delta h_0 - \hat{C}\hat{A}^{2M-1}(I - \hat{A}^{2M})^{-1}\hat{B}$$

and we obtain

$$\begin{aligned}\|\hat{D} - D\|_F \leq \|\Delta h_0\|_F + \|CA^{2M-1}(I - A^{2M})^{-1}B \\ - (C + \Delta C)(A + \Delta A)^{2M-1}(I - (A + \Delta A)^{2M})^{-1}(B + \Delta B)\|_F.\end{aligned}$$

The last term above requires some further study and we obtain

$$\begin{aligned}&\|CA^{2M-1}(I - A^{2M})^{-1}B \\ &\quad - (C + \Delta C)(A + \Delta A)^{2M-1}(I - (A + \Delta A)^{2M})^{-1}(B + \Delta B)\|_F \\ &\quad \leq \|\Delta C\|_F\|(A + \Delta A)^{2M-1}(I - (A + \Delta A)^{2M})^{-1}(B + \Delta B)\|_F \\ &\quad + \|C((A + \Delta A)^{2M-1} - A^{2M-1})(I - (A + \Delta A)^{2M})^{-1}(B + \Delta B)\|_F \\ &\quad + \|CA^{2M-1}(I - (A + \Delta A)^{2M})^{-1}\Delta B\|_F \\ &+ \|CA^{2M-1}(I - A^{2M})^{-1}((A + \Delta A)^{2M} - A^{2M})(I - (A + \Delta A)^{2M})^{-1}B\|_F\end{aligned} \tag{9.37}$$

We notice that

$$(A + \Delta A)^{2M} - A^{2M} = \sum_{k=1}^{2M} \binom{2M}{k} A^{2M-k}\Delta A^k \leq c\,\epsilon.$$

Since $(I - A^{2M})$ is nonsingular we can use Lemma A.2 in Appendix A to conclude that the inverses in expression (9.37) are bounded by some constant for all sufficiently small values of ϵ. Therfore we can conclude

$$\|\hat{D} - D\|_F \leq c\,\epsilon, \quad \forall \epsilon < \epsilon_D \tag{9.38}$$

for some constant $\epsilon_D > 0$. We have now established that the distances between the estimated state-space matrices converted to some basis and the state-space matrices of the true system indeed are bounded by ϵ whenever ϵ is sufficiently small.

Consider the transfer function error $\hat{G}(z) - G(z)$ which has a norm which can be written as

$$\begin{aligned}\|\hat{G}(z) - G(z)\|_F &= \|\hat{D} + \hat{C}(zI - \hat{A})^{-1}\hat{B} - D - C(zI - A)^{-1}B\|_F \\ &= \|\hat{D} + \hat{C}T^{-1}(zI - T\hat{A}T^{-1})^{-1}T\hat{B} - D - C(zI - A)^{-1}B\|_F\end{aligned}$$

for any nonsingular matrix $T \in \mathbb{R}^{n\times n}$. With straight forward algebraic calculations, this expression can be bounded as

$$\begin{aligned}\|\hat{G}(z) - G(z)\|_F \leq \|\hat{D} - D\|_F &+ \|\Delta C(zI - \hat{A})^{-1}\hat{B}\|_F \\ &+ \|C(zI - \hat{A})^{-1}\Delta B\|_F + \|C(zI - A)^{-1}\Delta A(zI - \hat{A})^{-1}B\|_F.\end{aligned}$$

Since G is a stable system $(zI - A)$ is nonsingular for all $|z| = 1$. Again we can use Lemma A.2 in Appendix A to conclude that the norm of $(zI - T\hat{A}T^{-1})$ is bounded by some constant. By using the bounds (9.34), (9.35), (9.36) and (9.38) we obtain (9.33) with $\epsilon_0 = \min(\epsilon_A, \epsilon_B, \epsilon_D)$ which concludes the proof. □

Definition 9.1 An identification algorithm is *robust* if

$$\lim_{\epsilon\to 0} \sup_{\|n_k\|_\infty \leq \epsilon} \|\hat{G}(z) - G(z)\|_\infty = 0.$$

□

This definition on robustness and the result from Theorem 9.2 yields the important property.

Corollary 9.1 *Identification Algorithm 9.1 is robust.*

9.3.3 First Order Perturbation Analysis

The perturbation analysis will be performed using a first order expansion. The analysis will then be valid whenever ϵ is sufficiently small. The route we will follow below is inspired by similar types of analysis of array signal processing algorithms [77, 78]. Although $\hat{U}_s$ is highly nonlinear in the data $\hat{H}$ we seek a first order perturbation matrix ΔU_s which is linear in the perturbation ΔH. An obvious but not tractable way is to find ΔU_s by differentiation. Instead a *backward error analysis* can be employed to find ΔU_s [78]. The following lemma gives the expression of the first order perturbation of the left singular vectors U_s.

Lemma 9.2 *The perturbed subspace spanned by $\hat{U}_s$ is spanned by $U_s + U_o P$ where P is a matrix with a norm of the order of $\|\Delta H\|$. Furthermore, a first order term expression of $\hat{U}_s$ is given by*

$$\hat{U}_s = U_s + \Delta U_s$$

where

$$\Delta U_s = U_o U_o^T \Delta H V_s \Sigma_s^{-1}. \tag{9.39}$$

Proof. See [77, 78]. □

The derived perturbation expression has the following two properties. It is exactly orthogonal to the unperturbed space and hence

$$\Delta U_s^T U_s = 0.$$

The perturbed subspace is orthonormal up to first order

$$(U_s + \Delta U_s)^T (U_s + \Delta U_s) = I + O(\|\Delta H\|_F^2).$$

If we assume $U_s = \mathcal{O}$ we obtain the alternative expression

$$\Delta U_s = U_o U_o^T \Delta H ((I - A^{2M})^{-1} \mathcal{C})^\dagger$$

since

$$\Sigma_s V_s^T = (I - A^{2M})^{-1} \mathcal{C}.$$

By the construction of ΔH from (9.25) and (9.26), the elements of ΔU_s are given by

$$[\Delta U_s]_{i,j} = \frac{1}{2M} \sum_{k=0}^{2M-1} c_{i,j}(k) n_k \tag{9.40}$$

where $c_{i,j}(k)$ are complex constants which are bounded since H is a bounded matrix and hence the factors in the SVD (9.27).

With the aid of this lemma it is straightforward to derive the corresponding first order perturbation expressions for the estimated system matrices $\hat{A}$ (9.12), $\hat{B}$ (9.14), $\hat{C}$ (9.13) and $\hat{D}$ (9.15).

In what follows we assume that (A, B, C, D) represents the corresponding state-space realization which is obtained from Algorithm 9.1 when $n_k = 0$. The only uniqueness imposed is that the extended observability matrix must satisfy

$$\mathcal{O}^T \mathcal{O} = I$$

which is guaranteed by the algorithm since $\mathcal{O} = U_s$.

Theorem 9.3 *Consider the Hankel matrix $\hat{H} = H + \Delta H$ where ΔH is the perturbations of the matrix. The first order perturbations of the estimated system matrices $\hat{A}, \hat{B}, \hat{C}$ and $\hat{D}$ from $\hat{H}$ using the algorithm (9.11)–(9.15) can be described by*

$$\hat{A} = A + \Delta A$$
$$\hat{B} = B + \Delta B$$
$$\hat{C} = C + \Delta C$$
$$\hat{D} = D + \Delta D$$

where

$$\begin{aligned}
\Delta A =& (J_1 U_s)^\dagger (J_2 \Delta U_s - J_1 \Delta U_s A) && (9.41)\\
\Delta B =& \left[(I - A^{2M}) U_s^T \Delta H - 2M A^{2M-1} \Delta A U_s^T H \right] J_4 && (9.42)\\
\Delta C =& J_3 \Delta U_s && (9.43)\\
\Delta D =& \Delta h_0 - \left[\Delta C A^{2M-1} + (2M-1) C A^{2M-2} \Delta A \right] (I - A^{2M})^{-1} B \\
& - C A^{2M-1} (I - A^{2M})^{-1} \left[2M A^{2M-1} \Delta A (I - A^{2M})^{-1} B + \Delta B \right] && (9.44)
\end{aligned}$$

and ΔU_s is given by (9.39). Furthermore, the first order perturbation of the transfer function is given by

$$\hat{G}(z) = G(z) + \Delta G(z)$$

where

$$\begin{aligned}
\Delta G(z) = \Delta D &+ \Delta C (zI - A)^{-1} B \\
&+ C (zI - A)^{-1} \Delta A (zI - A)^{-1} B + C (zI - A)^{-1} \Delta B. \quad (9.45)
\end{aligned}$$

Proof. In this proof all equality signs are valid up to first order. We will in the sequel encounter the inverse of a perturbed matrix and start by noting the following well known result. Assume $X = Y^{-1}$. Let $\hat{Y} = Y + \Delta Y$ and $\hat{Y}^{-1} = \hat{X} = X + \Delta X$. Then

$$\Delta X = -Y^{-1} \Delta Y Y^{-1} \tag{9.46}$$

is a first order approximation of the perturbation of the inverse.

From the algorithm we have $\hat{A} = (J_1 \hat{U}_s)^\dagger J_2 \hat{U}_s$. Hence, by post-multiplying with $J_1 \hat{U}_s$ we obtain

$$J_1 (U_s + \Delta U_s)(A + \Delta A) = J_2 (U_s + \Delta U_s). \tag{9.47}$$

By using the fact that $J_1 U_s A = J_2 U_s$ and by truncating the left-hand side of (9.47) up to first order terms yields

$$J_1 U_s \Delta A + J_1 \Delta U_s A = J_2 \Delta U_s,$$

which proves (9.41).

$\hat{B}$ is given by $\hat{B} = (I - \hat{A}^{2M}) \hat{\Sigma}_s \hat{V}_s^T J_4$. Notice that $\hat{U}_s^T \hat{H} = \hat{\Sigma}_s \hat{V}_s^T$. Using this equality we obtain $\hat{B} = (I - \hat{A}^{2M}) \hat{U}_s^T \hat{H} J_4$. For $\hat{A}^{2M}$ we have $(A + \Delta A)^{2M} = A^{2M} + 2M A^{2M-1} \Delta A$ up to first order terms. Using this yields

$$\begin{aligned}
B + \Delta B =& (I - (A + \Delta A)^{2M})(U_s + \Delta U_s)^T (H + \Delta H) J_4 \\
=& (I - A^{2M}) U_s^T H J_4 + \left[(I - A^{2M}) U_s^T \Delta H - 2M A^{2M-1} \Delta A U_s^T H \right. \\
& \left. + (I - A^{2M}) \Delta U_s^T H \right] J_4 \\
=& (I - A^{2M}) U_s^T H J_4 + \left[(I - A^{2M}) U_s^T \Delta H - 2M A^{2M-1} \Delta A U_s^T H \right] J_4,
\end{aligned}$$

where the last equality follows from the fact that $\Delta U_s^T H = 0$. $\hat{C} = J_3 \hat{U}_s$ directly gives

$$C + \Delta C = J_3 U_s + J_3 \Delta U_s.$$

$\hat{D}$ is given by (9.15). By using (9.46) we can simplify the factor

$$\begin{aligned}(I - (A + \Delta A)^{2M})^{-1} =& (I - A^{2M} - 2M A^{2M-1} \Delta A)^{-1} \\ =& (I - A^{2M})^{-1} + (I - A^{2M})^{-1} 2M A^{2M-1} \Delta A (I - A^{2M})^{-1}.\end{aligned}$$

which occurs in (9.15). A simple collection of the first order terms of (9.15) proves (9.44). The transfer function is given by

$$\hat{G}(z) = D + \Delta D + (C + \Delta C)(zI - A - \Delta A)^{-1}(B + \Delta B).$$

By using (9.46) for $(zI - A - \Delta A)^{-1}$ and collecting the first order terms we arrive at (9.45). □

By considering (9.40) and (9.41)-(9.45) notice that the elements of the first order perturbation of $G(z)$ can be written as

$$[\Delta G(z)]_{i,j} = \frac{1}{2M} \sum_{k=0}^{2M-1} c_{i,j}(k, z) n_k, \tag{9.48}$$

where $c_{i,j}(z, k)$ are bounded functions of z as long as $|z| = 1$ since the system G is stable and hence have no poles on the unit circle.

Remark 9.1 *Although we derived the expressions under the assumption that (A, B, C, D) is the noise free realization this particular choice of state-space basis do not influence the perturbation expression given in the theorem. This can easily been seen by introducing a orthonormal similarity transformation in the expression of $\Delta G(z)$. It is also possible to drop the requirement of orthonormality of the similarity transformation. However this would lead to a much more complex expression for (9.42).*

9.3.4 Stochastic Case

If we now adopt the view on n_k as being stochastic variables, the estimated transfer function $\hat{G}(z)$ will also be a stochastic variable. The aim of this section is first to show that the elements of ΔH converge with probability one (w.p. 1) to zero as M tends to infinity. This implies that the norm $\|\Delta H\|_F$ also tends to zero and strong consistency follows by Theorem 9.2. Furthermore, we will show that the estimate is asymptotically normal and derive the variance of the estimate.

Assumptions

Let us assume that the noise term n_k is a zero mean complex random variable with covariance

$$E \begin{pmatrix} \operatorname{Re} n_k \\ \operatorname{Im} n_k \end{pmatrix} \begin{pmatrix} \operatorname{Re} n_k^T & \operatorname{Im} n_k^T \end{pmatrix} = \begin{pmatrix} \frac{1}{2} R_k & 0 \\ 0 & \frac{1}{2} R_k \end{pmatrix}, \tag{9.49}$$

and hence

$$E\ \{n_k n_k^H\} = R_k. \tag{9.50}$$

In (9.50) $(\cdot)^H$ denotes the complex conjugate and transpose of a complex matrix. From (9.49) we see that the real and imaginary parts of n_k are assumed to be independent. Furthermore assume that all variance terms have a common bound

$$R_k \leq R. \tag{9.51}$$

We also assume that

$$E\, n_k n_l^H = 0, \quad l \neq k, \tag{9.52}$$

i.e., the noise terms for different frequencies are independent. For more information on these type of complex noise models see [21, 129]. The noise assumptions are rather weak and, for example, valid asymptotically if the frequency response is obtained as the empirical transfer function estimate, see [86].

Consistency

In this section we will show that the described method is strongly consistent,*i.e.*, the limiting transfer function estimate is equal to the true transfer function with probability one as the number of frequency points M tends to infinity. Let us introduce the notation $\hat{G}_M(z)$ to denote the transfer function estimate using M samples of the frequency function.

Theorem 9.4 *Let G be a stable linear system of order n and let G_k be given by (9.6) where n_k satisfies the assumptions (9.50) and (9.51). Let $\hat{G}_M$ denote the transfer function obtained by Algorithm 9.1 using a fixed dimension Hankel matrix $\hat{H}_{ij}$. Then*

$$\lim_{M\to\infty} \sup_{|z|=1} \|\hat{G}_M(z) - G(z)\|_F = 0, \quad \text{w.p. } 1 \tag{9.53}$$

Proof. The elements of ΔH given by (9.25) are all sample mean values of zero mean independent random variables with a common bound on the second moments. Applying Theorem 5.1.2 in [24] we directly obtain

$$\lim_{M\to\infty} \Delta h_k = 0, \quad \text{w.p. } 1$$

which implies that

$$\lim_{M\to\infty} \|\Delta H\|_F = 0, \quad \text{w.p. } 1$$

since ΔH has a fixed dimension. The result (9.53) now follows from Theorem 9.2. □

9.3.5 Asymptotic Distribution and Variance

The first order perturbation analysis has given us expressions for the estimation error dependence of the matrix ΔH and consequently the sums Δh_k. We have

$$\hat{G}_M(z) - G(z) = \Delta G_M(z) + O(\|\Delta H\|^2) \tag{9.54}$$

where, as shown in Theorem 9.3, $\Delta G_M(z)$ is a linear function of the noise n_k. This property can be utilized to prove asymptotic normality of the transfer function estimate. In order to guarantee a finite variance of the estimates we modify Algorithm 9.1 to always identify stable models. We do this by using the projection method outlined in Section 9.2 which gives us the bound

$$\|\hat{G}_M(z)\|_\infty \leq c < \infty$$

for some positive constant c.

Theorem 9.5 *Let G be a stable linear system of order n and let G_k be given by (9.6), where n_k satisfies the assumptions (9.50) and (9.51) and have bounded moments of order six. Let $\hat{G}_M$ denote the transfer function obtained by Algorithm 9.1. Then*

$$\sqrt{M}(\hat{G}_M(z) - G(z)) \in AsN(0, P(z)), \text{ as } M \to \infty, \tag{9.55}$$

where

$$P(z) = \lim_{M\to\infty} E\ M\, \Delta G_M(z) \Delta G_M(z)^H \tag{9.56}$$

and $\Delta G_M(z)$ is given by (9.39) and (9.41)-(9.45). By modifying the algorithm to guarantee that all estimated transfer functions satisfy the bound

$$\|\hat{G}_M(z)\|_\infty \leq c < \infty, \tag{9.57}$$

the covariance of the estimated transfer function satisfies

$$M\, E\, (\hat{G}_M(z) - E\, \hat{G}_M(z))(\hat{G}_M(z) - E\, \hat{G}_M(z))^H \to P(z), \text{ as } M \to \infty. \tag{9.58}$$

Proof. We will conduct the proof under the assumption that the transfer function is scalar valued. In the following let c, possibly with one or more indices, denote a bounded real or complex constant. From (9.48) we have

$$\sqrt{M}\Delta G_M(z) = \frac{1}{\sqrt{M}} \sum_{k=0}^{2M-1} c(k,z) n_k.$$

where $c(k,z)$ are functions of z bounded when $|z| = 1$ since the true system G is assumed to be stable. Let

$$X_{Mk} = \frac{c(k,z)n_k}{\sqrt{M}}$$

and

$$S_M = \sum_{k=0}^{2M-1} X_{Mk}.$$

Furthermore, using the properties of the noise n_k we obtain

$$E\,X_{Mk} = 0, \;\; E\,|X_{Mk}|^2 = \frac{1}{M}|c(k,z)|^2 R_k < \infty, \; \forall M, k. \tag{9.59}$$

For the third order moment of X_{Mk} we obtain

$$\gamma_{Mk} = E\,|X_{Mk}|^3 = \frac{1}{M^{3/2}} E\,|c(k,z)n_k|^3 \leq \frac{c}{M^{3/2}}, \;\; \forall M, k$$

where the last equality follows from the assumption of bounded moments of order six and Jensen's inequality [24]. This implies that

$$\lim_{M\to\infty} \sum_{k=0}^{2M-1} \gamma_{Mk} = 0. \tag{9.60}$$

(9.59) and (9.60) together with Theorem 7.1.2 in [24] implies that

$$\sqrt{M}\Delta G_M(z) \in AsN(0, P(z)). \tag{9.61}$$

Consider now the term $\sqrt{M}O(\|\Delta H\|_F^2)$. Let

$$X_M = \sqrt{M}\|\Delta H\|_F^2 = \frac{1}{M^{3/2}} \sum_{i=0}^{2M-1} \sum_{i=0}^{2M-1} c(i,z)c(j,z)^H n_i n_j^H$$

where the second equality follows from (9.25) and (9.26). This relation gives the expectation

$$E\,|X_M|^3 = \frac{1}{M^{9/2}} \sum_{i_1=0}^{2M-1} \cdots \sum_{i_6=0}^{2M-1} c(i_1,z)\ldots c(i_6,z)^H n_{i_1}\ldots n_{i_6}^H.$$

In this sum only terms in which there exists an index pairing such that each pair have equal index yield non-zero values. The number of such terms are asymptotically of order N^3 and together with the assumption on bounded moments of order six we conclude that

$$E\,|X_M|^3 \leq \frac{cM^3}{M^{9/2}} = \frac{c}{M^{3/2}}$$

holds asymptotically. Chebyshev's inequality then gives

$$P(|X_M| > \epsilon) \leq \frac{E|X_M|^3}{\epsilon^3} \leq \frac{c}{M^{3/2}}, \; \forall \epsilon > 0$$

and consequently

$$\lim_{M\to\infty} \sum_{k=0}^{2M-1} P(|X_M| > \epsilon) < \infty, \; \forall \epsilon.$$

Applying the Borel-Cantelli Lemma [24] gives

$$\lim_{M\to\infty} X_M = 0, \text{ w.p. } 1$$

which implies that $\sqrt{M}O(\|\Delta H\|_F^2) \to 0$ w.p. 1 as $M \to \infty$ which proves (9.55).

The asymptotic distribution result above does not necessarily imply (9.58). The rest of the proof will be devoted to this issue.

The perturbation expression (9.54) is valid for all sufficiently small norms of ΔH. When ΔH becomes large some small singular values of the n largest in (9.11) will change places. As shown in Lemma 9.1 the perturbation expression of the singular vectors are valid as long as

$$\sigma_n(H) > 4\|\Delta H\|_F.$$

Divide the event space Ω into two complementary sets

$$\Omega_1 = \{\omega \,|\, \sigma_n(H) > 4\|\Delta H\|_F\}$$

$$\Omega_2 = \overline{\Omega}_1$$

where ω is the elementary event variable. To bound the probability of Ω_2 we have

$$E\,\|\Delta H\|_F^4 \le \frac{c}{M^2}$$

where the inequality follows from the bounded sixth moments. Hence by Chebyshev's inequality we have

$$P(\|\Delta H\|_F > \sigma_n(H)/4) \le \frac{E\,\|\Delta H\|_F^4}{(\sigma_n(H)/4)^4} \le \frac{c}{M^2} \tag{9.62}$$

For events belonging to Ω_1 the expression

$$\hat{G}_M(z) = G(z) + \Delta G_M(z) + O(\|\Delta H\|_F^2)$$

holds and for Ω_2

$$\|\hat{G}_M(z)\| \le c$$

from assumption (9.57).

The variance of the estimated transfer function is given by

$$\int_\Omega M|\hat{G}_M(z) - E\,\hat{G}_M(z)|^2\,d\omega.$$

By dividing the integral over the two event sets we obtain asymptotically for Ω_2

$$\lim_{M\to\infty} \int_{\Omega_2} M|\hat{G}_M(z) - E\,\hat{G}_M(z)|^2\,d\omega \le \lim_{M\to\infty} \frac{c}{M} = 0,$$

where the inequality follows from (9.57) and (9.62). For the event set Ω_1 we thus obtain

$$\lim_{M\to\infty} \int_{\Omega_1} M|\Delta G_M(z) + O(\|\Delta H\|_F^2) - EO(\|\Delta H\|_F^2)|^2\,d\omega = P(z)$$

which concludes the proof. □

Remark 9.2 *The expressions given in Theorem 9.5 are valid for single-input multi-output transfer functions, i.e., when G_k is a column vector. The general case can be handled analogously by forming a long vector of columns of the transfer function matrix.*

Explicit Expression of the Asymptotic Variance

First we notice that the asymptotic covariance between elements Δh_k is

$$\begin{aligned} R_{\Delta h}(k-l) &= \lim_{M\to\infty} E\, M\, \Delta h_k \Delta h_l^T \\ &= \lim_{M\to\infty} E\, \frac{1}{4M} \sum_{t=0}^{2M-1} \sum_{s=0}^{2M-1} n_t n_s^H e^{j2\pi(kt-ls)/(2M)} \\ &= \lim_{M\to\infty} \frac{1}{4M} \sum_{t=0}^{2M-1} R_t e^{j2\pi(k-l)t/(2M)} \end{aligned} \tag{9.63}$$

which can be interpreted as the inverse DFT of the sequence of noise covariances R_k.

The asymptotic variance is given by the following expression

$$\begin{aligned} P(z) &= \lim_{M\to\infty} E\, M\, \{\Delta G_M(z) \Delta G_M(z)^H\} \\ &= \lim_{M\to\infty} E\, M\, \{(\Delta D + \Delta C(zI-A)^{-1}B \\ &\quad + C(zI-A)^{-1}\Delta A(zI-A)^{-1}B + C(zI-A)^{-1}\Delta B)(\dots)^H\} \\ &= \lim_{M\to\infty} E\, M\, \left\{\Delta D \Delta D^T + \Delta C(zI-A)^{-1}B(\dots)^H \right. \\ &\quad + C(zI-A)^{-1}\Delta A(zI-A)^{-1}B(\dots)^H + C(zI-A)^{-1}\Delta B(\dots)^H \\ &\quad + 2\,\mathrm{Re}\,\left[\Delta D \left[\Delta C(zI-A)^{-1}B + C(zI-A)^{-1}\Delta A(zI-A)^{-1}B \right.\right. \\ &\quad \left.\left. + C(zI-A)^{-1}\Delta B\right]^H \right. \\ &\quad \times C(zI-A)^{-1}\Delta A(zI-A)^{-1}BB^T(zI-A)^{-H}\Delta C^T \\ &\quad + C(zI-A)^{-1}\Delta A(zI-A)^{-1}B\Delta B^T(zI-A)^{-H}C^T \\ &\quad \left. + \Delta C(zI-A)^{-1}B\Delta B^T(zI-A)^{-H}C^T\right]\} \\ &= R_{\Delta h}(0) + V_1 + V_2 + V_3 + 2\,\mathrm{Re}\,(V_4 + V_5 + V_6 + V_7 + V_8 + V_9) \end{aligned} \tag{9.64}$$

where

$$\begin{aligned} V_1 &= \lim_{M\to\infty} E\, M\, \{\Delta C(zI-A)^{-1}B(\dots)^H\} \\ &= J_3 U_o U_o^T \lim_{M\to\infty} E\, M\, \left\{\Delta H \mathcal{C}^\dagger (zI-A)^{-1}B \right. \\ &\quad \left. \times B^T(zI-A)^{-H}(\mathcal{C}^T)^\dagger \Delta H^T\right\} U_o U_o^T J_3^T \end{aligned}$$

$$
\begin{aligned}
V_2 = &\lim_{M\to\infty} E\,M\,\{C(zI-A)^{-1}\Delta A(zI-A)^{-1}B(\dots)^H\}\\
=&C(zI-A)^{-1}(J_1\mathcal{O})^\dagger\,[\\
&J_2U_oU_o^T\lim_{M\to\infty} E\,M\,\left\{\Delta H\mathcal{C}^\dagger(zI-A)^{-1}B\right.\\
&\left.\times B^T(zI-A)^{-H}(\mathcal{C}^T)^\dagger\Delta H^T\right\}U_oU_o^TJ_2^T\\
&-2\,\mathrm{Re}\{J_1U_oU_o^T\lim_{M\to\infty} E\,M\,\left\{\Delta H\mathcal{C}^\dagger A(zI-A)^{-1}B\right.\\
&\left.\times B^T(zI-A)^{-H}(\mathcal{C}^T)^\dagger\Delta H^T\right\}U_oU_o^TJ_2^T\}\\
&+J_1U_oU_o^T\lim_{M\to\infty} E\,M\,\left\{\Delta H\mathcal{C}^\dagger A(zI-A)^{-1}B\right.\\
&\left.\times B^T(zI-A)^{-H}A^T(\mathcal{C}^T)^\dagger\Delta H^T\right\}U_oU_o^TJ_1^T\\
&]\,(\mathcal{O}^TJ_1^T)^\dagger(zI-A)^{-H}C^T
\end{aligned}
$$

$$
\begin{aligned}
V_3 = &\lim_{M\to\infty} E\,M\,\left\{C(zI-A)^{-1}\Delta B(\dots)^H\right\}\\
=&C(zI-A)^{-1}\mathcal{O}^T\lim_{M\to\infty} E\,M\,\left\{\Delta HJ_4J_4^T\Delta H^T\right\}\mathcal{O}(zI-A)^{-H}C^T
\end{aligned}
$$

$$
\begin{aligned}
V_4 = &\lim_{M\to\infty} E\,M\,\left\{\Delta D\left[\Delta C(zI-A)^{-1}B\right]^H\right\}\\
=&\lim_{M\to\infty} E\,M\,\left\{\Delta h_0B^T(zI-A)^{-H}(\mathcal{C}^T)^\dagger\Delta H^T\right\}U_oU_o^TJ_3^T
\end{aligned}
$$

$$
\begin{aligned}
V_5 = &\lim_{M\to\infty} E\,M\,\left\{\Delta D\left[C(zI-A)^{-1}\Delta A(zI-A)^{-1}B\right]^H\right\}\\
=&\Big[\lim_{M\to\infty} E\,M\,\left\{\Delta h_0B^T(zI-A)^{-H}(\mathcal{C}^T)^\dagger\Delta H^T\right\}U_oU_o^TJ_2^T\\
&-\lim_{M\to\infty} E\,M\,\left\{\Delta h_0B^T(zI-A)^{-H}A^T(\mathcal{C}^T)^\dagger\Delta H^T\right\}U_oU_o^TJ_1^T\Big]\\
&\times(\mathcal{O}^TJ_1^T)^\dagger(zI-A)^{-H}C^T
\end{aligned}
$$

$$
\begin{aligned}
V_6 = &\lim_{M\to\infty} E\,M\,\left\{\Delta D\left[C(zI-A)^{-1}\Delta B\right]^H\right\}\\
=&\lim_{M\to\infty} E\,M\,\left\{\Delta h_0J_4^T\Delta H^T\right\}\mathcal{O}(zI-A)^{-H}C^T
\end{aligned}
$$

$$
\begin{aligned}
V_7 = &\lim_{M\to\infty} E\,M\,\left\{C(zI-A)^{-1}\Delta A(zI-A)^{-1}BB^T(zI-A)^{-H}\Delta C^T\right\}\\
=&C(zI-A)^{-1}(J_1\mathcal{O})^\dagger\\
&\Big[J_2U_oU_o^T\lim_{M\to\infty} E\,M\,\left\{\Delta H\mathcal{C}^\dagger(zI-A)^{-1}BB^T(zI-A)^{-H}(\mathcal{C}^T)^\dagger\Delta H^T\right\}\\
&-J_1U_oU_o^T\lim_{M\to\infty} E\,M\,\left\{\Delta H\mathcal{C}^\dagger A(zI-A)^{-1}B\right.\\
&\left.\times B^T(zI-A)^{-H}(\mathcal{C}^T)^\dagger\Delta H^T\right\}\Big]\,U_oU_o^TJ_3^T
\end{aligned}
$$

$$
\begin{aligned}
V_8 = &\lim_{M\to\infty} E\,M\,\left\{C(zI-A)^{-1}\Delta A(zI-A)^{-1}B\Delta B^T(zI-A)^{-H}C^T\right\}\\
=&C(zI-A)^{-1}(J_1\mathcal{O})^\dagger\,[\\
&\times J_2U_oU_o^T\lim_{M\to\infty} E\,M\,\left\{\Delta H\mathcal{C}^\dagger(zI-A)^{-1}BJ_4^T\Delta H^T\right\}\\
&-J_1U_oU_o^T\lim_{M\to\infty} E\,M\,\left\{\Delta H\mathcal{C}^\dagger A(zI-A)^{-1}BJ_4^T\Delta H^T\right\}\Big]\\
&\times\mathcal{O}(zI-A)^{-H}C^T
\end{aligned}
$$

$$
\begin{aligned}
V_9 = &\lim_{M\to\infty} E\,M\,\left\{\Delta C(zI-A)^{-1}B\Delta B^T(zI-A)^{-H}C^T\right\}\\
=&J_3U_oU_o^T\lim_{M\to\infty} E\,M\,\left\{\Delta H\mathcal{C}^\dagger(zI-A)^{-1}BJ_4^T\Delta H^T\right\}\mathcal{O}(zI-A)^{-H}C^T
\end{aligned}
$$

In the expressions given above we have deliberately removed any factors A^{2M} although the limit is not "completely evaluated". However this abuse of notation does not change the asymptotic result. In the expressions two expectations occur frequently. For simplicity assume single input single output case. Then these expressions are given as follows.

Let X be a matrix of dimension $r\times r$. For matrix element i,j we obtain

$$
\begin{aligned}
\left[\lim_{M\to\infty} E\,M\,\{\Delta HX\Delta H^T\}\right]_{i,j} &= \sum_{k=1}^{r}\sum_{m=1}^{r}\lim_{M\to\infty} E\,M\,\{\Delta h_{i+k-1}x_{k,m}\Delta h_{m+j-1}\\
&= \sum_{k=1}^{r}\sum_{m=1}^{r} x_{k,m}R_{\Delta h}(i+k-m-j),
\end{aligned}
\tag{9.65}
$$

where $[X]_{i,j}$ denotes the element of the matrix X located at row i and column j.

Let X denote a $1\times r$ row vector which gives the expectation the value

$$
\left[\lim_{M\to\infty} E\,M\,\{\Delta h_0x\Delta H^T\}\right]_{1,i} = \sum_{k=1}^{r} x_kR_{\Delta h}(k+i-1). \tag{9.66}
$$

If we consider the special case when $R_k=\lambda\ \forall k$ then

$$
R_{\Delta h}(k) = \frac{\lambda}{2}\delta(k),
$$

where $\delta(k)$ is Kronecker's delta function. In this case (9.65) and (9.66) simplifies to

$$
\left[\lim_{M\to\infty} E\,M\,\{\Delta HX\Delta H^T\}\right]_{i,j} = \frac{\lambda}{2}\sum_{k=1}^{r}\sum_{m=1}^{r} x_{k,m}\delta(i+k-m-j)
$$

and

$$
\left[\lim_{M\to\infty} E\,M\,\{\Delta h_0x\Delta H^T\}\right]_{1,i} = \frac{\lambda}{2}\sum_{k=1}^{r} x_k\delta(k+i-1) = 0,\ \ \forall i.
$$

9.3.6 Verification by Monte Carlo Simulation

We shall in this section verify the validity of the asymptotic variance expression derived in section 9.3.5 for finite data. We do this by use of Monte Carlo simulations where we estimate the variance by calculating the sample variance of a large number of noise realizations.

The variance $P(z)$ given by (9.56) is only valid as M tends to infinity. However it is common to use such an expression [86] also for finite data to get an estimate of the resulting variance. In our case we have approximately

$$E\,|\hat{G}_M(z) - G(z)|^2 \approx \frac{1}{M} P(z)$$

where subscript M in $\hat{G}_M(z)$ explicitly shows the dependency of the data record length.

As an example the following second order system

$$y(t) = \frac{10^{-2}(6.376\,q^2 + 9.140\,q + 6.204)}{q^2 - 1.613\,q + 0.828}\,u(t) = G(q)\,u(t) \tag{9.67}$$

will be used. The magnitude of the transfer function is depicted in figure 9.1. Using the transfer function G 101 samples of the frequency response are generated using a linear frequency grid ranging from $\omega_0 = 0$ to $\omega_M = \pi$. Each frequency response sample is corrupted with independent complex Gaussian noise with three different variance levels $R = 1$, $R = 0.1$ and $R = 0.01$. Using different realizations of the noise 3×10000 different estimation data sets are generated.

From the data sets 3×10000 models of second order are estimated using Algorithm 9.1. Let the estimated models be denoted by $\hat{G}_k$ where subscript k indicates which data set is used in the identification. The estimated variance of the transfer function is evaluated as

$$P_{MC}(\omega_k) = \frac{1}{10000} \sum_{k=1}^{10000} |\hat{G}_k(e^{j\omega_k}) - G(e^{j\omega_k})|^2. \tag{9.68}$$

Results

The results of the simulations are depicted in Figure 9.2 and indicate an extremely good quality of the theoretical asymptotic variance expression (9.56). The theoretical and simulated values almost completely coincide for the two lower noise levels. A somewhat larger discrepancy can be seen from the highest noise level. This is in line with the analysis since the theoretical expression is derived under the assumption that the noise level is sufficiently low. However, a noise level with variance 1 is quite high compared with the maximal magnitude of the transfer function $\|G\|_\infty = 2.55$. In Figure 9.2 the Cramér-Rao lower bound is given. This bound is the lowest variance any unbiased estimator can obtain. By comparing with the lower bound we notice that Algorithm 9.1 is not an asymptotically efficient algorithm.

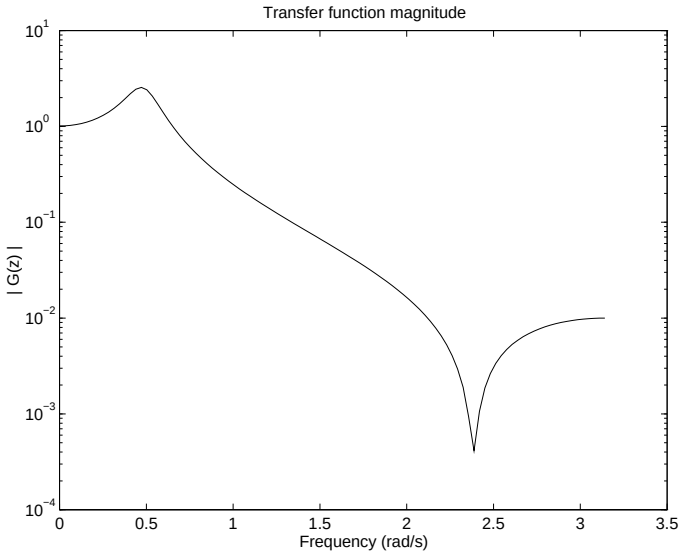

Figure 9.1: Magnitude of transfer function G(z) defined in (9.67)

This example clearly shows that the asymptotic variance expression (9.56) indeed can be used to accurately estimate the resulting variance of the estimated transfer function when using Algorithm 9.1. The sub-optimality of the algorithm with respect to the asymptotic variance is the price which has to be paid for using a non-iterative method.

9.3.7 Conclusions

In this section we have analyzed the non-iterative frequency domain state-space identification algorithm described by Algorithm 9.1. If the frequency data are noise free and generated by an nth order system we have shown that only $n+2$ equidistant frequency samples are required to exactly recover the true system. If the measurements are contaminated with unmodeled dynamics and/or noise, upper bounded by ϵ, we have shown that the resulting identification error is upper bounded by ϵ and hence the algorithm is robust.

Asymptotic stochastic analysis shows that the algorithm is consistent if each measurement is perturbed by an independent stochastic noise term with bounded covariance. Furthermore, we have shown that the resulting estimated transfer function is asymptotically normal distributed and have derived an analytical expression of the asymptotic variance.

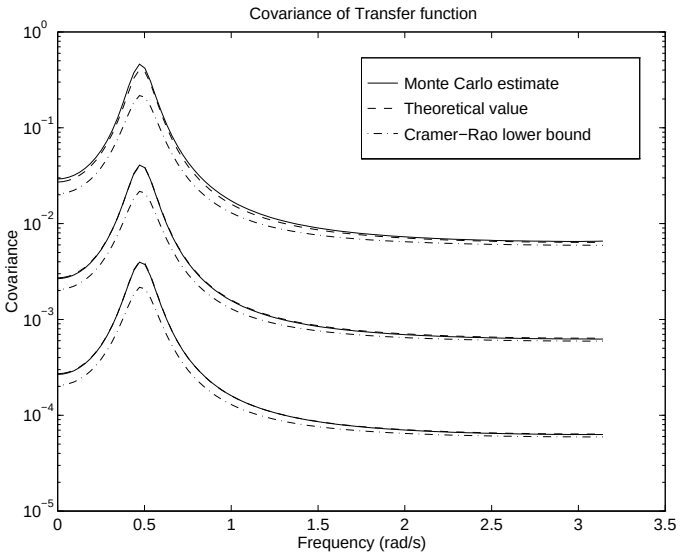

Figure 9.2: Result of Monte Carlo Simulations for three different noise levels, $R = 1$, $R = 0.1$ and $R = 0.01$. The solid line shows $P_{MC}(z)$ and the dashed line shows $\frac{1}{M}P(z)$ given by 9.56. For the two lower noise levels the theoretical and the Monte Carlo estimate almost completely coincide. The Cramér-Rao lower bound of the covariance is depicted as the dash-dotted line.

9.4 Infinite-Dimensional Systems

Identification of infinite-dimensional systems has been much studied recently in both the time and frequency domains [46, 91, 98]. Based on the disturbance characterization, problem formulations can be divided into two subgroups. In the traditional stochastic problem formulations, the disturbances are assumed to be random variables which lead to instrumental variable and prediction error methods. See for example, the books [86, 136]. The least-squares method is the archetype for such methods. Under suitable conditions on the unknown system and exogenous noise, letting the model order be large enough, one hopes to approximate an infinite-dimensional system well. Such a procedure called *black-box* identification algorithm having desired convergence properties is described in Ljung and Yuan [91]. In the deterministic problem formulations [46, 98], the disturbances are assumed to be deterministic and a *robust convergence* notion is introduced which requires nonlinear identification algorithms. The performance of the algorithm is measured by the worst-case identification error. In both formulations, a prejudice free model set of high complexity is the underlying model structure. In most practical applications, as in the design of model based controllers, the model is required to be of restricted complexity. Thus model reduction is a necessary additional step

to the identification if the model set is taken too large.

A direct method is then to realize low complexity models from the experimental data without passing through a high order model. In this section, we analyze Algorithm 9.1 described in Section 9.2 when applied to the low complexity identification problem of infinite-dimensional systems from equally spaced frequency response measurements. This analysis is a complement to our finite-dimensional analysis carried out in Section 9.3.

9.4.1 System Assumptions

In this section we focus on linear discrete time, multi-input multi-output systems which are bounded input bounded output stable. Then $G \in \mathcal{H}_\infty$ and $G(z)$ is continuous on the unit circle, where $\mathcal{H}_\infty$ denotes the Hardy space of bounded matrix valued functions analytical in the complement of the closed unit disc. Some further assumptions must be imposed on the system G to obtain good finite-dimensional approximations. A set of conditions can conveniently be stated in terms of the Hankel singular values of the system. Let ℓ_2^m denote the set of sequences $u = \{u_k\}_{k\geq 0}$, $u_k \in \mathbb{R}^m$ such that

$$\sum_{k=0}^{\infty} \|u_k\|_2^2 < \infty.$$

Recall that the Hankel operator with symbol $?$ is defined on ℓ_2^m by

$$(?\, u)(t) = \sum_{i=0}^{\infty} g_{t+i+1} u(i), \quad t = 0, 1, \ldots$$

which is a mapping into ℓ_2^p, where g_k is the impulse response (9.1) of G. Let $?^*$ be the adjoint of $?$. The squared Hankel singular values $?_i^2$ are defined to be the eigenvalues of $??^*$. Let v_i and w_i be the corresponding normalized eigenvectors of $??^*$ and $?^*?$, respectively. The pair (v_i, w_i) is called the Schmidt pair [167] and satisfies

$$?\, v_i = ?_i w_i; \qquad ?^* w_i = ?_i v_i,$$

where, $w_i \in \ell_2^p$ and $v_i \in \ell_2^m$. With the decomposition of the Hankel operator into Schmidt pairs and Hankel singular values we can describe the impulse response as

$$g_{k+j+1} = \sum_{i=1}^{\infty} w_i(k) ?_i v_i(j)^T, \quad k \geq 0,\ j \geq 0,$$

where $w_i(k) \in \mathbb{R}^p$ and $v_i(k) \in \mathbb{R}^m$. A system is said to be *nuclear* if its Hankel singular values are summable

$$\sum_{k=1}^{\infty} ?_k < \infty. \tag{9.69}$$

From (9.69) we see that all finite-dimensional stable linear systems form a subset of nuclear systems.

Optimal Hankel norm and truncated balanced realizations are two popular model reduction techniques for nuclear systems and they are known to produce the same upper bound on the approximation error by

$$\|G - G_n\|_\infty \leq 2 \sum_{k=n+1}^{\infty} ?_k, \tag{9.70}$$

where the summation is taken over the distinct $?_i$'s if G_n is an nth order approximant of G. The bound (9.70) also holds for any truncated model as long as the observability Gramian and the controllability Gramian of the full, possibly infinite-dimensional, realization remain diagonal and ordered in a non-decreasing order [146]. All realizations of this class can be obtained from the balanced realizations by using non-singular diagonal similarity transformations.

Definition 9.2 A state-space realization of a stable system G is *output-normal* if the observability Gramian W_o and the controllability Gramian W_c satisfies

$$W_o = I, \quad W_c = \text{diag}\,(?_1^2, ?_2^2, \dots)$$

where $?_k$ are the Hankel singular values of G in a non-increasing order. □

Since the output normal form is easily reached from the balanced realization via a diagonal similarity transformation it directly follows that (9.70) also holds for truncated output normal realizations.

A sufficient condition for the nuclearity [18] is given in terms of the impulse response as

$$\|g_k\| = \mathbf{O}(k^{-\alpha}) \quad \text{for some} \quad \alpha > 3/2. \tag{9.71}$$

It is not difficult to translate this condition into the frequency domain description. Hence, sufficient conditions for nuclearity can be stated in terms of the transfer function of the system.

9.4.2 Analysis

In this section, we discuss the properties of Algorithm 9.1 for identifying finite order models from infinite-dimensional systems whose impulse response coefficients asymptotically decay at the rate (9.71), given uniformly spaced, experimental frequency response data of the system

$$G_k = G(e^{jk\pi/M}) + n_k; \quad k = 0, \dots, M, \tag{9.72}$$

where the frequency response measurement noise n_k are assumed to have the properties described by (9.49)-(9.52) in Section 9.3.4

Since (9.70) is the best available bound on the approximation error, our objective is to achieve the same bound on the identification error asymptotically (with probability one), *i.e.*,

$$\lim_{M\to\infty} ||G - \hat{G}_n||_\infty \leq 2 \sum_{k=n+1}^{\infty} ?_k(G), \quad \text{w.p. 1} \tag{9.73}$$

where $\hat{G}_n$ is the nth order identified model.

The above objective is achieved by many two-stage algorithms. In the first stage of a black-box type two-stage algorithm, a linearly parametrized model structure is used to derive a *pre-identified* model and in the second stage, an nth order rational approximation of the pre-identified model gives $\hat{G}_n$. We refer the reader to [55] and references therein for some interesting parametrizations. Unless the model set is suitably parametrized, a lightly damped system yields high order pre-identified models and hence number of data and computations needed for the accuracy increase dramatically. Therefore, a potential identification algorithm in addition to satisfying (9.73) must have good performance for finite data sets . This is the case if the algorithm is exact when restricted to finite-dimensional systems and noise free data. Since Algorithm 9.1 has this property it stands as a good candidate also for the identification of infinite-dimensional systems.

The main results in this section are contained in the following theorem.

Theorem 9.6 *Suppose that $M+1$ equidistant frequency response measurements of G on $[0,\pi]$ are available. Let $\|g_k\| = \mathbf{O}(k^{-\alpha})$ for some $\alpha > 3/2$. Let r and q be $\mathbf{O}(M^{1/3}\ (\log M)^{-\beta})$ for some $\beta > 1/3$. Assume $?_n > ?_{n+1}$. Then Algorithm 9.1 converges w.p. 1 to an nth order truncated output normal realization of G as $M \to \infty$ if the noise n_k is zero mean and satisfying (9.49)-(9.52). Furthermore, the identification errors are bounded w.p. 1 by*

$$\lim_{M,q,r\to\infty} ||G - \hat{G}||_\infty \leq 2 \sum_{k=n+1}^{\infty} ?_k(G). \tag{9.74}$$

Proof: Let $\tilde{B}$ be defined by

$$\tilde{B} = \hat{\Sigma}_s \hat{V}_s^T J_4, \tag{9.75}$$

and suppose that $(\hat{A}, \tilde{B}, \hat{C}, D)$ converges to an output normal balanced realization of G w.p. 1 as $M \to \infty$. Let (A_n, B_n, C_n, D) denote this limit. Since (A_n, B_n, C_n, D) is stable [18], $\hat{A}^M \to 0$ w.p. 1 as $M \to \infty$. Notice that $\hat{h}_0 \to D$ w.p. 1 as $M \to \infty$ and $\hat{B}$ can be written as

$$\hat{B} = (I - \hat{A}^{2M})^{-1}\tilde{B}.$$

Thus $\hat{B} \to B_n$ and $\hat{D} \to D$ w.p. 1 as $M \to \infty$.

Now it remains to show $(\hat{A}, \tilde{B}, \hat{C}) \to (A_n, B_n, C_n)$. First, we will consider the noise free case. The proof is straightforward but tedious. To simplify notation in the calculations, without loss of generality we assume that $q = r$.

Let G_{q+r} denote the $(q+r-1)$th order transfer function of the truncated impulse response of G as follows

$$G_{q+r} = \sum_{k=0}^{q+r-1} g_k z^{-k}$$

and let G_{q+r}^n be the nth order truncated balanced realization for G_{q+r}. If $\|g_k\| = \mathbf{O}(k^{-\alpha})$, it is known that $?_k(G) = \mathbf{O}(k^{-\alpha+1/2})$ for any $\alpha > 1$ [18]. Hence

$\sum_{i=1}^{\infty} ?_i(G_{q+r})$ is a uniformly bounded sequence in $q+r$ if $\alpha > 3/2$ and by the dominated convergence theorem [127], we have

$$\lim_{q+r\to\infty} \sum_{i=1}^{\infty} ?_i(G - G_{q+r}) = \sum_{i=1}^{\infty} \lim_{q+r\to\infty} ?_i(G - G_{q+r}) = 0.$$

Thus $\{?(G_{q+r})\}_{q+r=2}^{\infty}$ is a sequence of finite-rank Hankel operators converging to $?(G)$ in the nuclear norm. Let (v_i, u_i) be the normalized Schmidt pair of G associated with $?_i(G)$. Let G^n be the transfer function of an nth order truncated balanced realization for G which is equal to the nth order truncated output normal realization since the two realizations are related by a diagonal similarity transformation matrix. Then G^n is given by, *c.f.* [18] or [168].

$$G^n = C_n(zI_n - A_n)^{-1}B_n + g_0$$

where A_n, row vectors of B_n and C_n are defined as

$$\begin{aligned}
[A_n]_{kl} &= \sum_{i=0}^{\infty} u_k^T(i)u_l(i+1), \quad k,l = 1,\ldots,n,\\
[B_n]_k &= \sum_{i=0}^{\infty} u_k^T(i)g_{i+1}, \quad k = 1,\ldots,n,\\
C_n &= \begin{pmatrix} u_1(0) & u_2(0) & \cdots & u_n(0) \end{pmatrix}.
\end{aligned}$$

Now consider the following Hankel matrix

$$S_{q+r} = \begin{pmatrix} g_1 & g_2 & \cdots & g_{q+r-1} \\ g_2 & g_3 & \cdots & 0 \\ \vdots & \vdots & \ddots & \vdots \\ g_{q+r-1} & 0 & \cdots & 0 \end{pmatrix}. \tag{9.76}$$

Since G_{q+r} has a finite impulse response, the following SVD for S_{q+r}

$$S_{q+r} = \begin{pmatrix} \bar{U}_s & \bar{U}_o \end{pmatrix} \begin{pmatrix} \bar{\Sigma}_s & 0 \\ 0 & \bar{\Sigma}_o \end{pmatrix} \begin{pmatrix} \bar{V}_s^T \\ \bar{V}_o^T \end{pmatrix} \tag{9.77}$$

is the polar decomposition of the Hankel operator $?(G_{q+r})$. Therefore, a transfer function of an nth order truncated balanced realization for G_{q+r} can be calculated from (9.77) as

$$G_{q+r}^n = \bar{C}_n\ (zI_n - \bar{A}_n)^{-1}\bar{B}_n + g_0$$

where

$$\bar{U}_s = \begin{pmatrix} \bar{u}_1(0) & \bar{u}_2(0) & \cdots & \bar{u}_n(0) \\ \bar{u}_1(1) & \bar{u}_2(1) & \cdots & \bar{u}_n(1) \\ \vdots & \vdots & \vdots & \vdots \\ \bar{u}_1(q+r-2) & \bar{u}_2(q+r-2) & \cdots & \bar{u}_n(q+r-2) \end{pmatrix} \tag{9.78}$$

$$\bar{U}_1^{'} = J_1 \bar{U}_s = \begin{pmatrix} \bar{u}_1(0) & \cdots & \bar{u}_n(0) \\ \vdots & \ddots & \vdots \\ \bar{u}_1(q+r-3) & \cdots & \bar{u}_n(q+r-3) \end{pmatrix},$$

and $(\bar{\Sigma}_s)_{ii} = \bar{\sigma}_i = ?_i(G_{q+r})$. $\bar{A}_n, \bar{B}_n$ and $\bar{C}_n$ are defined by

$$[\tilde{A}_n]_{kl} = \sum_{i=0}^{q+r-3} \bar{u}_k^T(i)\bar{u}_l(i+1), \quad k,l = 1,\ldots,n,$$

$$\bar{A}_n = [(\bar{U}_1^{'})^T \bar{U}_1^{'}]^{-1} \tilde{A}_n \tag{9.79}$$

$$[\bar{B}_n]_k = \sum_{i=1}^{q+r-2} \bar{u}_k^T(i) g_i, \quad k = 1,\ldots,n, \tag{9.80}$$

$$\bar{C}_n = (\bar{u}_1(0) \;\; \bar{u}_2(0) \;\cdots\; \bar{u}_n(0)). \tag{9.81}$$

After a suitable normalization of u_i, convergence in the nuclear norm imply [18]

$$(i) \quad \lim_{q+r\to\infty} |?_i(G_{q+r}) - ?_i(G)| = 0; \tag{9.82}$$

$$(ii) \quad \lim_{q+r\to\infty} \|\bar{u}_i - u_i\|_2 = 0. \tag{9.83}$$

Thus applying Schwarz inequality, we can bound for example $B_n - \bar{B}_n$ by

$$\|B_n(k) - \bar{B}_n(k)\| = \left\| \sum_{i=q+r-1}^{\infty} u_k^T(i) g_{i+1} + \sum_{i=0}^{q+r-2} [u_k(i) - \bar{u}_k(i)]^T g_{i+1} \right\|$$

$$\leq \|u_k\|_2 \left(\sum_{i=q+r}^{\infty} \|g_i\|^2 \right)^{1/2} + \|g\|_2 \, \|u_k - \bar{u}_k\|_2,$$

Hence by (9.82) and (9.83), it follows that $(\bar{A}_n, \bar{B}_n, \bar{C}_n, D) \to (A_n, B_n, C_n, D)$ and $G_{q+r}^n \to G^n$ as $q+r \to \infty$. Thus we have

$$\lim_{q+r\to\infty} \|G - G_{q+r}^n\|_\infty \leq \|G - G^n\|_\infty + \lim_{q+r\to\infty} \|G^n - G_{q+r}^n\|_\infty \leq 2 \sum_{i=n+1}^{\infty} ?_i(G),$$

where the second inequality is known to hold for truncated balanced realizations.

Now consider the following decomposition of S_{q+r}

$$S_{q+r} = \begin{pmatrix} g_1 - \hat{h}_1 & \cdots & g_r - \hat{h}_r & g_{r+1} & \cdots & g_{q+r-1} \\ \vdots & \ddots & \vdots & \vdots & \ddots & \vdots \\ g_q - \hat{h}_q & \cdots & g_{q+r-1} - \hat{h}_{q+r-1} & 0 & \cdots & 0 \\ g_{q+1} & \cdots & 0 & 0 & \cdots & 0 \\ \vdots & \ddots & \vdots & \vdots & \ddots & \vdots \\ g_{q+r-1} & \cdots & 0 & 0 & \cdots & 0 \end{pmatrix}$$

$$+\begin{pmatrix} \hat{h}_1 & \cdots & \hat{h}_r & 0 & \cdots & 0 \\ \vdots & \ddots & \vdots & \vdots & \ddots & \vdots \\ \hat{h}_q & \cdots & \hat{h}_{q+r-1} & 0 & \cdots & 0 \\ 0 & \cdots & 0 & 0 & \cdots & 0 \\ \vdots & \ddots & \vdots & \vdots & \ddots & \vdots \\ 0 & \cdots & 0 & 0 & \cdots & 0 \end{pmatrix} = -E_{qr} + H_{qr}^{'}.$$

The term E_{qr} which may be interpreted as a perturbation term is bounded in the Frobenius norm as

$$\begin{aligned} \|E_{qr}\|_F^2 &= \sum_{k=1}^{q}\sum_{l=1}^{r}\left\|\sum_{i=1}^{\infty} g_(k+l-1+2iM)\right\|_2^2 + \sum_{i=1}^{q-1} i\,\|g_{r+i}\|_2^2 + \sum_{i=1}^{r-1} i\,\|g_{q+i}\|_2^2 \\ &\le q^2 \max_{k\ge 1}\left(\sum_{i=1}^{\infty}\|g_(k+2iM)\|_2\right)^2 + q^2 \max_{q\le k}\|g_k\|_2^2 \\ &= \mathbf{O}(1)\; q^2 M^{-2\alpha}\left(\sum_{i=1}^{\infty} i^{-\alpha}\right)^2 + \mathbf{O}(q^{-2\alpha+2}) = \mathbf{O}(q^{-2\alpha+2}). \end{aligned} \tag{9.84}$$

Given the SVD (9.11) for $\hat{H}_{qr}$, the following is an SVD for $H_{qr}^{'}$

$$H_{qr}^{'} = \begin{pmatrix} \hat{U}_s & \hat{U}_o \\ 0 & 0 \end{pmatrix}\begin{pmatrix} \hat{\Sigma}_s & 0 \\ 0 & \hat{\Sigma}_o \end{pmatrix}\begin{pmatrix} \hat{V}_s^T & 0 \\ \hat{V}_o^T & 0 \end{pmatrix} = \hat{U}_s'\hat{\Sigma}_s(\hat{V}_s')^T + \hat{U}_o'\hat{\Sigma}_o(\hat{V}_o')^T.$$

Let $\bar{U} = [\bar{U}_s\, \bar{U}_o]$ and conformably $\bar{U} = [\bar{V}_s\, \bar{V}_o]$ and let

$$\bar{U}^T E_{qr}\bar{V}^T = \begin{pmatrix} \tilde{F}_{11} & \tilde{F}_{12} \\ \tilde{F}_{21} & \tilde{F}_{22} \end{pmatrix} = F. \tag{9.85}$$

It is known [43, Theorem 8.3.5] that the column range spaces of $\hat{U}_s^{'}$ and $\bar{U}_s + \bar{U}_o P$ are equal for some matrix P satisfying

$$\|P\|_F \le \frac{2\|\tilde{F}_{12}\tilde{F}_{21}^T\|_F}{\bar{\sigma}_n - \bar{\sigma}_{n+1} - \|\tilde{F}_{11}\|_F - \|\tilde{F}_{22}\|_F} \tag{9.86}$$

provided that

$$0 < \delta = \bar{\sigma}_n - \bar{\sigma}_{n+1} - \|\tilde{F}_{11}\|_F - \|\tilde{F}_{22}\|_F \tag{9.87}$$

and

$$\frac{\|\tilde{F}_{21}\tilde{F}_{12}^T\|_F}{\delta} \le \frac{1}{2}. \tag{9.88}$$

Since the Frobenius norm is unitarily invariant, we have from (9.84)

$$\|\tilde{F}\|_F = \|E_{qr}\|_F = \mathbf{O}(q^{-\alpha+1}). \tag{9.89}$$

From (9.82), we also have $\bar{\sigma}_i \to ?_i(G)$ for $i = 1, \ldots, n+1$ as $q, r \to \infty$. Thus as $q, r \to \infty$ and since $?_n > ?_{n+1}$, (9.87) and (9.88) is satisfied and we can write

$$\left(\bar{U}_s + \bar{U}_o P\right) Q = \hat{U}_s' \tag{9.90}$$

for some unique matrices $P = \mathbf{O}(q^{-\alpha+1})$ and Q satisfying

$$I_n = Q^T \left(I_n + P^T P\right) Q. \tag{9.91}$$

Without loss of generality, we can take $Q = I_n$ whenever $P = 0$ since $\hat{G}$ is invariant to similarity transformations.

Now we approximate G_{q+r}^n by $\hat{G}$ for noise free data. Let

$$\hat{A}_n' = \left(J_1 \hat{U}_s'\right)^\dagger J_2 \hat{U}_s' \tag{9.92}$$

where the shift matrix J_2 is defined by (*c.f.* (9.78))

$$J_2 \bar{U}_s = \begin{pmatrix} \bar{u}_1(1) & \cdots & \bar{u}_n(1) \\ \vdots & \ddots & \vdots \\ \bar{u}_1(q+r-2) & \cdots & \bar{u}_n(q+r-2) \end{pmatrix}.$$

Since

$$\|J_i \bar{U}_s P\|_F \le \|\bar{U}_o\|_F \|P\|_F \le (q-n)^{1/2} \|P\|_F = \mathbf{O}(q^{-\alpha+3/2});\ i = 1, 2, \tag{9.93}$$

from (9.83), (9.84), (9.86), (9.89-9.90), and (9.92) it follows that

$$\lim_{q,r\to\infty} \hat{A}_n' = \lim_{q,r\to\infty} Q^{-1} \left(J_1 \left[\bar{U}_s + \bar{U}_o P\right]\right)^\dagger J_2 \left[\bar{U}_s + \bar{U}_o P\right] Q = A_n. \tag{9.94}$$

In (9.92), only the first $q+1$ rows of $\hat{U}_s'$ are involved. Since $\hat{u}_i(q) \to 0$ for $i = 1, \ldots, n$ as $q \to \infty$, we get

$$A_n = \lim_{q,r\to\infty} \hat{A}_n' = \lim_{q,r\to\infty} \left(J_1 \hat{U}_s\right)^\dagger J_2 \hat{U}_s = \lim_{q,r\to\infty} \hat{A}.$$

From (9.13), (9.75), (9.83), (9.90), (9.91), and (9.93), we get

$$\lim_{q,r\to\infty} \hat{C} = C_n \qquad \lim_{q,r\to\infty} \hat{B} = B_n.$$

Now the following triangle inequality yields the desired result for noise-free data

$$\|G - \hat{G}\|_\infty \le \|G - G_{q+r}^n\|_\infty + \|G_{q+r}^n - \hat{G}\|_\infty. \tag{9.95}$$

Finally, we will prove consistency. Let E_{qr} denote the noisy part of the Hankel matrix in (9.10). Suppose we can show that

$$\|\sqrt{q} E_{qr}\|_F \to 0, \quad \text{w.p. } 1 \text{ as } M \to \infty. \tag{9.96}$$

Then from (9.86) and the inequality in (9.89), we have

$$\|\sqrt{q}P\|_F \to 0, \text{ w.p. } 1 \text{ as } M \to \infty,$$

where the perturbation matrix P is due to E_{qr}. Thus from (9.13), (9.75), (9.83), and (9.90)–(9.94), we conclude that $(\hat{A}, \hat{B}, \hat{C}) \to (A_n, B_n, C_n)$ w.p. 1 as $M \to \infty$.

Without loss of generality, we may assume that the system is single-input single-output. Let $w = 2M$ and $\phi(l+m) = 2\pi(l+m-1)$. The (l,m)th element of E_{qr} is then

$$[E_{qr}]_{l,m} = \frac{1}{w}\sum_{k=0}^{w-1} n_k e^{j\phi(l+m)k/w} = \frac{1}{w}S_w(l+m). \tag{9.97}$$

Let $\bar{R}$ over-bound noise covariances. We have by (9.97)

$$E\ |S_w(l+m)|^2 \le \bar{R}w.$$

Hence for each $\epsilon > 0$ by Chebyshev inequality [24]

$$P\left(\|\sqrt{q}E_{qr}\|_F > \epsilon\right) \le \frac{q}{\epsilon^2}E\ \|E_{qr}\|_F^2 = \frac{q}{w^2\epsilon^2}\sum_{1\le l,m\le q} E\ |S_w(l+m)|^2 \le \frac{q^3\bar{R}}{w\epsilon^2}.$$

Taking a subsequence $\sqrt{q}S_{w^2}$, we get

$$\sum_w P\left(\|\sqrt{q}S_{w^2}\|_F > w^2\epsilon\right) = \sum_w \frac{q^3\bar{R}}{w^2\epsilon^2} < \infty$$

since $q = \mathbf{O}(M^{1/3}\log(M)^{-\beta})$, $\beta > 1/3$. Hence by Borel-Cantelli lemma [24], we have

$$\frac{\|\sqrt{q}S_{w^2}\|_F}{w^2} \to 0, \text{ w.p. } 1 \text{ as } w \to \infty. \tag{9.98}$$

We have thus proved the desired result for a subsequence. Now it will be extended to the whole sequence. For $w^2 < k < (w+1)^2$ with

$$S_k(l+m) - S_{w^2}(l+m) = \sum_{i=0}^{w^2-1} n_i\left[e^{j\phi(l+m)i/k} - e^{j\phi(l+m)i/w^2}\right] + \sum_{i=w^2}^{k-1} n_i e^{j\phi(l+m)i/k},$$

we have

$$\begin{aligned} &E\ |S_k(l+m) - S_{w^2}(l+m)|^2 \\ &\quad\le 2\ E\left|\sum_{i=0}^{w^2-1} n_i\left[e^{j\phi(l+m)i/k} - e^{j\phi(l+m)i/w^2}\right]\right|^2 + 2\ E\left|\sum_{i=w^2}^{k-1} n_i e^{j\phi(l+m)i/k}\right|^2 \\ &\qquad\le 8\bar{R}w^2\left(\sin\frac{\phi(l+m)w^2}{kw}\right)^2 + 4\bar{R}\ w \le 4\bar{R}\left(2(4\pi q)^2 + w\right) \end{aligned}$$

since $m + l \leq 2q$. Let

$$D_w(l+m) = \max_{w^2<k<(w+1)^2} |S_k(l+m) - S_{w^2}(l+m)| .$$

Then we have

$$E\left[D_w^2(l+m)\right] \leq E\left[\sum_{k=w^2+1}^{(w+1)^2-1} |S_k(l+m) - S_{w^2}(l+m)|^2\right] \leq 8\bar{R}\left[2(4\pi q)^2 + w\right] w$$

and consequently applying Chebyshev inequality we obtain for some constant c that

$$P(\|\sqrt{q}D_w\|_F > w^2\epsilon) \leq \sum_{1\leq l,m\leq q} \frac{qE\left[D_w^2(l+m)\right]}{w^4\epsilon^2} \leq \frac{cq^3\left[2(4\pi q)^2 + w\right]}{w^3\epsilon^2}.$$

It follows as before that

$$\frac{\|\sqrt{q}D_w\|_F}{w^2} \to 0, \quad \text{w.p. 1 as } w \to \infty. \tag{9.99}$$

For $w^2 < k < (w+1)^2$ using the following inequality

$$\frac{|S_k(l+m)|}{k} \leq \frac{|S_{w^2}(l+m)| + D_w(l+m)}{w^2},$$

we get

$$\frac{\|\sqrt{q}S_w\|_F}{w} \leq \frac{\|\sqrt{2q}S_{w^2}\|_F}{w^2} + \frac{\|\sqrt{2q}D_w\|_F}{w^2}.$$

Hence from (9.98) and (9.99), (9.96) follows. □

9.4.3 Discussion

Algorithm 9.1 exactly identifies rational transfer functions using a minimum number of data given noise-free data. This is a remarkable advantage with respect to linear black-box identification algorithms like FIR or other model structures based on some orthogonal basis [162].

The least-squares procedure to estimate $\hat{B}$ and $\hat{D}$ used in Algorithm 9.2 is a particular case of the nonlinear least-squares identification algorithm (NLS) (8.6) in Chapter 8, where $\hat{A}$ and $\hat{C}$ also are estimated. The NLS is not suitable for narrow band data if the model fit is measured in the $\mathcal{H}_\infty$-norm. To reduce model mismatch, model orders should be increased. As this happens, the pole-zero sensitivity of the model increases.

Let $\hat{A}$, $\hat{C}$ be calculated as in Algorithm 9.1, $\hat{B}$ from

$$\hat{B} = \hat{\Sigma}_s \hat{V}_s^T J_4$$

and $\hat{D} = \hat{h}_0$. This algorithm was studied in a modal analysis context by Juang and Suzuki [64] and also discussed in [61]. It is a biased algorithm which has poor performance whenever A^{2M} is large, *e.g.* lightly damped systems. However it converges to a transfer function equal to the truncated balanced realization of the system under the system and noise assumptions (9.71) and (9.49)-(9.52), respectively.

9.4.4 Continuous-Time Systems

The results in this section apply to continuous-time systems if they are transformed into the discrete domain. The bilinear map and the zero-order hold sampling equivalence are two popular techniques to discretize continuous-time systems. Since Hankel singular values are invariant under the bilinear map, Theorem 9.6 holds for the continuous-time systems if the bilinear transformation is used.

The bilinear transformation requires frequency response at very high frequencies if the equivalent discrete-time data are to be equally spaced. Hence, the bilinear method is limited to narrow bandwidth systems for practical applications.

9.4.5 Example

We will consider the problem of approximating the infinite dimensional transfer function

$$G(s) = \frac{1}{s + 1 - e^{-2-s}} \tag{9.100}$$

with a finite dimensional linear model. This particular problem has also been studied by Gu *et al.* [48]. As in [48], we use 512 uniformly spaced noise free frequency response data on $[0, \pi]$ derived from (9.100) by use of the bilinear map and pre-warping of the frequencies. In Figure 9.3, the error between the frequency response of the estimated model and the true frequency response

$$\|G - \hat{G}\|_{m,\infty} = \max_{\omega_k} |G_k - \hat{G}(e^{j\omega_k})|$$

is plotted for model orders ranging from 1 to 28 using Algorithm 9.1 shown by "x" on the figure. The results shown by "o" are the error for models estimated with Algorithm 9.1 using the extra projection step to obtain stable models as described in Section 9.2. Here we take $q = r = 512$ which gives the Hankel matrix of maximal dimensions. From the figure we notice a deviation at model orders 21, 23, 24, 25, and 26 which are due to the unstable initial models which after the projection step obtain an increased, however still reasonable, model error. The first order approximation has the error 3.1×10^{-2} to be compared with the first order model in [48] with error 3.2×10^{-2}. The error is reduced by increasing the model order. Our 24th order stable approximation has a quite small error 1.1×10^{-6} to be compared with the 24th order approximant of Gu *et al.* with error 7.9×10^{-3}. A further increase of the model order to 27 gives almost negligible error 2.4×10^{-12}.

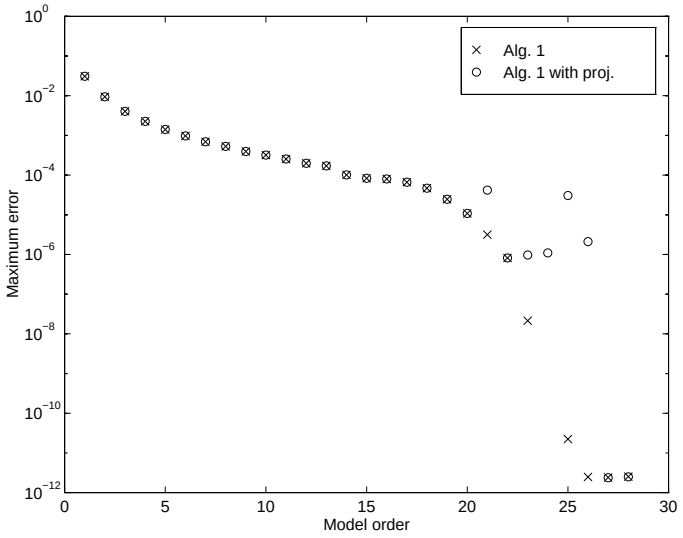

Figure 9.3: Plot of $\|G - \hat{G}\|_{m,\infty}$ for different model orders using Algorithm 9.1. "o": with projection of unstable eigenvalues of $\hat{A}$ into the unit disc. "x": without projection.

9.4.6 Conclusions

This section has analyzed the properties of Algorithm 9.1 when applied to data from an infinite-dimensional system. If the system is nuclear we show that the identification algorithm asymptotically yields a finite order estimated transfer function which is equal to the transfer function of the truncated balanced realization of the original system. The result also holds when the transfer function samples are corrupted with zero mean random variables with bounded covariances under certain conditions on the dimension of the Hankel matrix H_{qr}. The presented identification example illustrates the good performance of the new algorithm when compared with the method of Gu *et al.* [48].

9.5 Frequency Weighting

In most practical identification applications it is important to be able to shape the resulting identification error. Often prior information is available which can be used to improve the model quality. This knowledge is often in the form of known spectral densities of the excitation signal and the noise sources. For identification in the time domain, the resulting estimation error is shaped by pre-filtering input and output data [86, 136]. For frequency domain methods, *i.e.*, when samples of the frequency response functions are the primary data, it is often quite straightforward to use weightings since most methods are based on parametric optimization techniques.

The archetypical situation is the minimization of a frequency weighted norm

$$\hat{G}(z) = \arg \min_{G(z)\in\mathcal{M}} \sum_{k=0}^{M} \left\| F_k^y (G_k - G(e^{j\omega_k}))F_k^u \right\|^2, \tag{9.101}$$

where G_k are the $M+1$ measured frequency responses and $\hat{G}(z)$ the identified model from some model set $\mathcal{M}$. Here F_k^y is the output weight matrix and F_k^u the input weight matrix. For the single input and/or single output case it suffices with one weight matrix since $G(z)$ in this case is vector or scalar valued.

The aim of this section is to present an algorithm which produces a suboptimal solution to (9.101). The algorithm is based on Algorithm 9.1 augmented with frequency weighting properties. We do this by applying the technique of frequency weighted balanced truncation introduced by Enns [36, 37] and further analyzed in [69]. By introducing a particular frequency weighted state-space basis followed by state truncation a lower dimensional model results which has a frequency weighted truncation error. Successful applications are reported [9, 165] for controller reduction. In [150, 153] the frequency weighted balanced realizations are used to interpret in which state-space basis estimated models will belong to when using subspace based algorithms. Also the direct identification of a lower order model is discussed for various subspace algorithms. Our presentation of Enns's ideas are based on [150].

Most model reduction methods assume the knowledge of a high order system and the task is to find a lower order model with desired model error properties usually given as bounds of the frequency response of the model error. Here we instead assume that frequency response measurements of a high order or infinite-dimensional system are available and we directly identify a low order model. By using frequency weights we show that the user is free to tune the identification procedure in order to obtain a good fit for important frequency ranges.

9.5.1 The Identification Problem

The problem is as follows: Given $M+1$ noise corrupted measurements

$$G_k = G(e^{j\omega_k}) + n_k, \quad k = 0, \ldots, M \tag{9.102}$$

of the frequency response of the system at equidistant frequencies $\omega_k = \frac{k\pi}{M}$, $k = 0, \ldots, M$, find a finite dimensional state-space system (9.2) of order n, denoted by $\hat{G}$, such that the error between true system and the identified model, quantified by

$$\left\| F_y(z)(\hat{G} - G)F_u(z) \right\|_\infty, \tag{9.103}$$

is "small". In (9.103) $F_u(z)$ and $F_y(z)$ are user supplied stable filters which are used to shape the modeling error.

9.5.2 Frequency Weighted Balanced Model Reduction

The technique of balanced truncation introduced in [109] and [117] is a much used method for model reduction. This technique was extended [36, 37] to also enhance

the fit in certain frequency regions by user supplied weighting filters. This makes it possible to produce low order models which are accurate in the frequency region of interest.

Given a model $G(z) \in \mathbb{C}^{p\times m}$ of order n, the aim is to find a lower order model $G_l(z) \in \mathbb{C}^{p\times m}$, $l < n$ minimizing the norm

$$\|F_y(z)(G(z) - G_l(z))F_u(z)\|_\infty ,$$

where $F_y(z) \in \mathbb{C}^{p\times p}$ and $F_u(z) \in \mathbb{C}^{m\times m}$ are the output and input frequency filters, respectively. These filters are chosen by the user to influence the distribution of the error over the frequencies. The idea is based on considering the cascaded system

$$F_y(z)G(z)F_u(z). \tag{9.104}$$

A particular state-space basis is determined by diagonalizing parts of the observability and controllability Gramian for the cascaded system (9.104). Let (A, B, C, D) be a state-space realization of the transfer function $G(z)$, (A_y, B_y, C_y, D_y) a realization for the filter $F_y(z)$ and (A_u, B_u, C_u, D_u) the realization corresponding to $F_u(z)$.

Definition 9.3 The solution P_{11} of the Lyapunov equation:

$$\begin{pmatrix} A & BC_u \\ 0 & A_u \end{pmatrix} \begin{pmatrix} P_{11} & P_{12} \\ P_{12}^T & P_{22} \end{pmatrix} \begin{pmatrix} A & BC_u \\ 0 & A_u \end{pmatrix}^T$$

$$+ \begin{pmatrix} BD_u \\ B_u \end{pmatrix} \begin{pmatrix} BD_u \\ B_u \end{pmatrix}^T = \begin{pmatrix} P_{11} & P_{12} \\ P_{12}^T & P_{22} \end{pmatrix}$$

is called the $F_u(z)$ *weighted controllability Gramian* and is denoted by

$$W_c^u = P_{11}.$$

□

Of course we also have the dual Gramian.

Definition 9.4 The solution Q_{11} of the Lyapunov equation:

$$\begin{pmatrix} A & 0 \\ B_yC & A_y \end{pmatrix}^T \begin{pmatrix} Q_{11} & Q_{12} \\ Q_{12}^T & Q_{22} \end{pmatrix} \begin{pmatrix} A & 0 \\ B_yC & A_y \end{pmatrix}$$

$$+ \begin{pmatrix} D_yC & C_y \end{pmatrix}^T \begin{pmatrix} D_yC & C_y \end{pmatrix} = \begin{pmatrix} Q_{11} & Q_{12} \\ Q_{12}^T & Q_{22} \end{pmatrix}$$

is called the $F_y(z)$ *weighted observability Gramian* and is denoted by

$$W_o^y = Q_{11}.$$

□

If the realization of $G(z)$ undergoes a similarity transformation $T \in \mathbb{R}^{n\times n}$

$$\begin{aligned} A &\to TAT^{-1} \\ B &\to TB \\ C &\to CT^{-1}, \end{aligned}$$

it is easy to show [37] that

$$\begin{aligned} W_c^u &\to T^{-1}W_c^u T^{-T} \\ W_o^y &\to T^T W_o^y T. \end{aligned} \tag{9.105}$$

In a similar fashion as for the classical balancing problem [109] it is always possible to make the two Gramian matrices diagonal and equal for a proper choice of transformation matrix T.

Definition 9.5 A system $G(z)$ with realization (A, B, C, D) is *frequency weighted balanced* if

$$W_c^u = W_o^y = \Sigma(F_u, F_y)$$

where $\Sigma(F_u, F_y) = \text{diag}\,(\sigma_1, \sigma_2, \ldots, \sigma_n)$ are the frequency weighted Hankel singular values in a non-increasing order denoted by

$$\sigma_k(F_u, F_y).$$

□

From (9.105) we notice that the eigenvalues of $W_c^u W_o^y$ are equal to the squared frequency weighted Hankel singular values. It is also straightforward to see that frequency weighted singular values $\sigma_k(F_u, F_y)$ are independent of the realization of $G(z)$ or the realizations of the filters $F_y(z)$ and $F_u(z)$.

Let us now consider a state-truncation of a realization given in a frequency balanced realization. This leads to a reduced order model. If we partition the state-space matrices

$$\begin{aligned} A &= \begin{pmatrix} A_{11} & A_{12} \\ A_{21} & A_{22} \end{pmatrix}, \quad B = \begin{pmatrix} B_1 \\ B_2 \end{pmatrix} \\ C &= \begin{pmatrix} C_1 & C_2 \end{pmatrix}, \end{aligned} \tag{9.106}$$

with $A_{11} \in \mathbb{R}^{l\times l}$, $B_1 \in \mathbb{R}^{l\times m}$ and $C_1 \in \mathbb{R}^{p\times l}$, a reduced order model is given by the realization (A_{11}, B_1, C_1, D). The reduced order transfer function is then

$$G_l(z) = C_1(zI - A_{11})^{-1}B_1 + D.$$

A recent result gives a hard bound of the truncation error.

Theorem 9.7 ([69]) *Let $G(z)$ be a stable transfer function of order n and let $F_u(z)$ and $F_y(z)$ be stable weighting functions. Also let $G_l(z)$ be the frequency*

weighted balanced truncation (9.106) of order l. Assume $G_l(z)$ is stable. Then the following error bound holds:

$$\|F_y(z)(G(z)-G_l(z))F_u(z)\|_\infty \leq 2\sum_{k=l+1}^{n}\sqrt{\sigma_k^2+(\alpha_k+\beta_k)\sigma_k^{3/2}+\alpha_k\beta_k\sigma_k}$$

where $\sigma_k = \sigma_k(F_y, F_u)$, and α_k and β_k are finite.

For brevity we have omitted the expressions for α_k and β_k. The full expressions can be found in [69].

9.5.3 Frequency Weighted Identification

In this subsection we introduce a frequency weighted variant of Algorithm 9.1 by using the concepts of frequency weighted balanced realizations.

Let us first introduce two lower triangular block-Toeplitz matrices with elements from the impulse response of the two stable frequency filters $F_y(z)$ and $F_u(z)$.

$$F_y = \begin{pmatrix} D_y & 0 & 0 & \dots & 0 \\ C_yB_y & D_y & 0 & \dots & 0 \\ C_yA_yB_y & C_yB_y & D_y & \dots & 0 \\ \dots & \dots & \dots & \dots & \dots \\ C_yA_y^{q-2}B_y & C_yA_y^{q-3}B_y & C_yA_y^{q-4}B_y & \dots & D_y \end{pmatrix} \in \mathbb{R}^{qp\times qp}$$

$$F_u = \begin{pmatrix} D_u & 0 & 0 & \dots & 0 \\ C_uB_u & D_u & 0 & \dots & 0 \\ C_uA_uB_u & C_uB_u & D_u & \dots & 0 \\ \dots & \dots & \dots & \dots & \dots \\ C_uA_u^{r-2}B_u & C_uA_u^{r-3}B_u & C_uA_u^{r-4}B_u & \dots & D_u \end{pmatrix} \in \mathbb{R}^{rm\times rm}$$

Using F_y and F_u we can formulate a frequency weighted identification algorithm.

Algorithm 9.3

1.

$$G_{M+k} := G_{M-k}^*, \quad k = 1,\dots,M-1 \tag{9.107}$$

where $(\cdot)^*$ denotes complex conjugate.

2. Let $\hat{h}_i$ be defined by the $2M$-point Inverse Discrete Fourier Transform (IDFT)

$$\hat{h}_i = \frac{1}{2M}\sum_{k=0}^{2M-1} G_k\, e^{j2\pi ik/2M},\ i = 0,\dots,q+r-1. \tag{9.108}$$

3. Let the block Hankel matrix $\hat{H}_{qr}$ be defined as

$$\hat{H}_{qr} = \begin{pmatrix} \hat{h}_1 & \hat{h}_2 & \dots & \hat{h}_r \\ \hat{h}_2 & \hat{h}_3 & \dots & \hat{h}_{r+1} \\ \vdots & \vdots & \ddots & \vdots \\ \hat{h}_q & \hat{h}_{q+1} & \dots & \hat{h}_{q+r-1} \end{pmatrix} \in \mathbb{R}^{qp\times rm} \tag{9.109}$$

with number of block rows $q > n$ and block columns $r \geq n$. The dimension of $\hat{H}_{qr}$ is bounded by $q + r \leq M$.

4. *Let the singular value decomposition of the weighted Hankel matrix $F_y \hat{H}_{qr} F_u$ be denoted by*

$$F_y \hat{H}_{qr} F_u = \begin{pmatrix} \hat{U}_s & \hat{U}_o \end{pmatrix} \begin{pmatrix} \hat{\Sigma}_s & 0 \\ 0 & \hat{\Sigma}_o \end{pmatrix} \begin{pmatrix} \hat{V}_s^T \\ \hat{V}_o^T \end{pmatrix} \tag{9.110}$$

where $\hat{\Sigma}_s$ contains the n largest singular values.

5.

$$\hat{A} = (J_1 F_y^{-1} \hat{U}_s \hat{\Sigma}_s^{1/2})^\dagger J_2 F_y^{-1} \hat{U}_s \hat{\Sigma}_s^{1/2} \tag{9.111}$$

$$\hat{C} = J_3 F_y^{-1} \hat{U}_s \Sigma_s^{1/2} \tag{9.112}$$

6.

$$\hat{B} = (I - \hat{A}^{2M}) \hat{\Sigma}_s^{1/2} \hat{V}_s^T F_u^{-1} J_4 \tag{9.113}$$

$$\hat{D} = \hat{h}_0 - \hat{C} \hat{A}^{2M-1} (I - \hat{A}^{2M})^{-1} \hat{B} \tag{9.114}$$

where

$$J_1 = \begin{pmatrix} I_{(q-1)p} & 0_{(q-1)p \times p} \end{pmatrix}, \quad J_2 = \begin{pmatrix} 0_{(q-1)p \times p} & I_{(q-1)p} \end{pmatrix}$$
$$J_3 = \begin{pmatrix} I_p & 0_{p \times (q-1)p} \end{pmatrix}, \quad J_4 = \begin{pmatrix} I_m \\ 0_{(r-1)m \times m} \end{pmatrix}$$

and I_i denotes the $i \times i$ identity matrix, $0_{i \times j}$ denotes the $i \times j$ zero matrix and $X^\dagger = (X^T X)^{-1} X^T$ denotes the Moore-Penrose pseudo-inverse of the full column rank matrix X.

We also can consider an alternative way of determining B and D by using the frequency weighted version of Algorithm 9.2

Algorithm 9.4

1-5. Analogous to steps 1-5 in Algorithm 9.3.

6.

$$\hat{B},\ \hat{D} = \arg \min_{\substack{B \in \mathbb{R}^{n \times m} \\ D \in \mathbb{R}^{p \times m}}} \sum_{k=0}^{M} \left\| F_y(e^{j\omega_k})(G_k - D - \hat{C}(e^{j\omega_k} I - \hat{A})^{-1} B) F_u(e^{j\omega_k}) \right\|_F^2. \tag{9.115}$$

Denote by $\hat{G}$ the identified transfer function

$$\hat{G}(z) = \hat{C}(zI - \hat{A})^{-1} \hat{B} + \hat{D}.$$

When applied to data which are noise free and originate from a system of order n these two algorithms will deliver state-space realizations which are frequency weighted balanced as given in Definition 9.5 when $q, r \to \infty$. Before deriving this result we look at an alternative derivation of the frequency weighted Gramian matrices.

Lemma 9.3 ([150]) *If $G(z)$, $F_u(z)$ and $F_y(z)$ are stable then*

$$W_o^y = \lim_{q\to\infty} \mathcal{O}_q^T F_y^T F_y \mathcal{O}_q$$

$$W_c^u = \lim_{r\to\infty} \mathcal{C}_r F_u F_u^T \mathcal{C}_r^T$$

where $\mathcal{O}_q$ and $\mathcal{C}_r$ are the extended observability (9.18) and controllability (9.19) matrices of the realization (A, B, C, D) of $G(z)$.

We are now ready to present the main result of this section.

Theorem 9.8 *Suppose $M+1$ equidistant frequency samples of a stable linear system G of order n are given. Let $F_u(z)$ and $F_y(z)$ be any stable filters with D_u and D_y matrices of full rank. Then*

(i) If $q > n$, $r \geq n$ and $M \geq q + r$, the estimated system $\hat{G}$ using Algorithms 9.3 or 9.4 will equal G if the frequency response G_k is noise-free.

(ii) The realization of $\hat{G}$ will be frequency weighted balanced and

$$\hat{\Sigma}_s \to \Sigma(F_u, F_y) \quad \text{as } M, q, r \to \infty.$$

Proof: $\hat{H}_{qr}$ has rank n, see proof of Theorem 9.1. Since D_u and D_y are of full rank, F_u and F_y are matrices of full rank independently of q and r. Hence $F_y \hat{H}_{qr} F_u$ is still a matrix of rank n. Using (9.110) we can write

$$F_y \hat{H}_{qr} F_u = \hat{U}_s \hat{\Sigma}_s \hat{V}_s^T.$$

In (9.111) and (9.112) we implicitly use

$$\hat{\mathcal{O}}_q = F_y^{-1} \hat{U}_s \hat{\Sigma}_s^{1/2} \tag{9.116}$$

as the extended observability matrix. Equation (9.113) also implicitly defines

$$\hat{\mathcal{C}_r} = (I - \hat{A}^{2M}) \hat{\Sigma}_s^{1/2} \hat{V}_s^T F_u^{-1} \tag{9.117}$$

as the controllability matrix. Hence we obtain

$$\hat{\mathcal{O}}_q (I - \hat{A}^{2M})^{-1} \hat{\mathcal{C}_r} = F_y^{-1} F_y \hat{H}_{qr} F_u F_u^{-1} = \hat{H}_{qr}.$$

(i) now follows by the same arguments as in the proof of Theorem 9.1 in Section 9.3.

For the second part (ii), let $M, q, r \to \infty$ and drop the indices q and r. Then $A^{2M} \to 0$ and consequently, using (9.116) and (9.117), can we write

$$F_y \hat{\mathcal{O}} = \hat{U}_s \hat{\Sigma}_s^{1/2}.$$

and

$$\hat{\mathcal{C}} F_u = \hat{\Sigma}_s^{1/2} \hat{V}_s^T$$

Finally, using Lemma 9.3 we obtain the frequency weighted Gramians as

$$W_o^y = \hat{\mathcal{O}}^T F_y^T F_y \hat{\mathcal{O}} = \hat{\Sigma}_s$$

and

$$W_c^u = \hat{\mathcal{C}} F_u F_u^T \hat{\mathcal{C}}^T = \hat{\Sigma}_s$$

since $\hat{U}_s^T \hat{U}_s = I$ and $\hat{V}_s^T \hat{V}_s = I$. Both Gramians are diagonal and equal which implies that the identified state-space model is frequency weighted balanced and that

$$\hat{\Sigma}_s = \Sigma(F_u, F_y).$$

In Algorithm 9.4 A and C are determined as in Algorithm 9.3. Since the data are assumed to be noise-free there exist matrices B and D which makes the criterion (9.115) identical zero. This implies that the estimated transfer function is the true one. Since $\hat{A}$ and $\hat{C}$ are the same for the two algorithms, we conclude that $\hat{B}$ and $\hat{D}$ also are the same for the two algorithms. □

Notice that the frequency filters $F_u(z)$ and $F_y(z)$ only influence the realization obtained and not the transfer function itself. This holds only when dealing with noise free data and if the system has order n. In practice these two conditions are always violated and now the frequency filters will play an important role. In this case the singular values of $\hat{\Sigma}_o$ will not be zero and the algorithm will produce a model which is close to the truncated frequency weighted balanced realization.

Remark 9.3 *By applying the stochastic analysis given in Section 9.4 it follows that the stated result also holds with probability 1 if the measurements G_k are corrupted with zero mean random noise with bounded second moments if we let $q, r = \mathbf{O}(M^{1/3}(\log M)^{-\beta})$ for some $\beta > 1/3$.*

From Section 9.4 we know that if applied to data from an infinite-dimensional system the unweighted identification algorithm delivers models with transfer functions which converge to the truncated balanced realization. It would thus be appealing to extend this result for the new frequency weighted algorithm and show that the frequency weighted algorithm asymptotically will deliver models which are the frequency weighted balanced truncation of an infinite-dimensional system.

9.5.4 Applicability to Finite Data

In the previous subsection we have demonstrated that Algorithms 9.3 and 9.4 have the desired asymptotic behavior; frequency weighted balanced realizations

will result from the identification. Now we will investigate what properties the algorithm possess when used on finite data. We do this by considering an example.

Let G be a fourth order model with a frequency response with two resonant peaks. The following state-space model represents G

$$x(t+1) = \begin{pmatrix} 0.8876 & 0.4494 & 0 & 0 \\ -0.4494 & 0.7978 & 0 & 0 \\ 0 & 0 & -0.6129 & 0.0645 \\ 0 & 0 & -6.4516 & -0.7419 \end{pmatrix} x(t) + \begin{pmatrix} 0.2247 \\ 0.8989 \\ 0.0323 \\ 0.1290 \end{pmatrix} u(t)$$

$$y(t) = \begin{pmatrix} 0.4719 & 0.1124 & 9.6774 & 1.6129 \end{pmatrix} x(t) + 0.9626\, u(t).$$

The transfer function of G is sampled at 101 equidistant frequency points including frequency 0 and π. The solid line in Figure 9.4 represents the magnitude of the frequency function. Let us consider four different identification cases:

Case 1 Algorithm 9.3 with low pass frequency filter.

Case 2 Algorithm 9.3 with high pass frequency filter.

Case 3 Algorithm 9.4 with low pass frequency filter.

Case 4 Algorithm 9.4 with high pass frequency filter.

Since we are dealing with a SISO system we let $F_u(z) = F_y(z)$ and use a fifth order standard Butterworth filter with cut-off frequency $0.4/\pi$ rad/s in the low-pass form for cases 1 and 3 and in high-pass form for the other two cases. In Figure 9.4 the results of the four cases are presented. The solid graph is the magnitude of the original fourth order system. The dashed graph represents the estimated second order model for the four different cases. The magnitude of the frequency filters are shown as dotted lines and the dash-dotted line is the magnitude of the difference between the original model and the second order estimated model. In all four cases the peak is correctly estimated which indicates that the pole locations in the desired frequency band have been properly found. The final error in the weighted frequency band is lower for cases 3 and 4. This stems from improved DC-level and zero locations by the additional weighted least-squares step found in Algorithm 9.4. Based on this example it is clear that the frequency weights F_y and F_u indeed can make the algorithms focus on a selected frequency range.

9.5.5 Conclusions and Open Problems

In this section we have shown how the identification Algorithm 9.1 can be augmented with frequency weighting capabilities. We do this by using a technique closely related to frequency weighted balanced model reduction [36]. We show that as the size of the Hankel matrix tends to infinity the identification method yields models which are frequency weighted balanced. By considering an example, the applicability of the new frequency weighted algorithms to the case of finite data has been shown to be adequate. The algorithms are thus well suited for low order modeling directly from frequency data originating from systems of high complexity. This approach is thus a viable alternative to the two step approach of

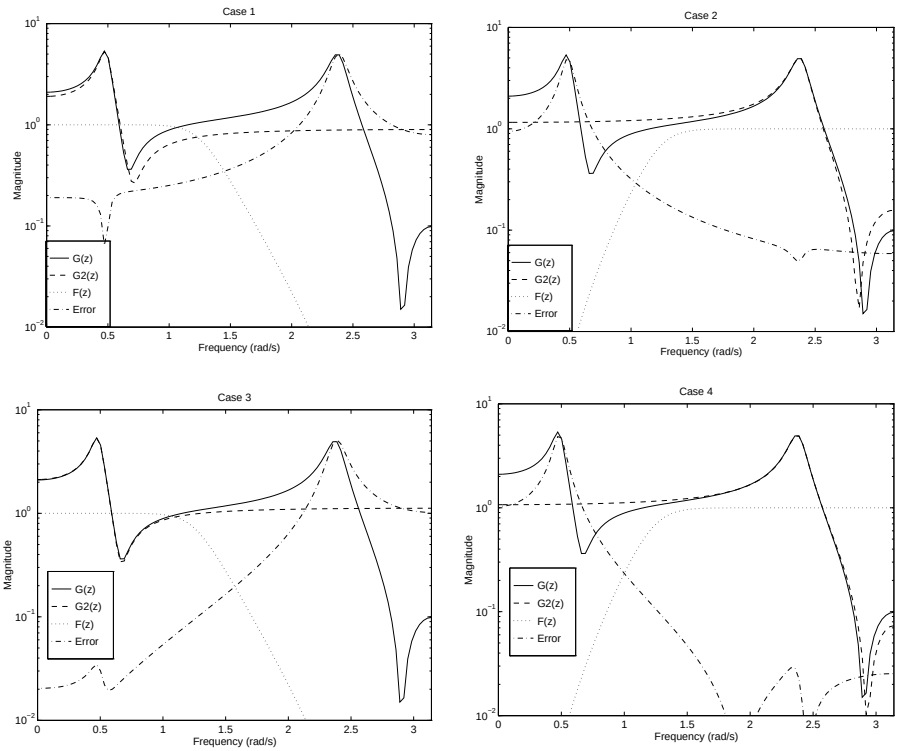

Figure 9.4: Results of the four different identification cases: Upper left; Case 1 using Alg. 9.3 with low-pass weighting. Upper right Case 2; Alg. 9.3 with high-pass weighting. Lower left Case 3; Alg. 9.4 with low-pass weighting. Lower right Case 4; Alg. 9.4 with high-pass weighting. The solid lines are the magnitude of the original fourth order system. The dashed lines represent the estimated second order models. The magnitude of the frequency filters are shown as dotted lines and the dash-dotted lines are the magnitude of the difference between the original model and the second order estimated model.

higher order modeling followed by model reduction. It is still an open question if the algorithm, when applied to data from infinite-dimensional systems, will yield finite-dimensional models which are frequency weighted balanced truncations of the original system.

10

Subspace Based Methods

10.1 Introduction

Methods which identify state-space models by means of geometrical properties of the input and output sequences are commonly known as subspace methods and have received much attention in the literature. The early subspace identification methods [31, 107, 155] focused on deterministic systems with errors present at the outputs only. These methods are consistent only if the noise is both spatially and temporally white [159]. By extending these methods, consistent algorithms have been obtained when the errors also affect the states or, equivalently, are described by colored output noise [152, 156, 157, 160]. One of the advantages with the methods is the absence of a parametric iterative optimization step. In classical prediction error minimization [86], such a step is necessary for most model structures. An excellent overview of time domain subspace methods is given in [158].

In this chapter we consider the case where data are given in the frequency domain, *i.e.*, when samples of the Fourier transform of the input and output signals are the primary measurements. In a number of applications it is common to fit models in the frequency domain [89, 129]. Subspace based algorithms formulated in the frequency domain have appeared recently. A frequency domain version of [85] (which is closely related to the basic projection algorithm [29, 31]) has been described in [84]. In a more recent contribution, [154], frequency domain formulations of the intersection algorithm [107] and N4SID [152] have been studied.

This problem formulation differs from the previous chapter where the frequency response of the system, given at equidistant frequencies, was considered the primary measurements. For single-input single-output systems with samples of the Fourier transform of the input and output given at equidistant frequencies, the two problem formulations coincide since

$$G(e^{j\omega}) = \frac{Y(\omega)}{U(\omega)}.$$

The goal of this chapter is to demonstrate that the recent subspace based identi-

fication algorithms, by simple modifications, can be used to identify systems using frequency domain data. In contrast to Algorithm 9.1 we will now assume the Fourier transform of the input and output signals to be given at arbitrary frequencies. The algorithm which we present is based on the time domain version called PI-MOESP [156]. Analysis will show that the algorithm is strongly consistent under mild assumptions on the noise.

10.2 Problem Description

Given samples of the discrete time Fourier transform of the input and output signals of a dynamic system, we seek an algorithm which identifies a state-space model of finite order.

Let us consider stable linear time-invariant discrete time systems of finite order n. One form of describing such a system is by the state-space equations

$$\begin{aligned} x(k+1) &= Ax(k) + Bu(k) \\ y(k) &= Cx(k) + Du(k) + n(k), \end{aligned} \tag{10.1}$$

where $u(k) \in \mathbb{R}^m$, $y(k) \in \mathbb{R}^p$ and $x(k) \in \mathbb{R}^n$. $n(k) \in \mathbb{R}^p$ is the noise term which we assume is independent of the input sequence $u(k)$. Here the time index k denotes normalized time. Hence $y(k)$ denotes the sample of the output signal $y(t)$ at time instant $t = kT$ where T denotes the sampling period. We also assume that the state-space realization (10.1) is minimal, which implies both observability and controllability [66]. A system with this type of noise model is commonly known as an output-error model [86]. Note that all such pairs (10.1) describing the same input/output behavior of the system are equivalent under a non-singular similarity transformation $T \in \mathbb{R}^{n \times n}$ [66], *i.e.*, the matrices $(T^{-1}AT, T^{-1}B, CT, D)$ will be an equivalent state-space realization.

The frequency response of the system (10.1) is

$$G(e^{j\omega}) = C(e^{j\omega}I - A)^{-1}B + D. \tag{10.2}$$

10.3 Subspace Identification

10.3.1 The Basic Relations

Let us introduce the vector of stacked outputs as

$$y_q(k) = \begin{pmatrix} y(k) \\ y(k+1) \\ \vdots \\ y(k+q-1) \end{pmatrix} \tag{10.3}$$

and conformally $u_q(k)$ and $n_q(k)$. The extended observability matrix is given as

$$\mathcal{O}_q = \begin{pmatrix} C \\ CA \\ \vdots \\ CA^{q-1} \end{pmatrix} \tag{10.4}$$

and the lower triangular Toeplitz matrix

$$?_q = \begin{pmatrix} D & 0 & \dots & 0 \\ CB & D & \dots & 0 \\ \vdots & \vdots & \ddots & \vdots \\ CA^{q-2}B & CA^{q-3}B & \dots & D \end{pmatrix}. \tag{10.5}$$

By recursive use of (10.1), we obtain [29] the relation

$$y_q(k) = \mathcal{O}_q x(k) + ?_q u_q(k) + n_q(k). \tag{10.6}$$

The extended observability matrix has a rank equal to the system order n if $q \geq n$ since the system is minimal.

The discrete time Fourier transform $\mathcal{F}$ of a sequence $f(k) \in \ell_1$ is defined as

$$\mathcal{F}f(k) = F(\omega) = \sum_{k=-\infty}^{\infty} f(k)e^{-j\omega k}. \tag{10.7}$$

From the definition (10.7) it follows immediately that the discrete Fourier transform of a time shifted sequence satisfies

$$\mathcal{F}f(k+n) = e^{j\omega n}F(w). \tag{10.8}$$

Let $Y(\omega) = \mathcal{F}y(k)$, $U(\omega) = \mathcal{F}u(k)$ and $N(\omega) = \mathcal{F}n(k)$. If we now apply the Fourier transform $\mathcal{F}$ on both sides of (10.6) we obtain

$$W_q(\omega) \otimes Y(\omega) = \mathcal{O}_q X(\omega) + ?_q W_q(\omega) \otimes U(\omega) + W_q(\omega) \otimes N(\omega), \tag{10.9}$$

where $\otimes$ denotes the Kronecker product [59] and

$$W_q(\omega) = \begin{bmatrix} 1 & e^{j\omega} & e^{j2\omega} & \dots & e^{j\omega(q-1)} \end{bmatrix}^T. \tag{10.10}$$

Notice that (10.9) is the frequency domain version of (10.6).

Assume we have samples of the Fourier transform of the input and output signals at M frequencies ω_k, $k = 1, \dots, M$. By collecting these samples in matrices

$$\mathbf{Y}_{q,M} = \begin{pmatrix} W_q(\omega_1) \otimes Y(\omega_1), & \cdots, & W_q(\omega_M) \otimes Y(\omega_M) \end{pmatrix}, \tag{10.11}$$

$$\mathbf{U}_{q,M} = \begin{pmatrix} W_q(\omega_1) \otimes U(\omega_1), & \cdots, & W_q(\omega_M) \otimes U(\omega_M) \end{pmatrix}, \tag{10.12}$$

$$\mathbf{N}_{q,M} = \begin{pmatrix} W_q(\omega_1) \otimes N(\omega_1), & \cdots, & W_q(\omega_M) \otimes N(\omega_M) \end{pmatrix}, \tag{10.13}$$

$$\mathbf{X}_M = \begin{pmatrix} X(\omega_1), & \cdots, & X(\omega_M) \end{pmatrix}, \tag{10.14}$$

where $\mathbf{Y}_{q,M} \in \mathbb{C}^{qp\times M}$, $\mathbf{U}_{q,M} \in \mathbb{C}^{qm\times M}$, $\mathbf{N}_{q,M} \in \mathbb{C}^{qp\times M}$, $\mathbf{X}_M \in \mathbb{C}^{n\times M}$ and using (10.9) we arrive at the matrix equation

$$\mathbf{Y}_{q,M} = \mathcal{O}_q \mathbf{X}_M + ?_q \mathbf{U}_{q,M} + \mathbf{N}_{q,M}. \tag{10.15}$$

By introducing

$$\mathbf{W}_{q,M} = \begin{pmatrix} W_q(\omega_1) & W_q(\omega_2) & \dots & W_q(\omega_M) \end{pmatrix}, \tag{10.16}$$

an alternative expression for $U_{q,M}$ can be formulated as

$$\mathbf{U}_{q,M} = \left(\begin{pmatrix} W(\omega_1) & \dots & W(\omega_M) \end{pmatrix} \otimes I_m \right) \operatorname{diag}(U(\omega_1), \dots, U(\omega_M)). \tag{10.17}$$

The rank of the matrix $\mathbf{U}_{q,M}$ is a measure of the excitation of the input signal. In the time domain this represents the concept of persistence of excitation [86]. In the single input case $\mathbf{U}_{q,M}$ is of full rank whenever $U(\omega_k)$ is non-zero for at least q distinct frequencies. The characterization of the rank condition for the multi-input case is more involved and from a user's point of view it suffices to check that $\mathbf{U}_{q,M}$ is of full rank for a given set of data.

Continuous-Time Formulation

In a continuous-time formulation a state-space model is given by the system of differential equations

$$\begin{aligned} \dot{x}^c(t) &= Ax^c(t) + Bu^c(t) \\ y^c(t) &= Cx^c(t) + Du^c(t) \end{aligned}$$

and the transfer function is given by

$$G^c(j\omega) = D + C(j\omega I - A)^{-1}B.$$

If we form vectors of time derivatives of the input and output signals as [108]

$$y_q^c(t) = \begin{pmatrix} y^c(t) \\ \frac{d}{dt}y^c(t) \\ \vdots \\ \frac{d^{q-1}}{dt^{q-1}}y^c(t) \end{pmatrix}$$

and conformally $u_q^c(t)$, we obtain the simple relation

$$y_q^c(t) = \mathcal{O}_q x^c(t) + ?_q u_q^c(t).$$

In the frequency domain (Laplace-domain) we obtain

$$W_q(\omega) \otimes Y^c(\omega) = \mathcal{O}_q X^c(\omega) + ?_q W_q^c(\omega) \otimes U^c(\omega),$$

where $Y^c(\omega)$ and $U^c(\omega)$ are the Fourier transform of $y^c(t)$ and $u^c(t)$ respectively, and $W_q^c(\omega)$ is given by

$$W_q^c = \begin{pmatrix} 1 \\ j\omega \\ \vdots \\ (j\omega)^{q-1} \end{pmatrix}.$$

By comparing with the discrete time formulation (10.9), we notice that only the elements of the vector W_q must be changed. Conceptually the distinction between the two domains is thus a minimum and the algorithms which will be presented are applicable to both domains. In practice the the continuous-time formulation suffers from a severe drawback: The Vandermonde matrix $\mathbf{W}_{q,M}^c$ easily becomes ill-conditioned since high powers of $j\omega$ becomes either very small or very large if $\omega < 1$ or $\omega > 1$. The matrix $\mathbf{W}_{q,M}^c$ will have elements with a large difference in magnitude, whenever the frequency samples cover a larger bandwidth. Although always of full rank $\mathbf{W}_{q,M}^c$ will become ill conditioned even for moderate values of q. In the discrete time case, all elements in $\mathbf{W}_{q,M}$ have a unit magnitude and $\mathbf{W}_{q,M}$ is well conditioned even for very large values of q and M. Hence, the continuous-time algorithm is only applicable for low order systems. Since the discrete time formulation is numerically much more robust, we recommend to use the bilinear transformation or the zero-order hold approach for identification of continuous-time systems as described in Chapter 8.

In the following discussion the subscripts which indicate the dimension of the matrices will be suppressed in order to simplify the notation.

10.3.2 Identification

The identification scheme we employ to find a state-space model $(\hat{A}, \hat{B}, \hat{C}, \hat{D})$ is based on a two step procedure. First the relation (10.15) is used to consistently determine a matrix $\hat{\mathcal{O}}_q$ with a range space equal to the extended observability matrix $\mathcal{O}_q$. From $\hat{\mathcal{O}}_q$ it is straightforward to find $\hat{A}$ and $\hat{C}$, as we already have shown in Chapters 4 and 9. In the second step $\hat{B}$ and $\hat{D}$ are determined by solving the minimization problem

$$\hat{B}, \hat{D} = \arg \min_{\substack{B \in \mathbb{R}^{n \times m} \\ D \in \mathbb{R}^{p \times m}}} \sum_{k=1}^{M} \left| Y(\omega_k) - (D + \hat{C}(e^{j\omega_k} I - \hat{A})^{-1} B) U(\omega_k) \right|^2 \tag{10.18}$$

which has an analytical solution since both B and D are linear functions of the transfer function G assuming $\hat{A}$ and $\hat{C}$ are fixed.

10.3.3 The Basic Projection Method

First consider the noise free case where $N(\omega_k) = 0$ and we restate the basic projection method [29, 31] in the frequency domain. In (10.15) the term $?_q\mathbf{U}$ can be

removed by the use of $\Pi^{-}_{\mathbf{U}^H}$ which is the orthogonal projection onto the null-space of $\mathbf{U}$,

$$\Pi^{-}_{\mathbf{U}^H} = I - \mathbf{U}^H(\mathbf{U}\mathbf{U}^H)^{-1}\mathbf{U}. \tag{10.19}$$

here $\mathbf{U}^H$ denotes the complex conjugate transpose of the matrix $\mathbf{U}$. The inverse in (10.19) will exist if the system is sufficiently excited by the input which implies that $\mathbf{U}$ has full rank. Since

$$\mathbf{U}\Pi^{-}_{\mathbf{U}^H} = 0$$

the effect of the input will be removed and we obtain

$$\mathbf{Y}\Pi^{-}_{\mathbf{U}^H} = \mathcal{O}_q\mathbf{X}\Pi^{-}_{\mathbf{U}^H}. \tag{10.20}$$

Provided

$$\text{rank}\,(\mathbf{X}\Pi^{-}_{\mathbf{U}^H}) = n, \tag{10.21}$$

$\mathbf{Y}\Pi^{-}_{U^H}$ and $\mathcal{O}_q$ will span the same column space. In the frequency domain formulation a small complication occurs at this stage. The state-space matrices (A, B, C, D) and thus also the extended observability matrices are usually real matrices but $\mathbf{Y}\Pi^{-}_{U^H}$ is a complex matrix. The real space can however be recovered by using both the real part and the imaginary part in a singular value decomposition [58]

$$\begin{pmatrix} \text{Re}\,(\mathbf{Y}\Pi^{-}_{U^H}) & \text{Im}\,(\mathbf{Y}\Pi^{-}_{U^H}) \end{pmatrix} = \begin{pmatrix} U_s & U_o \end{pmatrix} \begin{pmatrix} \Sigma_s & 0 \\ 0 & \Sigma_o \end{pmatrix} \begin{pmatrix} V_s^T \\ V_o^T \end{pmatrix} \tag{10.22}$$

where $U_s \in \mathbb{R}^{qp\times n}$ contains the n principal singular vectors and the diagonal matrix Σ_s the corresponding singular values. In the noise free case $\Sigma_o = 0$ and there exists a nonsingular matrix $T \in \mathbb{R}^{n\times n}$ such that

$$\mathcal{O}_q = U_s T$$

since both U_s and $\mathcal{O}_q$ share the same range space. This shows that U_s is an extended observability matrix $\hat{\mathcal{O}}$ of the original system in some realization. From U_s we proceed, as in step 5 of Algorithm 9.1 in Chapter 9, to calculate A and C as

$$\hat{A} = (J_1U_s)^{\dagger}J_2U_s \tag{10.23}$$

$$\hat{C} = J_3U_s \tag{10.24}$$

where J_i, are the selection matrices defined by (9.16) and (9.17). With the knowledge of $\hat{A}$ and $\hat{C}$, $\hat{B}$ and $\hat{D}$ are easily determined from (10.18).

Efficient Implementation

A more efficient way of forming the matrix $\mathbf{Y}\Pi^{-}_{\mathbf{U}^H}$ is by the use of the QR factorization of the matrix [155]

$$\begin{pmatrix} \mathbf{U} \\ \mathbf{Y} \end{pmatrix} = \begin{pmatrix} \mathbf{R}_{11} & 0 \\ \mathbf{R}_{21} & \mathbf{R}_{22} \end{pmatrix} \begin{pmatrix} \mathbf{Q}_1^H \\ \mathbf{Q}_2^H \end{pmatrix}. \tag{10.25}$$

Straightforward calculations show that

$$\mathbf{Y}\Pi_{\mathbf{U}^H}^{-} = \mathbf{R}_{22}\mathbf{Q}_2^H$$

and the column space of $\mathbf{R}_{22}$ equals the column space of $\mathbf{Y}\Pi_{\mathbf{U}^H}^{-}$ and it suffices to use $\mathbf{R}_{22}$ in the SVD (10.22).

Let us summarize the basic projection algorithm:

Algorithm 10.1

1 *Form the matrices* $\mathbf{Y}$ *(10.11) and* $\mathbf{U}$ *(10.12) with the number of block rows* q *satisfying* $q > n$.

2 *Calculate the QR factorization*

$$\begin{pmatrix} \mathbf{U} \\ \mathbf{Y} \end{pmatrix} = \begin{pmatrix} \mathbf{R}_{11} & 0 \\ \mathbf{R}_{21} & \mathbf{R}_{22} \end{pmatrix} \begin{pmatrix} \mathbf{Q}_1^H \\ \mathbf{Q}_2^H \end{pmatrix}$$

3. *Calculate the SVD of* $\mathbf{R}_{21}$

$$\begin{pmatrix} Re\,(\mathbf{R}_{21}) & Im\,(\mathbf{R}_{22}) \end{pmatrix} = U_s\Sigma_s V_s^T + U_o\Sigma_o V_o^T$$

were U_s *contain the left singular vectors of the* n *dominating singular values.*

4. *Determine* $\hat{A}$ *and* $\hat{C}$*:*

$$\hat{A} = (J_1U_s)^{\dagger}J_2U_s$$
$$\hat{C} = J_3U_s$$

5. *Solve the least-squares problem for* $\hat{B}$ *and* $\hat{D}$*:*

$$\hat{B},\hat{D} = \arg\min_{\substack{B\in\mathbb{R}^{n\times m}\\ D\in\mathbb{R}^{p\times m}}} \sum_{k=1}^{M} \left| Y(\omega_k) - (D + \hat{C}(e^{j\omega_k}I - \hat{A})^{-1}B)U(\omega_k) \right|^2$$

Relation With Other Projection Methods

The frequency domain method described in [83, 84] is closely related to the basic projection method presented above. Extend the Fourier transform samples $U(\omega_k)$ and $Y(\omega_k)$ with their corresponding negative frequency values

$$U(-\omega_k) = U(\omega_k)^*, \quad Y(-\omega_k) = Y(\omega_k)^*$$

and form $\mathbf{U}$ and $\mathbf{Y}$ including both negative and positive frequencies and form the projection matrix $\Pi_{\mathbf{U}^H}^{-}$. By determining the observability range space from the matrix

$$\mathbf{Y}\Pi_{U^H}^{-}\mathbf{Y}^H \tag{10.26}$$

we end up with the method described in [84]. If the columns are ordered in a particular way $\mathbf{Y}\Pi_{\mathbf{U}^H}^{-}\mathbf{Y}^H$ is a real matrix [83] and the extraction of the imaginary part done in (10.22) becomes superfluous. Comparing with (10.20) we conclude that the method of [83] and the basic projection algorithm outlined above will give identical estimates of the observability range space.

Consistency Issues

As we have seen, the basic projection algorithm will estimate a state-space model which is similar to the original realization in the noise free case. If we now let the noise term $N(\omega)$ be a zero mean complex random variable the issue of consistency becomes important. Does the estimate converge to the true system as M, the number of data, tends to infinity? For the time domain formulation the basic projection algorithm is consistent if the noise is spatially and temporally white [159], *i.e.*, the output errors must be independent in time and have a covariance matrix proportional to the identity matrix. For the frequency domain version similar restrictions apply in order to guarantee consistency.

Theorem 10.1 *Let the following assumptions hold:*

(i) The true system G is an nth order system and there exist constants c and M_0 such that

$$\mathbf{U}\mathbf{U}^H > cMI$$

for all $M > M_0$ and let $|U(\omega_k)|$ be uniformly bounded for all frequencies.

(ii)

$$\operatorname{rank} \mathbf{X}\Pi_{\mathbf{U}^H}^- = n.$$

(iii) The noise $N(\omega)$ is an independent zero mean complex random variable with covariance

$$E\, N(\omega)N(\omega)^H = \sigma^2 I$$

for some scalar σ, and let $N(\omega)$ have bounded fourth moments.

(iv) The Fourier transforms of the input $U(\omega)$ and output $Y(\omega)$ are given at M equidistant frequencies ω_k covering the full unit circle

$$\omega_k = \frac{2\pi(k-1)}{M}, \quad k = 1, \ldots, M$$

where we assume that samples for the negative frequencies are obtained by complex symmetry $Y(-\omega) = Y(\omega)^*$.

Then the identified transfer function $\hat{G}$ using Algorithm 10.1 satisfy

$$\hat{G} \to G, \quad \text{w.p. 1 as } M \to \infty.$$

Proof: In the analysis, we introduce the "sample covariance matrix" of size $qp \times qp$

$$\hat{\mathcal{G}} = \frac{1}{M}\mathbf{Y}\Pi_{\mathbf{U}^H}^- \mathbf{Y}^H \tag{10.27}$$

which is bounded as M tends to infinity but has the same range space as $\mathbf{Y}\Pi_{\mathbf{U}^H}^-$. We also assume that the frequencies are ordered so that the imaginary parts of (10.27) are zero [83]. By using the relation (10.15), (10.27) becomes

$$\hat{\mathcal{G}} = \frac{1}{M}\left(\mathcal{O}_q \mathbf{X}\Pi_{\mathbf{U}^H}^- \mathbf{X}^H \mathcal{O}_q^T + \mathbf{N}\Pi_{\mathbf{U}^H}^- \mathbf{N}^H + \mathcal{O}_q \mathbf{X}\Pi_{\mathbf{U}^H}^- \mathbf{N}^H + \mathbf{N}\Pi_{\mathbf{U}^H}^- \mathbf{X}^H \mathcal{O}_q^T\right) \tag{10.28}$$

Our aim is now to show that the range space of $\hat{\mathcal{G}}$ will converge to the range space of $\mathcal{O}_q$ with probability one. By assumption (i) it follows that $\Pi^-_{\mathbf{U}^H}$ given by (10.19) has bounded elements. In (10.28) we recognize one deterministic term and three stochastic terms. The elements of the fourth term in (10.28) can be described by

$$S_{ij}(M) := \left[\frac{1}{M}\mathbf{N}\Pi^-_{\mathbf{U}^H}\mathbf{X}^H\mathcal{O}_q^T\right]_{ij} = \frac{1}{M}\sum_{k=1}^{M} N(\omega_k)c_{ij}(k)$$

for some bounded constants $c_{ij}(k)$. From the zero mean assumption and bounded moments of $N(\omega_k)$ and by applying the limit result [24, Theorem 5.1.2] we conclude that

$$\lim_{M\to\infty} S_{ij}(M) = 0, \quad \text{w.p. } 1, \quad \forall i,j$$

which of course holds also for the third term in (10.28).

By using the explicit expression (10.19), the second term in (10.28) naturally divides into two terms

$$\frac{1}{M}\mathbf{N}\Pi^-_{\mathbf{U}^H}\mathbf{N}^H = \frac{1}{M}\mathbf{N}\mathbf{N}^H + \frac{1}{M}\mathbf{N}\mathbf{U}^H(\mathbf{U}\mathbf{U}^H)^{-1}\mathbf{U}\mathbf{N}^H \tag{10.29}$$

By assumption (i) $\mathbf{U}\mathbf{U}^H > cMI$ and hence

$$(\mathbf{U}\mathbf{U}^H)^{-1} = \mathbf{O}(1/M).$$

The block-elements of the second matrix in (10.29) are of the form

$$\left[\frac{1}{M}\mathbf{N}\mathbf{U}^H(\mathbf{U}\mathbf{U}^H)^{-1}\mathbf{U}\mathbf{N}^H\right]_{ij} = \frac{1}{M^2}\sum_{k=1}^{M}\sum_{l=1}^{M} c_{ij}(k,l)N_(\omega_k)N(\omega_l)^H$$

for some constants $c_{ij}(k,l)$ which are bounded since $\mathbf{U}$ has full rank and bounded elements. The second moment of these block-elements are bounded as

$$E\left\|\left[\frac{1}{M}\mathbf{N}\mathbf{U}^H(\mathbf{U}\mathbf{U}^H)^{-1}\mathbf{U}^H\mathbf{N}^H\right]_{ij}\right\|_F^2 \le \frac{c_3}{M^3} + \frac{c_4}{M^2}$$

for some bounded constants c_i. By applying Chebyshev's inequality and the Borel-Cantelli lemma [24], we conclude that this term also converges to zero w.p. 1.

The first term in (10.29) is simply

$$\begin{aligned}&\frac{1}{M}\mathbf{N}\mathbf{N}^H\\ &= \frac{1}{M}\left(\mathbf{W}\otimes I_p\right)\,\mathrm{diag}\left(N(\omega_1)N(\omega_1)^H,\ldots,N(\omega_M)N(\omega_M)^H\right)\left(\mathbf{W}^H\otimes I_p\right)\end{aligned} \tag{10.30}$$

Assumption (iv) implies $\mathbf{W}\mathbf{W}^H = MI_q$ and we obtain

$$\frac{1}{M}\left(\mathbf{W}\otimes I_p\right)\left(\mathbf{W}\otimes I_p\right)^H = I_{qp}. \tag{10.31}$$

Hence, the expected value of $\mathbf{N}\mathbf{N}^H/M$ is equal to the scaled identity matrix $\sigma^2 I_{qp}$. Consider

$$\frac{1}{M}\mathbf{N}\mathbf{N}^H - \sigma^2 I_{qp} \tag{10.32}$$

which is zero mean. Let

$$\epsilon_k = N(\omega_k)N(\omega_k)^H - \sigma^2 I.$$

Then ϵ_k is zero mean and have bounded second moments since $N(\omega_k)$ has bounded fourth moments. It is straightforward to see that the (i,j)th block-element in the matrix (10.32) is given by

$$\left[\frac{1}{M}\mathbf{N}\mathbf{N}^H - \sigma^2 I_{qp}\right]_{ij} = \sum_{k=1}^{M} c_{i,j}(k)\epsilon_k \tag{10.33}$$

for some constants $c_{i,j}(k)$ which are bounded since all elements in $\mathbf{W}$ are bounded. The expression (10.33) is a sum of zero mean random variables with bounded second moments and we conclude as before that $\frac{1}{M}\mathbf{N}\mathbf{N}^H \to \sigma^2 I_{qp}$ w.p. 1 as $M \to \infty$. Finally, we arrive at

$$\mathcal{G} := \lim_{M\to\infty} \hat{\mathcal{G}} = \lim_{M\to\infty} \frac{1}{M}\mathcal{O}_q \mathbf{X}\Pi^{-}_{\mathbf{U}^H}\mathbf{X}^H\mathcal{O}_q^T + \sigma^2 I_{qp}, \quad \text{w.p. } 1 \tag{10.34}$$

The signal part has the following (asymptotic) SVD

$$\lim_{M\to\infty} \frac{1}{M}\mathcal{O}_q \mathbf{X}\Pi^{-}_{\mathbf{U}^H}\mathbf{X}^H\mathcal{O}_q^T = \begin{pmatrix} U_s & U_o \end{pmatrix} \begin{pmatrix} \Sigma_s & 0 \\ 0 & 0 \end{pmatrix} \begin{pmatrix} U_s^T \\ U_o^T \end{pmatrix} \tag{10.35}$$

where, by assumption (ii), Σ_s is a diagonal matrix with n positive elements , we obtain

$$\mathcal{G} = \begin{pmatrix} U_s & U_o \end{pmatrix} \begin{pmatrix} \Sigma_s + \sigma^2 I & 0 \\ 0 & \sigma^2 I \end{pmatrix} \begin{pmatrix} U_s^T \\ U_o^T \end{pmatrix}. \tag{10.36}$$

Thus we have shown that the n left singular vectors corresponding to the n largest singular values of $\hat{\mathcal{G}}$ converge w.p. 1 to a set of basis vectors for the observability range space as $M \to \infty$. Thus A and C, up to a similarity transformation, will be consistently estimated. Thus given $\hat{A}$ and $\hat{C}$, it follows from (10.18) that $\hat{B}$ and $\hat{D}$ are consistent since the estimate is a linear function of $Y(\omega_k)$, and hence also a linear function of the noise $N(\omega_k)$. □

The requirements on the noise and the need for a uniform frequency distribution of the samples limit the practical use of the basic projection algorithm to the case when a high signal to noise ratio is guaranteed.

10.3.4 Instrumental Variable Techniques

The conditions for consistency, given by assumption (*iii*) in Theorem 10.1, is a severe drawback for the basic projection method. The origin of the problem stems from the fact that the noise influence does not disappear from the estimate but is required to converge to an identity matrix. We would like to find some instruments which are uncorrelated with the noise but preserves the rank condition (10.21). The time domain instrumental variable technique by Verhaegen [156,157] will here be adopted to yield a frequency domain instrumental variable method.

Partition $\mathbf{Y}$, $\mathbf{U}$ and $\mathbf{N}$ as

$$\mathbf{Y} = \begin{pmatrix} \mathbf{Y}_p \\ \mathbf{Y}_f \end{pmatrix}, \quad \mathbf{U} = \begin{pmatrix} \mathbf{U}_p \\ \mathbf{U}_f \end{pmatrix}, \quad \mathbf{N} = \begin{pmatrix} \mathbf{N}_p \\ \mathbf{N}_f \end{pmatrix}.$$

By following the nomenclature of the time domain case, we call $\mathbf{U}_p$ and $\mathbf{Y}_p$ the "past" inputs and outputs, respectively, and conformally $\mathbf{U}_f$ and $\mathbf{Y}_f$, the "future" inputs and outputs. The partition is done such that each sub-matrix will have α block rows and consequently $2\alpha = q$ block rows. The size requirement of this partition is that $\alpha > n$ where n is the system order. It is straightforward to show that

$$\mathbf{Y}_f = \mathcal{O}_\alpha \mathbf{X}_f + ?_\alpha \mathbf{U}_f + \mathbf{N}_f, \tag{10.37}$$

where $\mathbf{X}_f$ is given by

$$\mathbf{X}_f = \begin{pmatrix} e^{j\alpha\omega_1} X(\omega_1) & e^{j\alpha\omega_2} X(\omega_2) & \dots & e^{j\alpha\omega_M} X(\omega_M) \end{pmatrix}.$$

We now have the possibility to remove the future inputs by a projection and then use the past inputs in order to remove the noise [156]. Using (10.37) we get

$$\mathbf{Y}_f \Pi^-_{\mathbf{U}_f^H} \mathbf{U}_p^H = \mathcal{O}_\alpha \mathbf{X}_f \Pi^-_{\mathbf{U}_f^H} \mathbf{U}_p^H + \mathbf{N}_f \Pi^-_{\mathbf{U}_f^H} \mathbf{U}_p^H \tag{10.38}$$

where $\Pi^-_{\mathbf{U}_f^H}$ denotes the orthogonal projection onto the null-space of $\mathbf{U}_f$ and is given by

$$\Pi^-_{\mathbf{U}_f^H} = I - \mathbf{U}_f^H (\mathbf{U}_f \mathbf{U}_f^H)^{-1} \mathbf{U}_f. \tag{10.39}$$

The inverse in (10.19) exists whenever $\mathbf{U}_f$ has full rank. If we assume $N(\omega_k)$ to be zero mean independent random variables with uniformly bounded second moments

$$E\, N(\omega_k) N(\omega_k)^H = R(\omega_k) \leq R, \quad \forall \omega_k$$

and assume that $U(\omega_k)$ to be uniformly bounded and that $\mathbf{U}_f$ has full rank, the following relation follows from a standard limit result [24, Theorem 5.1.2]

$$\lim_{M \to \infty} \frac{1}{M} \mathbf{N}_f \Pi^-_{\mathbf{U}_f^H} \mathbf{U}_p^H = 0, \quad \text{w.p. } 1.$$

Assume the following rank condition is fulfilled

$$\operatorname{rank} \left(\frac{1}{M} \mathbf{X}_f \Pi^-_{\mathbf{U}_f^H} \mathbf{U}_p^H \right) = n, \tag{10.40}$$

In the time domain setting, this corresponds to requirements on the excitation signal [156]. If the rank condition (10.40) is fulfilled, the n principal left singular vectors of

$$\mathbf{Y}_f \Pi^{-}_{\mathbf{U}_f^H} \mathbf{U}_p^H$$

will constitute a strongly consistent estimate of the range space of the extended observability matrix (10.4).

Implementation

Just as for the basic projection algorithm an efficient implementation involves a QR factorization of the data matrices. By following [156] we form the QR factorization

$$\begin{pmatrix} \mathbf{U}_f \\ \mathbf{U}_p \\ \mathbf{Y}_f \end{pmatrix} = \begin{pmatrix} \mathbf{R}_{11} & 0 & 0 \\ \mathbf{R}_{21} & \mathbf{R}_{22} & 0 \\ \mathbf{R}_{31} & \mathbf{R}_{32} & \mathbf{R}_{33} \end{pmatrix} \begin{pmatrix} \mathbf{Q}_1^H \\ \mathbf{Q}_2^H \\ \mathbf{Q}_3^H \end{pmatrix} \tag{10.41}$$

By using (10.41) and (10.39) simple calculations show that

$$\mathbf{Y}_f \Pi^{-}_{\mathbf{U}_f^H} \mathbf{U}_p^H = \mathbf{R}_{32} \mathbf{R}_{22}^H.$$

Since $\mathbf{R}_{22}$ is of full rank whenever $\mathbf{U}$ has full rank, we use $\mathbf{R}_{32}$ in a SVD to estimate the range space of the observability matrix. The real valued observability range space is extracted as $U_s \in \mathbb{R}^{\alpha p \times n}$ from

$$\begin{pmatrix} \mathrm{Re}\,(\mathbf{R}_{32}) & \mathrm{Im}\,(\mathbf{R}_{32}) \end{pmatrix} = \begin{pmatrix} U_s & U_o \end{pmatrix} \begin{pmatrix} \Sigma_s & 0 \\ 0 & \Sigma_o \end{pmatrix} \begin{pmatrix} V_s^H \\ V_o^H \end{pmatrix}. \tag{10.42}$$

Notice that the orthogonal matrix $\mathbf{Q}$ in (10.41) is not needed in the estimation and that the QR factorization constitutes a considerable data reduction since the size of $\mathbf{R}_{32} \in \mathbb{C}^{\alpha p \times \alpha m}$ is independent of the number of data samples M. As before, we use U_s as the estimate of the extended observability matrix and determine $\hat{A}$ and $\hat{C}$ according to (10.23) and (10.24), while $\hat{B}$ and $\hat{D}$ are determined from (10.18). By using the $\hat{A}$ and $\hat{C}$ from the consistent estimates of the observability range space, the solution of $\hat{B}$ and $\hat{D}$ from (10.18) is a linear function of the output Fourier transforms $Y(\omega_k)$ and hence also in the noise. By similar arguments as before, this shows that $\hat{B}$ and $\hat{D}$ also will be be consistently estimated.

We summarize this discussion in the form of an identification algorithm.

Algorithm 10.2

1 Form the matrices $\mathbf{Y}$ *(10.11) and* $\mathbf{U}$ *(10.12) and partition them as*

$$\mathbf{Y} = \begin{pmatrix} \mathbf{Y}_p \\ \mathbf{Y}_f \end{pmatrix}, \quad \mathbf{U} = \begin{pmatrix} \mathbf{U}_p \\ \mathbf{U}_f \end{pmatrix}$$

such that each sub-matrix has $\alpha > n$ *block rows.*

2 *Calculate the QR factorization*

$$\begin{pmatrix} \mathbf{U}_f \\ \mathbf{U}_p \\ \mathbf{Y}_f \end{pmatrix} = \begin{pmatrix} \mathbf{R}_{11} & 0 & 0 \\ \mathbf{R}_{21} & \mathbf{R}_{22} & 0 \\ \mathbf{R}_{31} & \mathbf{R}_{32} & \mathbf{R}_{33} \end{pmatrix} \begin{pmatrix} \mathbf{Q}_1^H \\ \mathbf{Q}_2^H \\ \mathbf{Q}_3^H \end{pmatrix}$$

3. *Calculate the SVD of* $\mathbf{R}_{32}$

$$\begin{pmatrix} Re\,(\mathbf{R}_{32}) & Im\,(\mathbf{R}_{32}) \end{pmatrix} = U_s \Sigma_s V_s^T + U_o \Sigma_o V_o^T$$

were U_s *contains the left singular vectors of the* n *dominating singular values.*

4. *Determine* $\hat{A}$ *and* $\hat{C}$*:*

$$\hat{A} = (J_1 U_s)^\dagger J_2 U_s$$
$$\hat{C} = J_3 U_s$$

5. *Solve the least-squares problem for* $\hat{B}$ *and* $\hat{D}$*:*

$$\hat{B}, \hat{D} = \arg \min_{\substack{B \in \mathbb{R}^{n \times m} \\ D \in \mathbb{R}^{p \times m}}} \sum_{k=1}^{M} \left| Y(\omega_k) - (D + \hat{C}(e^{j\omega_k} I - \hat{A})^{-1} B) U(\omega_k) \right|^2$$

We also summarize the theoretical discussion in the following theorem.

Theorem 10.2 *Assume that the following conditions are satisfied:*

(i) The frequency data are generated by a stable linear system $G(z)$ *of order* n*.*

(ii) $\text{rank}\,(\mathbf{U}) = 2\alpha m$ *and* $U(\omega_k)$ *is uniformly bounded.*

(iii) $\text{rank}\,(\mathbf{X}_f \Pi^-_{\mathbf{U}_f^H} \mathbf{U}_p^H) = n$

(iv) The noise $N(\omega_k)$ *are zero mean independent random variables with bounded covariances*

$$EN(\omega_k)N(\omega_k)^H = R_k \leq R < \infty, \quad \forall \omega_k$$

Let $\hat{G}(z)$ *be the resulting transfer function when applying Algorithm 10.2. Then*

$$\hat{G} \to G, \quad w.p\ 1\ as\ M \to \infty$$

10.4 Illustrative Example

This section describes an identification example based on simulated data. From the results of the example we will clearly see the limits of the basic projection algorithm when faced with data which do not comply with the assumptions needed for consistence. On the other hand the new instrumental variable algorithm performs as expected from the theoretical analysis summarized by Theorem 10.2.

10.4.1 Experimental Setup

Let the true system $G(z)$ be a fourth order system with an output error noise model $H(z)$. In the frequency domain we thus assume

$$Y(\omega) = G(e^{j\omega})U(\omega) + H(e^{j\omega})E(\omega)$$

where $Y(\omega)$, $U(\omega)$ and $E(\omega)$ are the Fourier transforms of the time domain quantities; outputs $y(t)$, inputs $u(t)$ and innovations $e(t)$. The system $G(z)$ is given by

$$G(z) = C(zI - A)^{-1}B + D$$

with

$$A = \begin{pmatrix} 0.8876 & 0.4494 & 0 & 0 \\ -0.4494 & 0.7978 & 0 & 0 \\ 0 & 0 & -0.6129 & 0.0645 \\ 0 & 0 & -6.4516 & -0.7419 \end{pmatrix}, \quad B = \begin{pmatrix} 0.2247 \\ 0.8989 \\ 0.0323 \\ 0.1290 \end{pmatrix}$$
$$C = \begin{pmatrix} 0.4719 & 0.1124 & 9.6774 & 1.6129 \end{pmatrix}, \quad D = 0.9626.$$

The noise transfer function is of second order and is given by

$$H(z) = C_n + (zI - A_n)^{-1}B_n + D_n$$

with

$$A_n = \begin{pmatrix} 0.6296 & 0.0741 \\ -7.4074 & 0.4815 \end{pmatrix}, \quad B_n = \begin{pmatrix} 0.0370 \\ 0.7407 \end{pmatrix}$$
$$C_n = \begin{pmatrix} 1.6300 & 0.0740 \end{pmatrix}, \quad D_n = 0.2000.$$

The Fourier transform of the noise $E(\omega)$ is modeled as a complex Gaussian distributed random variable with unit variance and is assumed to be independent over different frequencies. In the output error formalism we obtain the output error as

$$N(\omega) = H(e^{j\omega})E(\omega)$$

which thus is a complex Gaussian random variable with frequency dependent variance equal to $|H(e^{j\omega})|^2$. The Fourier transform of the input signal is defined to be $U(\omega) = 1$, $\forall\omega$, *i.e.*, all frequencies are equally excited.

To examine the consistency properties of the basic projection algorithm and the IV algorithm we perform Monte Carlo simulations estimating the system given samples of $U(\omega)$ and $Y(\omega)$ using different noise realizations of $E(\omega)$ and an increasing number of samples of the transforms. The frequency grid will be logarithmically spaced between $\omega_1 = 0.3$ and $\omega_M = \pi$. Data lengths of 30, 50, 100, 200 and 400 frequency samples will be used. For each data length 100 different noise realizations are generated and both algorithms estimate 100 models. To assess the quality of the resulting model the infinity norm of the estimation error

$$\|G(z) - \hat{G}(z)\|_\infty$$

is determined for each estimated model and averaged over the 100 estimated models.

	Average $\|G - \hat{G}\|_\infty$	
M	Alg. 10.1	Alg. 10.2
30	1.7886	1.0425
50	1.3829	0.7737
100	1.2867	0.5078
200	1.2638	0.3751
400	1.2378	0.2550

Table 10.1: Monte Carlo simulations comparing the basic projection algorithm and the IV algorithm. The estimation error decreases for an increasing amount of identification data which is predicted from Theorem 10.2. The projection algorithms fail to capture the true system which shows that the assumption of evenly spaced frequencies and equal covariances are essentially necessary for the projection algorithm to be consistent.

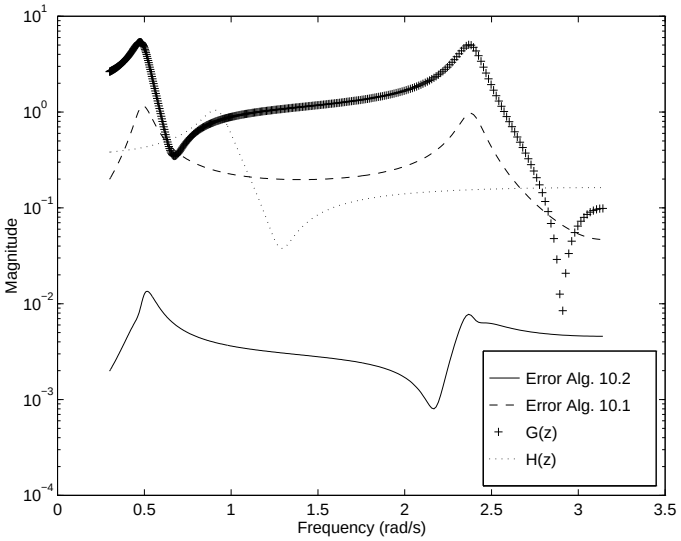

Figure 10.1: Result from Monte Carlo simulations using data length $M = 400$. The true transfer function $G(z)$ is depicted as "+" and the noise transfer function $H(z)$ is shown as the dotted line. The absolute value of the mean transfer function errors calculated over 100 estimated models are shown as a solid line for the Algorithm 10.2 and as a dashed line for Algorithm 10.1.

10.4.2 Estimation Results

As expected from the analysis, the quality of the estimates from the instrumental variable algorithm (IV) improves as the number of samples of the Fourier transform

increases. In Table 10.1 the averaged maximum identification error is presented. The results clearly indicate that the basic projection algorithm is not consistent for these data. We have in this example violated the requirement of equally spaced frequencies and equal noise covariances required for consistency of the basic projection algorithm given in Theorem 10.1. By judging from the example these requirements seem to be essential for consistency. In Figure 10.1 the magnitude of samples of the true transfer function is shown as "+". Notice the logarithmic frequency scale. The dotted line shows the magnitude of the transfer function of the noise. The average transfer function error, calculated over 100 estimated models, is shown as a solid line for Algorithm 10.2 and as a dashed line for Algorithm 10.1.

10.5 Relation to Realization Based Methods

This section will show the relation between the subspace based methods of this chapter and the realization based method described in Chapter 9.

Let us consider the single input noise-free case when $U(\omega_k) = 1, \ \forall k$. The Fourier transform of the output $Y(\omega_k)$ is then equal to the frequency response of the system $G(e^{j\omega_k})$. Furthermore, let us also assume that the transform samples are given at equidistant frequencies

$$\omega_k = \frac{2\pi(k-1)}{M}, \quad k = 1, \ldots, M.$$

We know that

$$\mathbf{Y} = \mathcal{O}_q \mathbf{X} + ?_q \mathbf{U}.$$

The basic projection method described in Algorithm 10.1 estimates the observability range space from

$$\mathbf{Y}\Pi_{\mathbf{U}^H}^{-}.$$

Since $U(\omega) = 1$, the exact nature of $\mathbf{U}$ is

$$\mathbf{U} = \mathbf{W}_{q,M},$$

where $\mathbf{W}_{q,M}$ is given by (10.16). This knowledge can be used in order to find a different matrix which annihilates $\mathbf{U}$. It is easy to verify that

$$\mathbf{W}^{-} = \frac{1}{M} \begin{pmatrix} 1 & 1 & \cdots & 1 \\ e^{j2\pi/M} & e^{j4\pi/M} & \cdots & e^{j2\pi r/M} \\ \vdots & \vdots & \ddots & \vdots \\ e^{j2\pi(M-1)/M} & \cdots & \cdots & e^{j2\pi r(M-1)/M} \end{pmatrix} \in \mathbb{C}^{M \times r} \tag{10.43}$$

has the property

$$\mathbf{U}\mathbf{W}^{-} = 0.$$

Furthermore, (i_1, i_2)-th block entry of $\mathbf{YW}^-$ is calculated as

$$\begin{aligned}\left[\mathbf{YW}^-\right]_{i_1,i_2} &= \frac{1}{M}\sum_{k=0}^{M-1} Y(\omega_k) e^{j2\pi k(i_2+i_1-1)/M} \\ &= \frac{1}{M}\sum_{k=0}^{M-1} G(e^{jk2\pi/M})\ e^{j2\pi k(i_2+i_1-1)/M} \\ &= \hat{h}_{i_2+i_1-1}, \quad i_1 = 1,\dots,q,\ i_2 = 1,\dots,r, \end{aligned} \tag{10.44}$$

which we recognize from (9.9) in Chapter 9 as the M-point inverse DFT of the full frequency response data and we directly see that

$$\hat{H}_{qr} = \mathbf{YW}^-,$$

where $\hat{H}_{qr}$ is defined by (9.10). The projection algorithm with the special choice of annihilator matrix (10.43) is thus equal to the realization based Algorithm 9.2. The particular choice $\mathbf{W}^-$ is possible since the samples are assumed to be at equidistant frequencies and that $Y(\omega) = G(e^{j\omega})$.

10.6 Conclusions

In this chapter we have shown that the time domain subspace based identification algorithms have a frequency domain counterpart when the primary measurements are given as samples of the Fourier transform of the input and output signals. Particularly, we have studied the basic projection algorithm and an instrumental variable algorithm. Stochastic analysis reveals that the instrumental variable algorithm has superior noise rejection properties over the basic projection algorithm. An example was presented which illuminated the theoretical discussion.

11

ML Identification

The time domain prediction error method, with a quadratic criterion function, can be interpreted as the maximum-likelihood estimator if the innovation sequence has a normal distribution [86]. Frequency domain methods which fit a rational function to the noisy data by minimizing the weighted squared sum of the model error can also be considered as maximum-likelihood (ML) estimators [89, 129]. If the spectrum of the noise model is known the ML-estimator for the single output case is equal to a weighted least-squares fit [129]. This chapter will discuss maximum-likelihood estimation using frequency data when the noise model is unknown. The single-output case has previously been discussed in [89, 90] and we will here present the corresponding ML-estimator for the more general case of multi-output systems. Also we highlight the similarities but also the differences of the time and frequency domain ML-estimators. In our presentation we focus on discrete time models and refer to Chapter 8 for a general discussion on the close relationship between frequency domain models in continuous-time and discrete time.

11.1 Preliminaries

Let us consider parametrized discrete time linear models

$$y(t) = G(q,\theta)u(t) + H(q,\theta)e(t), \tag{11.1}$$

where $y(t) \in \mathbb{R}^p$, $u(t) \in \mathbb{R}^m$ and $e(t) \in \mathbb{R}^p$ are the output, input and innovation signals, respectively. $G(q,\theta)$ is the transfer function matrix of the system parametrized by a vector $\theta \in \mathbb{R}^d$. q denotes the forward shift operator. One particular parameter value represents a model from the model set spanned by the model structure. Furthermore, assume the noise model $H(q,\theta)$ to be a proper, stable and inversely stable transfer function matrix.

11.1.1 Time Domain ML-Estimator

If the predictor $\hat{y}(t|\theta)$ is given by

$$\hat{y}(t|\theta) = H(q,\theta)^{-1}G(q,\theta)u(t) + (I - H(q,\theta)^{-1})y(t),$$

the prediction errors

$$\epsilon(t,\theta) = y(t) - \hat{y}(t|\theta)$$

equal the innovations $e(t)$ if the output $y(t)$ was generated by (11.1) for some sequences $u(t)$ and $e(t)$. Assume that N samples of measured data is available

$$\{u(1), y(1), \ldots, u(N), y(N)\}.$$

If $e(t)$ is normal distributed zero mean random variables with covariance Λ, *i.e.*,

$$e(t) \in N(0,\Lambda),$$

the estimator

$$\hat{\theta}_N = \arg\min_\theta \det \frac{1}{N}\sum_{k=1}^{N} \epsilon(t,\theta)\epsilon(t,\theta)^T \tag{11.2}$$

$$\hat{\Lambda}_N = \frac{1}{N}\sum_{k=1}^{N} \epsilon(t,\hat{\theta}_N)\epsilon(t,\hat{\theta}_N)^T$$

is the maximum-likelihood estimator of θ [86, 136].

11.2 The Complex Normal Distribution

For a frequency domain formulation we need a complex representation of the innovations. One possible characterization is given by the complex normal distribution.

Let $X \in \mathbb{C}^p$ be a complex random vector. If the real valued random vector

$$\begin{pmatrix} \operatorname{Re} X \\ \operatorname{Im} X \end{pmatrix}$$

has normal distribution,

$$N\left(\begin{pmatrix} \operatorname{Re} m_X \\ \operatorname{Im} m_X \end{pmatrix}, \frac{1}{2}\begin{pmatrix} \operatorname{Re}\Sigma_{XX} & -\operatorname{Im}\Sigma_{XX} \\ \operatorname{Im}\Sigma_{XX} & \operatorname{Re}\Sigma_{XX} \end{pmatrix}\right)$$

for some $m_X \in \mathbb{C}^p$ and some non-negative definite Hermitian matrix $\Sigma_{XX} \in \mathbb{C}^{p\times p}$, then X is *complex normal* [21]

$$X \in N^c(m_X, \Sigma_{XX}).$$

If X is complex normal, it has mean value

$$E\,X = m_X,$$

and covariance matrix

$$E\,(X-m)(X-m)^H = \Sigma_{XX}.$$

Here $(\cdot)^H$ denote complex conjugate transpose. We also notice that

$$E\,(X-m)(X-m)^T = 0.$$

Furthermore, if Σ_{XX} is non-singular the probability density function of X is given by [21]

$$p(\operatorname{Re} X,\, \operatorname{Im} X) = \frac{1}{\pi^p \det \Sigma_{XX}} \exp\left[-(X-m_X)^H \Sigma_{XX}^{-1}(X-m_X)\right] \tag{11.3}$$

An important application of the complex normal distribution is to characterize the Fourier transform of a noise sequence. If the noise $x(t)$ is a stationary process with zero mean and spectrum $\Phi_x(\omega)$, then the appropriately scaled asymptotic Fourier transform of $x(t)$, $X(\omega)$, is complex normal [21]

$$X(\omega) \in N^c(0, \Phi_x(\omega)), \tag{11.4}$$

Furthermore, $X(\omega_1)$ and $X(\omega_2)$ are asymptotically uncorrelated whenever $\omega_1 \neq \omega_2$.

11.3 Frequency Domain Formulation

Consider the relation (11.1). By applying the discrete Fourier transform we obtain

$$Y(\omega) = G(e^{j\omega}, \theta)U(\omega) + H(e^{j\omega}, \theta)E(\omega). \tag{11.5}$$

Here $Y(\omega)$, $U(\omega)$ and $E(\omega)$ denote the transforms of the time domain signals. If $e(t)$ is a white noise signal with covariance Λ it follows from (11.4) that $Y(\omega)$ will be complex normal as

$$Y(\omega) \in N^c(G(e^{j\omega}, \theta)U(\omega), H(e^{j\omega}, \theta)\Lambda H(e^{j\omega}, \theta)^H). \tag{11.6}$$

Since Λ is the time domain covariance matrix of the noise it is real, symmetric and positive semi-definite.

11.3.1 The ML-estimator

We are now ready to derive a maximum-likelihood estimator for the frequency domain identification problem. We will base our estimation formulation in a somewhat more general setting by assuming Λ to be a positive definite Hermitian complex matrix.

Given samples of the Fourier transform of the input and output at M frequencies

$$\{U(\omega_1), Y(\omega_1), \ldots, U(\omega_M), Y(\omega_M)\},$$

we can formulate the maximum-likelihood estimator of θ. From (11.6) and (11.3), the θ dependent part of the negative logarithm of the likelihood function becomes

$$V_M(\theta) = \sum_{k=1}^{M} \Big[\log\det\left(H(e^{j\omega_k})\Lambda H(e^{j\omega_k})^H\right) + \left(Y(\omega_k) - G(e^{j\omega_k},\theta)U(\omega_k)\right)^H \left(H(e^{j\omega_k})\Lambda H(e^{j\omega_k})^H\right)^{-1} \times \left(Y(\omega_k) - G(e^{j\omega_k},\theta)U(\omega_k)\right)\Big]. \quad (11.7)$$

If Λ is known the maximum-likelihood estimate of θ is simply

$$\hat{\theta}_M = \arg\min_{\theta} V_M(\theta). \quad (11.8)$$

For the case when Λ is unknown, we can remove Λ by first deriving the optimal Λ for each fixed value of θ, by analytical optimization.

By introducing the notation

$$Z_k(\theta) = Y(\omega_k) - G(e^{j\omega_k},\theta)U(\omega_k)$$

and

$$H_k(\theta) = H(e^{j\omega_k},\theta)$$

we can reformulate $V_M(\theta)$ as

$$\begin{aligned} V_M(\theta) &= \sum_{k=1}^{M} \left[\log\det(H_k(\theta)\Lambda H_k(\theta)^H) + Z_k(\theta)^H (H_k(\theta)\Lambda H_k(\theta)^H)^{-1} Z_k(\theta)\right] \\ &= \sum_{k=1}^{M} \left[\log\det(H_k(\theta)H_k(\theta)^H) + \log\det\Lambda \right. \\ &\quad \left. + \ \mathrm{tr}\, H_k(\theta)^{-1} Z_k(\theta) Z_k(\theta)^H H_k(\theta)^{-H}\Lambda^{-1}\right] \\ &= M\left(\log\det\Lambda + \bar{H} + \ \mathrm{tr}\,\bar{Z}\Lambda^{-1}\right), \end{aligned}$$

where

$$\bar{H} = \frac{1}{M}\sum_{k=1}^{M} \log\det(H_k(\theta)H_k(\theta)^H)$$

and

$$\bar{Z} = \frac{1}{M}\sum_{k=1}^{M} H_k(\theta)^{-1} Z_k(\theta) Z_k(\theta)^H H_k(\theta)^{-H}.$$

Let us now assume that $V_M(\theta)$ is minimized with respect to Λ by the choice

$$\Lambda = \bar{Z}. \quad (11.9)$$

This is equivalent to the following sequence of inequalities

$$\begin{aligned} \log\det\Lambda + \ \mathrm{tr}\,\bar{Z}\Lambda^{-1} &\geq \log\det\bar{Z} + \ \mathrm{tr}\, I_p \\ \log\det(\Lambda\bar{Z}^{-1}) + \ \mathrm{tr}\,\bar{Z}\Lambda^{-1} &\geq p \\ \mathrm{tr}\,\bar{Z}\Lambda^{-1} - \log\det(\bar{Z}\Lambda^{-1}) &\geq p. \end{aligned}$$

Assume $\bar{Z}$ to be positive definite and define $PP^H = \bar{Z}$ and $X = P^H\Lambda^{-1}P$. By construction, X is positive definite with eigenvalues $\lambda_i > 0,\ i = 1, \ldots, p$. Using the factorization of $\bar{Z}$, we can continue the inequalities as

$$\begin{aligned} \operatorname{tr} PP^H\Lambda^{-1} - \log\det(PP^H\Lambda^{-1}) &\geq p \\ \operatorname{tr} X - \log\det X &\geq p \\ \sum_{k=1}^{p} (\lambda_i - \log\lambda_i - 1) &\geq 0 \end{aligned}$$

The last inequality is always true since $\lambda - \log\lambda - 1 \geq 0$ for all $\lambda > 0$ with equality for $\lambda = 1$, *i.e.,* when $\Lambda = \bar{Z}$. This proves that $V_M(\theta)$ is minimized with respect to Λ by the choice (11.9). If we insert (11.9) into (11.7), the maximum-likelihood estimate for unknown noise covariance emerges as

$$\begin{aligned} \hat{\theta}_M &= \arg\min_\theta \left[\log\det W_M(\theta) + \frac{1}{M}\sum_{k=1}^{M} \log\det\left(H_k(\theta)H_k(\theta)^H\right) \right] \\ W_M(\theta) &= \frac{1}{M}\sum_{k=1}^{M} H_k(\theta)^{-1} Z_k(\theta) Z_k(\theta)^H H_k(\theta)^H \\ \hat{\Lambda}_M &= W_M(\hat{\theta}_M). \end{aligned} \tag{11.10}$$

As already mentioned, this estimator assumes Λ to be positive definite and Hermitian. If we would like to strengthen the estimator to only consider the case when Λ is a real matrix, the ML-estimator becomes more complicated and less intuitive.

For the single output case $p = 1$ the ML-estimator (11.10) simplifies to

$$\begin{aligned} \hat{\theta}_M &= \arg\min_\theta \left[\log W_M(\theta) + \frac{1}{M}\sum_{k=1}^{M} \log|H(e^{j\omega_k},\theta)|^2 \right] \\ W_M(\theta) &= \frac{1}{M}\sum_{k=1}^{M} \frac{|Y(\omega_k) - G(e^{j\omega_k},\theta)U(\omega_k)|^2}{|H(e^{j\omega_k},\theta)|^2} \\ \hat{\lambda}_M &= W_M(\hat{\theta}_M). \end{aligned} \tag{11.11}$$

In the single output case the scalar λ is a real constant since a Hermitian scalar is by definition real.

11.3.2 Discussion

Let us briefly return to the time-domain formulation and the prediction error estimate $\hat{\theta}_N$ given by (11.2) and for simplicity we consider the single output case. A straightforward application of Parseval's relation to (11.2) reveals that

$$\hat{\theta}_N \sim \arg\min_\theta \int_{-\pi}^{\pi} |E_N(\omega,\theta)|^2\, d\omega,$$

where E_N is the discrete Fourier transform of ϵ calculated on N data, *i.e.*,

$$E_N(\omega,\theta) = H(e^{j\omega},\theta)^{-1}\left(Y_N(\omega) - G(e^{j\omega},\theta)U_N(\omega)\right).$$

Altogether this yields the approximate expression

$$\hat{\theta}_N \sim \arg\min_{\theta} \int_{-\pi}^{\pi} \frac{|Y_N(\omega_k) - G(e^{j\omega_k},\theta)U_N(\omega_k)|^2}{|H(e^{j\omega_k},\theta)|^2}\, d\omega. \tag{11.12}$$

A few points are worth noticing. For a fixed known noise model $H(q,\theta) = H(q)$, as assumed in [129], the frequency domain ML-estimates (11.11) and (11.12) are essentially the same. Whenever the noise model also has to be estimated, the additional term

$$\frac{1}{M}\sum_{k=1}^{M} \log|H(e^{j\omega_k},\theta)|^2$$

occurs in the criterion. This difference can be explained by the different character of the errors of the observations. In the time domain, the prediction errors are normal distributed variables with a constant covariance. In the frequency formulation, the errors $H(e^{j\omega},\theta)E(\omega)$ are complex normal distributed with a frequency dependent covariance matrix.

If the frequencies ω_k are equidistantly distributed between 0 and 2π this additional term again becomes less important since

$$\int_{-\pi}^{\pi} \log|H(e^{j\omega},\theta)|^2\, d\omega = 0$$

for any stable and inversely stable monic transfer function.

11.4 Asymptotic Properties

The asymptotic properties ($M \to \infty$) of the ML-estimator (11.10) can be derived in a straightforward fashion, using standard techniques [90]. We limit the presentation to the single-input single-output case. The extension to the multivariable case is straightforward but notationally more complex.

Let us assume that the data is generated from

$$Y(\omega) = G_0(e^{j\omega})U(\omega) + H_0(e^{j\omega})E_0(\omega). \tag{11.13}$$

Here G_0 and H_0 can be any bounded complex valued functions. Furthermore, we assume $E_0(\omega)$ to be zero mean complex random variables satisfying

$$E\, E_0(\omega_k)E_0(\omega_l)^H = \lambda_0\delta(k-l), \tag{11.14}$$

with bounded fourth moments which are uncorrelated over the frequencies. We also assume that the noise $E_0(\omega)$ and the input $U(\omega)$ are uncorrelated. The frequency errors

$$V_0(\omega) = H_0(e^{j\omega})E_0(\omega),$$

are thus zero mean random variables with bounded fourth moments and with moments up to the fourth moments jointly uncorrelated with the input and itself.

Consider the case when a fixed noise model, $H(q,\theta) = H(q)$, is assumed. Suppose, as $M \to \infty$, the frequencies ω_k cover the frequency interval $[-\omega, \omega]$ with a frequency density function $W(\omega)$. That is, let $w_M(\Omega_1, \Omega_2)$ denote the number of frequency samples in the interval Ω_1 to Ω_2 when the total number of frequencies are M. Then

$$\lim_{M\to\infty} \frac{1}{M} w_M(\Omega_1, \Omega_2) = \int_{\Omega_1}^{\Omega_2} W(\omega)\, d\omega.$$

For a fixed noise model, the ML-criterion for the single output case is

$$V_M(\theta) = \frac{1}{M} \sum_{k=1}^{M} \frac{|Y(\omega_k) - G(e^{j\omega_k}, \theta)U(\omega_k)|^2}{|H(e^{j\omega_k})|^2}.$$

By regarding the generation of $Y(\omega)$ from (11.13), we get

$$V_M(\theta) = \frac{1}{M} \sum_{k=1}^{M} \frac{|(G_0(e^{j\omega_k}) - G(e^{j\omega_k}, \theta))U(\omega_k) + H_0(e^{j\omega_k})E_0(\omega_k)|^2}{|H(e^{j\omega_k})|^2}.$$

With the noise assumptions (11.14), the standard limit result [24, Theorem 5.1.2] gives

$$\lim_{M\to\infty} \frac{1}{M} \sum_{k=1}^{M} c_k E_0(\omega_k), \quad \text{w.p. } 1$$

for any bounded constants c_k independent of $E_0(\omega_k)$. This implies that $V_M(\theta)$ converges [90], uniformly in θ and with probability 1 to

$$\begin{aligned} \bar{V}(\theta) &= \lim_{M\to\infty} V_M(\theta) \\ &= \int_{-\Omega}^{\Omega} \frac{|G_0(e^{j\omega}) - G(e^{j\omega}, \theta)|^2 \Phi_u(\omega) W(\omega) + \Phi_v(\omega) W(\omega)}{|H(e^{j\omega})|^2} d\omega, \end{aligned} \quad (11.15)$$

where $\Phi_u(\omega) = |U(\omega)|^2$ and $\Phi_v(\omega) = \lambda_0 |H_0(e^{j\omega})|^2$ are the input and noise spectra, respectively.

Let us denote by

$$D_c = \arg\min_{\theta} \bar{V}(\theta)$$

the set of limiting estimates as $M \to \infty$. If $\bar{V}(\theta)$ has a unique minimum, D_c is a singleton. By discarding the θ-independent term of (11.15), the characterization of the limiting estimate becomes

$$D_c = \arg\min_{\theta} \int_{-\Omega}^{\Omega} \frac{|G_0(e^{j\omega}) - G(e^{j\omega}, \theta)|^2 \Phi_u(\omega) W(\omega)}{|H(e^{j\omega})|^2}\, d\omega, \quad \text{w.p. } 1.$$

The asymptotic estimate is thus the best model in weighted mean-square sense. The weight is dependent on the input spectrum, the frequency density function

and the assumed noise model. It is quite surprising that the true noise model does not influence the bias of the limiting estimate. However, the variance of the estimate is highly dependent on the true noise model.

Let us now consider the case when the true model belongs to the set of models spanned by the model structure, *i.e.*, there exists a θ_0 such that

$$G(q,\theta_0) = G_0(q).$$

If $\Phi_u(\omega)W(\omega)$ is different from zero at sufficiently many frequencies, it follows that

$$\hat{\theta}_M \to \theta_0 \quad \text{as} \quad M \to \infty, \quad \text{w.p. } 1,$$

which shows that the estimator is strongly consistent.

In this case the covariance matrix of $\hat{\theta}_M$ will be, asymptotically, *c.f.* [86, p. 249],

$$\operatorname{Cov}\hat{\theta}_M \sim \frac{1}{M} R^{-1} Q R^{-1}, \tag{11.16}$$

with

$$R = \lim_{M\to\infty} E\ \frac{d^2}{d\theta^2} V_M(\theta)\bigg|_{\theta=\theta_0} = \int_{-\Omega}^{\Omega} \frac{G'_\theta(e^{j\omega},\theta_0)\Phi_u(\omega)G'_\theta(e^{j\omega},\theta_0)^H W(\omega)}{|H(e^{j\omega})|^2}\, d\omega$$

$$Q = \lim_{M\to\infty} E\left\{V'_M(\theta_0)V'_M(\theta_0)^H\right\} = \int_{-\Omega}^{\Omega} \frac{G'_\theta(e^{j\omega},\theta_0)\Phi_u(\omega)G'_\theta(e^{j\omega},\theta_0)^H \Phi_v(\omega)W(\omega)}{|H(e^{j\omega})|^4}\, d\omega,$$

where the column vector $G'_\theta(q,\theta)$ denotes the gradient of $G(q,\theta)$ with respect to θ. From (11.16) we see that the covariance is dependent on the true noise spectrum $\Phi_v(\omega)$.

If we compare the noise assumptions (11.14) with the assumptions required for consistency of the errors-in-variables ML-estimator [129], we note one significant difference. The ratio between the input and output noise spectra have to be known to guarantee consistency of the errors-in-variables ML-estimator [129]. For the output error ML-estimator we do not need any spectral information of the noise for consistency. However, if noise is present in the input signal, the output error ML-estimator will in general be inconsistent.

11.5 Conclusions

We have derived the multivariable output-error ML-estimator for the case when data is given in the frequency domain. If the noise spectrum is known, the resulting estimator is equal to a weighted non-linear least squares estimator. However, if the noise spectrum is unknown, an additional sum of the logarithm of the noise spectrum appears in the criterion. The asymptotic properties of the estimator was discussed, and it was pointed out that the ML-estimator is consistent under rather general noise assumptions.

12

An Application

Although theoretical analysis is indispensable when developing new identification methods, practical experience is probably even more important. The real world is neither linear, nor are the measurements errors stochastic variables drown from some probability distribution. New methods can never be accepted unless proved to be successful when faced with real experimental data.

This chapter deals with identification of linear models from measured data. The experimental data originate from a flexible mechanical structure which has a large number of lightly damped vibrational modes. Both discrete time models as well as continuous-time models will be estimated. We use both the new algorithms as well as some classical methods. This gives us the ability to perform a fair comparison.

12.1 The Data

This application considers the identification of the transfer function between a force-actuator and an accelerometer located on a flexible mechanical structure. The structure is the Advanced Reconfigurable Control (ARC) testbed at the Jet Propulsion Laboratory (JPL), California Institute of Technology, Pasadena, California.[1] The ARC testbed is a mechanical truss structure with several active struts and accelerometers at different locations.

The frequency data are obtained with a sampling frequency of 200 Hz using a multisine input [129] with 512 equidistant spectral lines. The frequency response data are shown in Figure 12.1. As clearly seen from the phase plot in the figure the frequency response data below 8 Hz is only noise. The response above 8 Hz appears to have a rather high signal to noise ratio. A quick look at the magnitude curve reveals about 16 peaks.

[1]The author thanks Dr. David S. Bayard at JPL for providing the experimental data.

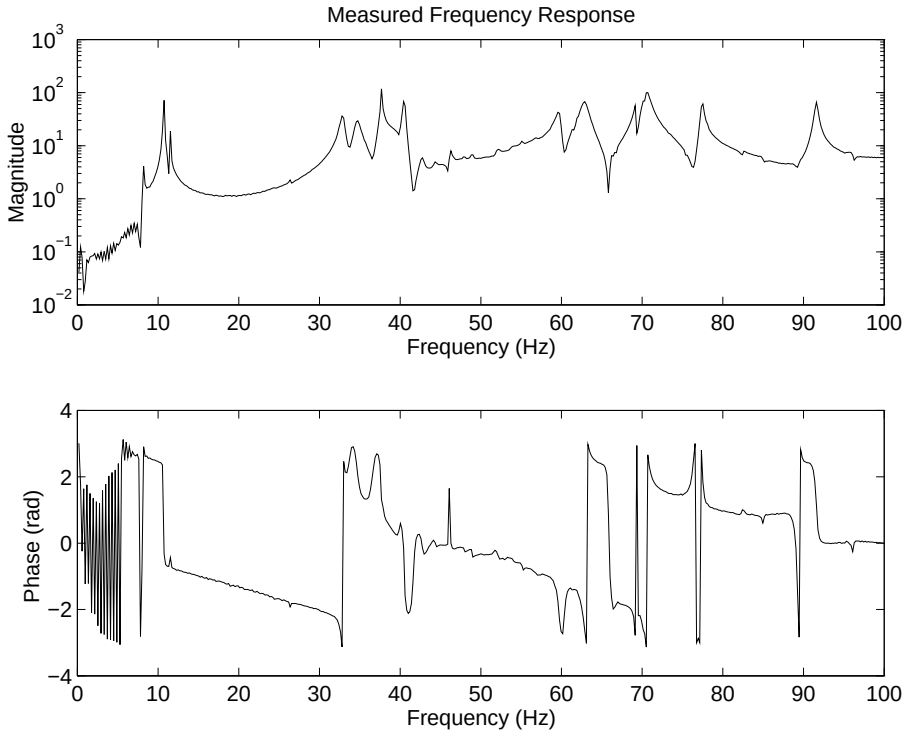

Figure 12.1: Measured Frequency Response of the ARC testbed at JPL. The frequency response is given at 512 equidistant frequency points between 0 and 100 Hz. The sample period is 200 Hz.

12.2 Quality Measures

To assess the quality of estimated models we will use two measures based on the fit between the data and the model. The following two norms for the error between the predicted and measured frequency responses will be used. The maximum error

$$\|G - \hat{G}\|_{m,\infty} = \max_{\omega_k} \left| G_k - \hat{G}(e^{j\omega_k}) \right|, \tag{12.1}$$

and the root mean square error (RMS)

$$\|G - \hat{G}\|_{m,2} = \sqrt{\frac{1}{N} \sum_{k=1}^{N} \left| G_k - \hat{G}(e^{j\omega_k}) \right|^2}. \tag{12.2}$$

First we will use the realization based algorithms from Chapter 9 to estimate discrete time models based on the zero-order hold assumption. Secondly, we will assume that the data is band limited and that the frequency response are samples

of the continuous-time Fourier transform. Continuous-time models are estimated by use of the bilinear transformation.

12.3 Discrete Time Modeling

In this section we will estimate discrete time models assuming the frequency response are equidistant samples of the discrete time frequency function. We start by trying to determine an appropriate model order. We do this by by the technique of cross-validation as described in Chapter 8. The data set is divided into two disjunct sets, the estimation data and the validation data. The division is made such that every second frequency response sample is put in the estimation set and every other in the validation set. Frequency response samples at frequencies below 8 Hz are removed from the validation data since these are only noise.

Using Algorithms 9.1 and 9.2, a sequence of models of order 20–90 are estimated. The algorithms are augmented with the projection scheme to guarantee stable models, as described in Section 9.2. The frequency response of each estimated model is calculated at the frequencies of the validation data and the two error criteria, the maximum error (12.1) and the RMS error (12.2), are determined using the validation data set. The results are shown in Figure 12.2. From the two graphs we can see no "knee" in the error curves, which, if present, would indicate an appropriate model order [136]. Instead the model error (on an average) decreases slowly with the model order. A noticeable decrease in error can be seen at model orders 42, 70 and 82 which then could be possible choices. The result indicates that the frequency data has a high signal to noise ratio and the best linear model has a high dimension.

Let us now study the performance of the new algorithms in comparison with some established estimation procedures. As estimation data we now use all 512 frequency samples. The procedures we compare with are the simple linear least squares estimate (LS) (8.7) introduced by Levy [75], the non-linear least squares (NLS) (8.6), and the realization approach described by Juang *et al.* [64] and Jacques and Miller [61]. The LS estimate is calculated by using the model structure (8.4), *i.e.*, a fraction of two polynomials. The NLS estimate uses the LS estimate as an initial model before proceeding with Gauss-Newton iterative search. The LS and NLS estimates are implemented in the command `invfreqz` in MATLAB's Signal Processing Toolbox [82]. The realization based approach starts by calculating the approximate impulse response by forming the inverse DFT of the data and then Kung's realization algorithm [71] is used.

Models of order 20 to 64 are estimated using all four approaches. Algorithm 9.2 used the projection method to ensure stable models. This is necessary for all the estimated models between 43-64 since the initial A matrix has eigenvalues outside the unit circle. The dimension of the Hankel matrix H_{ij} (9.10) in Algorithm 9.1 is chosen to be 512×512. This choice gives the best accuracy. The resulting maximum errors calculated on the estimation data are shown in Figure 12.3. The performance of Algorithm 9.2 is significantly better than the other three methods. We notice an erratic behavior of the NLS estimate, which probably is due to local minima.

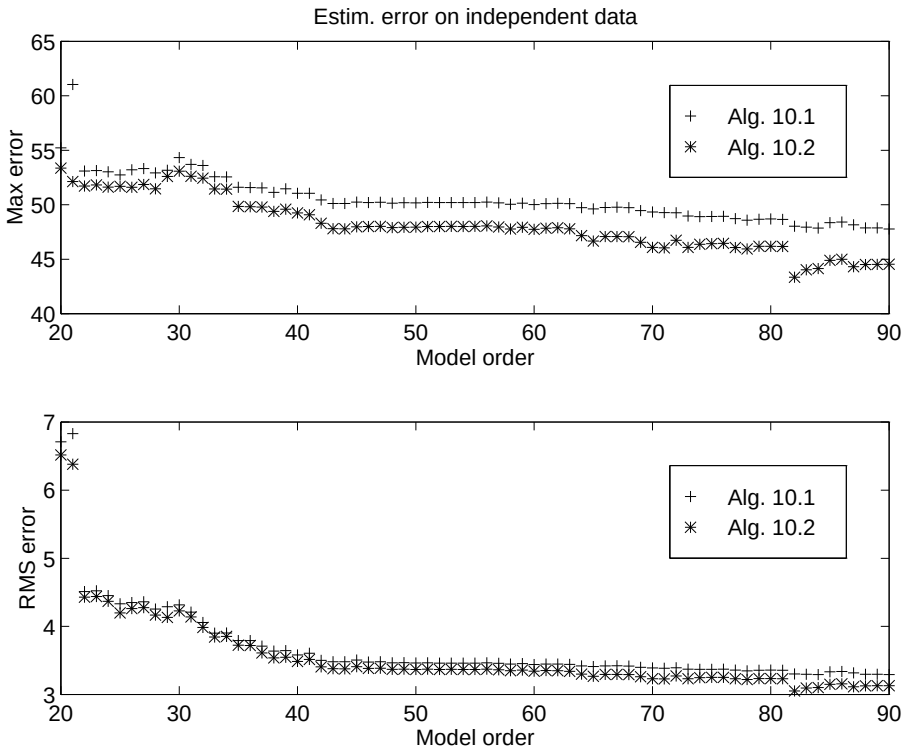

Figure 12.2: Model errors calculated on independent validation data plotted versus order of the estimated models.

The increase in error for the 61th order NLS estimate from the LS estimate, is due to numerical problems during the iterative search. The straightforward approach using Kung's algorithm gives a large error which increases with an increasing model order. The poor behavior of this approach stems from the lack of correction for finite number frequency samples as discussed in Chapter 9. The estimation errors using Algorithm 9.1 are not shown in Figure 12.3 since these are almost identical to Algorithm 9.2. The RMS error for all four methods behaves similar as the shown maximum error.

If the model order is increased above 65-70, the LS and NLS estimates become quite bad since the estimation procedure run into severe numerical problems. For these data, the realization based algorithms show no such behavior. Accurate models of order 400 can be estimated without any numerical problems.

With the full data set, we now estimate models using the input-output subspace approach described in Chapter 10. More precisely, we use the basic projection method, Algorithm 10.1, and the instrumental variable method, Algorithm 10.2. Since only frequency response data are given, we let $Y(\omega_k) = G_k$ and $U(\omega_k) = 1$. Based on resulting model quality considerations, the number of block rows q in

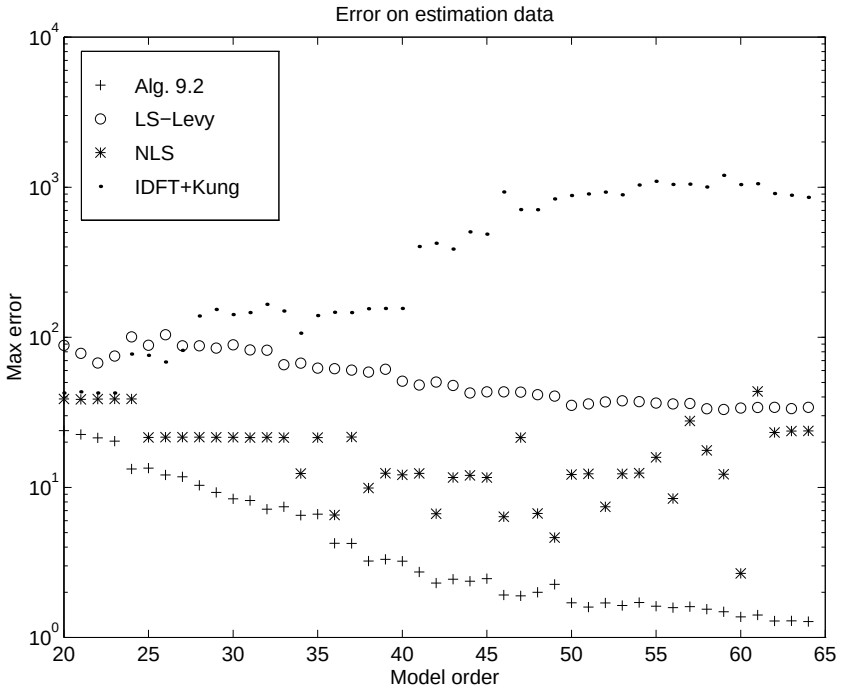

Figure 12.3: Estimation errors for four different methods. The error is calculated using the estimation data.

the algorithms were chosen to be 256. The quality of the resulting models are presented in Figure 12.4 together with the results of Algorithm 9.1. The two input-output subspace methods has a larger error for almost all model orders, especially when the order is high. However, comparing with the results of the least-squares methods from Figure 12.3, the two algorithms perform well. The basic projection method and the IV method show almost equal performance. This indicates that the measured data contain very little noise.

The same data has been used by Gu and Khargonekar [47]. They estimate discrete time stable models with an algorithm inspired by the recent theory of identification in $\mathcal{H}_\infty$. For model orders 24 and 42, they obtain maximum errors 13 and 6.1, respectively. The maximum errors obtained by Algorithm 9.1 are 13.2 and 2.4, respectively, for the same model orders. Bayard has also successfully estimated models from these data [15, 16]. However, in [16] the estimated transfer functions are shown without any explicit quantitative results.

Finally we conclude by showing the excellent fit obtained for a 60th order model estimated with Algorithm 9.1. The transfer function of the estimated stable trans-

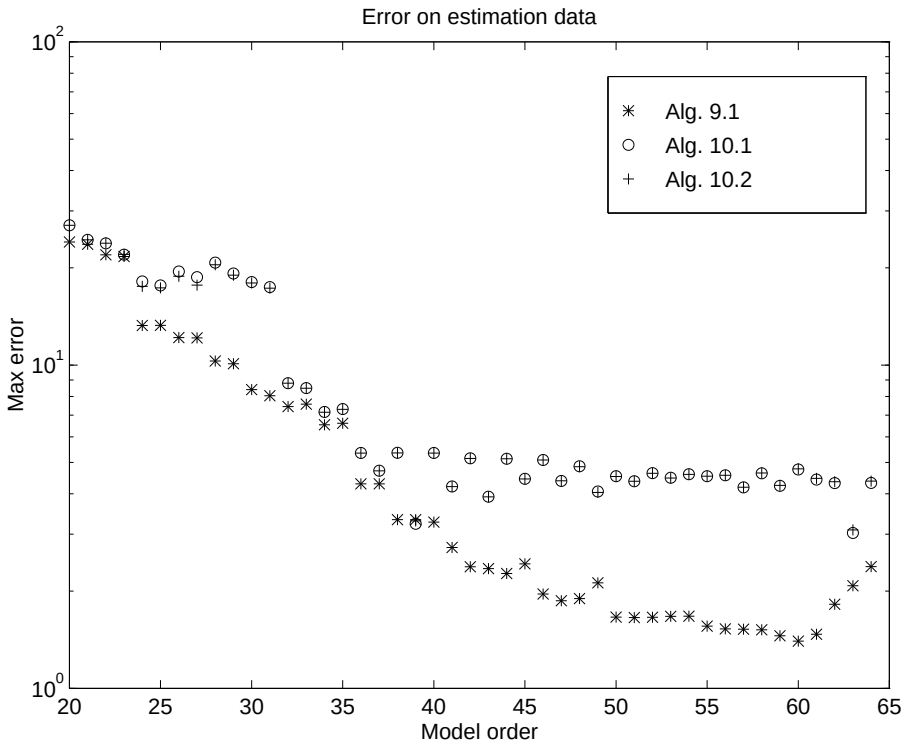

Figure 12.4: Estimation results using the input-output subspace based identification methods.

fer function is shown in Figure 12.5. For this model the maximum error is

$$\|G - \hat{G}\|_{m,\infty} = 1.37$$

and the RMS error is

$$\|G - \hat{G}\|_{m,2} = 0.41.$$

The estimated model is converted to the block-diagonal form and parametrized according to Chapter 6. With this as an initial model, the NLS criterion (8.6) was minimized using a Gauss-Newton iterative numerical search. The iterations decreased the maximum error to 1.36 and the RMS error to 0.37.

12.4 Continuous-Time Modeling

In this section we will consider the frequency data as samples of the continuous-time transfer function. This would be the case if we assume the input and output

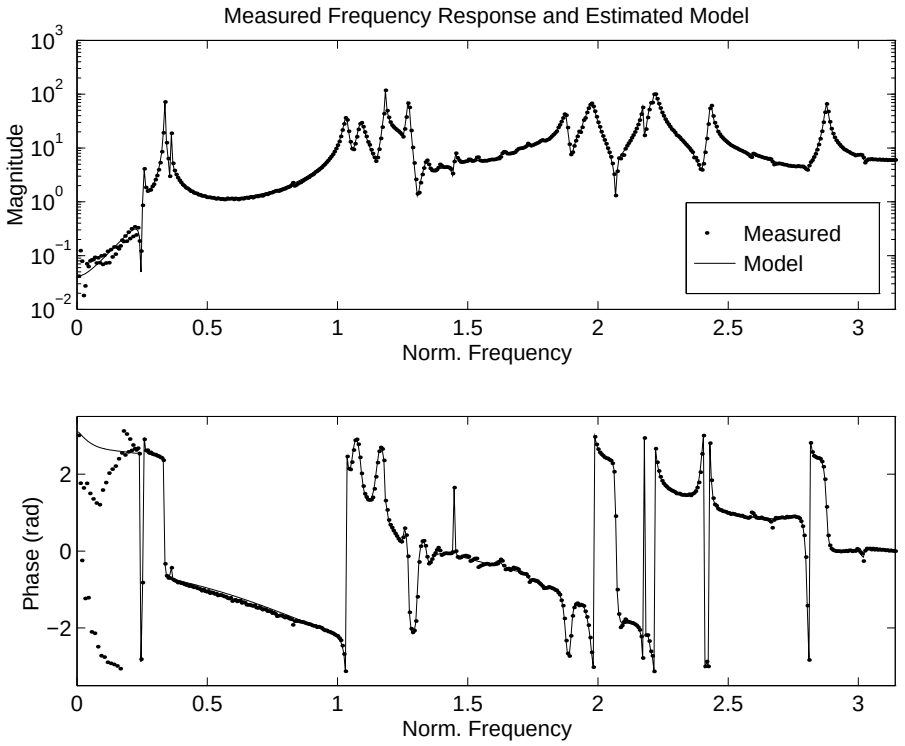

Figure 12.5: Measured frequency response and estimated model using Algorithm 9.1. The estimated model is stable and of order 60.

signals to be band limited. The validity of this assumption for these data is not known to us but we will derive a continuous-time model as if the BL assumption were correct. We will follow the strategy outlined in Section 8.5 of Chapter 8:

- Convert the measured frequency data do discrete time by pre-warping the frequencies as (8.15).
- Estimate a discrete time initial model using the input-output subspace algorithm described by Algorithm 10.2.
- Convert the obtained initial model to the block-diagonal realization (6.32) and minimize the non-linear least squares criterion (8.6).
- The final continuous-time model is obtained by the bilinear transformation (8.17).

The pre-warping step of the frequencies leads to non-uniformly spaced frequencies and we cannot use the accurate realization based Algorithm 9.1. Instead we

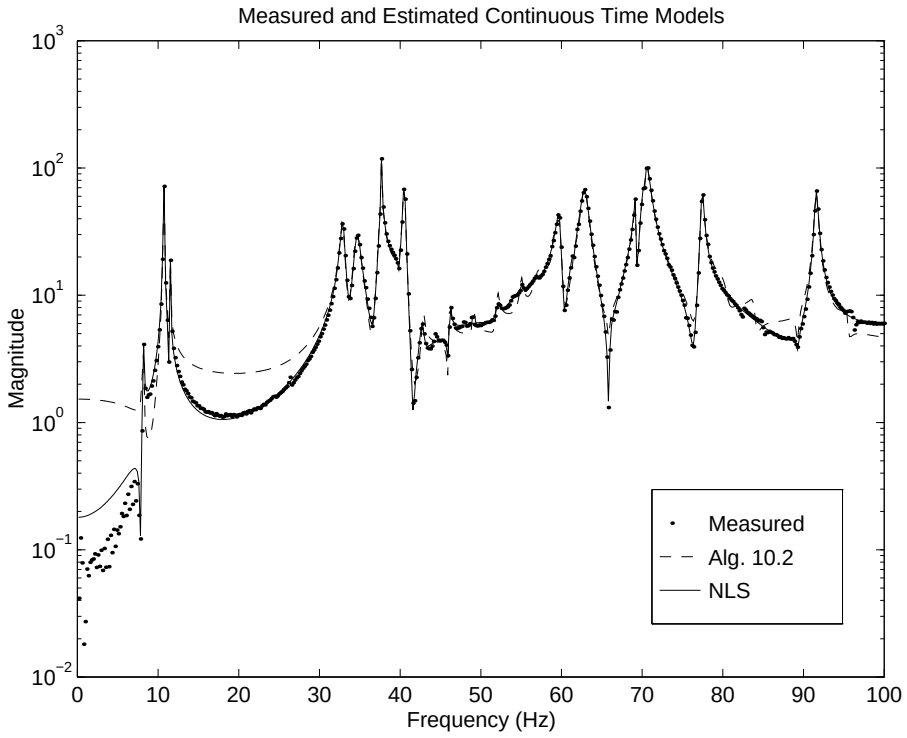

Figure 12.6: Measured data and estimated models.

turn to the input-output subspace based IV method of Algorithm 10.2. The initial model of order 60 obtained from Algorithm 10.2 has a maximum error of 7.79 and an RMS error of 2.00. The initial model is converted to the block diagonal form (6.32) and parametrized according to Section 6.3.3. After the iterative minimization of the NLS criterion (8.6), the maximum error decreased significantly to 2.37 while the RMS error also decreased to 0.42. The errors are calculated from the continuous-time models. During the iterations no numerical problems occured and the Hessian matrix remained well-conditioned. These good properties can be traced back to the block-diagonal parametrization. With a parametrization using un-factored polynomials (8.4) numerical problems occur during the minimization.

In Figure 12.6 the magnitudes of the measured data, the initial model and the final model are shown. The deficiencies of the initial model are removed by the NLS minimization, leading to a final continuous-time model of very high quality.

12.5 Computational Complexity

The main computation time for the realization based Algorithm 9.1 and Algorithm 9.2 is spent in the singular value decomposition (9.11). For this application, with a 512×512 Hankel matrix, this is equivalent to 3 minutes on a Sun Sparc-10 workstation. After the factorization is accomplished, models of order up to 511 can be estimated. Given the SVD factorization, a model of order 60 is estimated in 6 seconds.

The input-output based subspace algorithms spend most of the time in the QR factorization followed by an SVD. For the row size $q = 256$ this equals 2 minutes on a Sparc-10. After this step, models of order up to 255 can be estimated. A model of order 60 is estimated in 4 seconds, given the SVD factorization.

Iterative minimization for models of high order is considerably slower. The NLS minimization of the 60th order model requires about 1 hour of computation time, depending on the stopping criterion. However, the implementation of the iterative algorithm does not take advantage of the particular structure of the block diagonal realization. If the structure of the problem is utilized, a considerable reduction in computation time is expected.

12.6 Conclusions

High order models have successfully been estimated from real measured data, using the new algorithms discussed and analyzed in this thesis. The application shows that high order state-space models of high quality easily are derived with the realization based Algorithms 9.1 and 9.2, or with the input-output subspace Algorithms 10.1 and 10.2. By using the realization and subspace based approach we obtain high quality models without the need for an explicit parametrization or an iterative optimization. Once this initial model is found it can be converted to a form suited for a numerical stable parametrization, *e.g.*, the block diagonal form, and as a second step a parametric optimization can be applied to refine the quality of the model.

A

Some Matrix Lemmata

The following lemma describes the resulting perturbation of the pseudo inverse of a perturbed matrix.

Lemma A.1 [138] *Let $A \in \mathbb{C}^{m \times n}$, where $m \geq n$ and $\hat{A} = A + \Delta A$. If* $\operatorname{rank}(A) = \operatorname{rank}(\hat{A})$*, then*

$$\|\hat{A}^\dagger - A^\dagger\|_F \leq \|A^\dagger\|_2 \|\hat{A}^\dagger\|_2 \|\Delta A\|_F. \tag{A.1}$$

Proof. See Theorem 3.9 in [138]. □

In the next lemma we show that the norm of the perturbed pseudo inverse is always bounded if the perturbation is sufficiently small.

Lemma A.2 *Let $A, \Delta A \in \mathbb{R}^{m \times n}$, $m \geq n$, let $\|\Delta A\| \leq \epsilon$ and let $\|\cdot\|$ be any consistent matrix norm. Also let A be of full rank n, then*

$$\|(A + \Delta A)^\dagger\| \leq c, \quad \forall \epsilon < \epsilon_0 \tag{A.2}$$

with

$$\epsilon_0 = \sqrt{\|A\|^2 + \|(A^T A)^{-1}\|^{-1}} - \|A\|$$

and

$$c = \frac{\|(A^T A)^{-1}\|}{1 - \|A^T A\|(\epsilon_0 + 2\|A\|)\epsilon_0}(\|A\| + \epsilon_0).$$

Proof. Let $X = A^T A$ and $\Delta X = \Delta A^T \Delta A + \Delta A^T A + A^T \Delta A$. We then get

$$\|(A + \Delta A)^\dagger\| = \|(X + \Delta X)^{-1}(A + \Delta A)^T\| \leq \|(X + \Delta X)^{-1}\| \|A + \Delta A\| \tag{A.3}$$

From the construction of X we conclude that

$$\|\Delta X\| \leq (\|\Delta A\| + 2\|A\|)\|\Delta A\| \leq (\epsilon + 2\|A\|)\epsilon$$

X is of full rank since A is of full rank. $\|X^{-1}\|$ is therefore bounded. Then from the definition of ϵ_0

$$\|X^{-1}\Delta X\| \leq \|X^{-1}\|(\epsilon + 2\|A\|)\epsilon < 1, \ \ \forall\, \epsilon < \epsilon_0.$$

By the use of Theorem 2.3.4 in [43] we obtain

$$\|(X + \Delta X)^{-1}\| \leq \frac{\|X^{-1}\|}{1 - \|X^{-1}\Delta X\|} \leq c_2, \ \ \forall \epsilon < \epsilon_0 \tag{A.4}$$

where $c_2 = \frac{\|X^{-1}\|}{1-\|X^{-1}\|(\epsilon_0+2\|A\|)\epsilon_0}$ By inserting (A.4) into (A.3) we obtain

$$\|(A + \Delta A)^{\dagger}\| \leq c_2(\|A\| + \epsilon) \leq c, \ \ \forall \epsilon < \epsilon_0$$

□

Remark A.1 *For the inverse of a perturbed square matrix, Lemma A.2 is also applicable by setting $m = n$.*

B

Notations

The following notation is used in the thesis.

Operators and Notational Conventions

$\mathbb{R}^d$	Euclidian d-dimensional space
$\mathbb{C}^d$	Complex d-dimensional space
$\otimes$	The Kronecker matrix product
X^*	Complex conjugate
$\operatorname{tr} X$	$\sum_i x_{ii}$, the trace of X
X^T	Matrix transpose of X
X^H	Matrix conjugate transpose, $(X^*)^T$
X^{-1}	Matrix inverse
X^{-T}	$(X^{-1})^T$
$X^\dagger$	Moore-Penrose pseudo-inverse to the matrix X
$\lvert\cdot\rvert$	Euclidian vector norm
$\lVert\cdot\rVert$	Any matrix Norm
$\lVert\cdot\rVert_F$	The Frobenius norm
$\lVert\cdot\rVert_H$	The Hankel norm
$E\,x$	Mathematical expectation of the random vector x
$\operatorname{Cov} x$	The covariance matrix of x
$\operatorname{Re}(z)$	The real part of z
$\operatorname{Im}(z)$	The imaginary part of z
$\arg\min_x f(x)$	The minimizing argument of $f(x)$
$O(x)$	An arbitrary function with the property $\lvert O(x)/x\rvert \leq c < \infty$ as $x \to 0$
$\beta_k = \mathbf{O}(\alpha_k)$	Given two sequences of real numbers $\{\alpha_k\}_{k\geq 1}$ and $\{\beta_k\}_{k\geq 1}$, there exists an integer M and a constant c such that $\lvert\beta_k\rvert \leq c\lvert\alpha_k\rvert$ for all $k \geq M$

$\delta(t)$	Kronecker's delta, $\delta(t) = 1$ if $t = 0$ and 0 otherwise
$\mathrm{diag}(d_1, d_2, \ldots, d_n)$	Diagonal matrix with d_i as diagonal elements
$\dim \theta$	Dimension of vector θ
$\lambda_i(X)$	ith eigenvalue of X
$\sigma_i(X)$	The ordered singular values of X, $\sigma_1 \geq \sigma_2 \geq, \ldots$
$\bar{\sigma}(X)$	The largest singular value of X
$V'(\theta)$	Gradient of V with respect to the argument
$V''(\theta)$	Hessian of V with respect to the argument
$\|G\|_\infty$	Sup norm of $G \in \mathcal{H}_\infty$, $= \sup_\omega \bar{\sigma}(G(e^{j\omega}))$
$?$	Hankel operator of a linear system
$?_i$	The ordered Hankel singular values, $?_1 \geq ?_2 \geq \ldots$

Symbols used in text

$c, c_{ij}, c(i,j)$	Arbitrary bounded complex or real constants
$\mathcal{C}_j$	Extended controllability matrix with j block columns
$D_\mathcal{M}$	Space of θ corresponding to stable predictors $\mathcal{M}(\theta)$
D_T	Space of θ corresponding to input-output equal models $\mathcal{M}(\theta)$
D_N	Space of θ corresponding to input-output equal models $\mathcal{M}(\theta)$ which are norm-minimal
d	Dimension of parameter vector θ
$e(t)$	Disturbance vector at time t
E_{ij}	Zero matrix except for a 1 in row i column j
e_k	Zero vector except for a 1 in position k
f	Sampling frequency
$G(q)$	Transfer function from u to y
g_k	Impulse response coefficient
$H(q)$	Transfer function from e to y
$\mathcal{H}_{ij}$	Block Hankel matrix formed from Markov parameters with block dimensions $i \times j$
H_{ij}	Block Hankel matrix formed from biased Markov parameters with block dimensions $i \times j$
$H(\theta)$	Approximate Hessian of $V_N(\theta)$ or $W_N^\delta(\theta)$
$\mathcal{H}_\infty$	Hardy space of bounded matrix valued functions analytical in the complement of the closed unit disc.
I_m	Identity matrix of size $m \times m$
j	$\sqrt{-1}$
ℓ_2^m	Set of sequences $u = \{u_k\}_{k \geq 0}$, $u_k \in \mathbb{R}^m$ such that $\sum_{k=0}^\infty \|u_k\|^2 < \infty$
$\mathcal{M}$	Model structure
$\mathcal{M}_F$	Fully parametrized model structure
$\mathcal{M}_I$	Identifiable model structure
$\mathcal{M}(\theta)$	Predictor model resulting from $\mathcal{M}$ and θ
$\mathcal{M}^*$	Model set

m	Dimension of input vector $u(t)$
n	System order, dimension of the state vector $x(t)$
$\mathcal{O}_i$	Extended observability matrix with i block rows
p	Dimension of output vector $y(t)$
q, q^{-1}	Forward and backward shift operators
$\mathcal{S}$	True system
T	Similarity transformation matrix
U_s	Left singular vectors of the signal subspace
U_o	Left singular vectors to the orthogonal subspace
$U(\omega)$	Fourier transform of the signal $u(t)$
$u(t)$	Input vector at time t
V_s	Right singular vectors of the signal subspace
V_o	Right singular vectors of the orthogonal subspace
$V_N(\theta)$	Prediction error criterion
$\hat{\bar{V}}$	Sample prediction error variance
$v(t)$	Disturbance at time t
$W_N^\delta(\theta)$	Prediction error criterion with regularization
W_c	Controllability Gramian
W_o	Observability Gramian
w_k	Impulse response disturbance
$x(t)$	State vector at time t
$Y(\omega)$	Fourier transform of the signal $y(t)$
$y(t)$	Output vector at time t
$\hat{y}(t\|\theta)$	Predicted output at time t using a model $\mathcal{M}(\theta)$
Z^N	$\{u(1), y(1), \ldots, u(N), y(N)\}$
$0_{i\times j}$	Zero matrix of dimension $i \times j$
γ	Modal Coherence Indicator (MCI)
δ	Regularization parameter
$\varepsilon(t,\theta)$	Prediction errors $y(t) - \hat{y}(t\|\theta)$
ζ	Damping ratio of vibrational mode
θ	Parameter vector
$\hat{\theta}$	Parameter vector estimated from Z^N
Λ_0, λ_0	Variance of the innovations $e_0(t)$
$\bar{\nu}_n$	Multi-index describing a particular identifiable model structure of order n
$\psi(t,\theta)$	Gradient of $\hat{y}(t,\theta)$ with respect to θ
Σ_s	Diagonal matrix with the singular values of the signal subspace
Σ_o	Diagonal matrix with the singular values of the orthogonal subspace
Ω	Event set
ω	Frequency

Abbreviations and Acronyms

ARX	Auto Regressive with eXternal input
DFT	Discrete Fourier Transform
ERA	Eigensystem Realization Algorithm
FEM	Finite Element Modeling
FFT	Fast Fourier Transform
IDFT	Inverse discrete Fourier Transform
PEM	Prediction Error Minimization
MCI	Modal Coherence Indicator
MIMO	Multiple Input Multiple Output
SISO	Single Input Single Output
SVD	Singular Value Decomposition
w.p. 1	with probability one (convergence)

Bibliography

[1] T. Abrahamsson, T. McKelvey, and L. Ljung. A study of some approaches to vibration data analysis. In *Proc. of the 10th IFAC Symposium on System Identification*, volume 3, pages 289–294, Copenhagen, Denmark, July 1994.

[2] V. M. Adamjan, D. Z. Arov, and M. G. Krein. Analytical properties of Schmidt pairs for a Hankel operator and the generalized Schur-Takagi problem. *Math. USSR Sbornik*, 15:31–73, 1971.

[3] J. L. Adcock. Curve fitter for pole-zero analysis. *Hewlett-Packard Journal*, pages 33–36, January 1987.

[4] H. Akaike. Fitting autoregressive models for prediction. *Ann. Inst. Stat. Math.*, 21:243–247, 1969.

[5] H. Akaike. Modern development of statistical methods. In P. Eykhoff, editor, *Trends and Progress in System Identification*. Pergamon Press, Elmsford, N.Y., 1981.

[6] U. M. Al-Saggaf and G. F. Franklin. Model reduction via balanced realizations: An extension and frequency weighting techniques. *IEEE Trans. on Automatic Control*, 33(7):687–692, July 1988.

[7] B. D. O Anderson. Identification of scalar errors-in-variables models with dynamics. *Automatica*, 21(6):709–716, 1985.

[8] B. D. O Anderson and M. Deistler. Identifiability in dynamic errors-in-variables models. *Journal of Time Series Analysis*, 5(1):1–13, 1984.

[9] B. D. O. Anderson and J. B. Moore. *Optimal Control - Linear Quadratic Methods*. Prentice-Hall, Englewood Cliffs, New Jersey, 1989.

[10] J. D. Aplevich. Approximation of discrete linear systems. *Int. J. Control*, 17(3):565–575, 1973.

[11] K. J. Åström and B. Wittenmark. *Computer Controlled Systems.* Prentice-Hall, Englewood Cliffs, New Jersey, 1984.

[12] M. Basseville, A. Benveniste, B. Gach-Devauchelle, M. Goursat, D. Bonnecase, P. Dorey, M. Prevosto, and M. Olagnon. Damage monitoring in vibration mechanics: issues in diagnostics and predictive maintenance. *Mechanical Systems and Signal Processing*, 7(5):401–423, Sept. 1993.

[13] M. Basseville, A. Benveniste, G. Moustakides, and A. Rougée. Detection and diagnosis of changes in the eigenstructure of nonstationary multivariable systems. *Automatica*, 23(4):479–489, 1987.

[14] D. S. Bayard. An algorithm for state-space frequency domain identification without windowing distortions. In *Proc. of the 31st IEEE Conference on Decision and Control, Tucson, Arizona*, pages 1707–1712, December 1992.

[15] D. S. Bayard. Multivariable state-space identification in the delta and shift operators: Algorithms and experimental results. In *Proc. of the American Control Conference, San Francisco, CA, June*, pages 3038–3042, 1993.

[16] D. S. Bayard. High-order multivariable transfer function curve fitting: Algorithms, sparse matrix methods and experimental results. *Automatica*, 30(9):1439–1444, 1994.

[17] A. Benveniste and J. J. Fuchs. Single sample modal identification of a nonstationary stochastic process. *IEEE Trans. on Automatic Control*, 30(1):66–74, 1985.

[18] C. Bonnet. Convergence and convergence rate of the balanced realization truncations for infinite-dimensional discrete-time systems. *Systems & Control Letters*, 20:353–359, 1993.

[19] G. E. P. Box and G. M. Jenkins. *Time Series Analysis, Forecasting and Control.* Holden-Day, Oakland, California, 1976.

[20] E. O. Brigham. *The Fast Fourier Transform.* Prentice Hall, New Jersey, 1974.

[21] D. R. Brillinger. *Time Series: Data Analysis and Theory.* McGraw-Hill Inc., New York, 1981.

[22] C. W. Chen, J. N. Juang, and G. Lee. Frequency domain state-space system identification. In *Proc. of the American Control Conference, San Francisco, CA, June*, 1993.

[23] C. T. Chou. *Geometry of Linear Systems and Identification.* PhD thesis, Trinity Collage, Cambridge, England, March 1994.

[24] K. L. Chung. *A Course in Probability Theory.* Academic Press, San Diego, CA, 1974.

[25] H. C. Cramér and M. R. Leadbetter. *Stationary and Related Stochastic Processes.* John Wiley & Sons, Inc., New York, 1967.

[26] R. L. Dailey and M. S. Lukich. Mimo transfer function curve fitting using Chebyshev polynomials. In *Proc. of the SIAM 35th Anniversary Meeting, Denver, Colorado*, 1987.

[27] A. A. H. Damen, R. P. Guidorzi, A. K. Hajdasinski, and P. M. J. Van den Hof. On multivariable partial realization. *Int. J. Control*, 41(3):589–613, 1985.

[28] P. De Groen and B. De Moor. The fit of a sum of exponentials to noisy data. *Journal of Computational and Applied Mathematics*, 20:175–187, 1987.

[29] B. De Moor. *Mathematical Concepts and Techniques for Modeling of Static and Dynamic Systems.* PhD thesis, Katholieke Universiteit Leuven, Kard. Mercierlaan 94, 3001 Leuven (Heverlee), Belgium, June 1988.

[30] B. De Moor, M. Gevers, and G. Goodwin. l_2-overbiased, l_2-underbiased and l_2-unbiased estimation of transfer functions. *Automatica*, 30(5):893–898, 1994.

[31] B. De Moor and J. Vandewalle. A geometrical strategy for the identification of state space models of linear multivariable systems with singular value decomposition. In *Proc. of the 3rd International Symposium on Applications of Multivariable System Techniques, April 13-15, Plymouth, UK*, pages 59–69, 1987.

[32] G. R. de Prony. Essai expérimental et analytic, etc. *J. L'Ecole Polytechnique, Paris*, 1(2):24–76, 1795.

[33] M. J. Denham. Canonical forms for the identification of multivariable linear systems. *IEEE Trans. on Automatic Control*, 19(6):646–656, 1974.

[34] J. E. Dennis and R. B. Schnabel. *Numerical Methods for Unconstrained Optimization and Nonlinear Equations.* Prentice-Hall, Englewood Cliffs, New Jersey, 1983.

[35] N. R. Draper and R. C. Van Nostrand. Ridge regression and James-Stein estimation: Review and comments. *Technometrics*, 21(4):451–466, November 1979.

[36] D. F. Enns. *Model reduction for control system design.* PhD thesis, Department of Aeronautics and Astronautics, Stanford University, Stanford, CA, 1984.

[37] D. F. Enns. Model reduction with balanced realizations: An error bound and a frequency weighted generalization. In *Proc. of the 23rd IEEE Conference on Decision and Control, Las Vegas, NV*, pages 127–132, 1984.

[38] E. G. Forsythe. Generation and use of orthogonal polynomials for data fitting with a digital computer. *J. Soc. Indust. Appl. Math.*, 5(2):74–88, 1957.

[39] M. Gevers and G. Li. *Parametrizations in Control, Estimation and Filtering Problems.* Springer-Verlag, 1993.

[40] M. Gevers and V. Wertz. Uniquely identifiable state-space and ARMA parametrizations for multivariable linear systems. *Automatica*, 20(3):333–347, 1984.

[41] K. Glover. All optimal Hankel-norm approximations of linear multivariable systems and their L^∞-error bounds. *Int. J. Control*, 39(6):1115–1193, 1984.

[42] K. Glover and J. C. Willems. Parametrizations of linear dynamical systems: Canonical forms and identifiability. *IEEE Trans. on Automatic Control*, 19(6):640–645, 1974.

[43] G. H. Golub and C. F. Van Loan. *Matrix Computations.* The Johns Hopkins University Press, Baltimore, Maryland, second edition, 1989.

[44] G. C. Goodwin. Some observations on robust stochastic estimation. In *Proc. IFAC Identification and System Parameter Estimation, Beijing, PRC*, 1988.

[45] A. Graham. *Kronecker Products and Matrix Calculus With Applications.* Ellis Horwood Limited, Chichester, England, 1981.

[46] G. Gu and P. P. Khargonekar. A class of algorithms for identification in $\mathcal{H}_\infty$. *Automatica*, 37:299–312, 1992.

[47] G. Gu and P. P. Khargonekar. Frequency domain identification of lightly damped systems: The JPL example. In *Proc. of the American Control Conference*, pages 3052–3056, San Francisco, CA, 1993.

[48] G. Gu, P. P. Khargonekar, and E. B. Lee. Approximation of infinite-dimensional systems. *IEEE Trans. on Automatic Control*, 34:610–618, 1989.

[49] G. Gu and P. Misra. Identification of linear time-invariant systems from frequency response data corrupted by bounded noise. *IEE Proceedings-D*, 139(2):135–140, March 1992.

[50] R. Guidorzi. Canonical structures in the identification of multivariable systems. *Automatica*, 11:361–374, 1975.

[51] R. Guidorzi. Invariants and canonical forms for systems structural and parametric identification. *Automatica*, 17(1):117–133, 1981.

[52] P. Guillaume, R. Pintelon, and J. Schoukens. Robust parametric transfer function estimation using complex logarithmic frequency response data. In *Proc. 10th IFAC Symposium on System Identification*, volume 2, pages 495–502, Copenhagen, Denmark, July 1994.

[53] R. G. Hakvoort. Frequency domain curve fitting with maximum amplitude criterion and guaranteed stability. In *Proc. 2nd European Control Conference*, pages 252–257, Groningen, The Netherlands, 1993.

[54] U. Helmke. Balanced realizations for linear systems: A variational approach. *SIAM J. Control and Optimization*, 31(1):1–15, January 1993.

[55] P. S. C. Heuberger, P. M. J. Van den Hof, and O. H. Bosgra. A generalized orthonormal basis for linear dynamical systems. *IEEE Trans. on Automatic Control*, 40(3):451–465, 1995.

[56] F. B. Hildebrand. *Introduction to Numerical Analysis.* McGraw-Hill, New-York, 1956. ch. 9.

[57] B. L. Ho and R. E. Kalman. Effective construction of linear state-variable models from input/output functions. *Regelungstechnik*, 14(12):545–548, 1966.

[58] R. A. Horn and C. R. Johnson. *Matrix Analysis.* Cambridge University Press, Cambridge, NY, 1985.

[59] R. A. Horn and C. R. Johnson. *Topics In Matrix Analysis.* Cambridge University Press, Cambridge, NY, 1991.

[60] M. Iwatsuki, M. Kawamata, and T. Higuchi. Statistical sensitivity structures with fewer coefficients in discrete time linear systems. *IEEE Trans. on Circuits and Systems*, 37(1):72–80, January 1989.

[61] R. N. Jacques and D. W. Miller. Multivariable model identification from frequency response data. In *Proc. IEEE 32nd Conference on Decision and Control*, pages 3046–3051, San Antonio, Texas, December 1993.

[62] J. N. Juang and R. S. Pappa. An eigensystem realization algorithm for modal parameter identification and model reduction. *J. of Guidance, Control and Dynamics*, 8(5):620–627, 1985.

[63] J. N. Juang and R. S. Pappa. Effects of noise on modal parameters identified by the eigensystem realization algorithm. *J. of Guidance, Control and Dynamics*, 9(3):294–303, May-June 1986.

[64] J. N. Juang and H. Suzuki. An eigensystem realization algorithm in frequency domain for modal parameter identification. *Journal of Vibration, Acoustics, Stress, and Reliability in Design*, 110:24–29, January 1988.

[65] P. T. Kabamba. Balanced forms: Canonicity and parameterization. *IEEE Trans. on Automatic Control*, 30(11):1106–1109, 1985.

[66] T. Kailath. *Linear Systems.* Prentice-Hall, Englewood Cliffs, New Jersey, 1980.

[67] R. E. Kalman. Identifiability and modeling in econometrics. In P. R. Krishnaiah, editor, *Developments in Statistics*, volume 4. Academic Press, New York, 1983.

[68] S. M. Kay. *Modern Spectral Estimation, Theory & Application.* Prentice-Hall, Englewood Cliffs, New Jersey, 1988.

[69] S. W. Kim, B. D. O. Anderson, and A. G. Madievski. Error bound for transfer function order reduction using frequency weighted balanced truncation. *Systems & Control Letters*, 24(3):183–192, February 1995.

[70] L. Kronecker. Zur theorie der elimination einer variabeln aus zwei algebraischen gleichungen. *Trans. Royal Prussian Academy of Science.*, 1881. see collected works Vol. 2.

[71] S. Y. Kung. A new identification and model reduction algorithm via singular value decomposition. In *Proc. of 12th Asilomar Conference on Circuits, Systems and Computers, Pacific Grove, CA*, pages 705–714, 1978.

[72] C. Lanczos. *Applied Analysis.* Prentice Hall, Englewood Cliffs, NJ, 1956.

[73] A. J. Laub. Computation of balancing transformations. In *Proc. JACC, San Francisco*, pages paper FA8–E, 1980.

[74] A. J. Laub, M. T. Heath, C. C. Page, and R. C. Ward. Computation of balancing transformations and other applications of simultaneous diagonalization algorithms. *IEEE Trans. on Automatic Control*, 32(1):115–122, 1987.

[75] E. C. Levy. Complex curve fitting. *IRE Trans. on Automatic Control*, AC-4:37–44, May 1959.

[76] J. S. Lew, J. N. Juang, and R. W. Longman. Comparison of several system identification methods for flexible structures. *J. of Sound and Vibration*, 167(3):461–480, 1993.

[77] F. Li and R. J. Vaccaro. Unified analysis for DOA estimation algorithms i array signal processing. *Signal Processing*, 25:147–169, 1991.

[78] F. Li, R. J. Vaccaro, and D. W. Tufts. Performance analysis of the state-space realization (TAM) and ESPRIT algorithms for DOA estimation. *IEEE Trans. on Antennas and Propagation*, 39(3):418–423, March 1991.

[79] G. Li, B. D. O. Anderson, and M. Gevers. Optimal FWL design of state-space digital systems with weighted sensitivity minimization and sparseness considerations. *IEEE Trans. on Circuits and Systems Vol I: Fundamental Theory and Applications*, 39(5):365–377, May 1992.

[80] G. Li and M. Gevers. Data filtering, reparametrization, and the numerical accuracy of parameter estimators. In *Proc. 31'th IEEE Conference on Decision and Control, Tuscon, Arizona*, 1992.

[81] P. L. Lin and Y. C. Wu. Identification of multi-input multi-output linear systems from frequency response data. *Trans. ASME, J. Dyn. Syst., Measurement and Control*, 104:58–64, 1982.

[82] J. Little and L. Shure. *Signal Processing Toolbox*. The Mathworks, Inc., 1988.

[83] K. Liu, R. N. Jacques, and D. W. Miller. Frequency domain structural system identification by observability range space extraction. Technical report, Space Engineering Research Center, MIT Cambridge, MA 02139, September 1993. Submitted for review for 1994 ACC and ASME Journal of Dynamic Systems, Measurement and Control.

[84] K. Liu, R. N. Jacques, and D. W. Miller. Frequency domain structural system identification by observability range space extraction. In *Proc. of the American Control Conference, Baltimore, Maryland*, volume 1, pages 107–111, June 1994.

[85] K. Liu and R. E. Skelton. Q-markov covariance equivalent realization and its application to flexible structure identification. *AIAA Journal of Guidance, Control and Dynamics*, 16(2):308–319, 1993.

[86] L. Ljung. *System Identification: Theory for the User*. Prentice-Hall, Englewood Cliffs, New Jersey, 1987.

[87] L. Ljung. Issues in system identification. *IEEE Control Systems Magazine*, 11(1):25–29, January 1991.

[88] L. Ljung. *System Identification Toolbox*. The Mathworks, Inc, 1991.

[89] L. Ljung. Some results on identifying linear systems using frequency domain data. In *Proc. 32nd IEEE Conference on Decision and Control, San Antonio, Texas*, pages 3534–3538, December 1993.

[90] L. Ljung. Building models from frequency domain data. In *IMA Workshop on Adaptive Control and Signal Processing*, Minneapolis, Minnesota, 1994.

[91] L. Ljung and Z. D. Yuan. Asymptotic properties of black-box identification of transfer functions. *IEEE Trans. on Automatic Control*, 30:514–530, 1985.

[92] D. G. Luenberger. Canonical forms for linear multivariable systems. *IEEE Trans. on Automatic Control*, AC-12:290, 1967.

[93] D. G. Luenberger. *Linear and Nonlinear Programming*. Addison Wesley, Reading, Massachusetts, 1984.

[94] W. J. Lutz and S. L. Hakimi. Design of multi-input multi-output systems with minimum sensitivity. *IEEE Trans. on Circuits and Systems*, 35(9):1114–1121, September 1988.

[95] J. M. Maciejowski. Balanced realizations in system identification. In *Proc. 7'th IFAC Symposium on Identification & parameter Estimation*, York, UK, 1985.

[96] J. M. Maciejowski. *Multivariable Feedback Design*. Addison-Wesley, Wokingham, England, 1989.

[97] J. M. Maciejowski. Guaranteed stability with subspace methods. *Systems & Control Letters*, 26(2):153–156, 1995.

[98] P. M. Mäkilä and J. R. Partington. Robust approximation and identification in $\mathcal{H}_\infty$. In *Proceedings of the 1991 American Control Conference*, pages 70–76, Boston, MA, 1991.

[99] D. Q. Mayne. A canonical model for identification of multivariable linear systems. *IEEE Trans. on Automatic Control*, 17:728–729, 1972.

[100] T. McKelvey. A combined state-space identification algorithm applied to data from a modal analysis experiment on a separation system. In *Proc. 33rd IEEE Conference on Decision and Control, Lake Buena Vista, Florida*, pages 2286–2287, December 1994.

[101] T. McKelvey. Fully parametrized state-space models in system identification. In *Proc. of the 10th IFAC Symposium on System Identification*, volume 2, pages 373–378, Copenhagen, Denmark, July 1994.

[102] T. McKelvey. Model validation using geometric arguments. In *Proc. Third European Control Conference*, volume 2, pages 423–428, Rome, Italy, 1995.

[103] T. McKelvey and H. Akçay. An efficient frequency domain state-space identification algorithm. In *Proc. 33rd IEEE Conference on Decision and Control, Lake Buena Vista, Florida*, pages 3359–3364, December 1994.

[104] T. McKelvey and H. Akçay. An efficient frequency domain state-space identification algorithm: Robustness and stochastic analysis. In *Proc. 33rd IEEE Conference on Decision and Control, Lake Buena Vista, Florida*, pages 3348–3353, December 1994.

[105] T. McKelvey and H. Akçay. Subspace based system identification with periodic excitation signals. In *Proc. Third European Control Conference*, volume 1, pages 423–428, Rome, Italy, 1995.

[106] T. McKelvey, L. Ljung, and H. Akçay. Identification of infinite dimensional systems from frequency response data. In *Proc. Third European Control Conference*, volume 3, pages 2106–2111, Rome, Italy, 1995.

[107] M. Moonen, B. De Moor, L. Vandenberghe, and J. Vandewalle. On- and off-line identification of linear state-space models. *Int. J. Control*, 49(1):219–232, 1989.

[108] M. Moonen, B. De Moor, and J. Vandewalle. Svd-based subspace methods for multivariable continuous-time identification. In N. K. Sinha and G. P. Rao, editors, *Identification of Continuous-Time Systems*, pages 473–488. Kluwer Academic Publishers, The Netherlands, 1991.

[109] B. C. Moore. Principal component analysis in linear systems: Controllability, observability, and model reduction. *IEEE Trans. on Automatic Control*, 26(1):17–32, 1981.

[110] C. T. Mullis and R. A. Roberts. Roundoff noise in digital filters: Frequency transformations and invariants. *IEEE Trans. on Acoustics, Speech and Signal Processing*, 24(6):538–550, December 1976.

[111] C. T. Mullis and R. A. Roberts. Synthesis of minimum roundoff noise fixed point digital filters. *IEEE Trans. on Circuits and Systems*, 23(9):551–562, September 1976.

[112] B. M. Ninness. *Stochastic and Deterministic Modelling.* PhD thesis, Electrical and Computer Engineering, University of Newcastle, New South Wales, Australia, 1993.

[113] B. Noble. *Applied Linear Algebra.* Prentice-Hall, Engelwood Cliffs, N. J., 1969.

[114] R. J. Ober. Balanced realizations: Canonical form, parametrization, model reduction. *Int. J. Control*, 46(2):643–670, 1987.

[115] A. V. Oppenheim and R. W. Schafer. *Discrete-Time Signal Processing.* Prentice-Hall, Englewood Cliffs, NJ, 1989.

[116] B. Ottersten and M. Viberg. A subspace based instrumental variable method for state-space system identification. In *Proceedings of the 10th IFAC Symposium on System Identification*, volume 2, pages 139–144, Copenhagen, Denmark, July 1994.

[117] L. Pernebo and L. M. Silverman. Model reduction via balanced state space representations. *IEEE Trans. on Automatic Control*, 27(2):382–387, 1982.

[118] L. E. Pfeffer. The RPM toolbox: A system for fitting linear models to frequency response data. In *Proc. of 1993 MATLAB Conference, Cambridge, MA*, October 1993.

[119] R. Pintelon, P. Guillaume, Y. Rolain, J. Schoukens, and H. Van Hamme. Parametric identification of transfer functions in the frequency domain, a survey. In *Proc. 32nd IEEE Conference on Decision and Control, San Antonio, Texas*, pages 557–566, 1993.

[120] R. Pintelon, P. Guillaume, Y. Rolain, J. Schoukens, and H. Van Hamme. Parametric identification of transfer functions in the frequency domain – A survey. *IEEE Trans. of Automatic Control*, 94(11):2245–2260, November 1994.

[121] R. Pintelon and J. Schoukens. Robust identification of transfer functions in s- and z- domains. *IEEE Trans. Instrum. Meas.*, 39(4):565–573, 1990.

[122] R. Pintelon, J. Schoukens, and H. Chen. On the basic assumptions in the identification of continuous time systems. In *Proc. 10th IFAC Symposium on System Identification*, volume 3, pages 143–152, Copenhagen, Denmark, July 1994.

[123] M. Prevosto, M. Olagnon, A. Benveniste, and M. Basseville. State space formulation: A solution to modal parameter estimation. *Journal of Sound and Vibration*, 148(2):329–342, 1991.

[124] Y. Rolain, R. Pintelon, K. Q. Xu, and H. Vold. On the use of orthogonal polynomials in high order frequency domain system identification and its application to modal parameter estimation. In *Proc. 33rd IEEE Conference on Decision and Control, Lake Buena Vista, Florida*, volume 4, pages 3365–3373, December 1994.

[125] R. Roy and T. Kailath. ESPRIT - Estimation of signal parameters via rotational invariance techniques. *IEEE Trans. on Acoustics, Speech and Signal Processing*, 37(7):984–995, July 1989.

[126] R. Roy, A. Paulray, and T. Kailath. ESPRIT-A subspace rotation approach to estimation of parameters of cisoids in noise. *IEEE Trans. on Acoustics, Speech and Signal Processing*, ASSP-34(5):1340–1342, October 1986.

[127] W. Rudin. *Real and Complex Analysis.* McGraw-Hill, 1987.

[128] C. K. Sanathanan and J. Koerner. Transfer function synthesis as a ratio of two complex polynomials. *IEEE Trans. on Automatic Control*, 8:56–58, January 1963.

[129] J. Schoukens and R. Pintelon. *Identification of Linear Systems: a Practical Guideline to Accurate Modeling.* Pergamon Press, London, UK, 1991.

[130] J. Schoukens, R. Pintelon, and P. Guillaume. On the advantage of periodic excitation in system identification. In *Proceedings of the 10th IFAC Symposium on System Identification*, volume 3, pages 153–158, Copenhagen, Denmark, 1994.

[131] M. D. Sidman, F. E. DeAngelis, and G. C. Verghese. Parametric system identification on logarithmic frequency response data. *IEEE Trans. on Automatic Control*, 36(9):1065–1070, 1991.

[132] L. M. Silverman. Realization of linear dynamical systems. *IEEE Trans. on Automatic Control*, 16(6):554–567, 1971.

[133] N. K. Sinha and G. P. Rao. *Identification of Continuous-Time Systems.* Kluwer Academic Publishers, 1994.

[134] J. Sjöberg. Regularization issues in neural network models of dynamical systems. Linköping Studies in Science and Technology. Thesis no.366, LiU-Tek-Lic-1993:08, Department of Electrical Engineering, Linköping University, Sweden, 1993.

[135] J. Sjöberg, T. McKelvey, and L. Ljung. On the use of regularization in system identification. In *Proc. 12th World Congress International Federation of Automatic Control, Sydney, Australia*, volume 7, pages 381–386, 1993.

[136] T. Söderström and P. Stoica. *System Identification*. Prentice-Hall International, Hemel Hempstead, Hertfordshire, 1989.

[137] J. T. Spanos and D. L. Mingori. Newton algorithm for fitting transfer functions to frequnecy response measurements. *Journal of Guidance, Control and Dynamics*, 16(1):34–39, 1993.

[138] G. W. Stewart and J. G. Sun. *Matrix Perturbation Theory*. Academic Press, Inc., 1990.

[139] P. Stoica, P. Eykhoff, P. Janssen, and T. Söderström. Model structure selection by cross validation. *Int. J. Control*, 43:1841–1878, 1986.

[140] P. Stoica, R. Moses, B. Friedlander, and T. Söderström. Maximum likelihood estimation of the parameters of multiple sinusoids from noisy measurements. *IEEE Trans. on Acoustics, Speech and Signal Processing*, 37(3):378–392, March 1989.

[141] L. Swindlehurst, R. Roy, B. Ottersten, and T. Kailath. A subspace fitting method for identification of linear state-space models. *IEEE Trans. on Automatic Control*, 40(2):311–316, February 1995.

[142] V. Tavsanoglu and L. Thiele. Optimal design of state-space digital filters by simultaneous minimization of sensitivity and roundoff noise. *IEEE Trans. on Circuits and Systems*, 31(10):884–888, October 1984.

[143] The MathWorks Inc. *MATLAB, Reference Guide*. 1992.

[144] L. Thiele. Design of sensitivity and round-off noise optimal state-space discrete systems. *Circuit Theory and Applications*, 12:39–46, 1984.

[145] L. Thiele. On the sensitivity of linear state-space systems. *IEEE Trans. on Circuits and Systems*, 33:502–510, 1986.

[146] R. J. Vaccaro. Deterministic balancing and stochastic model reduction. *IEEE Trans. on Automatic Control*, 30(9):921–923, September 1985.

[147] A. W. M. Van den Enden and G. A. L. Leenknegt. Design of optimal filters with arbitrary amplitude and phase requirements. In L. T. Young *et al.*, editor, *Signal Processing III: Theories and Applications*, pages 183–186. North Holland: Elsevier Science, 1986.

[148] A. J. van der Veen, E. F. Deprettere, and A. L. Swindlehurst. SVD-based estimation of low-rank system parameters. In E. F. Deprettere and A. J. van der Veen, editors, *Algorithms and Parallel VLSI Architectures*. Elsevier Science Publishers, 1991.

[149] A. J. M. van Overbeek and L. Ljung. On-line structure selection for multivariable state space models. *Automatica*, 18(5):529–543, 1982.

[150] P. Van Overschee. *Subspace Identification, Theory - Implementation - Application*. PhD thesis, Katholieke Universiteit Leuven, Kard. Mercierlaan 94, 3001 Leuven (Heverlee), Belgium, February 1995.

[151] P. Van Overschee and B. De Moor. Two subspace algorithms for the identification of combined deterministic-stochastic systems. In *Proc. 31'st IEEE Conference on Decision and Control, Tuscon, Arizona*, pages 511–516, 1992.

[152] P. Van Overschee and B. De Moor. N4SID: Subspace algorithms for the identification of combined deterministic-stochastic systems. *Automatica*, 30(1):75–93, 1994.

[153] P. Van Overschee and B. De Moor. A unifying theorem for subspace identification algorithms and its interpretation. In *Proceedings of the 10th IFAC Symposium on System Identification*, volume 2, pages 145–150, Copenhagen, Denmark, July 1994.

[154] P. Van Overschee and B. De Moor. Frequency domain subspace identification algorithms. In *14'th Benelux Meeting on Systems and Control, Houthalen, Belgium*, 1995.

[155] M. Verhaegen. A novel non-iterative MIMO state space model identification technique. In *Proc. 9th IFAC/IFORS Symp. on Identification and System parameter estimation, Budapest, Hungary*, pages 1453–1458, July 1991.

[156] M. Verhaegen. Subspace model identification, Part III: Analysis of the ordinary output-error state space model identification algorithm. *Int. J. Control*, 58:555–586, 1993.

[157] M. Verhaegen. Identification of the deterministic part of MIMO state space models given in innovations form from input-output data. *Automatica*, 30(1):61–74, 1994.

[158] M. Viberg. Subspace methods in system identification. In *10th IFAC Symposium on System Identification*, volume 1, pages 1–12. IFAC, 1994.

[159] M. Viberg, B. Ottersten, B. Wahlberg, and L. Ljung. A statistical perspective on state-space modeling using subspace methods. In *Proc. 30th IEEE Conference on Decision and Control, Brighton, England*, pages 1337–1342, 1991.

[160] M. Viberg, B. Ottersten, B. Wahlberg, and L. Ljung. Performance of subspace based state-space system identification methods. In *Proc. 12th World Congress International Federation of Automatic Control, Sydney, Australia*, volume 7, pages 369–372, 1993.

[161] H. Vold and R. Russel. Advanced analysis methods improve modal test results. *Sound and Vibration*, pages 36–40, 1983.

[162] B. Wahlberg. System identification using Laguerre models. *IEEE Trans. on Automatic Control*, 36:551–562, May 1991.

[163] B. Wahlberg. System identification using Kautz models. *IEEE Trans. on Automatic Control*, 39(6):1276–1282, June 1994.

[164] A. H. Whitfield. Asymptotic behaviour of transfer function synthesis methods. *Int. J. Control*, 45(3):1083–1092, 1987.

[165] P. M. R. Wortelboer and O. H. Bosgra. Generalized frequency weighted balanced reduction. In O. H. Bosgra and P. M. J. Van den Hof, editors, *Selected Topics in Identification, Modeling and Control*, volume 5, pages 29–36. Delft University Press, 1992.

[166] D. C. Youla and P. Tissi. n-port synthesis via reactance extraction - Part I. *IEEE Conv. Rec.*, 14(7):183–205, March 1966.

[167] N. Young. *An introduction to Hilbert space*. Cambridge University Press, 1995.

[168] N. J. Young. Balanced realizations in infinite dimensions. In *Operator Theory: Advances and Applications*, volume 19. Birkhäuser Verlag, Basel, 1986.

[169] H. P. Zeiger and A. J. McEwen. Approximate linear realizations of given dimension via Ho's algorithm. *IEEE Trans. on Automatic Control*, 19:153, April 1974.